Synthesis and Characterization of TiO_2 Doped with Fluoride Ion

Sutatip Jainsiri

A Thesis Submitted in Partial Fulfillment of the Requirements for the Degree of
Master of Science in Inorganic Chemistry
Prince of Songkla University
2012

Thesis Title	Synthesis and Characterization of TiO_2 Doped with Fluoride Ion
Author	Miss Sutatip Jainsiri
Major Program	Inorganic Chemistry

Major Advisor :	**Examining Committee :**
....	.... Chairperson
(Assoc. Prof. Dr. Sumpun Wongnawa)	(Dr. Anob Kantacha)
	....
	(Assoc. Prof. Dr. Sumpun Wongnawa)
	....
	(Asst. Prof. Dr. Chaveng Pakawatchai)
	....
	(Asst. Prof. Dr. Pongsaton
Amornpitoksuk)	

The Graduate School, Prince of Songkla University, has approved this thesis as partial fulfillment of the requirements for the Master of Science Degree in Inorganic Chemistry

....
(Prof. Dr. Amornrat Phongdara)
Dean of Graduate School

ชื่อวิทยานิพนธ์ การสังเคราะห์และการศึกษาคุณลักษณะของไทเทเนียมไดออกไซด์เจือด้วยไอออนฟลูออไรด์
ผู้เขียน นางสาวสุธาทิพย์ เจียรศิริ
สาขาวิชา เคมีอนินทรีย์
ปีการศึกษา 2554

บทคัดย่อ

สังเคราะห์ไทเทเนียมไดออกไซด์เจือฟลูออรีนด้วยวิธีอิมเพรกเนชันและวิธีตกตะกอนรวมโดยใช้ $TiCl_4$ และ $NH_4F \cdot HF$ เป็นสารตั้งต้น ศึกษาลักษณะของสารตัวอย่างด้วยเทคนิค XRD, SEM, PL, UV-DRS, BET, FT-IR, TGA, XAS และ UV-Vis พร้อมทั้งทดสอบความสามารถในการเป็นโฟโตคะตะลิสต์ด้วยการสลายสีย้อมอินดิโกคาร์มีน ภายใต้ช่วงแสงอัลตราไวโอเลตและช่วงแสงที่มองเห็น จากผลการทดลองพบว่าไทเทเนียมไดออกไซด์ที่ใช้เป็นสารตั้งต้นเป็นไทเทเนียมไดออกไซด์อสัณฐาน ส่วนผลิตภัณฑ์ที่เจือด้วยฟลูออรีนเป็นไทเทเนียมไดออกไซด์อสัณฐานที่มีผลึกแบบอนาเทสปนอยู่เล็กน้อยและมีองค์ประกอบของธาตุไทเทเนียม ออกซิเจน คาร์บอนและฟลูออรีน ทั้งไทเทเนียมไดออกไซด์บริสุทธิ์และที่เจือด้วยฟลูออรีนมีพื้นที่ผิวสูง การเจือธาตุฟลูออรีนมีผลทำให้แถบการดูดกลืนแสงของไทเทเนียมไดออกไซด์เลื่อนเขามาอยูในชวงแสงที่มองเห็น ทำให้ค่าพลังงานของแถบช่องว่างลดลง ซึ่งจะช่วยเพิ่มประสิทธิภาพการตอบสนองในช่วงแสงที่มองเห็น

ได้ทำการเปรียบเทียบประสิทธิภาพไทเทเนียมไดออกไซด์เจือด้วยฟลูออรีนด้วยวิธีอิมเพรกเนชัน และวิธีตกตะกอนรวม ในการสลายสีย้อมอินดิโกคาร์มีนภายใต้ช่วงแสงอัลตราไวโอเลตและช่วงแสงที่มองเห็นพบว่าไทเทเนียมไดออกไซด์ซึ่งเจือด้วยฟลูออรีนสามารถสลายสีย้อมอินดิโกคาร์มีนได้ดีกว่าไทเทเนียมไดออกไซด์อสัณฐาน โดยภายใต้การฉายแสงอัลตราไวโอเลต 1 ชั่วโมงและแสงที่มองเห็น 4 ชั่วโมง มีประสิทธิภาพในการสลายสีย้อมได้ 100 เปอร์เซ็นต์ ขณะที่ไทเทเนียมไดออกไซด์อสัณฐาน ไม่มีประสิทธิภาพในการสลายสีย้อมอินดิโกคาร์มีนภายใต้การฉายแสงอัลตราไวโอเลตและแสงที่มองเห็น

Thesis Title	Synthesis and Characterization of TiO_2 Doped with Fluoride Ion
Author	Miss Sutatip Jainsiri
Major Program	Inorganic Chemistry
Academic Year	2011

Abstract

Fluorine doped TiO_2 ($F\text{-}TiO_2$) was synthesized via the impregnation and co-precipitation methods by using $TiCl_4$ and $NH_4F{\cdot}HF$ as titanium and fluorine sources, respectively. The prepared samples were characterized by XRD, SEM, UV-DRS, PL, BET surface area, FT-IR, TGA, XAS, UV-Vis techniques. The photocatalytic activity was evaluated by decomposing indigo carmine under UV and visible light. The characterization results showed that the undoped powder was amorphous TiO_2 while the doped sample $F\text{-}TiO_2$ contained small amount of anatase. Analysis of $F\text{-}TiO_2$ showed the presence of Ti, O, C and F elements. Both the doped and undoped samples exhibited high surface area. The absorption edge shifted toward longer wavelength indicating a decrease in the band gap energy of $F\text{-}TiO_2$. Narrowing of the band gap of TiO_2 upon doping was responsible for the enhanced visible light activity.

Comparative assessment of the efficiency of fluorine doped TiO_2 prepared by two doping methods was carried out with the photocatalytic degradation of indigo carmine in aqueous solution under UV and visible light irradiation. $F\text{-}TiO_2$ showed higher activity for indigo carmine photodegradation than that of amorphous TiO_2. Under UV light, $F\text{-}TiO_2$ degraded about 100% of dye in about 1 h, and about 4 h under visible light, while the undoped amorphous TiO_2 barely showed any activities under both UV and visible light irradiation.

Contents

Page

Contents (Continued)

Contents (Continued)

List of Tables

List of Tables (Continued)

Table **Page**

List of Figures

Figure **Page**

List of Figures (Continued)

List of Figures (Continued)

Figure **Page**

List of Figures (Continued)

Figure **Page**

List of Figures (Continued)

Figure **Page**

List of Figures (Continued)

CHAPTER 1

Introduction

1.1 Introduction

Environmental pollution by chemical substances has become a serious problem throughout the world. Wastewater effluents in some industries, such as dyestuff, textiles, leather, paper, and plastics, contain several kinds of synthetic dyestuffs. A very small amount of dye in water is highly visible and can be toxic to life and harmful to human beings. Hence, the removal of color from process or waste effluents becomes of fundamental importance to the environment (Mohamed, *et al.*, 2007). Heterogeneous photocatalysis based on titanium dioxide (TiO_2) has been extensively studied in various fields, especially for the environmental application to the destruction of toxic pollutants (Wang, *et al.*, 2008). TiO_2 is a promising photocatalyst due to its high oxidation power, long-term stability, low cost and nontoxicity (Yang, *et al.*, 2008). However, it can only work under ultraviolet (UV) light (wavelength $\lambda < 388$ nm) due to its wide bandgap of 3.0-3.2 eV, which means only ~4% of the incoming solar energy on the surface can be utilized. As a result, the widespread technological use of TiO_2 photocatalyst has been hampered (Xie, *et al.*, 2007). Several works reported that doping TiO_2 with nonmetallic elements, such as fluorine, nitrogen, sulphur, carbon, shift the optical absorption edge of TiO_2 toward lower energy, thereby increasing the photocatalytic activity in visible region (Xu, *et al.*, 2008). F-doping into TiO_2 is also effective for enhancing the photocatalytic activity (Mori, *et al.*, 2008). Fluorinated TiO_2 has been often investigated in relation to doping ($TiO_{2-x}F_x$) or surface complexation (F-TiO_2). It was reported that fluoride doping improves the crystallinity of anatase and the photocatalytic reactivity. In addition, $TiO_{2-x}F_x$ has fewer anion vacancies with a lower density of midgap states and is more stable against photocorrosion. On the other hand, surface fluorination of TiO_2 (F-TiO_2) is a simple ligand exchange between fluoride anions (F^-) and surface hydroxyl groups on TiO_2 in water (Park and Choi, 2004). A variety of anionic species in aqueous solution undergoes inner-sphere ligand substitution reaction with the surface hydroxyl as follows:

$$\equiv TiOH + X^- \longrightarrow \equiv TiX + OH^- \qquad (1.1)$$

The reaction rate was strongly dependent on the surface coverage by Ti-F species (concentration of fluoride ions and pH) (Minero, *et al*., 2000). Fluorine-doped TiO_2 is more stable against photocorrosion and can increase the surface OH radicals that are beneficial for the photocatalytic reactions. Furthermore, Fluorination is a very effective way to increase the surface acidity of a material because of the strongest electronegativity of fluorine (Tang, *et al*., 2007). It was also demonstrated that F-doped TiO_2 is effective for enhancing photocatalytic activity. F-doping converts Ti^{4+} to Ti^{3+} by charge compensation, and the existence of Ti^{3+} can reduce the electron-hole recombination rate and subsequently enhances the photocatalytic activity (Yu, *et al*., 2002). F-doping produced several beneficial effects including the creation of surface oxygen vacancies, the enhancement of surface acidity and the increase of Ti^{3+} ions (Li, *et al*., 2005). Surface-fluorinated TiO_2 (F-TiO_2) particles were prepared via the HF etching method. The surface characteristics of fluorinated TiO_2, the adsorption modes of dyes, and the reaction pathways for the photocatalytic degradation of dye pollutants under visible light irradiation were investigated. It was found that, in the treatment of TiO_2 by HF etching, F^- not only displaces surface HO^- but also substitutes some surface lattice oxygen. As a result, both the adsorption modes and degradation of the dyes were greatly altered. The adsorption mode of zwitterionic dyes was reversed from anionic group adsorption on pure TiO_2 to nitrogen-alkyl group adsorption on F-TiO_2. Dyes with positively charged nitrogen-alkyl groups underwent a rapid *N*-dealkylation process on F-TiO_2, while on pure TiO_2 direct cleavage of the dye chromophore ring structures predominated. It was proposed that the increase in the degradation kinetics after fluorination was derived from the enhanced adsorption and the lowered flat-band potential. The promotion of *N*-dealkylation is likely to be due to the changes in the electron density, the energy level structure of the dye excited state, and the dye cationic radical after inversion of the adsorption modes (Wang, *et al*., 2008). The design of highly efficient photocatalytic systems is of vital interest and one of the most desirable goals in the research on environmentally friendly catalysts. The utilization of extremely small TiO_2 particles as photocatalysts has attracted a great deal of attention, especially for the degradation of organic pollutants diluted in air and water (Yamashita, *et al*., 2008). Indigo carmine (IC) is one of the oldest dyes and still one of the most important used. Its major industrial application is the dyeing of clothes (blue jeans) and other blue denim (Othman, *et al*., 2007). The discharge of highly coloured wastewater into the ecosystem involves environmental problems like aesthetic pollution (even a small amount of dye is clearly apparent), and perturbation of aquatic life. Thus, keeping the toxicity of this dye, various attempts have been made for the removal of indigo carmine from water and wastewater (Barka, *et al*., 2008).

On the other hand, it has been reported that amorphous TiO_2 has very low photocatalytic efficiency with very few studies. There are few investigations for improving its activity by doping with some anions. In this work, we focus on doping with F^- ion on amorphous titania in order to improve its photocatalytic activity under UV and visible irradiation. The physico-chemical properties of the products were characterized by X-ray diffractometry (XRD), scanning electron microscopy (SEM), Ultraviolet-visible diffused reflectance (UV-Vis DRS), Photoluminescence spectroscopy (PL), Fourier transformed infrared spectroscopy (FT-IR), X-ray absorption spectroscopy (XAS), Thermogravimetric analysis (TGA), Differential scanning calorimetry (DSC), UV-Vis spectroscopy, and surface area measurement by BET techniques.

1.2 Review of Literatures

1.2.1 Titanium dioxide (TiO_2)

(1) General background

Titanium, the world's fourth most abundant metal (exceeded only by aluminium, iron, and magnesium) and the ninth most abundant element (constituting about 0.63% of the Earth's crust), was discovered in 1791 in England by Reverend William Gregor, who recognized the presence of a new element in ilmenite. The element was rediscovered several years later by the German chemist Heinrich Klaporth in rutile ore who named it after Titans, mythological first sons of the goddess Ge (Earth in Greek mythology) (Carp, *et al.*, 2004). TiO_2 is found in nature as the three minerals rutile, anatase and brookite, and also as a constituent in ilmenite ($FeTiO_3$), perovskite ($CaTiO_3$) and titanite ($CaTiSiO_5$). TiO_2 is chemically and mechanically very stable (Pore, *et al.*, 2010). TiO_2 belongs to the family of transition metal oxides. In the beginning of the 20th century, industrial production started with titanium dioxide replacing toxic lead oxides as pigments for white paint. At present, the annual production of TiO_2 exceeds 4 million tons. It is used as a white pigment in paints (51% of total production), plastic (19%), and paper (17%), which represents the major end-use sectors of TiO_2. The consumption of TiO_2 as a pigment increased in the last few years in a number of minor end-use sectors such as textiles, food, leather, pharmaceuticals, and various titanate pigments (Carp, *et al.*, 2004). Scientific studies on such photoactivity of TiO_2 have been reported since the early part of the 20th century. For example, there was a report on the photobleaching of dyes by TiO_2 both in vacuo and in oxygen in 1938. It was reported that UV absorption produces active oxygen species on the TiO_2 surface, causing the photobleaching of dyes. It was also known that TiO_2 itself does not change through the photoreaction, although the photocatalyst terminology was not used for TiO_2 in the report, but called a photosensitizer (Hashimoto, *et al.*, 2005). In 1972, Fujishima and Honda discovered the phenomenon of photocatalytic splitting of water on a TiO_2 electrode under ultraviolet (UV) light. Since then, enormous efforts have been devoted to the research of TiO_2 material, which has led to many promising applications in areas ranging from photovoltaics and photocatalysis to photo/electrochromics and sensors. These applications can be roughly divided into energy and environmental categories, many of which depend not only on the properties of the TiO_2 material itself but also on the modifications of the TiO_2 material host (e.g., with inorganic and organic dyes) and on the interactions of TiO_2 materials with the environment (Chen and Mao, 2007).

(2) Crystal structures and properties

TiO_2 usually crystallizes in one of the three major crystal structures; antase, rutile, and brookite (Figure 1.1). Brookite is rarer and much more difficult to prepare. From the application perspective, anatase and rutile are, therefore, by far the most important structures and their properties have been studied much more than those of brookite (Pore, *et al.*, 2010). Two different crystal structures of TiO_2, rutile and anatase are commonly used in photocatalysis with anatase showing a higher photocatalytic activity.

(a) Anatase

(b) Rutile

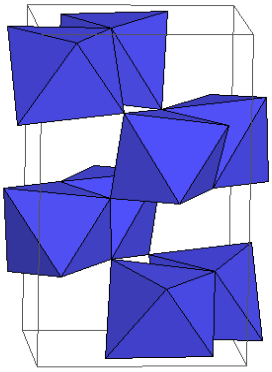

(c) Brookite

Figure 1.1 Crystal structures of TiO_2; (a) anatase, (b) rutile, and (c) brookite (http://ruby.colorado.edu/~smyth/min/tio2.html)

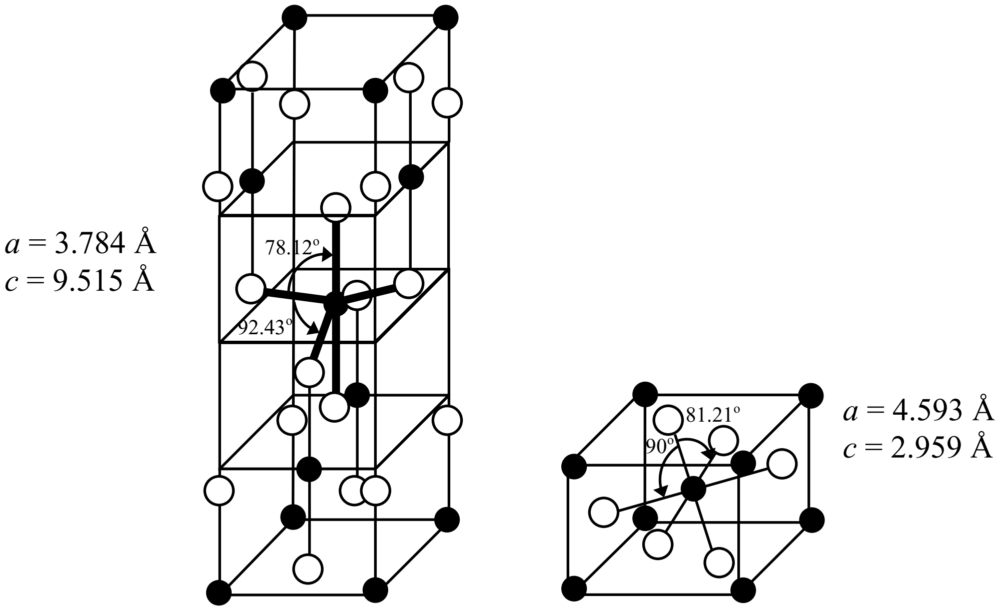

Figure 1.2 The unit cell structures of the anatase and rutile crystal (Linsebigler, *et al.*, 1995).

The unit cell structures of the rutile and anatase crystal are shown in Figure 1.2. Each Ti^{4+} ion is surrounded by an octahedron of six O^{2-} ions. The octahedron in rutile is not regular, showing a slight orthorhombic distortion. The octahedron in anatase is significantly distorted so that its symmetry is lower than orthorhombic. The Ti-Ti distances in anatase are greater (3.79 and 3.04 Å vs 3.57 and 2.96 Å in rutile) whereas the Ti-O distances are shorter than in rutile (1.934 and 1.980 Å in anatase vs 1.949 and 1.980 Å in rutile). In the rutile structure each octahedron is in contact with 10 neighbor octahedrons (two sharing edge oxygen pairs and eight sharing corner oxygen atoms) while in the anatase structure each octahedron is in contact with eight neighbors (four sharing an edge and four sharing a corner) (Linsebigler, *et al.*, 1995). Both anatase and rutile have tetragonal crystal structures but belong to different space groups. Anatase has the space group $I4_1/amd$ with four formula units in one unit cell and rutile has the space group $P4_2/mnm$ with two TiO_2 formula units in one unit cell. The low-density solid phases are less stable and undergo transition rutile in the solid state. The transformation is accelerated by heat treatment and occurs at temperatures between 450 and 1200 °C. This transformation is dependent on several parameters such as initial particle size, initial phase, dopant concentration, reaction atmosphere and annealing temperature, etc (Ahmad, *et al*., 2006). Some bulk properties of the three main polymorphs of TiO_2 are shown in Table 1.1.

Table 1.1 Some bulk properties of the three main polymorphs of TiO_2. (anatase, rutile, and brookite) (Carp, *et al*., 2004).

Crystal structure	System	Space group	Lattice constants (nm)			
			a	*b*	*c*	*c/a*
Rutile	Tetragonal	D_{4h}^{14}-P4_2/mmm	0.4584	-	0.2953	0.644
Anatase	Tetragonal	D_{4h}^{19}-I4_1/amd	0.3733	-	0.937	2.51
Brookite	Rhombohedral	D_{2h}^{15}-Pbca	0.5436	0.9166	-	0.944
Density (kg/m^3)						
Rutile	4240					
Anatase	3830					
Brookite	4170					
Dielectric properties	Frequency (Hz)	Temperature (K)	Dielectric constant			
Rutile, perpendicular to optical *c*-axis	10^8	290-295	86			
Rutile, parallel to optical *c*-axis	-	290-295	170			
Rutile, perpendicular to optical *c*-axis	10^4	298	160			
Rutile, along *c*-axis	10^7	303	100			
Anatase, average	10^4	298	55			
Band gap (eV)						
Rutile	3.05					
Anatase	3.26					
Refractive index	n_g	n_p				
Rutile	2.9467	2.6506				
Anatase	2.5688	2.6584				
Brookite	2.809	2.677				

1.2.2 Synthesis of TiO_2

TiO_2 pigments are either manufactured using the older sulfate or newer chloride processes. The economics of the two processes are very much dependent upon the raw materials available. The sulfate process (Figure 1.3) utilizes ilmenite or titaniferous slage. The finely ground raw material are digested in an exothermic reaction with concentrated sulfuric acid, the digested cake dissolved cold water and the residue separated off. To prevent their precipitation during the subsequent hydrolysis the iron (III) ions are reduced to iron (II) by adding a Ti (III) solution or scrap-iron. Upon evaporating the solution, the large quantities of iron (II) sulfate heptahydrate produced when ilmenite is used, crystallize out. The titanium sulfate is then hydrolyzed by heating the clarified solution with steam at 95-110 C. TiO_2 seed crystals are added or are formed before hydrolysis to ensure yields of 93 to 96 % TiO_2 and to obtain a hydrolysis product which yields the optimum particle size of *ca.* 0.2 m upon firing dilute sulfuric acid remains as waste acid. The hydrolysis product is washed, treated with a Ti (III) solution to remove adsorbed heavy metal ions (Fe, Cr, Mn, V) and then calcined at temperatures between 800 and 1000 C (Buchner, *et al.*, 1989).

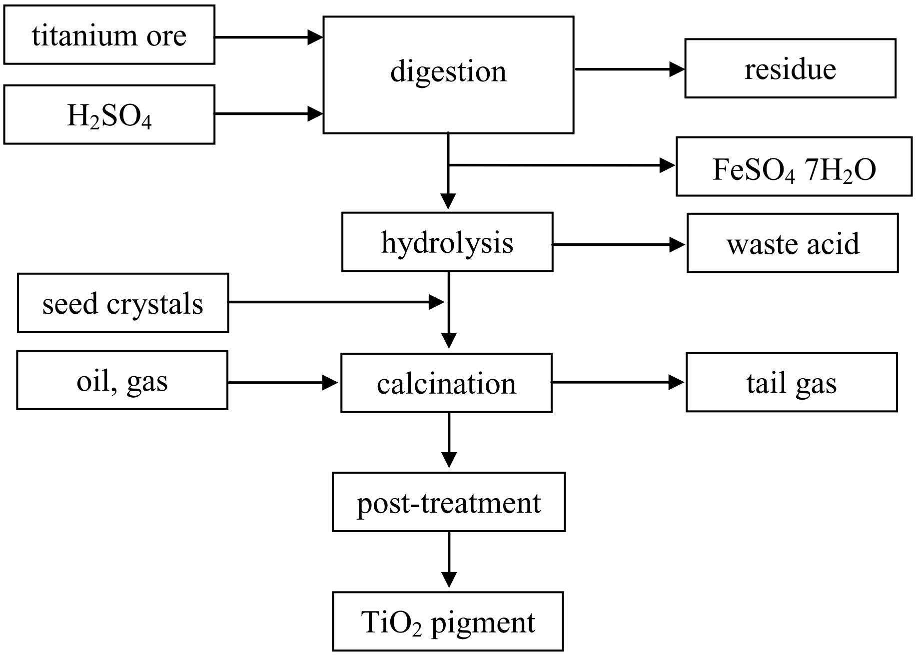

Figure 1.3 TiO_2 pigment manufacture using the sulfate process (Buchner, *et al.*, 1989).

In the chloride process natural or synthetic rutile ore with a TiO_2 content of *ca.* 96 % is chlorinated in a fluidized bed with oil coke and chlorine. The raw $TiCl_4$ produced is mixed with reducing agents to convert impurities such as vanadium oxychloride to lower valency state compounds. It is then distilled yielding titanium tetrachloride in almost any required purity. Finally it is combusted with pure oxygen to TiO_2 and chlorine, which is reused in the chlorination (Figure 1.4). The formation of metal chlorides other than $TiCl_4$ is dependent upon the raw material. If there were sufficient rutile available, this process would be particularly ecologically favorable. However, in view of its scarcity and hence its high price, raw materials with low titanium content, such as 85% RBM slag, are currently being used in the chloride process. Allowance has then to be made for the resulting increased metal chloride formation. TiO_2 pigment manufacture without by products is impossible. These are disposed of in similar ways to those already described for the sulfate process (Buchner, *et al.*, 1989).

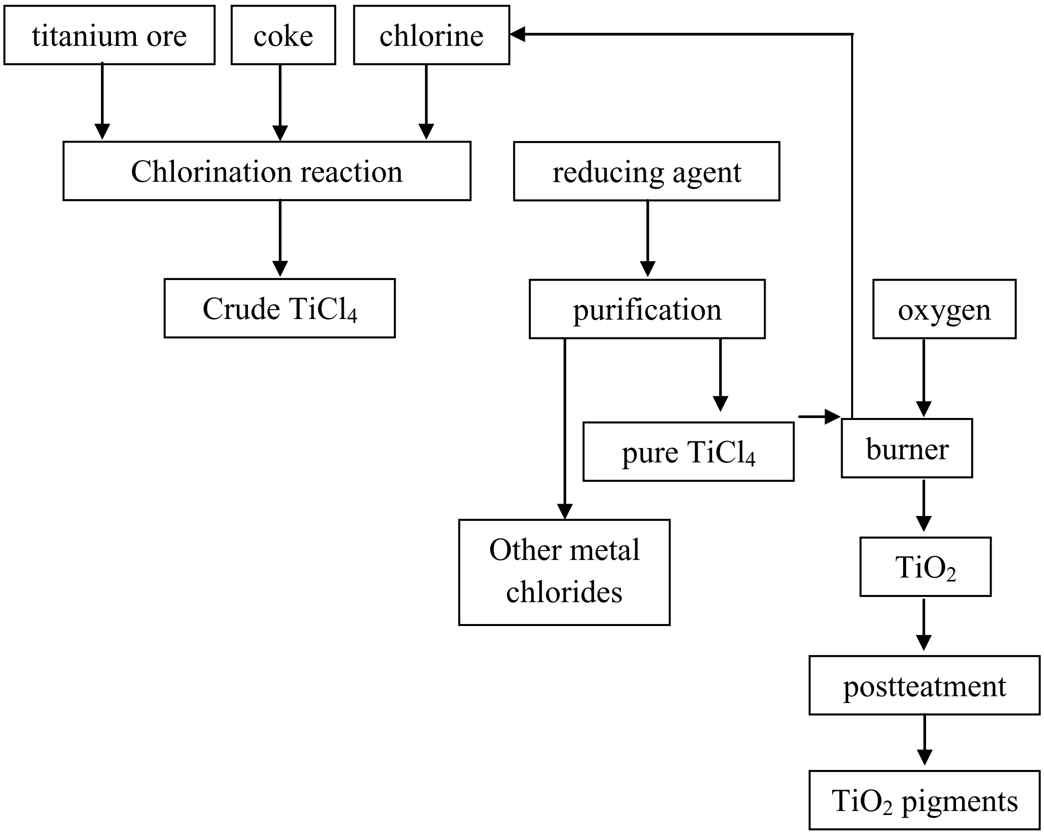

Figure 1.4 TiO_2 manufacture by the chloride process (Buchner, *et al.*, 1989).

Kanna and Wongnawa, (2008) studied mixed TiO_2 powders of various amorphous-anatase-rutile contents prepared by acid-catalyzed sol-gel method. Titanium tetrachloride ($TiCl_4$), 20 mL, was added slowly to 200 mL of cold distilled water which had been cooled in an ice-water bath at least 10 min prior to the addition. The solution was then mixed with each corresponding acid (acts as hydrolysis catalyst) and refluxed at 80 °C for 1 h under vigorous stirring. The solution was then treated with ammonia solution until the pH value was 7 and maintained at the same temperature for 24 h. The product was dried overnight and ground to fine powder. The physico-chemical properties of the powder were investigated by powder XRD, SEM, BET surface area, FT-IR, EDX, and UV-vis spectroscopy. The results showed that the products were mixtures of mainly amorphous TiO_2 with small amount of anatase and rutile phases when prepared by without using acid catalyst and by adding small amount of acid catalyst (hydrochloric acid, nitric acid, and acetic acid). Positive photocatalytic activities of these products were found and some could be compared favorably with Degussa P25.

Zhang, *et al.*, (2000) studied an economic inorganic compound $TiCl_4$ was used as precursor of nanosized TiO_2 powder. By controlling the hydrolysis conditions, either nanocrystalline or amorphous TiO_2 powders can be prepared. The powders were characterised by TEM, HREM, XRD, EDX, and BET techniques. The particle size in the crystalline samples was ultra fine (3.5 nm for anatase and 4.3 nm for rutile, respectively.) and the BET surface area of this powder was much higher than that of alkoxide-derived powders. The amorphous powders had mesoporous structure as well as high BET surface area. The addition of a small amount of $(NH_4)_2SO_4$ promoted the formation of anatase phase and inhibited the anatase-rutile transformation such that the powder was in completely anatase phase after calcining at 650 °C for 2 h, and rutile occurred at around 700 °C. However, in the absence of SO_4^{2-} ions, the powder prepared by hydrolysis of $TiCl_4$ solution at 70 °C was in both rutile and anatase phases. When it was calcined at 600 °C, anatase starts to transform to rutile. While aqueous solution of $TiCl_4$ hydrolysed at 20 °C, either the presence of SO_4^{2-} ions or not, the rate of nucleation was too slow to form crystalline TiO_2 powders. This amorphous TiO_2 powders had a BET surface area in the range 470-501 m^2g^{-1}, after calcining at 400 °C, they transformed to anatase completely.

In earlier reported studies, fluorine doping of TiO_2 was achieved by different methods such as spray pyrolysis, solvothermal, hydrothermal, hydrolysis, wet impregnation and sol-gel method (Li, *et al*., 2005; Todorova, *et al*., 2008; Chen and Mao, 2007; Dong, *et al*., 2009; Xu, *et al*., 2008; Mori, *et al*., 2008). In this work, F-TiO_2 was prepared by impregnation and co-precipitation method.

Impregnation method

Incipient wetness impregnation is a commonly used technique for the synthesis of heterogeneous catalysts. Typically, the active metal precursor is dissolved in an aqueous or organic solution. Then the metal-containing solution is added to a catalyst support containing the same pore volume as the volume of solution that was added. Capillary action draws the solution into the pores. The catalyst can then be dried and calcined to drive off the volatile components within the solution, depositing the metal on the catalyst surface. The maximum loading is limited by the solubility of the precursor in the solution. The concentration profile of the impregnated compound depends in the mass transfer conditions within the pores during impregnation and drying (http://en.wikipedia.org/wiki/Incipient_wetness_impregnation).

Preparative chemistry has for many years been critical to heterogeneous catalysis. One frequently used route to real heterogeneous catalysts involves impregnation of a porous solid support, using a solution of a precursor to the active phase. Impregnation is technically and superficially simple, but is in fact rather complex and multistep, involving:

(i) Support wetting,
(ii) Drying, and
(iii) Calcinations or reduction

Within the first of these (i) ion-exchange/ adsorption, (ii) ligand exchange reaction and (iii) support modification and dissolution may occur to an equilibrium extent (Alexiou and Sermon, 1993). Usually, the active catalyst constituent is coated by filling the granulated carrier with the theoretical volume of a solution of given chemical composition and later holding in static conditions while mixing. The volume ratio of solvent and pores is most often 1 to 1.5. The term “impregnation” implies several physical and chemical processes: wetting of carrier, capillary solution suction, diffusion of dissolved substances in the external solution and in the pore body, phase conversion of dissolved substances caused by chemical changes during impregnation with changes of temperature, solution concentration and composition, and also medium pH, and adsorption by reaction between dissolved substances and surface groups of carrier. Two types of impregnation technology, for heterogeneous catalysts, are recognized: dry and diffusion. In the former, the baking carrier is mixed with the impregnating solution containing all the required constituents. In diffusion technology, most widely adopted industrially, the impregnating solution contacts with the carrier whose pores are already filled with the solvent. The process commences with the diffusion of substances dissolved in the external solution and in the pore body. In the system carrier-solution of dissociated compound, the main adsorption mechanisms are ion exchange or ligand substitution (Duplyakin, *et al.*, 1991). However, in the impregnation method, the ion substitution may take place on the surfaces instead of in the bulk TiO_2 crystals (Qiu, *et al.*, 2006).

1.2.3 Semiconductor photocatalysis

The origin of semiconductors goes back to Faraday and Becquerel. Faraday discovered in 1833 that silver sulphate has a negative temperture coefficient, and in 1839 Becquerel studied the properties of various electrolytes. Galena was first used as a detector in about 1915, and in 1920 selenium and copper oxide rectifiers were introduced. In 1993 Schottky published his theory of dry rectifiers, which inaugurated the study of the theory of semiconductors, a study for which quantum mechanics are all-important. The development of radar resulted in an increasing use of the semiconductor diode, since the gap between the electrodes in the vacuum diode is of the same order as the wavelength employed in radar. In 1948 Brattain and Barden of the Bell Laboratorier in the U.S.A. discovered the point-contact transistor, and a few months later Shockley produced the junction transistor which, after extensive improvements, replanced the point-contact transistor and is now manufactured on a large scale. Semiconductors now soon became of increasing importance in modern technology (Cassignol, 1996). TiO_2 pigments are used in the manufacture of paints and coating materials, plastics, printing inks, fiber (delustering), paper, laminate papers (laminates based on melamine or urea-formaldehyde resins), construction materials, enamel and ceramics, cosmetic powders, ointments and toothpaste. There is hardly a white-colored or tinted object in our environment which does not contain TiO_2 pigments (Buchner, *et al*., 1989). Table 1.2 summarizes the properties of TiO_2 and the resulting applications (Eufinger, 2007). Semiconductor photocatalysis has been intensively investigated for its application to environmental pollutants degradation. The photocatalyst used is mainly focused on TiO_2 semiconductor due to its low cost, high stability and environmental friendly features. However, the photocatalytic activity of TiO_2 is not high enough for the requirements of practical applications. So improving its photocatalytic activity is still a principal challenge (Yang, *et al*., 2010). Scientific studies on photocatalysis started about two and a half decades ago. TiO_2 which is one of the most basic materials in our daily life has emerged as an excellent photocatalyst material for environmental purification. This story began with photoelectrochemical solar energy conversion and then shifted into the area of environmental photocatalysis, including self-cleaning surfaces, and most recently into the area of photoinduced hydrophilicity, which involves not only self-cleaning surfaces, but also antifogging ones. One of the most interesting aspects of TiO_2 is that the types of photochemistry responsible for photocatalysis and hydrophilicity are completely different, even though both can occur simultaneously on the same surface (Fujishima, *et al*., 2000).

Table 1.2 Applications of TiO_2 (Eufinger, 2007).

Property	Material type	Crystal phase	application
Dielectric constant	1) bulk 2) thin film	rutile amorphous	Capacitors
Biocompatibility	thick/thin film	rutile	Bone substituent, reinforcing mechanical supports
Refractive index: High reflectivity	1) powder 2) thin film	mostly rutile rutile	White pigment (paint, cosmetics) optical interference coatings
Dependence of electrical conductivity on concentration of surface species	thin film	rutile, other	Gas sensing
Chemical activity (1)	powder, granulate, thin film	anatase, rutile	Thermally activated catalyst
Chemical activity (2)	powder, thin film	anatase, rutile, (brookite)	Photo-activated catalyst (at room temperature)
Superhydrophilicity, amphiphilicity	thin film	anatase, rutile,	Self-cleaning, antifogging

Semiconductors like $Bi_{12}TiO_2$, Nb_2O_5, $Sm_2Ti_2S_2O_5$, Bi_2O_3, $ZnWO_4$, Bi_2WO_6, $NaTaO_3$, $CaIn_2O_4$, WO_3, TiO_2, Fe_2O_3, ZnO, etc, finds extensive application either in water splitting/degradation of organic compounds (Devi, *et al.*, 2011). An important step of the photoreaction is the formation of electron-hole pairs, which needs energy to overcome the band gap between the valence and conduction bands. Position of conduction and valence bands and band gap values for some semiconductors are presented in Figure 1.5. Electron-hole pairs are created at the semiconductor surface by irradiation, thus, a charge will transfer between electron-hole pairs and adsorbed species (reactants) onto semiconductor surface, resulting in the photodegradation of contaminants. Among the semiconductors, TiO_2 is the most suitable for the photodegradation of contaminants due to its low band gap value (3.2 eV). Heterogeneous photocatalysis is a significant green technology for application in water purification. Thus, environmental studies are necessary to remove this contaminant from water (Prado, *et al.*, 2008).

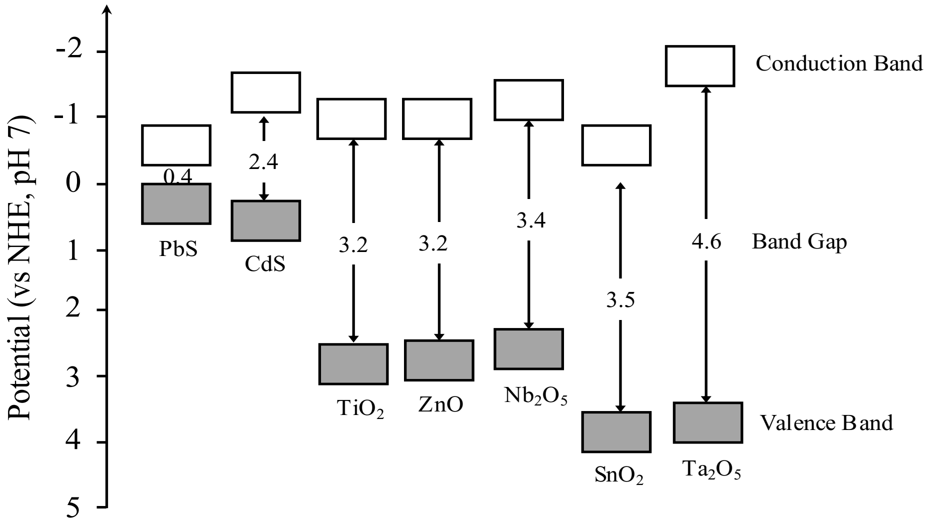

Figure 1.5 The band edge positions of several semiconductors (Prado, *et al.*, 2008).

Heterogeneous photocatalysis is a discipline which includes a large variety of reactions: mild or total oxidations, dehydrogenation, hydrogen transfer, $^{18}O_2$ - $^{16}O_2$ and deuterium-alkane isotopic exchange, metal deposition, water detoxification, gaseous pollutant removal, etc. In line with the two latter points, it can be considered as one of the new advanced oxidation technologies (AOT) for air and water purification treatment. Heterogeneous photocatalysis can be carried out in various media: gas phase, pure organic liquid phases or aqueous solutions. As for classical heterogeneous catalysis, the overall process can be decomposed into five independent steps:

(1) Transfer of the reactants in the fluid phase to the surface

(2) Adsorption of at least one of the reactants

(3) Reaction in the adsorbed phase

(4) Desorption of the product
(5) Removal of the products from the interface region

The photocatalytic reaction occurs in the adsorbed phase (Step No. 3). The activation mode is not concerned with Steps 1, 2, 4 and 5, although photoadsorption and photodesorption of reactants, mainly oxygen, do exist (Herrmann, *et al.*, 1999). Photocatalytic degradation is a part of AOP which has proven to be a promising technology for degrading organic compounds. The photocatalytic discoloration of a dye is believed to take place according to the following mechanism. When a catalyst is exposed to UV radiation, electrons are promoted from the valence band to the conduction band. As a result of this, an electron-hole pair is produced (Rauf, *et al.*, 2009). The detailed mechanism of the process has been discussed previously in the literature and will be only briefly summarized here. It is well established that conduction band electrons (e^-) and valence band holes (h^+) are generated when aqueous TiO_2 suspension is irradiated with light energy greater than its band gap energy (E_g, 3.2 eV). The photogenerated electrons could reduce the dye or react with electron acceptors such as O_2 adsorbed on the Ti(III)-surface or dissolved in water, reducing it to superoxide radical anion $O_2^{\bullet-}$. The photogenerated holes can oxidize the organic molecule to form R^+, or react with OH^- or H_2O oxidizing them into $OH^\bullet$ radicals. Together with other highly oxidant species (peroxide radicals) they are reported to be responsible for the heterogeneous TiO_2 photodecomposition of organic substrates as dyes. According to this, the relevant reactions at the semiconductor surface causing the degradation of dyes can be expressed as follows:

$$TiO_2 + h\ \ (UV) \longrightarrow TiO_2\,(e_{CB}^- + h_{VB}^+) \tag{1.2}$$

$$TiO_2\,(h_{VB}^+) + H_2O \longrightarrow TiO_2 + H^+ + OH^\bullet \tag{1.3}$$

$$TiO_2\,(h_{VB}^+) + OH^- \longrightarrow TiO_2 + OH^\bullet \tag{1.4}$$

$$TiO_2\,(e_{CB}^-) + O_2 \longrightarrow TiO_2 + O_2^{\bullet-} \tag{1.5}$$

$$O_2^{\bullet-} + H^+ \longrightarrow HO_2^\bullet \tag{1.6}$$

$$\text{Dye} + OH^\bullet \longrightarrow \text{degradation products} \tag{1.7}$$

$$\text{Dye} + h_{VB}^+ \longrightarrow \text{oxidation products} \tag{1.8}$$

$$\text{Dye} + e_{CB}^- \longrightarrow \text{reduction products} \tag{1.9}$$

The resulting $^{\bullet}OH$ radical, being a very strong oxidizing agent (standard redox potential +2.8V) can oxidize of dyes to the mineral end-products. Substrates not reactive toward hydroxyl radicals are degraded employing TiO_2 photocatalysis with rates of decay highly influenced by the semiconductor valence band edge position. The role of reductive pathways (Eq. (1.9)) in heterogeneous photocatalysis has been envisaged also in the degradation of several dyes but in a minor extent than oxidation (Konstantinou, *et al.*, 2004). The mechanisms of generation of oxidative species in a photocatalytic study are shown in Figure 1.6 (Rauf, *et al.*, 2009).

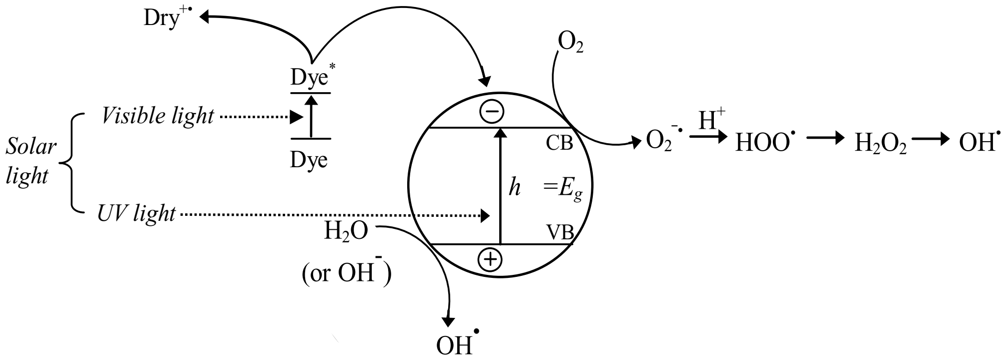

Figure 1.6 The generation of oxidative species in a photocatalytic.

The characteristic time for each elementary reaction has been reported in Table 1.3. The $\{\equiv Ti^{IV}OH^{\bullet+}\}$ and $\{\equiv Ti^{III}OH\}$ represent the surface-trapped valence band electron and surface-trapped conduction band electrons, respectively. The surface-bound OH radical represented by $\{\equiv Ti^{IV}OH^{\bullet+}\}$ is chemically equivalent to the surface-trapped hole allowing the use of the former and latter terms interchangeably. There exist a good correlation between charge carrier dynamics, their surface densities and the efficiency of the photocatalytic degradation over TiO_2 (Gaya and Abdullah, 2008). According to the mechanism illustrated in Figure 1.7, the overall quantum efficiency for interfacial charge transfer is determined by two critical processes. They are the competition between charge carrier recombination and trapping (picoseconds to nanoseconds) followed by the competition between trapped carrier recombination and interfacial charge transfer (microseconds to milliseconds).

An increase in either the recombination lifetime of charge carriers or the interfacial electron-transfer rate constant is expected to result in higher quantum efficiencies for steady-state photolysis (Hoffmann, *et al.*, 1995).

Table 1.3 Major processes and their characteristic times for TiO_2-sensitized photooxidative mineralization of organic compounds by dissolved oxygen in aqueous solutions (Carp, *et al.*, 2004; Gaya and Abdullah, 2008).

Primary process	Characteristic time
1. Charge carrier generation	
$TiO_2 + h \longrightarrow e_{cb}^- + h_{vb}^+$	fast (fs)
2. Charge carrier trapping	
$h_{vb}^+ + \equiv Ti^{IV}OH \longrightarrow \{\equiv Ti^{IV}OH^\bullet\}^+$	fast (10 ns)
$e_{cb}^- + \equiv Ti^{IV}OH \longrightarrow \equiv Ti^{III}OH\}$	(100 ps)
(Shallow traps, dynamic equilibrium)	
$e_{cb}^- + \equiv Ti^{IV}OH \longrightarrow Ti^{III}$	(10 ns)
(deep trap, irreversible)	
3. Charge carrier recombination	
$e_{cb}^- + \{\equiv Ti^{IV}OH^\bullet\}^+ \longrightarrow \equiv Ti^{IV}OH$	slow (100 ns)
$h_{vb}^+ + \{\equiv Ti^{III}OH\} \longrightarrow \equiv Ti^{IV}OH$	fast (10 ns)
4. Interfacial charge transfer	
$\{\equiv Ti^{IV}OH^\bullet\}^+ + Red \longrightarrow \equiv Ti^{IV}OH + Red^{\bullet +}$	slow (100 ns)
$e_{cb}^- + Ox \longrightarrow Ti^{IV}OH + Ox^{\bullet -}$	very slow (ms)

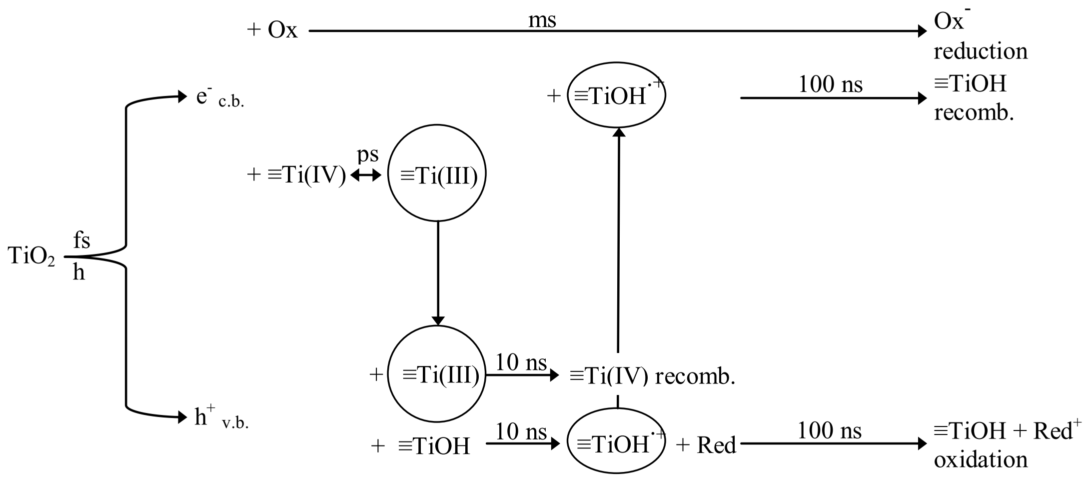

Figure 1.7 Kinetics of the primary steps in photoelectron chemical mechanism. Recombination is mediated primarily by ≡Ti(III) in the first 10 ns. Valence band holes are sequestered as long-lived ≡$TiOH^{\bullet+}$ after 10 ns. ≡TiOH is reformed by recombination with conduction band electrons or oxidation of the substrate on the time scale of 100 ns. The arrow lengths are representative of the respective time scales (Hoffmann, *et al.*, 1995).

1.2.4 Dye and photocatalytic degradation of indigo carmine

(1) Dyes

A dye is a colored substance that has an affinity to the substrate to which it is being applied. The dye is generally applied in an aqueous solution, and may require a mordant to improve the fastness of the dye on the fiber. Both dyes and pigments appear to be colored because they absorb some wavelengths of light more than others. In contrast with a dye, a pigment generally is insoluble, and has no affinity for the substrate. Some dyes can be precipitated with an inert salt to produce a lake pigment, and based on the salt used they could be aluminum lake, calcium lake or barium lake pigments. The first human-made (synthetic dye) organic dye, mauveine, was discovered by William Henry Perkin in 1856. Many thousands of synthetic dyes have since been prepared. Synthetic dyes quickly replaced the traditional natural dyes. They cost less, they offered a vast range of new colors, and they imparted better properties to the dyed materials. Dyes are now classified according to how they are used in the dyeing process and have been divided to nine types, the details of which can be found elsewhere (http://en.wikipedia.org/wiki/Dye). Synthetic dyestuffs are extensively used in textile, printing industries, paper, and dye houses due to their ease of production, variety of colors, and fastness compared to natural dyes. Many commercially available dyes are known and approximately one million tons of these dyes are produced annually worldwide. It has been estimated that more than 10% of the total dyestuff used in dyeing processes is released into the environment (Habibi and Esfahani, 2007). Organic dyes are one of the largest groups of pollutants released into wastewaters from textile and other industrial processes. Because of potential toxicity of the dyes and their visibility in surface waters, removal and degradation of organic dyes have been a matter of considerable interest. A wide range of methods have been developed, amongst which the heterogeneous photocatalysis involving titanium dioxide (TiO_2) appears to be the most promising technology (Han, *et al.*, 2009). In the present work, indigo carmine as anionic dye (Figure 1.8) was selected as a model of dye pollutant with which the degradation efficiencies of the as-prepared catalysts are to be investigated.

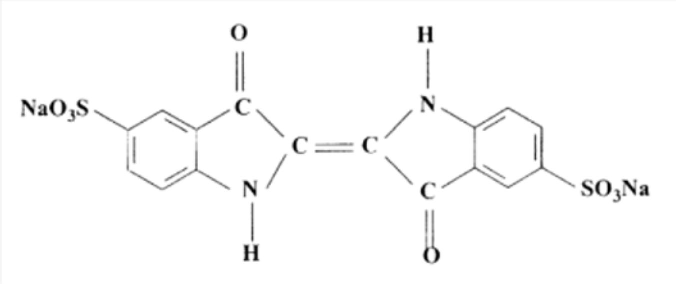

Figure 1.8 Chemical structure of indigo carmine.

Indigo carmine (IC), disodium salt of 3,3-dioxobi-indolin-2,2-ylidine-5,5- disulfonate, is one of the oldest dyes and still one of the most important used. Its major industrial application is the dyeing of clothes (blue jeans) and other blue denim (Gemeay, *et al.*, 2003). Indigo carmine is also used for medical diagnostic purposes in conjunction with acetic acid the dye facilitate diagnosis of Barrett's esophagus. It can also help to target biopsies even better, since in homogeneously stained or unstained areas seem to correlate with intraepithelial neoplasia. Indigo carmine, however, is not readily metabolized but is rather freely filterable by the kidneys, giving intravenous injection of indigo carmine for intra-operative cystoscopy is a safe technique that can detect otherwise undetected intra-operative compromise of the urinary tract (Othman, *et al*., 2007). A common dye also used as food coloring, as indicator in analytical chemistry, and as a microscopic stain in biology (Ammar, *et al*., 2006). Indigo carmine is a dye which occurs as a dusky, purplish-blue powder or blue granules having a coppery lustre. The chemical formula of indigo carmine is $C_{16}H_8N_2Na_2O_8S_2$ and molecular weight is 466.36 g/mol. The dye forms blue or bluish-purple solutions (Mohamed, *et al*., 2007). Its solubility in water and the indigo carmine solution has “H”- chromophore consisted of electron donating group (N-H, C=O) and also the double bond of C causing the blue color (Yano, *et al*., 2009). These chemical structures yield principal absorption spectrums at 610 nm (Sriwong, *et al*., 2010). The UV-vis absorption spectrum of IC is presented in Figure1.9. The indigo carmine is considered as highly toxic indigoid class of dye. Contact with it can cause skin and eye irritations. It can also cause permanent injury to cornea and conjunctiva. The consumption of the dye can also prove fatal, as it is carcino-genic and can lead to reproductive, developmental, neuron and acute toxicity. It has also been established that the dye leads to tumours at the site of application. When administered intravenously to determine potency of the urinary collecting system, it is also known to cause mild to severe hypertension, cardiovascular and respiratory effects in patients. It may also cause gastrointestinal irritations with nausea, vomiting and diarrhea. The toxicity tests of the dye revealed long term toxicity in mice and short-term toxicity in the pig. Thus, keeping the toxicity of this dye in view, various attempts have been made for the removal of indigo carmine from water and wastewater (Barka, *et al*., 2008).

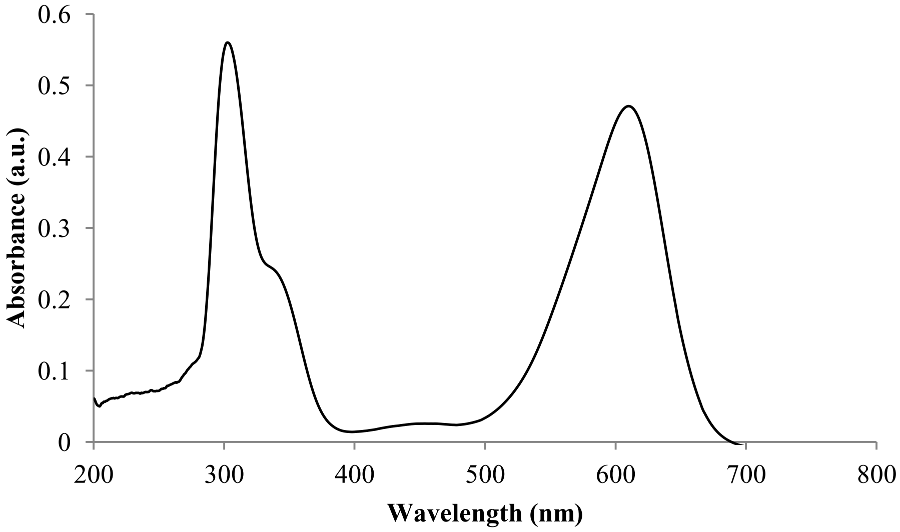

Figure 1.9 UV-vis spectrum of indigo carmine (2.5×10^{-5} M).

(2) Photocatalytic degradation of indigo carmine

The main pathway of photomineralization carried out in aerated solution may be easily summarized by the following reaction: (Mills and Hunte, 2004; Carp, *et al.*, 2004).

$$\text{Organic compound} \xrightarrow[h \quad E_g]{TiO_2} CO_2 + H_2O + \text{mineral acid} \qquad (1.10)$$

Many elementary mechanistic processes have been described in the photocatalytic degradation of organic compounds over TiO_2 surface. TiO_2 semiconductor material is known as one of the most stable and highly reactive photocatalysts. Because TiO_2 photocatalyst can completely mineralize toxic and non biodegradable organics to CO_2, H_2O, and inorganic constituents, many researches have been undertaken to design highly efficient TiO_2 photocatalytic systems which can be applied especially to purify polluted water (Yamashita, *et al.*, 2008). Nowadays, TiO_2 has attracted the attention of scientists in the catalysis field, due to its effective utilization of visible light to degrade organic pollutants (Mohamed, *et al.*, 2009). Several works reported that photocatalytic degradation of indigo carmine by using TiO_2.

Subramani, *et al.*, (2007) studied the photocatalytic degradation of indigo carmine dye was studied using hydrothermally prepared TiO_2 impregnated activated carbon (TiO_2:AC). TiO_2:AC was employed in the degradation of indigo carmine dye. A comparative study of the degradation efficiency of commercial TiO_2 and TiO_2:AC has shown the efficiency of prepared catalyst. The optimization studies revealed the dependence of the degradation of indigo carmine on initial dye concentration and amount of the catalyst. This study highlights that the TiO_2:AC can be used as an alternative for the conventional isolated use of the TiO_2 photocatalyst.

Othman, *et al.*, (2007) studied a detailed comparative investigation on the discoloration and mineralization (in the presence of UV irradiation) of indigo carmine dye over four photocatalysts TiO_2-D (from Degussa), TiO_2-SG (prepared with a sol-gel method), Mn/TiO_2-imp (prepared with an impregnation method) and Mn/TiO_2-SG (prepared with a sol-gel method) is presented. The experimental results show that Mn/TiO_2-imp gives the highest photocatalytic activity. However, the influence of pH, catalyst amount and time on the decolorization rate of IC on Mn/TiO_2-imp was thoroughly discussed and correlated with ZPC of MnO_x species, various exposed species of MnO_x and surface properties.

Barka, *et al.*, (2008) studied the degradation of indigo carmine dye was successfully carried out using coated TiO_2 on paper fibres. A correlation between the adsorption of the dye onto photocatalyst material and the rate of degradation has been found. pH influences both the photocatalyst surface and the dye structure. The maximum dye adsorption was achieved for pH less than 4 in relation with the pzc of the pair TiO_2/SiO_2. The photocatalytic degradation was obviously affected by the initial concentration with respect to Langmuir-Hinshelwood kinetic model.

Vautier, *et al.*, (2001) studied the TiO_2/UV photocatalytic degradations of indigo and of indigo carmine have been investigated both in aqueous heterogeneous suspensions and in the solid state. In addition to prompt removal of the color, TiO_2/UV-based photocatalysis was simultaneously able to oxidize the dye, with almost complete mineralization of carbon and of nitrogen and sulfur heteroatom into CO_2, NH_4^+, NO_3^- and SO_4^{2-} , respectively. Figure 1.10 represents an energy diagram under UV and visible irradiation. Under UV, titania gets excited and indigo carmine can cede an electron to its valence band either directly or indirectly via an attack by $OH^\bullet$ radicals. Under visible light, only indigo carmine becomes excited at > 440 nm with the promotion of an electron in an upper orbital, whose relative energy level enables the transfer of one electron into the conduction band of the catalyst. This transfer could be favored by a driving force consisting of a subsequent electron transfer to an adsorbed oxygen molecule. The photocatalytic degradation of IC used TiO_2 under UV irradiation. A tentative mechanism of degradation inferred from these data is reported in Figure 1.11. The first acids formed after 20 min of UV irradiation are oxalic, anthranilic, and malic acids, in line with the complete bleaching of the dye in 8 min. The shorter carboxylic acids appear subsequently, with a maximum amount obtained after *ca.* 30 min of UV irradiation. All the intermediate products, except acetic acid, are degraded within 1 h of UV irradiation, in agreement with the time of formation of CO_2 (1 h). Acetic acid requires a longer time for mineralization, as generally observed.

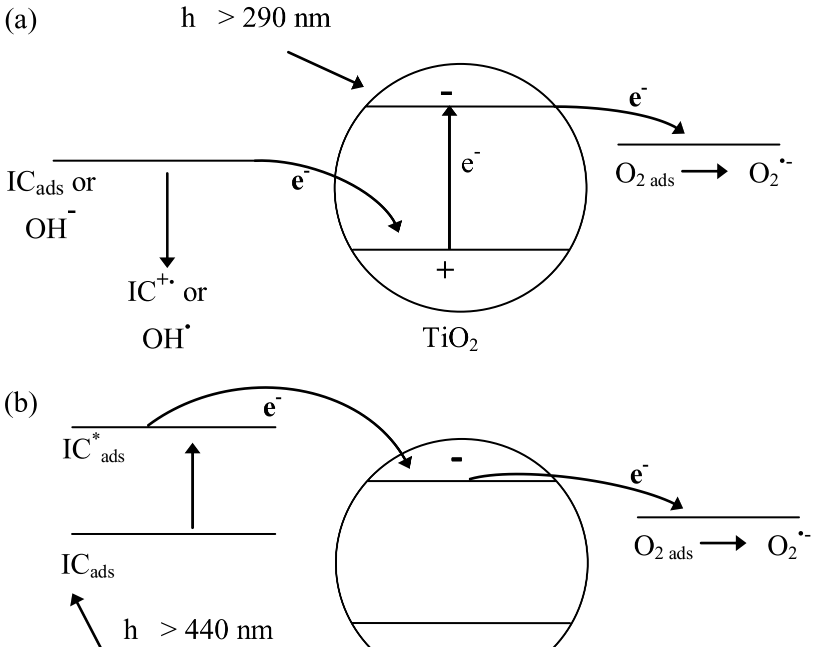

Figure 1.10 Mechanism of TiO_2-assisted photodecolorization; (a) under UV irradiation and (b) under visible light (Vautier, *et al.*, 2001).

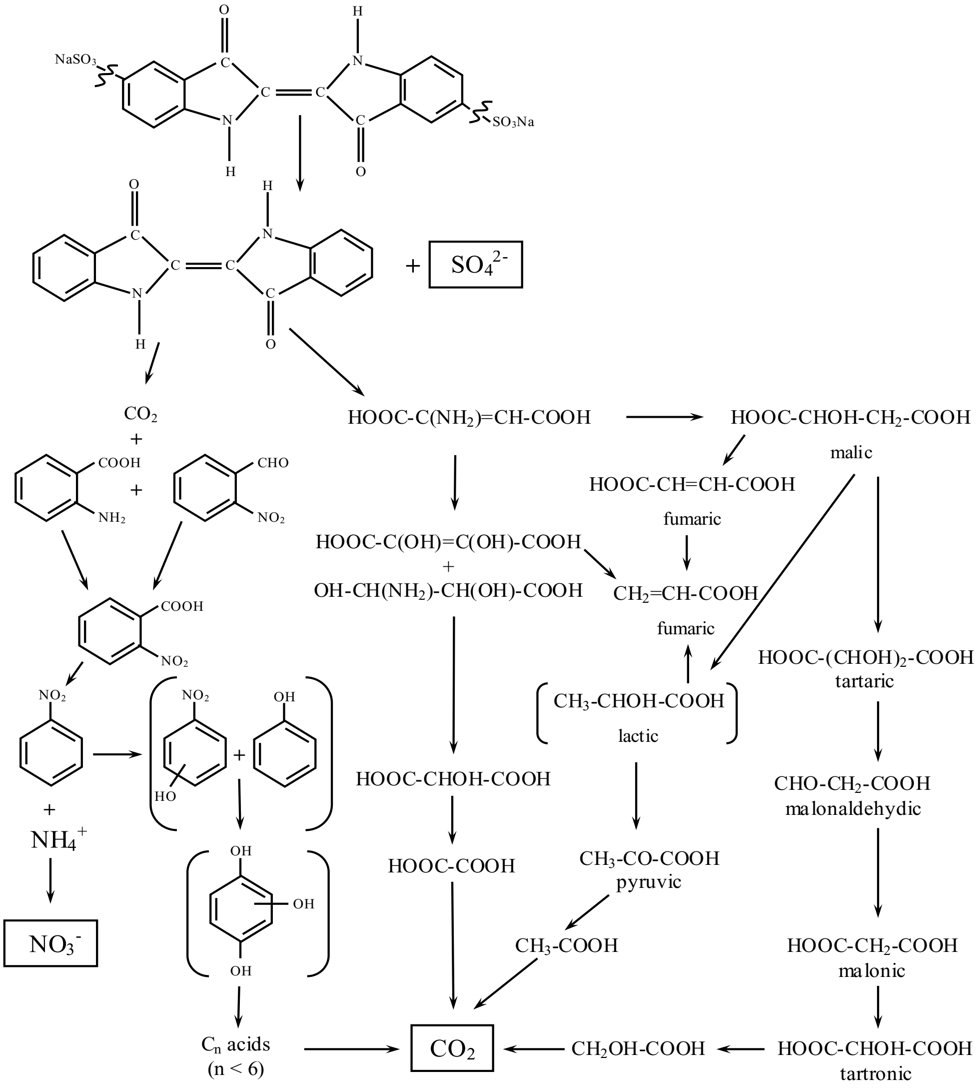

Figure 1.11 Photocatalytic degradation pathway of indigo carmine (Vautier, *et al.*, 2001).

1.2.5 Doping method

In semiconductor production, doping intentionally introduces impurities into an extremely pure (also referred to as intrinsic) semiconductor for the purpose of modulating its electrical properties. The impurities are dependent upon the type of semiconductor. Lightly and moderately doped semiconductors are referred to as extrinsic. A semiconductor doped to such high levels that it acts more like a conductor than a semiconductor is referred to as degenerate (http;//en.wikipedia.org/wiki/Doping_(semiconductor)). In both n-type and p-type semiconductors the existence of electrons or holes free to conduct electricity result from the presence of foreign impurity atoms in the crystal, rather than from the properties of the pure crystal. Such materials are therefore called extrinsic semiconductors, as distinguished from intrinsic semiconductors. Note that, as in Figure 1.12, the Fermi level is located near the donor levels in an n-type semiconductor and near the acceptor levels in a p-type semiconductor. This is so because the conduction band levels in n-type crystals have more electrons than they would in the intrinsic situation, which indicates that the Fermi level must be located nearby. Just the reverse is true for p-type crystals (Brophy, 1964).

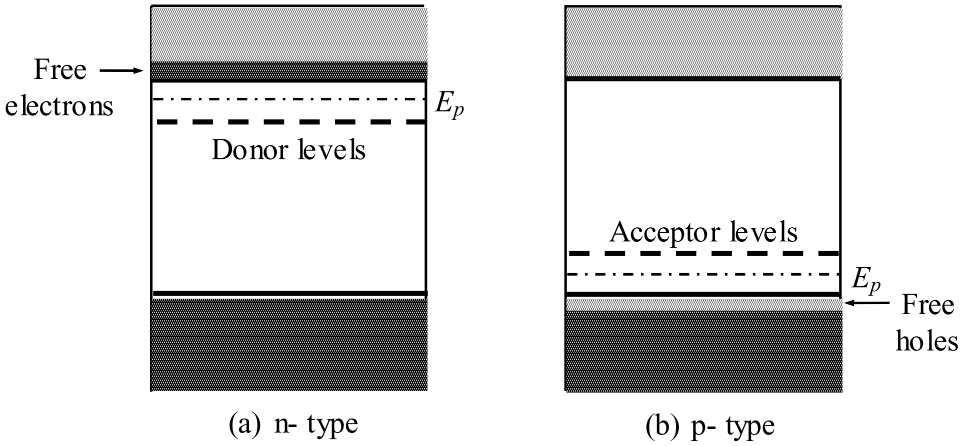

(a) n- type (b) p- type

Figure 1.12 Energy band model of an n-type and n-type extrinsic semiconductor (Brophy, 1964).

The inorganic material doping method is by far more popular because of its good activity and application, and has mainly three design types: (1) cation doping (Fe, Co, Ni, Cu), (2) anion doping (N, C, F, S) and (3) composite photocatalyst (CdS-TiO_2). Although suitable metal ion dopants could increase the absorption region, they acted either as recombination center for the photogenerated charge carriers or were simply ineffective in aiding the surface redox reaction. However, even though the modified TiO_2 by doping with metal ion has been prepared successfully. Furthermore, transition metals are toxic and will diffuse from photocatalysts to the environment during the operation, which may lead to a second pollution. For these reasons, anion doped photocatalysts are better than cation doped types as a result of their good activity and non-toxic feature (Huang, *et al.*, 2009). Anion doping is an effective approach to prepare titanium dioxide (TiO_2) materials having photocatalytic activity under visible light irradiation (Gil, *et al.*, 2006). On the other hand, fluorine doped TiO_2 can improve the visible light response of TiO_2 photocatalysts.

Mori, *et al.*, (2008) synthesized TiO_2 by hydrothermal method from tetraisopropyl orthotitanate (TPOT) in the presence of NH_4F with different NH_4F/Ti molar ratios (HT-TiO_2 : (F = 0, 0.01, 0.05, 0.25, and 1)). The formation of well-crystallized anatase phase of TiO_2 and suppression of phase transition to rutile were observed even at high calcination temperature. The amount of employed NH_4F influenced on the crystal size and surface area. XPS analysis showed that F^- ions coordinated with Ti in the lattice. In comparison to the commercial TiO_2 powder (P-25), the HT-TiO_2 samples with high F^- ion contents exhibited high absorption in the UV-visible range with a shift to the longer wavelength in the band gap transition. The HT-TiO_2 samples exhibited high photocatalytic activity for the degradation of i-BuOH diluted in water. The photocatalytic activities were apparently affected by surface area and crystallinity of TiO_2 phase depending on the amount of employed NH_4F.

Park and Choi, (2004) prepared fluorine doped TiO_2. The formation of surface fluorides on TiO_2 (F-TiO_2), which can be easily attained by a simple addition of F^- to aqueous TiO_2 suspensions, uniquely affects both photocatalytic reactions and photoelectrochemical behaviors. The fluoride adsorption is favored at acidic pH and greatly reduces the positive surface charge on TiO_2 by replacing $\equiv Ti\text{-}OH_2^+$ by ≡Ti-F species. Effects of surface fluorination on the photocatalytic reactivities are very different depending on the kind of substrates to be degraded. F-TiO_2 is more effective than pure TiO_2 for the photocatalytic oxidation of Acid Orange 7 and phenol, but less effective for the degradation of dichloroacetate. F-TiO_2 was studied by XPS and UV-vis DRS. The results from XPS indicated that the F-TiO_2 sample clearly shows the peak of F 1s as well as those of Ti, O, and C elements (Figure 1.13). The F 1s peak is originated from the surface fluoride (≡Ti-F) formed by ligand exchange between F- and surface hydroxyl group on TiO_2. The surface fluorination of TiO_2 hardly takes place at pH 10.6, which indicates that the fluoride adsorption is greatly reduced at alkaline pH.

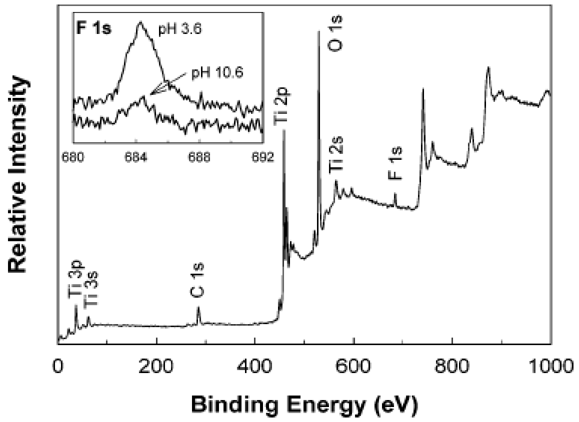

Figure 1.13 XPS survey spectrum of fluorinated TiO_2 (F-TiO_2) powder prepared at pH 3.6. The inset compares the F 1s peak intensity of F-TiO_2 samples prepared at pH 3.6 and 10.6.

The UV-vis DRS spectra of F-TiO_2 (Figure 1.14) prepared at pH 3.6 is higher than that of pure TiO_2 at $\lambda < 400$ nm, whereas the absorption edge region is unaffected by the surface fluorination. Figure 1.15 shows the variation of zeta potentials of suspended TiO_2 particles in water as a function of pH and [F^-]. The point of zero zeta potential (PZZP) of TiO_2 is measured to be *ca.* pH 6.2. In the presence of F^-, the PZZP is shifted to lower pH values and the positive charge on TiO_2 surface at acidic pH region is much reduced since the surface ≡Ti-OH_2^+ groups are replaced by ≡Ti-F species.

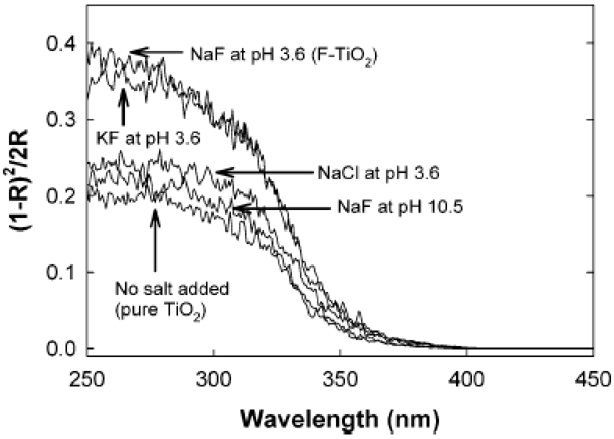

Figure 1.14 UV-vis DRS spectra of naked TiO_2 and F-TiO_2 powders prepared at pH 3.6 and 10.6.

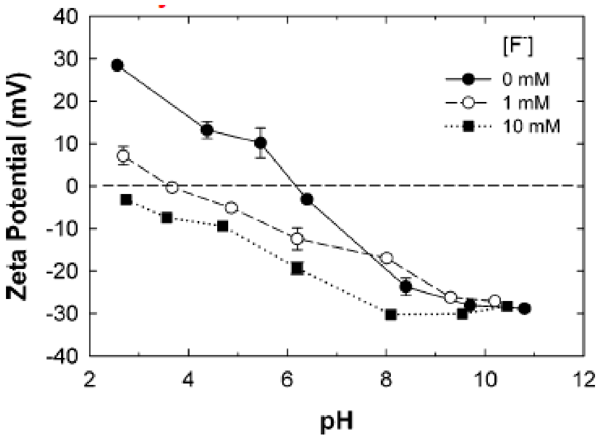

Figure 1.15 Zeta potentials of TiO_2 particles in aqueous suspensions ([TiO_2] = 2 mg/L) as a function of pH and [F^-].

Minero, *et al.*, (2000) studied the effect of fluoride ions on the photocatalytic degradation of phenol in an aqueous suspension of TiO_2. Fluoride ions displaced surficial hydroxyl groups and coordinated surface-bound titanium atoms directly. For 0.01M fluoride concentration and 0.10 gL^{-1} of TiO_2 in the range pH 2-6, the degradation rate of phenol was up to 3 times that in the absence of fluoride ions. At [F^-] = 0.01 M a large part of the surficial hydroxyl groups was displaced. The degradation rate of phenol increased as a function of the fluoride concentration, and its dependence on pH reflected that of the ≡TiF distribution. This rate increase was explained by the major extent of homogeneous $^{\bullet}OH$ reaction and direct electron transfer from the aromatic ring to the hole. The extent of formation of catechol and quinol ensured that these two dihydroxybenzenes were the main intermediates irrespective of $\equiv TiO^{\bullet}$, free $^{\bullet}OH$, or h^+ -mediated processes. Although displaced from the TiO_2/F surface, catechol was degraded faster than that on naked TiO_2. Then, the role of adsorption had to be analyzed under different aspects (increased surface availability vs detrimental recombination centers). The degradation rate vs phenol concentration showed different profiles for TiO_2/F (saturative) and naked TiO_2 (which goes through a maximum), which might be explained through the possibility that in the former case the backreaction was diminished. On TiO_2/F, phenol was degraded even in an inert atmosphere, although the rate was 25 times slower than that in the presence of oxygen. Virtually no depletion of TOC was observed, confirming that oxygen was crucial for mineralization when the initial oxidation number of carbon was < 4. Balanced oxidation/reduction processes on initially formed oxidation intermediates gave products, which could be rationalized as originating from photocatalytically induced hydrolysis.

Minero, *et al.*, (2000) studied the photocatalytic transformation of phenol had been investigated on naked TiO_2 and on TiO_2/F (0.01M F^-) at pH 3.6 in the presence of different alcohols (tert-butyl alcohol, 2-propanol, and furfuryl alcohol). On the basis of a detailed kinetic analysis and the time evolution of the intermediates, it was suggested that on naked TiO_2 the oxidation of phenol proceeded for 90 % through the reaction with surficial bound hydroxyl radical, the remaining 10 % via a direct interaction with the holes. On TiO_2/F the reaction proceeded almost entirely via homogeneous hydroxyl radicals because of the unavailability of surface-bound hydroxyl in the presence of fluoride ions. The kinetic analysis demonstrated that three oxidant species might be present in the photocatalytic system, namely the hole, the surface-trapped hole ($\equiv TiO^{\bullet}$), and the free $^{\bullet}OH$ radical. Their presence and their role in the oxidation of phenol depended both on photocatalyst surface characteristics and solution composition.

Li, *et al.*, (2005) synthesized F-doped TiO_2 powders by spray pyrolysis (SP) from an aqueous solution of H_2TiF_6. The resulting FTO powders possessed spherical particles with a rough surface morphology and a strong surface acidity. The fluorine concentrations in the FTO powders calculated from XPS spectra significantly depended on SP temperature and ranged from 2.76 to 9.40 at %. The doped fluorine atoms existed in two chemical forms, one was in $TiOF_2$, and another was in substitutional fluorine atoms in TiO_2 crystal lattice. The latter might take a positive role in photocatalysis. The FTO powder prepared at SP temperature of 1173 K demonstrated the highest photocatalytic activity for the decomposition of gas-phase acetaldehyde under both ultraviolet (UV) and visible light (vis) irradiations, and it was higher than that of commercial P 25. This high photocatalytic activity was ascribed to several beneficial effects produced by F-doping: enhancement of surface acidity, creation of oxygen vacancies, and increase of active sites. It was interesting to point out that the vis photocatalytic activity of FTO powders was achieved by the creation of surface oxygen vacancies rather than the improvement of optical absorption property of bulk TiO_2 in vis region.

Czoska, *et al.*, (2008) synthesized TiO_2 powders by sol-gel method. Titanium (IV) isopropoxide was mixed with a solution of isopropyl alcohol in water also containing hydrofluoric acid. This mixture was stirred at ambient temperature to complete the hydrolysis with formation of a gel. The gel was left aging for 20 h at room temperature, then dried at 340 K, and eventually calcined in air at 770 K for 1 h. The final sample is a white powder. Fluorine-doped TiO_2 (F_{surf}-TiO_2) by impregnation technique suspending 1 g of pure TiO_2 powder in 1 L of aqueous HF solution [0.01M] with continuous stirring for 1 h. The material was then filtered and washed with water. The material was finally dried at 40 $^{\circ}$C for 4 h. Fluorine-doped TiO_2 were characterized by XRD, UV-vis DRS, EPR and XPS. Fluorine doping of TiO_2 using a wet chemistry technique (sol-gel) caused the appearance of two types of fluorine species in the solid. The former species consisted of fluoride F^- ions that substituted O^{2-} ions in the solid lattice yielding a bridging Ti-F-Ti bond. This induced the formation of bulk Ti^{3+} species in an octahedral environment that introduced localized states just below the conduction band. The doped samples did not show absorption in the visible region and did not react with adsorbed O_2 to form superoxide anions, suggesting that the defect centers were located inside the material and not on the external layers. The second species consists of F^- ions at the solid surface (both external and internal) where they substitute OH^- hydroxyl groups yielding a terminal Ti-F bond without generating reduced centers.

Lokshin, *et al*., (2008) synthesized fluorine doped anatase using $TiCl_4$, $(NH_4)_2TiF_6$, HF, 24% NH_4OH and distilled water. Fluorine doped anatase were prepared by hydrolysis method. The results showed that a higher photocatalytic activity compared to undoped anatase obtained under identical conditions and retains this activity after thermal treatment in a temperature range of 400-700 °C. The photocatalytic activity of the evaluated fluorine-doped titanium oxohydroxide with an allowance for its titanium content was insignificantly lower than the photocatalytic activity of fluorine-doped anatase.

Yu, *et al*., (2002) prepared F^--doped TiO_2 photocatalyst with anatase and brookite phase was developed by hydrolysis of titanium tetraisopropoxide in a mixed NH_4F-H_2O solution. F^--doped TiO_2 powders were characterized by DTA-TG, XRD, XPS, UV-vis spectroscopy, PL, TEM, and BET surface areas. The results showed that the crystallinity of anatase was improved upon F^- doping. Moreover, fluoride ions not only suppressed the formation of brookite phase but also prevented phase transition of anatase to rutile. The F^--doped TiO_2 samples exhibited stronger absorption in the UV-visible range with a red shift in the band gap transition. The photocatalytic activity of F^--doped TiO_2 powders prepared by this method exceeded that of Degussa P25 when the molar ratio of NH_4F to H_2O was kept in the range of 0.5-3. The photocatalytic activity was evaluated by the photocatalytic oxidation of acetone in air. Figure 1.16 shows the energy level diagram for Ti^{3+} and charge-carrier dynamics in F^--doped TiO_2. Upon UV excitation, photogenerated electrons accumulated at the lower lying surface state of Ti^{3+}, whereas holes accumulated at the valence band of TiO_2. Accumulated electrons at the surface state of Ti^{3+} was transferred to oxygen adsorbed on the surface. This slowed down the recombination of the electron-hole pairs.

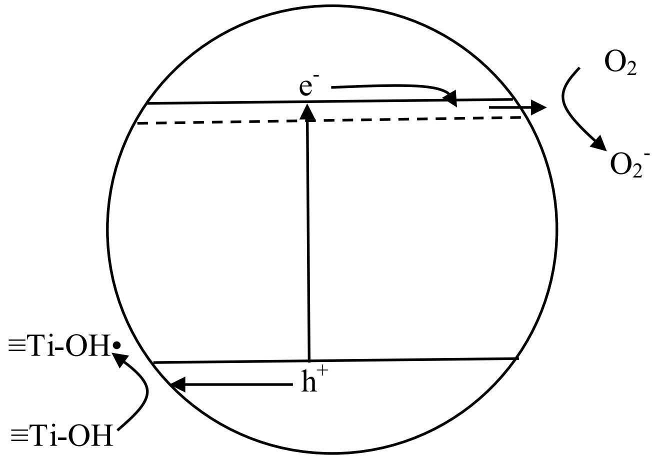

Figure 1.16 Energy level diagram for Ti^{3+} and charge-carrier dynamics in F^--doped TiO_2.

Todorova, *et al.*, (2008) synthesized F-doped TiO_2 powders by sol-gel route. Tetraethyl orthotitanate (TEOTi) Merck was used as titanium source. Different amounts of fluoroacetic acid (atomic ratios F/Ti = 0, 10/90, 20/80) were dissolved in deionized water (molar ratio H_2O/TEOTi = 18) under stirring at room temperature and the TEOTi was added to the solution dropwise. The sols were stirred in closed beakers at room temperature for 24 hours for completion of the hydrolysis process. Consequently, they were dried at 90 °C in air for 12 h for water and alcohol evaporation. The as-prepared xerogels were calcinated at 400, 500, and 600 °C for 1 h in a Carbolite muffle furnace with heating rate of 5 °C/min. The results showed that the crystallization of pure rutile or anatase/rutile mixture at low temperatures was attributed to the acidic character of the fluorine precursor. Improved crystallinity and enhanced absorbance of the powders in the UV-vis region were recorded upon F-doping. The fluorine was presented in the powders mainly as metal (Ti) fluoride. The width of the TiO_2 band gap was not affected by the presence of fluorine. The red shift of the absorption edge was attributed to the increased rutile content in the fluorine doped TiO_2 powders. The prepared fluorine doped TiO_2 powders calcinated at 400 °C exhibited higher photocatalytic activity than that of Degussa P25 for decomposition of acetone under UV-vis illumination.

Todorova, *et al.*, (2008) studied and synthesized fluorine-doped nanocrystalline TiO_2 powders with controlled anatase-rutile phase content by a sol-gel route using NH_4F and CF_3COOH as fluorine sources. The X-ray diffraction (XRD) study revealed that fluorine-doping through NH_4F led to the formation of anatase crystalline phase, whereas F-doping through CF_3COOH favored the formation of rutile along with anatase phase. These results were connected to the influence of the fluorine precursor on the pH of the starting solutions. The measured UV-vis diffuse reflectance spectra and the calculated band gap widths using Kubelka-Munk phenomenological theory were in good agreement with the crystallographic results. The calculations revealed no change in the band gap values due to fluorine doping. The enhanced absorbance in the visible region and the red shift of the absorption edge were attributed to the presence of fluorine and the anatase/rutile phase composition of the TiO_2 powders.

Huang, *et al.*, (2007) synthesized anatase fluoride doped TiO_2 sol (F-TiO_2) catalyst by a modified sol-gel hydrothermal method, using tetra butyl titanate as a precursor. The titanium in the initial tetra butyl titanate had 4-fold coordination, when the tetra butyl titanate reacted with water, the titanium ion increased its co-ordination by using its vacant d-orbital to accept oxygen lone pairs from nucleophilic ligands (such as OH groups) by co-ordination expansion. Consequently, titanium ions in solution existed as 6-fold co-ordinate structures. The reaction was performed in an acidic medium, the groups of -OH, NH_4^+, and F^- would be presented and the composition of this solution was $[Ti(OH)_xF_y(OH_2)_{6-x-y}]^{(6-x-y)+}$. These 6-fold structural units underwent condensation and became the octahedral that was incorporated into the final amorphous gel structure. Formed mechanism of anatase F-TiO_2 under hydrothermal conditions was possibly as follows: owing to the doping of fluoride, few TiO_6 octahedral deformed and formed polarity surface and edge; two discrete single TiO_6 octahedral join at corner through oxolation initially, by further condensation, they would become joined along polarity edges to form a dimer, the dimers tended to form screw chains of polymer by sharing polarity edge with further oxolation reaction, which were similar to anatase in structure and the screw chains could form the anatase nuclei by oxolation reaction. The microstructure and morphology of sol sample were characterized by XRD, TEM, FTIR, UV-Vis-DRS, particle size distribution (PSD) and XPS. The results showed that F-TiO_2 particles in sol were spherical and partly crystallized to anatase structure, and dispersed in the aqueous medium homogeneously and that the average particle size was *ca.* 10.5 nm calculated from XRD and TEM results. FT-IR spectra of the TiO_2 sol particles were shown in Figure 1.17. The TiO_2 sol particles showed the main bands at 400-700 cm^{-1}, which were attributed to Ti-O stretching and Ti-O-Ti bridging stretching modes. The small peak at 889 cm^{-1} was attributed to Ti-F vibration. The peak at 1384 cm^{-1} was produced by NO_3^-. The stronger peak at 1626 cm^{-1} was attributed to bending vibrations of O-H and N-H. The IR spectra of the sol sample dried at 110 °C revealed that Ti-O, Ti-F, N-H, Ti-OH, H-O-H groups existed in the as-prepared sample by sol-gel-hydrothermal method. The forming of Ti-F indicated that F atoms were incorporated into the TiO_2 crystal lattice. It was also found that the addition of fluorine could improve the crystallization and adsorption of particles significantly, the photocatalytic activity for decomposition of formaldehyde were enhanced remarkably with the doping of fluorine.

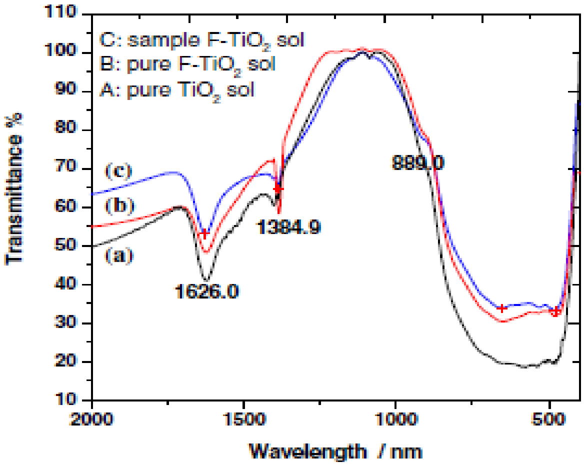

Figure 1.17 FT-IR spectra of TiO_2 sol particles (Huang, *et al.*, 2007).

Huang, *et al.*, (2007) synthesized nitrogen and fluoride codoped TiO_2 anatase (N-F-TiO_2) by a modified sol-gel hydrothermal method using tetrabutyl titanate as precursor. TiO_2 samples were characterized by XRD, TEM, UV-vis-DRS and XPS. The results from XRD showed that the addition of a small amount of anion

F could promote amorphous TiO_2 transformation to anatase TiO_2 and enhance the crystallinity of TiO_2 significantly. Figure 1.18 showed the assumed band structure of pure anatase TiO_2 sol, F-TiO_2 sol, N-TiO_2 sol, and N-F-TiO_2 sol particles. The isolated levels of the N 2p orbitals situated above the valence band led to a narrowing of the band gap, and the absorption edge shifted toward longer wavelengths. F-doping in TiO_2 converted some Ti^{4+} to Ti^{3+} by charge compensation, and the Ti^{3+} surface states in TiO_2 formed a donor level between the band gaps of TiO_2 and would thus somewhat improve its visible-light absorption. The N-F-codoped TiO_2 sol particles showed strong visible-light response and high photocatalytic activity for formaldehyde degradation under irradiation by visible light (400-500 nm).

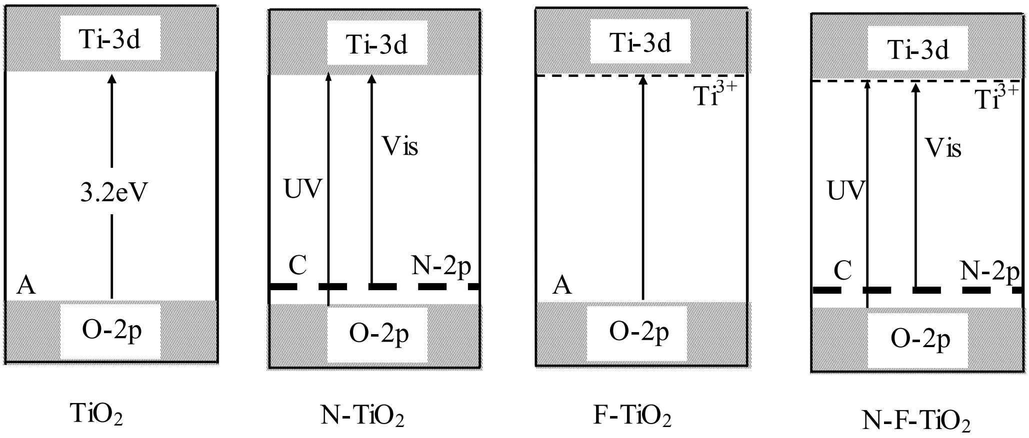

Figure 1.18 Energy diagrams for the anatase TiO_2 sol particles (Huang, *et al.*, 2007).

Xie, *et al.*, (2007) synthesized F-N-codoped TiO_2 photocatalysts with anatase at 100 °C using $TiCl_4$ and NH_4F as titanium and fluorine, nitrogen sources, respectively. The as-prepared yellow or white yellow photocatalysts were characterized by XRD, TEM, SEM, BET surface area, XPS and UV-vis DRS. The results showed that the F-N-codoping extended the absorbance spectra of TiO_2 into visible region. The BET surface area of the as-prepared F-N-codoped TiO_2 photocatalyst was high up to 191 m^2g^{-1}. The results of degradation of methyl orange (MO) solution showed that the F-N-codoped samples exhibited much higher visible-light-induced catalytic activities than that of Degussa P25 and the as-prepared pure TiO_2. This property was attributed to the synergetic effects of absorption in the visible-light region, red shift in adsorption edge, good crystallization, porous structure and large surface area of the F-N-codoped TiO_2.

Pelaez, *et al.*, (2009) developed nonmetal-doped TiO_2 nanoparticles (N-F-TiO_2) by a novel synthesis route employing a simple sol-gel method containing a nonionic fluorosurfactant as pore template material to tailor-design the structural properties of TiO_2 and fluorine dopant as well as ethylenediamine as nitrogen source for the photocatalytic response towards visible light. The N-F-TiO_2 was characterized by XRD, UV-vis spectroscopy, XPS, HR-TEM, ESEM and porosimetry measurements. The resulting nanoparticles exhibited enhanced structural properties such as high surface area (141 m^2g^{-1}), high porosity (49%), mesoporous structure (2-10 nm pore size) and low degree of agglomeration (1.07). A reduction in the effective band gap (2.75 eV) was observed compared with reference TiO_2 (3.00 eV) due to the red-shift in the optical absorption spectrum of the nonmetal-doped TiO_2 photocatalyst.

Meng, *et al.*, (2009) synthesized F-N-codoped anatase TiO_2 nanocrystals by sol-gel method. In a typical procedure, 2 mL tetrabutyl titanate (TBOT) was dissolved in 10 mL ethanol with 20 mL of $N(Et)_3$ (in excess). Under continuously stirring for 10 min, a given amount of NH_4F was added to the above solution. The pH value of the mixed solution was adjusted with diluent HNO_3 solution. Such mixture was roughly stirred for 24 h at room temperature. The solution was then transferred to a culture dish and was kept in an oven at 60 C about 2 h, getting a monolith gel. Finally, this gel was calcined in air at different temperatures for 4 h, getting powder. The results from XPS suggested that the substitutional N and F species replaced the lattice oxygen atoms in TiO_2 nanocrystals. Such nanocrystals showed strong absorption from 400 to 550 nm, which was mainly induced by nitrogen doping. The N-F-codoped TiO_2 nanocrystals showed satisfying photocatalytic activity on the photo-degradation of methylene blue under visible light.

Li, *et al.*, (2005) studied N-doped, F-doped, and N-F-codoped TiO_2 powders (NTO, FTO, NFTO) synthesized by spray pyrolysis in order to elucidate the origin of their visible-light-driven photocatalysis. The comparisons in their experimentally obtained characteristics were based on the analysis of XPS, UV-Vis, PL, NH_3-TPD and ESR spectra. The comparisons in their theoretically predicted properties were based on the analysis of the calculated electronic structures. As a result, N-doping into TiO_2 resulted in not only the improvement in visible-light absorption but also the creation of surface oxygen vacancies. F-doping produced several beneficial effects including the creation of surface oxygen vacancies, the enhancement of surface acidity and the increase of Ti^{3+} ions. Doped N atoms formed a localized energy state above the valence band of TiO_2, whereas doped F atoms themselves had no influence on the band structure. The photocatalytic tests indicated that the NFTO demonstrated the highest visible-light activity for decompositions of both acetaldehyde and trichloroethylene.

1.3 Objectives

The objectives of this research are as follows:

- To prepare amorphous TiO_2 from reaction between $TiCl_4$ and diluted ammonia solution at below room temperature.
- To prepare fluorine doped TiO_2 via impregnation method.
- To prepare fluorine doped TiO_2 via co-precipitation method.
- To investigate the physical and photocatalytic properties of fluorine doped TiO_2 powder.

CHAPTER 2

Experimental and characterization techniques

2.1 Synthesis of fluorine doped TiO_2 powders

2.1.1 Materials

1. Ammonium hydroxide (Ammonia solution), 28.0-30.0%, NH_4OH, AR., Code no. 9721-03, J.T. Baker, U.S.A.
2. Ammonium bifluoride, $NH_4F{\cdot}HF$, code no. 6155780, BDH Chemicals Ltd, England.
3. Hydrochloric acid, HCl, A.R., code no. 9535-03, J.T. Baker, U.S.A.
4. Indigo Carmine, $C_{16}H_8N_2Na_2O_8S_2$; A.R., code no. 57000, Fluka, U.S.A.
5. Silver nitrate, $AgNO_3$, A.R., code no 102333J, BDH, England.
6. Sodium hydroxide, NaOH, A.R., code no. K 2001, LAB-SCAN Analytical Science, Ireland
7. Sodium chloride, NaCl, A.R., code no. 479686, CARLO REBA REAGENTI, Italy.
8. Titanium dioxide (Degussa P25), code no. D-60287, Degussa AG, Frankfurt, Germany.
9. Titanium dioxide (Anatase), A.R., code no. 488257, Carlo Erba, Italy.
10. Titanium tetrachloride, $TiCl_4$, A.R. code no. 8.12382.1000, Merck, Germany.
11. Potassium hydrogen phthalate ($C_8H_5KO_4$), code no. CH-9470, Fluka Chemika, Switzerland.

2.1.2 Instruments

Chemistry Department, Faculty of Science, PSU.

1. Centrifuse, EBA 20, Hettich, Germany.

2. UV-vis diffuse reflectance spectrophotometer, UV-vis DRS, UV-2401, Shimadzu, Japan.
3. Fourier- transformed infrared spectrophotometer, FT-IR, Spectrum GX, Perkin Elmer, U.S.A.
4. Photoluminescence spectrophotometer, LS55, Perkin Elmer, U.S.A.
5. Ultraviolet-visible spectrophotometer, SPECORD S100, Analytik Jena GmbH, Germany.
6. Reaction compartment (UV light; 75m × 75m × 75m,Visible light; 70m × 70m × 70m).
7. pH meter, pH Testr 10, Eutech Instruments/ Oakton Instruments, U.S.A.

Chemical Engineering Department, Faculty of Engineering, PSU.

1. BET surface area, SA 3100, Coulter, U.S.A.

Scientific Equiment Center, PSU.

1. X-ray diffractometer, XRD, PHILIPS X'Pert MPD, the Netherlands.
2. Scanning electron microscope, SEM, JEOL JSM-5800LV, Japan.
3. Scanning electron microscope, SEM, JEOL JSM-5200, Japan.
4. Energy dispersive X-ray spectrometer, ISIS 300, Oxford, England.
5. Thermogravimetric analyzer, TGA7, Perkin Elmer, U.S.A.
6. Differential scanning calorimeter, DSC7, Perkin Elmer., U.S.A.

Siam Photon Laboratory Synchrotron Light Research Institute , Public organization, Nakhon Ratchasima, Thailand.

1. X-ray Absorption Spectroscopy (XAS)

The Petroleum and Petrochemical College, Chulalongkorn University, Bangkok, Thailand.

1. BET surface area, Quantachrome / Autosorb-1, Thermo Finnigan / Sorptomatic 1990.

2.1.3 Methods

This work is divided into 2 parts : Part 1 synthesis of fluorine doped TiO_2 via impregnation method, characterization and studies of photocatalytic degradation of indigo carmine under UV and visible light irradiation; Part 2: synthesis of fluorine doped TiO_2 via co-precipitation method, characterization and studies of photocatalytic degradation of indigo carmine under UV and visible light irradiation.

2.1.3.1 Synthesis of fluorine doped TiO_2 via impregnation method

Amorphous TiO_2 was prepared by the following method: titanium tetrachloride ($TiCl_4$, 30 mL) was added in a 2-necked round bottom flask which was placed in an ice water bath. Then, ammonia solution (NH_3, 240 mL) was added slowly to $TiCl_4$ with vigorous stirring to yield the white precipitate. The precipitate was filtered gravimetrically with Whatman no. 42 filter paper followed by washing with distilled water until free of chloride ions (tested with 0.1 M $AgNO_3$ solution). The white powder was dried at 40 °C for 24 h and ground to fine powder. Figure 2.1 shows flow chart for the synthesis of amorphous TiO_2.

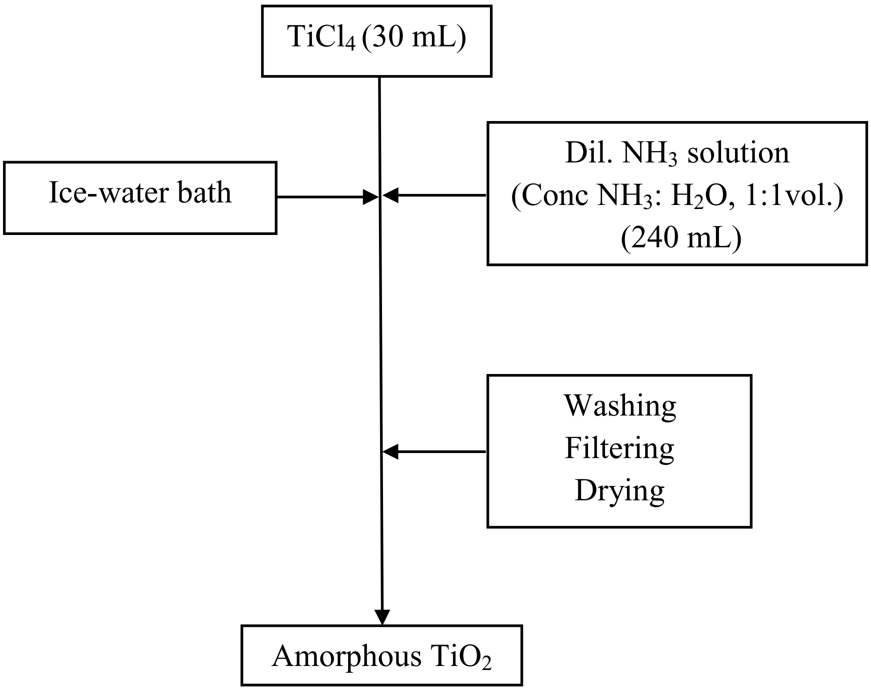

Figure 2.1 Flow chart of the synthesis of amorphous TiO_2.

Detailed procedure for the preparation of fluorine doped TiO_2 via impregnation method is as follows. The required amount of dopant was dissolved in distilled water and then added to amorphous TiO_2. The solution was treated by hydrochloric acid until the pH value was 3.6 and then stirred for 24 h. The precipitate was filtered gravimetrically with Whatman no. 42 filter paper followed by washing with distilled water until free of chloride ions (tested with 0.1 M $AgNO_3$ solution). The white powder was dried at 40 °C for 24 h and ground to fine powder. TiO_2 samples were referred to as ***xF-TiO$_2$-imp***. where *x* is the fluorine content in mM. A flow chart for the synthesis of F- TiO_2 is shown in Figure 2.2.

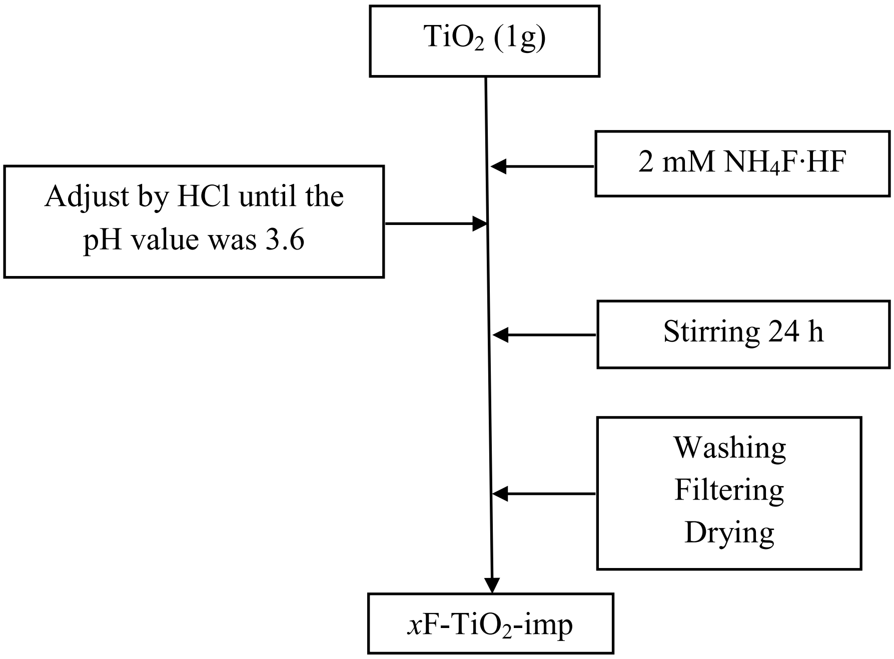

Figure 2.2 Flow chart of the synthesis of F-TiO_2 via impregnation method.

2.1.3.2 Synthesis of fluorine doped via co-precipitation method

Figure 2.3 shows flow chart for the synthesis of undoped TiO_2. Detailed procedure for the preparation is as follows: titanium tetrachloride ($TiCl_4$, 5 mL) was added in a 2-necked round bottom flask which was placed in an ice water bath. Then, ammonia solution (NH_3, 60 mL) was added slowly to $TiCl_4$ with vigorous stirring to yield the white precipitate. The solution was stirred for 24 h. The precipitate was filtered gravimetrically with Whatman no. 42 filter paper followed by washing with distilled water until free of chloride ions (tested with 0.1 M $AgNO_3$ solution). The white powder was dried at 40 °C for 24 h and ground to fine powder.

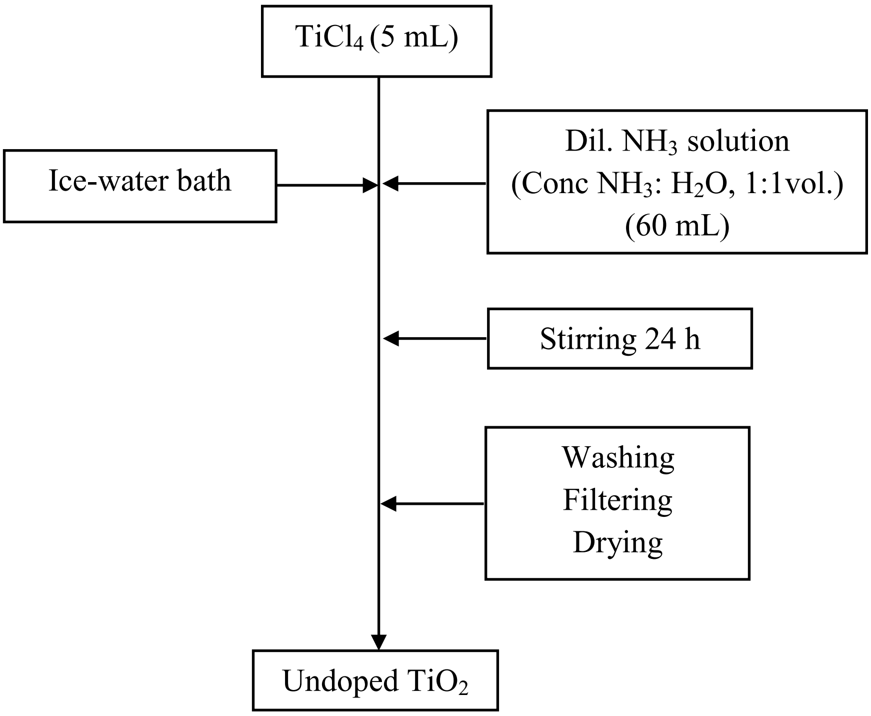

Figure 2.3 Flow chart of the synthesis of undoped TiO_2.

Detailed procedure for the preparation of fluorine doped TiO_2 via co-precipitation method (Figure 2.4) is as follows: titanium tetrachloride ($TiCl_4$, 5 mL) was added in a 2-necked round bottom flask which was placed in an ice water bath. Then, ammonia solution (NH_3, 60 mL) was added slowly to $TiCl_4$ with vigorous stirring. The required amount of dopant was dissolved in distilled water and then added to TiO_2. The solution was treated until the pH value was 3.6 and then stirred for 24 h. The pH value was adjusted using dilute HCl and NaOH. The precipitate was filtered gravimetrically with Whatman no. 42 filter paper followed by washing with distilled water until free of chloride ions (tested with 0.1 M $AgNO_3$ solution). The white powder was dried at 40 °C for 24 h and ground to fine powder. This TiO_2 sample was referred to as ***xF-TiO$_2$-PC***.

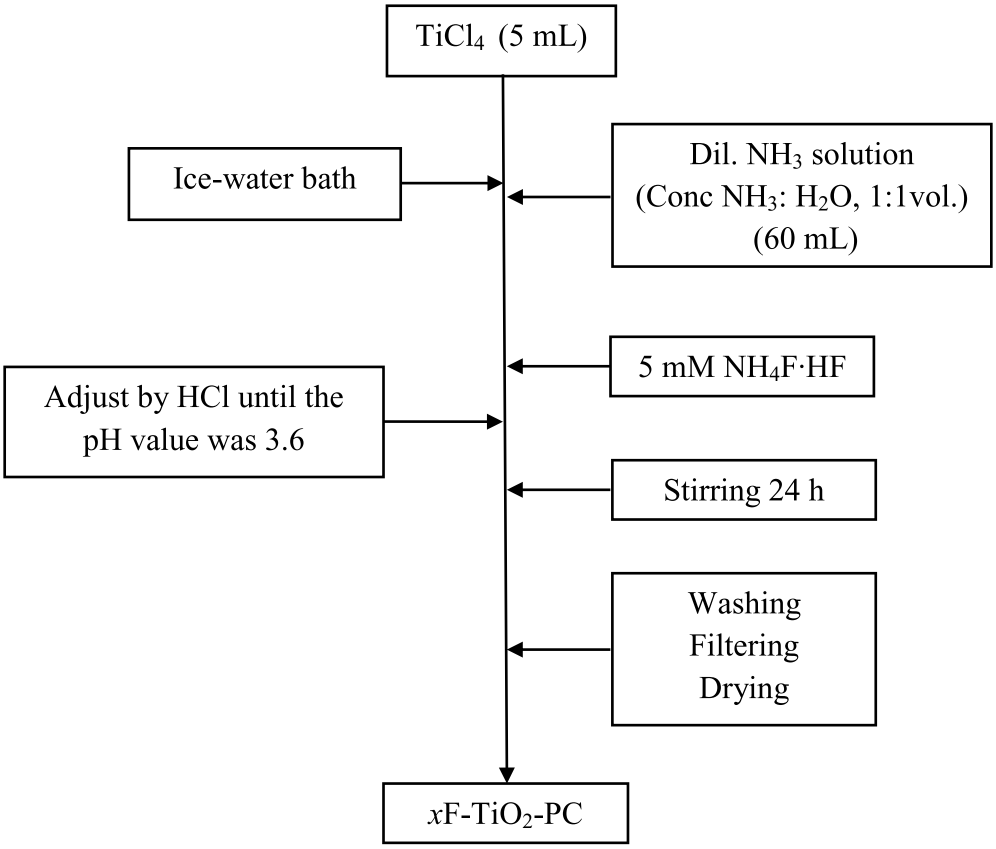

Figure 2.4 Flow chart of the synthesis of F-TiO_2 via co-precipitation method.

2.2 Characterization techniques

The synthesized TiO_2 powders were characterized by various techniques like XRD, SEM, EDX, UV-Vis DRS, PL, BET surface area, FT-IR, TGA, DSC and XAS techniques.

2.2.1 X-ray diffraction (XRD)

TiO_2 samples were observed by the Philips PW 3710 powder diffractometer (PHILIPH X'Pert MPD) used Cu K radiation and equipped with a Ni filter over the range of 2 = 5-90° at room temperature. The crystallite size was calculated from the Scherrer equation (Eq. (2.1)).

$$d = 0.9 \ / \ (\ \cos \ ) \qquad (2.1)$$

In Eq. (2.1), d is the crystallite size, is the full width at half-maximum (fwhm, in radians), is the wavelength of the X-ray radiation (1.5406 Å) and is the diffraction angle of the reflection (Lakshminarasimhan, *et al.*, 2007).

The percentage of anatase phase existed in sample was determined by standard addition method employing the standard curve of anatase. The standard curve was constructed from mixed pure amorphous phase with anatase phase (10%, 20%, 30% by weight) then measure the phase by XRD technique. The plot of area and percentage of anatase phase was applied to estimate the percentage of anatase phase in samples. Standard curve for the calculation of % anatase phase in TiO_2 sample is a straight line defined by $Y = 15.029X$, $R^2 = 0.9933$ (Suwanchawalit, *et al.*, 2008). On the other hand, the fraction of rutile in Degussa P25 was determined via the usually accepted quantitative method. This method consists of measuring the relative XRD intensities of the anatase and rutile from the following equation:

$$= 1/[1+ 0.8(I_A/I_R)] \qquad (2.2)$$

where is the mass fraction of rutile in the powder, while I_A and I_R are the X-ray integrated intensities of the (101) reflection of anatase and (110) reflection of rutile, respectively (Zhang, *et al.*, 2000).

2.2.2 Electron microscopy

The surface morphology and size of TiO_2 samples were observed with a SEM (JEOL JSM-5800LV, JEOL JSM-5200). An analytical technique used for the elemental analysis or chemical characterization of TiO_2 samples were investigated by using a SEM mode JEOL JSM-5800 LV. A SEM can be utilized for high magnification imaging of almost all materials. With SEM in combination with EDX mode ISIS 300 it is also possible to find out which elements different parts of sample contain.

2.2.3 Diffuse reflectance UV-Vis spectroscopy (DRS)

UV-vis diffuse reflectance spectra of all TiO_2 samples were recorded with a UV-Vis absorption spectrophotometer (Shimadzu UV-2401, Japan) in the wavelength range 200-800 nm and using $BaSO_4$ as a reference. The band gap energies of all TiO_2 samples were calculated by the Planck's equation:

$$E_g = \frac{hc}{} = \frac{1240}{} \qquad (2.3)$$

Where E_g is the band gap energy (eV)
h is the Planck's constant (6.63×10^{-34} J.s.)
c is the light velocity (3×10^{8} ms^{-1})
is the wavelength (nm)

2.2.4 Photoluminescence spectroscopy (PL)

TiO_2 samples were studied with a photoluminescence spectroscopy (LS 55, Perkin Elmer, U.S.A.). The PL spectra were recorded in the range 200-800 nm at room temperature. The band gap energies of all TiO_2 samples were calculated by the Planck's equation (E_g =1240/).

2.2.5 BET surface area (BET method)

The Brunauer-Emmett-Teller (BET) surface area was determined from the N_2 adsorption-desorption isotherm at -196 °C by using the BET method (Coulter, model SA3100, U.S.A.). The average particle size was estimated by assuming all the particles to have same spherical shape and size. The particle size, *D* is given by Eq (2.4),

$$D_{BET} = \frac{6000}{(S_{BET} \cdot \quad)} \qquad (2.4)$$

where S_{BET} is the BET-specific surface area and is the true density (Joseph, *et al.*, 2009). The densities of the three crystalline TiO_2, i.e., anatase, brookite, and rutile, are 3.90, 4.13, and 4.27 g/cm^3, respectively (Kanna, *et al.*, 2010, Pelaez, *et al.*, 2009).

2.2.6 Fourier-transformed infrared spectroscopy (FTIR)

The infrared spectra were recorded using Fourier-transformed infrared (FT-IR) spectrophotometer (Spectrum GX, Perkin Elmer, U.S.A.) in diffused reflectance mode at 400-4000 cm^{-1} and using KBr as blank.

2.2.7 Thermogravimetric analysis (TGA)

The crystal phase and phase transformation of the synthesized TiO_2 were characterized by TGA (TGA7, Perkin Elmer, U.S.A.) with the temperature range of 50-1000 °C at the heating rate of 10 °C/min.

2.2.8 Differential scanning calorimetry (DSC)

The synthesized TiO_2 powders were studied with the differential scanning calorimetry (DSC7, Perkin Elmer., U.S.A.). The heat transfer rate used in the investigation was 10 °C/min and the applied temperature interval was 50-500 °C.

2.2.9 UV-Vis spectroscopy

The concentration of IC in the solution was determined by measuring the absorbance intensity at 610 nm (Specord S100, Analytik Jena GmbH, Germany) and with the use of calibration curves.

2.2.10 X-ray absorption spectroscopy (XAS)

The oxidation states of TiO_2 samples were determined by X-ray absorption spectroscopy (XAS). XAS spectra were obtained at Synchrotron Light Research Institute (Public Organization), 111 University Avenue, Muang District, Nakhon Ratchasima 30000, Thailand.

2.3 The pH of the point of zero charge (pH_{pzc})

The pH of the point of zero charge (pH_{pzc}) was measured by the so-called pH drift method (Utrilla, *et al*., 2001; Bessekhouad, *et al*., 2004). A 0.05 g amount of TiO_2 sample was added into 50 ml of 0.01M NaCl solutions at various pH values and the suspensions were magnetically stirred for 3 h. The pH was adjusted to a value between 2 to 12 by addition of 0.1 M HCl or 0.1 M NaOH solutions. All solutions were prepared using distilled water. The final pH (reached after 3 h) was measured at room temperature and plotted as a function of initial pH. The pH of the suspension was measured using a pH meter. We used two methods for determining the point of zero charge: the first one reported by Bessekhouad, *et al*., 2004, the pH at which the curve crosses the line pH (final) = pH (initial) is the pH_{pzc} of the given catalyst. The second is a commonly used method. The salt addition methods provide another means of determining the pH_{pzc}. The pH_{pzc} is obtained from the shifts $\Delta pH = pH_{final} - pH_{initial}$. The pH_{pzc} is identified as the pH at which $\Delta pH = 0$ (Mullet, *et al*., 1997).

2.4 Titration of the synthesized TiO_2 powders

(a) Standardization of NaOH solution.

Potassium hydrogen phthalate ($C_8H_5KO_4$, 25 mL) solution of accurately known concentration was added in the flask. Phenolphthalein indicator was added prior to the titration with NaOH solution. NaOH was added from the burette until reaching the end point when the solution turned to pink colour. Record the amount of NaOH from the burette. Repeat the experiment and take an average of these results to use in the calculation and to find the unknown concentration of base.

(b) Standardization of HCl solution.

Hydrochloric acid (0.01 M HCl, 25 mL) was added in the flask. Phenolphthalein indicator was added prior to the titration with NaOH solution. NaOH was added from the burette until reaching the end point when the solution turned to pink colour. Repeat the experiment and take an average of these results to use in the calculation and to find the unknown concentration of acid.

(c) Detailed procedure for titration of the synthesized TiO_2 powders

The synthesized TiO_2 powders (TiO_2, 0.1 g) was added to distilled water (H_2O, 50 mL) and then added phenolphthalein indicator. The slurry was titrated with HCl or NaOH from the burette. Record the amount of HCl or NaOH from the burette. Repeat the experiment and take an average of these results to use in the calculation and to find the unknown concentration.

2.5 Photocatalytic test

Photoactivity of F-TiO_2 was studied by indigo carmine (IC, a representative of polluting dyes in textile effluents) degradation in aqueous solution under both UV and visible light irradiation. In a typical experiment, 0.1 g of TiO_2 powders was added into 100 mL of IC solution with a concentration of 2.5×10^{-5} M. The experiments were performed in a closed compartment (0.75m × 0.75m × 0.75m for UV light and 0.70m × 0.70m × 0.70m for Visible light). The suspensions were magnetically stirred for 1 h in the dark to establish the equilibrium of IC adsorption/desorption followed by switching on the light source (20 watt black light F20T12-BLB, G.E., U.S.A. or visible light (18 watts fluorescence TL-D 18W/54-765, PHILIPS, the Netherlands.)). Samples of 5 mL (every 1 h) were collected from the suspension and were immediately centrifuged at 6000 rpm for 10 min. The concentration of IC dye after photodegradation was analysed by using a UV-Vis spectrophotometer (Specord S100, Analytik Jena, Germany) by measuring the change in absorbance at 610 nm. The experiment was repeated three times. A flow chart of the photodegradation of of IC by TiO_2 samples is shown in Figure 2.5.

In a blank test, IC solution (2.5×10^{-5} M) was added in a peaker. The suspensions were magnetically stirred for 6 h under UV or visible light, repeat the experiment three times. The concentration of IC dye after photodegradation was analysed by using a UV-Vis spectrophotometer.

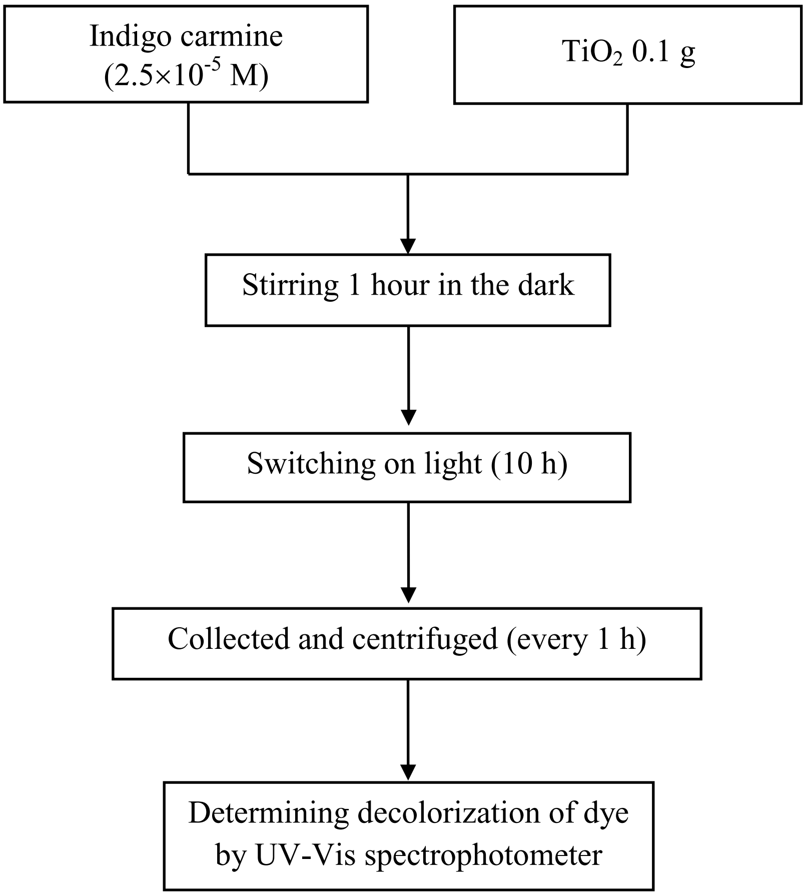

Figure 2.5 Flow chart of the photodegradation of IC by TiO_2 samples.

The percentage of IC decrease was followed by measuring absorbance at wavelength 610 nm using a UV-vis spectrophotometer (Specord S100, Analytik Jena GmbH, Germany). Photocatalytic efficiency (%) of IC was measured by applying the following equation:

$$\text{Photocatalytic efficiency (\%)} = \frac{(C_0 - C_t)}{C_0} \times 100 \qquad (2.5)$$

where C_0 is the initial concentration of IC solution and C_t is the concentration of IC solution at specific time interval for the collected sample.

CHAPTER 3

Results and discussion

3.1 Synthesis and characterzations of amorphous TiO_2

In this work, amorphous TiO_2 was synthesized via the sol-gel method by using titanium (IV) tetrachloride and diluted ammonia solution as a starting material. Amorphous TiO_2 exists as a white powder solid. The physico-chemical properties of amorphous TiO_2 were characterized by XRD, SEM, EDX, DRS, PL, FT-IR, TGA, and DSC techniques. Many studies on the synthesis of TiO_2 powder have been done using titanium compounds, such as titanium alkoxides ($Ti(OR)_4$) or titanium tetrachloride ($TiCl_4$), as the starting material (Sun, *et al.*, 2002). $TiCl_4$ is the primary starting material for the commercial production of titania powders, known as the chloride process in the titania industry. The sol-gel method typically entails hydrolysis of a solution of a precursor molecule aiming to obtain first a suspension of colloidal particles (the sol) and then a gel composed of aggregated sol particles. The gel is then thermally treated to yield the desired material. The pH value of the precursor solution is a decisive factor in controlling the final particle size and shape, crystal phase and agglomeration due to its influence on the relative rates of hydrolysis and polycondensation. The reaction can be written as follows (Golubovic, *et al.*, 2009):

$$TiCl_4 \longrightarrow Ti(OH)_4 \longrightarrow \text{alcogel} \qquad (3.1)$$

The corresponding chemical reactions are:

$$TiCl_4 + 4NH_4OH \longrightarrow Ti(OH)_4 + 4NH_4Cl \qquad (3.2)$$

$$Ti(OH)_4 \longrightarrow TiO_2 + 2H_2O \qquad (3.3)$$

When $TiCl_4$ hydrolyses, it generates TiO_2 particle as well as H^+ and Cl^- ions, the process is described by Eq. (3.4) (Zhang, *et al.*, 2000):

$$TiCl_4 + 2H_2O \longrightarrow TiO_2 + 4H^+ + 4Cl^- \qquad (3.4)$$

In general, the initial reaction product of sol-gel reaction is the mixture of hydrolysis product (hydroxylated titanium) and condensation product with Ti-O-Ti structure (oxide compound). The content of hydrolysis product is dependent upon the degree of being condensated (Liu, *et al.*, 2008). The hydrolysis reaction occurs upon the addition of water, when a hydroxyl ion attaches onto the metal atom resulting in the removal of the alkyl group (OR). This is followed by condensation, which involves the formation of (M-O-M) bonds and depending on the conditions, either water or alcohol is formed (Watson, *et al.*, 2004). However, the subsequent calcination was excluded. Since no calcination was employed, the product powder was mostly present in an amorphous form with some hydrated water molecules (Kanna, *et al.*, 2010).

3.1.1 Characterization of amorphous TiO_2

3.1.1.1 X-ray diffraction (XRD)

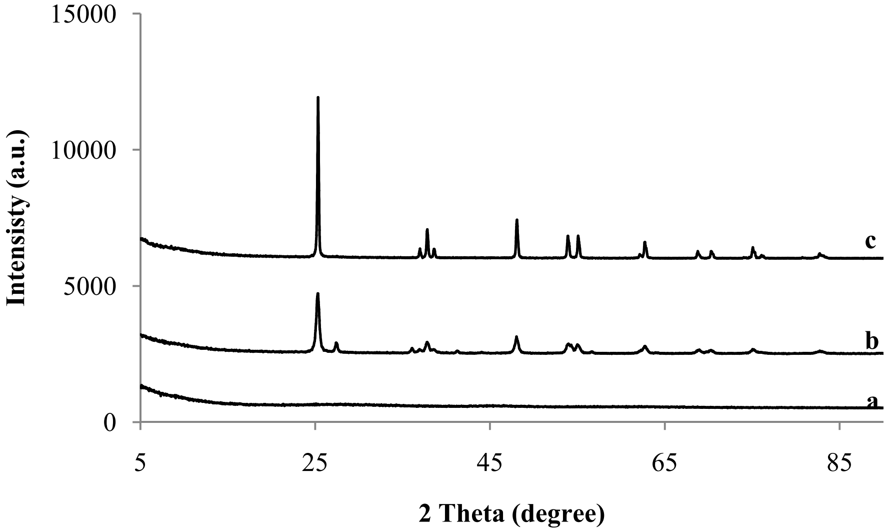

Figure 3.1 X-ray diffraction patterns of TiO_2 samples; (a) amorphous TiO_2, (b) Degussa P25, (c) anatase.

The X-ray diffraction patterns of TiO_2 samples were recorded with the Philips PW 3710 powder diffractometer (PHILIPH X'Pert MPD) using Cu Kα radiation. The diffractometer was equipped with a Ni filter. TiO_2 samples were scanned in the 2θ range of 5-90°. It was shown that amorphous TiO_2 was synthesized via the sol-gel method by using titanium (IV) tetrachloride and diluted ammonia solutions. The XRD pattern of the amorphous TiO_2 is given in Figure 3.1a. From the

XRD data, only flat base line with no peak at all was observed indicating that the TiO_2 existed mainly in the amorphous form. XRD spectra of Degussa P25 and anatase are shown in Figure 3.1b and Figure 3.1c, respectively. Degussa P25 as shown in Figure 3.1b consists of mixed phase in the ratio of anatase (75%) and rutile (25%) and the XRD peak at 2θ of 25.29°, 27.44°, 36.09°, 37.77°, 38.59°, 41.27°, 44.01°, 48.02°, 53.87°, 54.99°, 56.64°, 62.73°, 68.88°, 70.26°, 75.10°, 82.72°, respectively. The anatase phase was identified at 2θ of 25.33°, 36.98°, 37.83°, 38.59°, 48.07°, 53.90°, 55.10°, 62.13°, 62.70°, 68.76°, 70.29°, 75.04°, 75.32°, 76.06°, 82.70°, respectively. Degussa P25 shows the strongest peak at 2θ = 25.29° is representative of anatase phase (101) reflections. The crystallite size of Degussa P25 is 23.67 nm, and the crystallite size of anatase is 41.42 nm which are similar to the reported values. Phase, crystallinity and crystallite size of amorphous TiO_2 and commercial are shown in Table 3.1.

Table 3.1 Phase, crystallinity and crystallite size of amorphous and commercial TiO_2.

TiO_2 samples	Phase	Crystallinity (%)	Crystallite size (nm)	
			This work[b]	Literatures[c]
Amorphous TiO_2	Amorphous	-	-	-
Anatase	Anatase	Anatase (100)	41.42	48.00
Degussa P25	Anatase , Rutile	Anatase (81)[a], Rutile (19)	23.67	21.00

[a] Determined by XRD using $\chi = 1/[1+ 0.8(I_A/I_R)]$, Zhang, *et al.*, 2000.

[b] Calculated from XRD data using Scherrer's formula.

[c] Raj and Viswanathan, 2009.

The amorphous phase represents the highest state of disorder, i.e. has a completely random structure. With TiO_2 the definition of amorphous is difficult, as there is always some degree of local ordering observed. Here we will define amorphous as the TiO_2 phase where no signal can be detected in XRD. This states only that the material has crystalline domains of a size below the XRD detection limit (< 3-5 nm). Usually grains around 5 nm are detected as very broad peaks around the position expected from the diffraction spectrum of the material. The absence of any XRD signal can be caused not only by a very small crystallite size but also by a very low degree of crystallinity. One can, therefore, state that XRD 'amorphous' TiO_2 contains a certain degree of local ordering which can extend to crystallites of grain size smaller than 3 nm, which may or may not be enclosed by a matrix of low structural ordering. Very little is known on the electronic structure of amorphous TiO_2. Most discussions agree that the high defect state should result in poor charge carrier conduction. As a result, only rarely the photocatalytic activity of amorphous films or powders is measured (Eufinger, 2007).

3.1.1.2 Electron microscopy

(1) Scanning electron microscopy (SEM)

The surface morphology of amorphous and commercial TiO_2 were investigated by using a scanning electron microscope (SEM) model JEOL JSM-5800 LV. The surface and morphology of amorphous TiO_2 determined by SEM are shown in Figure 3.2a. The SEM results showed high agglomerated particles with various sizes of particles as shown in Figure 3.2a (low magnification, 1,000×). At high magnifications (5,000× and 10,000×), the amorphous-like structure with low crystalline phase of TiO_2 can be detected. Figure 3.2b and Figure 3.2c show the SEM images of Degussa P25 and anatase, respectively. The morphology of Degussa P25 showed high agglomerated of smaller particles. Anatase has spherical particles and agglomerated of particles.

(a) Amorphous TiO_2

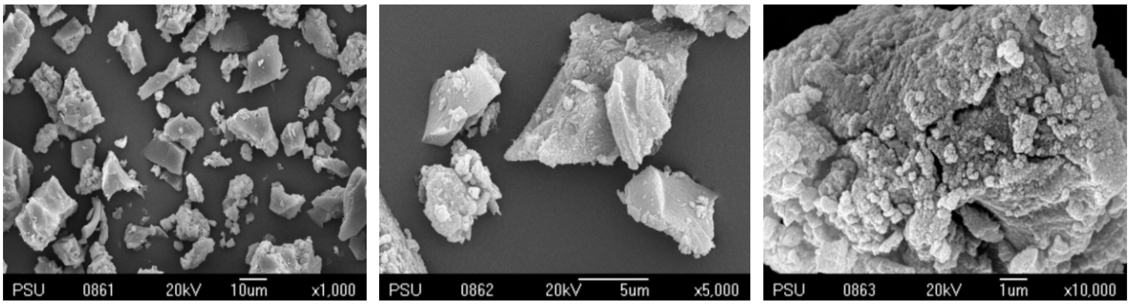

(b) Degussa P25

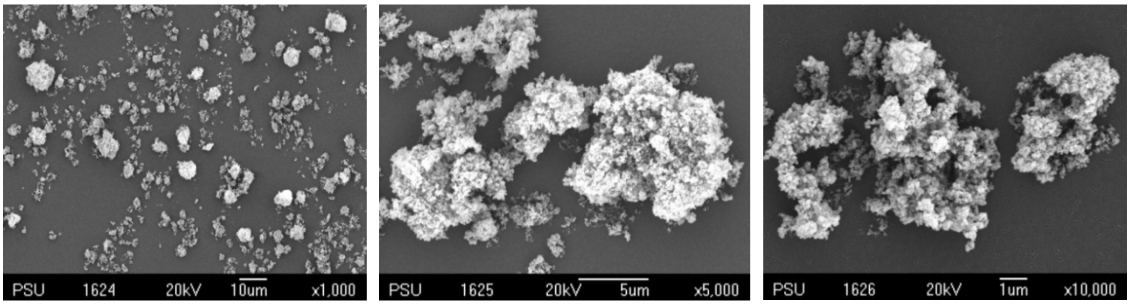

(c) Anatase

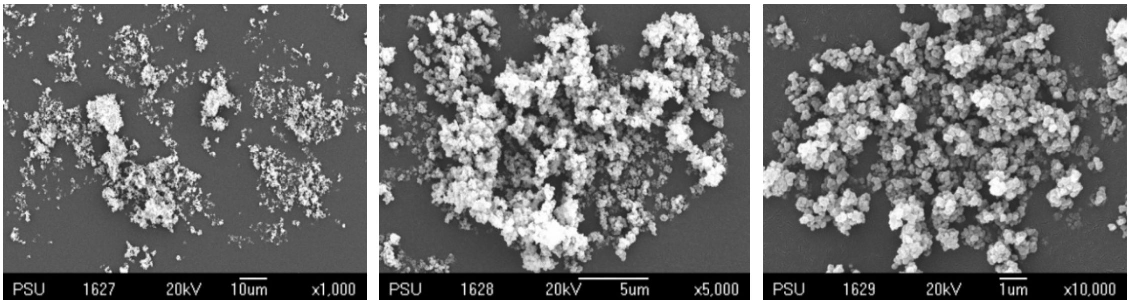

Figure 3.2 SEM images of TiO_2 samples; (a) amorphous TiO_2, (b) Degussa P25, (c) anatase. Each sample was magnified at low (1,000×) and high (5,000× and 10,000×) magnefication.

(2) Energy-dispersive X-ray spectroscopy (EDX)

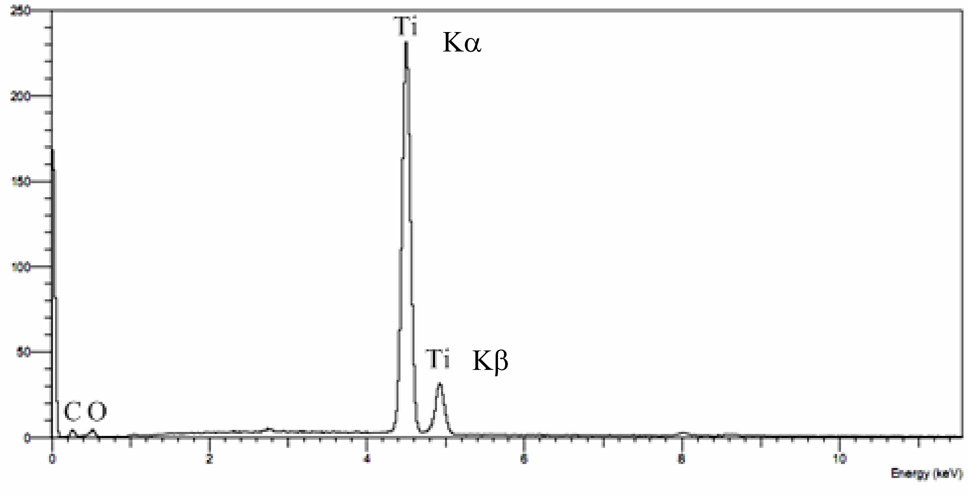

Figure 3.3 EDX spectra of amorphous TiO_2.

The elemental analysis of amorphous TiO_2 was investigated by using a scanning electron microscope (SEM) model JEOL JSM-5800 LV. SEM and EDX data were recorded by using scanning electron microscope coupled with energy dispersive X-ray spectroscopy (SEM-EDX). Figure 3.3 shows EDX spectra of amorphous TiO_2 and elemental analysis of amorphous TiO_2 revealed the presence of Ti, O and C elements.

3.1.1.3 Diffused reflectance UV-Vis spectroscopy (DRS)

UV-vis diffused reflectance spectra of TiO_2 samples were recorded with a UV-Vis absorption spectrophotometer (Shimadzu UV-2401, Japan) in the wavelength range 200-800 nm. Diffused reflectance UV-Vis spectra of amorphous and commercial TiO_2 are shown in Figure 3.4. It was found that amorphous and commercial TiO_2 have absorption only in the UV region. Amorphous TiO_2, Degussa P25 and anatase show edges of absorption band at 387 nm, 395 nm and 385 nm, respectively. The band gap energies of amorphous and commercial TiO_2 were calculated by the Planck's equation. The band gap energy of amorphous TiO_2, Degussa P25 and anatase were 3.20, 3.14 and 3.22 eV, respectively. The wavelength at onset of absorption and the band gap energy of amorphous and commercial TiO_2 are summarized Table 3.2.

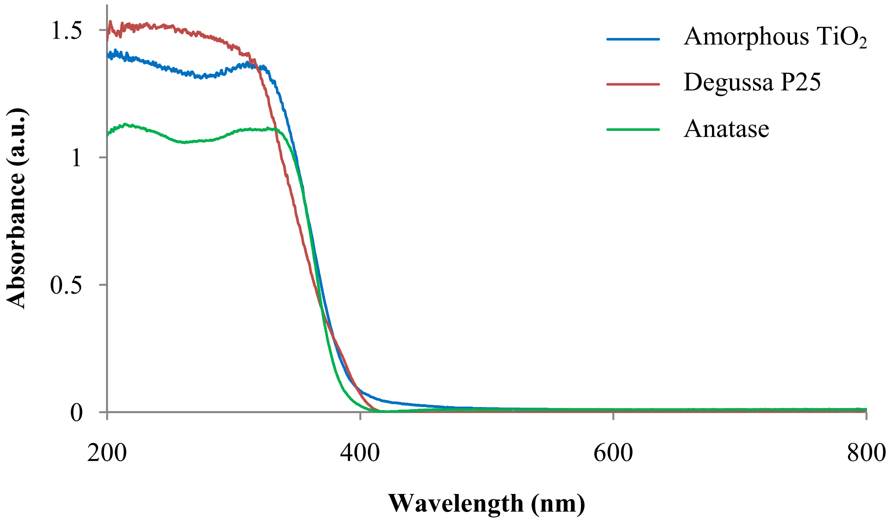

Figure 3.4 Diffused reflectance UV-Vis spectra of amorphous and commercial TiO_2.

Table 3.2 The wavelength at onset of absorption and the band gap energy of amorphous and commercial TiO_2.

TiO_2 samples	DRS		
	λ_{onset} of absorption (nm)	E_g (eV)	Literatures
Amorphous TiO_2	387	3.20	3.25^a
Degussa P25	395	3.14	3.10^b
Anatase	385	3.22	3.20^c

[a] Kanna, *et al.*, 2010.

[b] Stengl, *et al.*, 2009.

[c] Ngamsopasiriskun, *et al.*, 2010.

3.1.1.4 Photoluminescence spectroscopy (PL)

The photoluminescence spectra were studied with a photoluminescence spectroscopy (LS 55, Perkin Elmer, U.S.A.) in the range 200-800 nm. Amorphous TiO_2 displays the sharp UV emission at 386 nm. While Degussa P25 and anatase display the sharp UV emission at 395 nm and 390 nm, respectively. The peak at 650 nm could be ascribed to electron transition mediated by defects level in the band gap (Suwanchawalit and Wongnawa, 2008). The photoluminescence spectra of amorphous and commercial TiO_2 are shown in Figure 3.5. The data of emission wavelength and band gap energy of amorphous and commercial TiO_2 are summarized in Table 3.3.

Table 3.3 The wavelength at emission of absorption and the band gap energy of amorphous and commercial TiO_2.

TiO_2 samples	PL	
	$\lambda_{emission}$ (nm)	E_g (eV)
Amorphous TiO_2	386	3.21
Degussa P25	395	3.14
Anatase	390	3.18

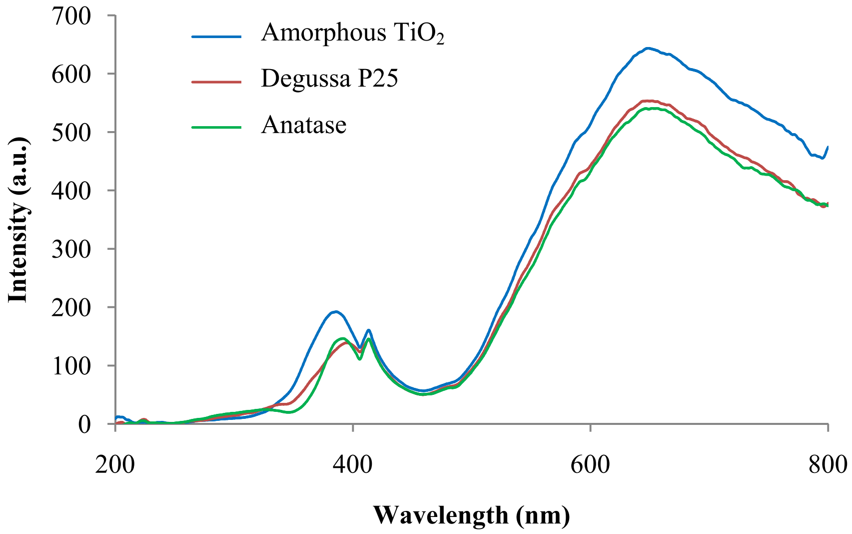

Figure 3.5 Photoluminescence spectra of amorphous and commercial TiO_2.

3.1.1.5 Fourier-transformed infrared spectroscopy (FT-IR)

(a) Amorphous TiO_2

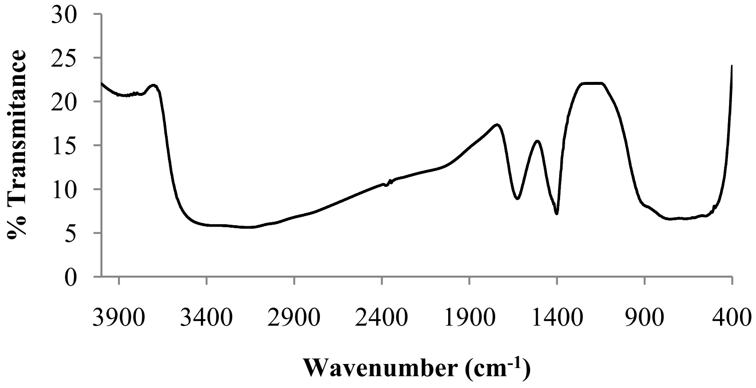

(b) Degussa P25

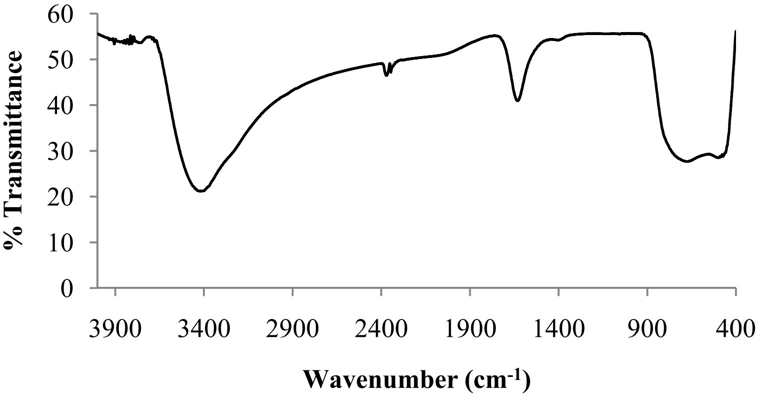

(c) Anatase

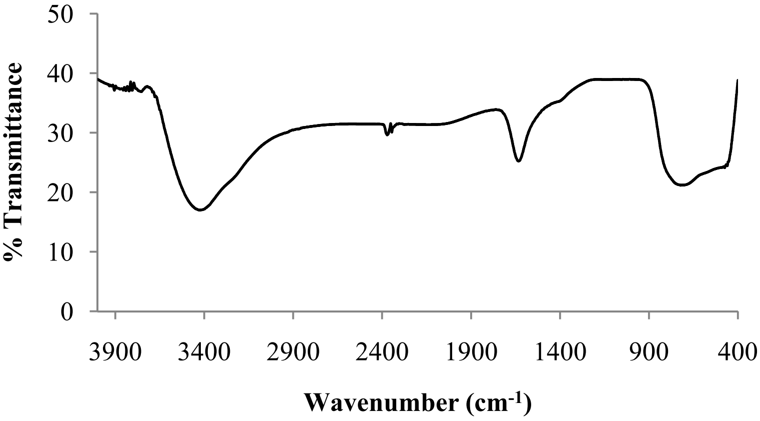

Figure 3.6 FT-IR spectrum of TiO_2 samples; (a) amorphous TiO_2, (b) Degussa P25, (c) anatase.

The infrared spectra of amorphous and commercial TiO_2 were recorded using Fourier-transformed infrared (FT-IR) spectrophotometer (Spectrum GX, Perkin Elmer, U.S.A.). The infrared spectra of all TiO_2 samples in the range 4000-400 cm^{-1} are shown in Figure 3.6. The FT-IR spectra of amorphous TiO_2 showed vibrational bonds at 3500-3000 cm^{-1}, 1639 cm^{-1}, 1402 cm^{-1}, and below 800 cm^{-1}. The bands at 3500-3000 and 1640-1630 cm^{-1} were assigned to the O-H stretching vibration and the adsorbed H_2O bending vibration. The bands at 1402 cm^{-1} can be assigned to NH_4^+ and the bands at 800-400 cm^{-1} can be assigned to the formation of the O-Ti-O lattice. The data of vibrational bands, assignments, functional groups and literatures of TiO_2 samples are summarized in Table 3.4.

Table 3.4 The FT-IR bands of amorphous and commercial TiO_2.

TiO_2	Vibrational bands (cm^{-1})	Assignments	Functional groups	Literatures
Amorphous TiO_2	3500-3000	ν_{OH} and ν_{NH}	H_2O and NH_4^+	Tong, *et al.*, 2008
	2380	ν_{co}	CO_2	Liao, *et al.*, 2003
	1639	δ_{OH}	OH groups	Khalil and Zaki, 1997
	1402	δ_{NH}	NH_4^+ group	Youn,*et al.*, 1999
	below 800	$\nu_{Ti\text{-}O}$	Ti-O bond	Jensen, *et al.*, 2005
Degussa P25	3500-3000	ν_{OH} and ν_{NH}	H_2O and NH_4^+	Tong, *et al.*, 2008
	2385	ν_{co}	CO_2	Liao, *et al.*, 2003
	1630	δ_{OH}	OH groups	Youn,*et al.*, 1999
	below 800	$\nu_{Ti\text{-}O}$	Ti-O bond	Yang, *et al.*, 2010
Anatase	3500-3000	ν_{OH} and ν_{NH}	H_2O and NH_4^+	Tong, *et al.*, 2008
	2384	ν_{co}	CO_2	Liao, *et al.*, 2003
	1632	δ_{OH}	OH groups	Khalil and Zaki, 1997
	below 800	$\nu_{Ti\text{-}O}$	Ti-O bond	Yang, *et al.*, 2010

3.1.1.6 Thermogravimetric analyzer (TGA)

(a) Amorphous TiO_2

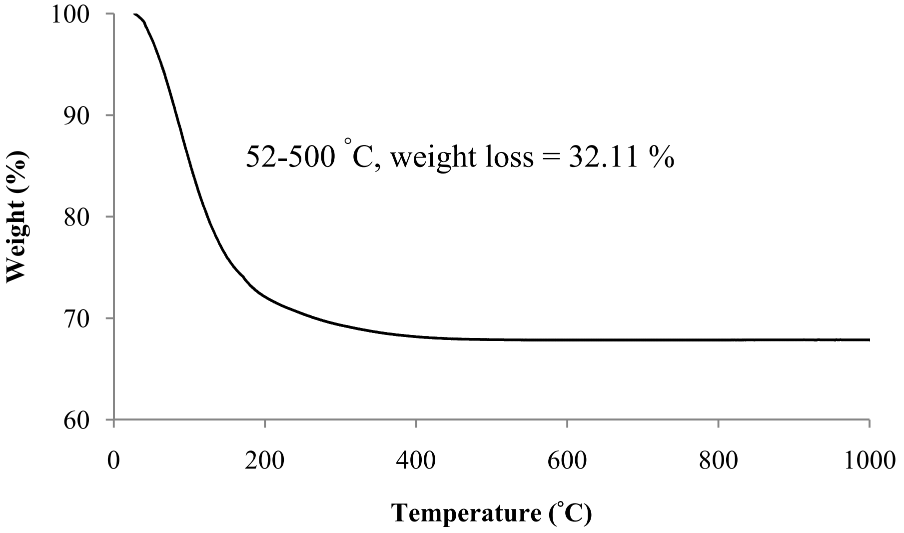

(b) Degussa P25

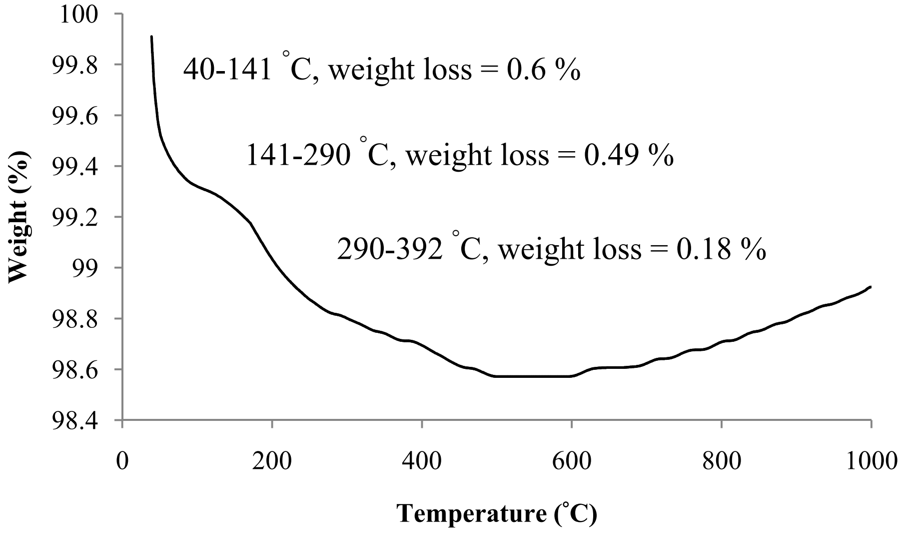

(c) Anatase

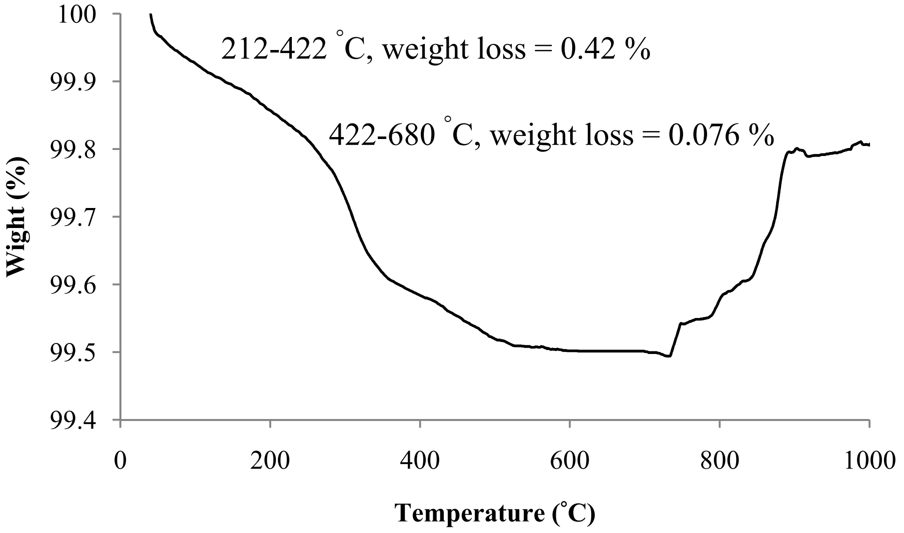

Figure 3.7 TGA spectra of TiO_2 samples; (a) amorphous TiO_2, (b) Degussa P25, (c) anatase.

The TiO_2 samples were studied with the thermogravimetric analyzer (TGA7, Perkin Elmer, U.S.A.) at temperatures ranging from 50 °C to 1,000 °C. TGA spectra of amorphous TiO_2 (Figure 3.7a) shows the weight loss of 32.11% in the range of 52-500 °C attributed to the evaporation of water and alcohol. A similar result was reported by Kanna, *et al.*, (2010) who studied the TGA spectra of amorphous TiO_2 with a gradual weight loss commencing near 50 °C and coming to completion near 450 °C. The initial weight loss in the range 50-150 °C occurred at higher rate than that taking place at higher temperatures. The total weight loss of the product was about 25.98% equivalent to the decomposition of the product $TiO_2 \cdot 1.6H_2O$ to TiO_2. The TGA results of Degussa P25 in Figure 3.7b shows that the weight loss is about 0.60% from 40 °C up to 141 °C which represents the loss of physically adsorbed water. In the temperature range of 141-290 °C, the weight loss was about 0.49%, due to the removal of strongly bound water or surface hydroxyl groups and the temperature range of 290-392 °C, the weight loss was about 0.18%, due to the crystallization of anatase phase. A similar result of Nagaveni, *et al.*, (2004) studied the TGA spectra of Degussa P25 showed 0.8% weight loss from room temperature to

150 °C, 0.9% between 150 and 500 °C, and remained constant thereafter. The TGA spectra of anatase is shown in Figure 3.7c and can be divided into two stages. The first stage ranges from 212 °C to 422 °C with the weight loss of 0.42% due to the evaporation of water and confirms the crystallization of anatase phase (Shi, *et al.*, 2009). In the temperature range of 422-680 °C, the weight loss is about 0.076% which is attributed to the loss of strongly bound water or surface hydroxyl groups (Nagaveni, *et al.*, 2004).

3.1.1.7 Differential scanning calorimetry (DSC)

TiO_2 samples were studied with the differential scanning calorimetry (DSC7, Perkin Elmer, U.S.A.). The heat transfer rate used in the investigation was 10 °C/min and the applied temperature interval was 50-500 °C. The endothermic peaks at 104 °C in the DSC spectra (Figure 3.8a) of amorphous TiO_2 correspond to desorption of physical adsorbed water and hydroxyl groups. The DSC results of Degussa P25 and anatase are shown in Figure 3.8b and Figure 3.8c, respectively. It was also demonstrated that the exothermic peak at about 319 °C of Degussa P25 and anatase corresponds to the crystallization of the anatase phase.

(a) Amorphous TiO_2

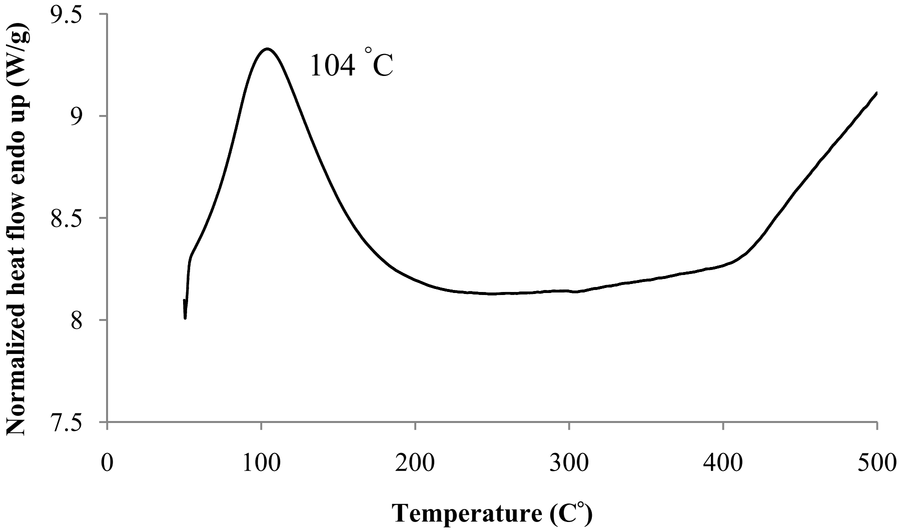

(b) Degussa P25

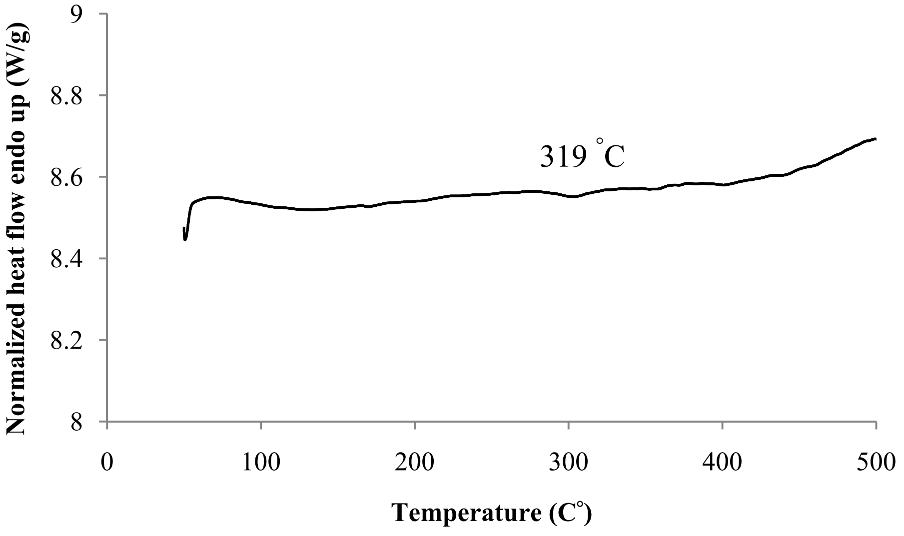

(c) Anatase

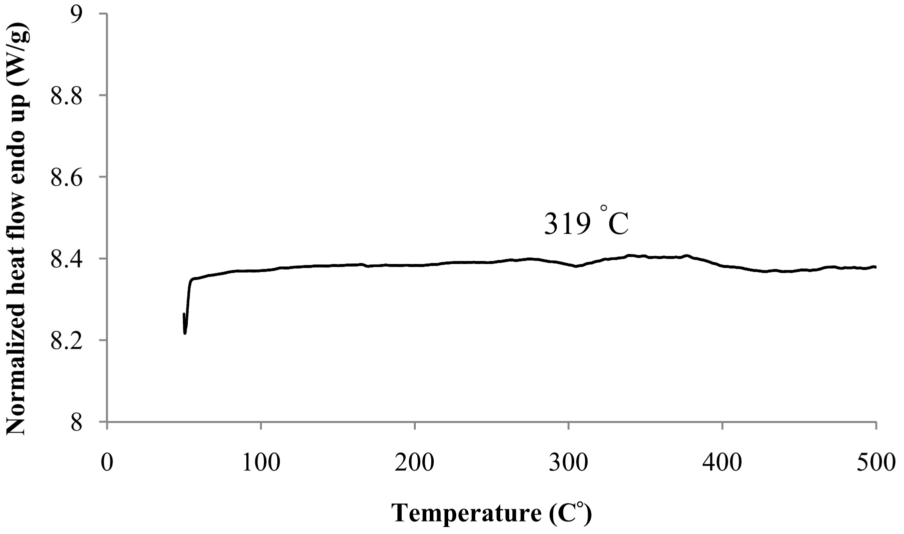

Figure 3.8 DSC spectra of TiO_2 samples; (a) amorphous TiO_2, (b) Degussa P25, (c) anatase.

3.2 Fluorine doped TiO_2 via impregnation method and the photocatalytic activity

Fluorine doped amorphous TiO_2 (F-TiO_2-imp) was prepared by the wet impregnation method using $NH_4F \cdot HF$ as a source of dopant with the aim to improve the photocatalytic activity of amorphous TiO_2. The obtained F-TiO_2-imp existed as a white powder solid and characterized by XRD, SEM, EDX, DRS, PL, BET surface area, FT-IR, TGA, and DSC techniques.

3.2.1 Characterization of fluorine doped TiO_2

3.2.1.1 X-ray diffraction (XRD)

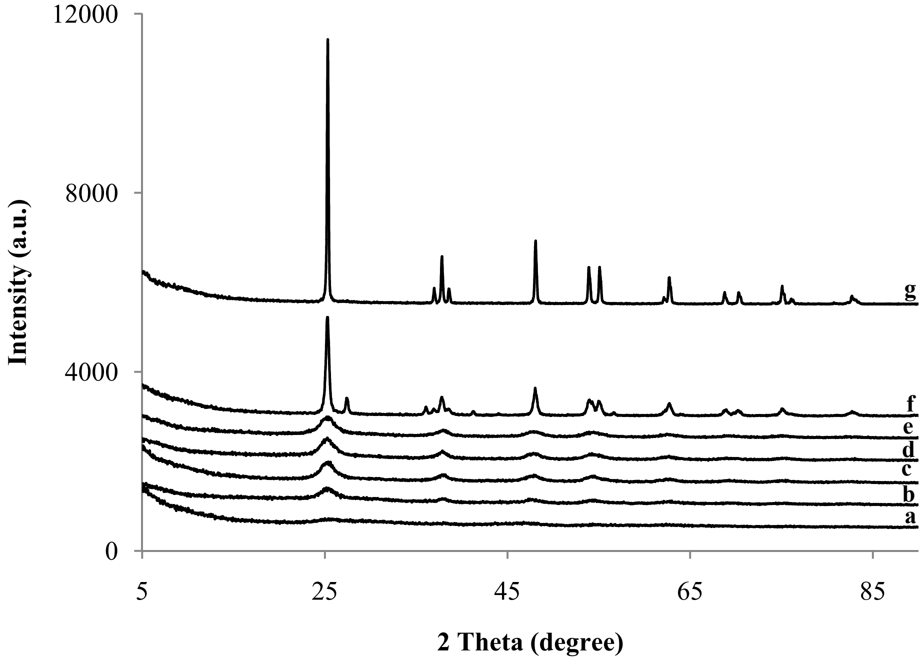

Figure 3.9 X-ray diffraction patterns of the synthesized TiO_2 powders; (a) undoped TiO_2, (b) undoped-pH 3.6, (c) 5F-TiO_2-imp, (d) 7F-TiO_2-imp, (e) 10F-TiO_2-imp, (f) Degussa P25, (g) anatase.

The X-ray diffraction patterns of the synthesized TiO_2 powders are presented in Figure 3.9. The undoped powder was amorphous TiO_2 showing a flat base line without any diffraction pattern. The doped sample F-TiO_2-imp showed broad characteristic diffraction peak of anatase phase, four characteristic peaks of 5F-TiO_2-imp are detected corresponding to the anatase phase (major peaks: 25.33°, 38.02°, 47.90°, 54.70°) with the complete absence of rutile and brookite phases. The undoped-pH 3.6 TiO_2, Figure 3.9b, shows peaks at 25.18°, 37.88°, 47.53° and 54.50°. The peaks are broad and of low intensity indicating little degree of crystallinity of the anatase phase. The broaden diffraction peak of anatase is observed and the crystal size calculated by the Scherrer equation formula from anatase peak. The crystallite sizes of the undoped-pH 3.6 TiO_2 and 5F-TiO_2-imp, calculated from the (101) peak of the XRD patterns are 11.21 and 5.64 nm, respectively. The crystallite size of Degussa P25 and anatase are larger than 5F-TiO_2-imp. Undoped-pH 3.6 and 5F-TiO_2-imp showed a small amount of crystalline anatase phase (~11.29% for undoped-pH 3.6 TiO_2, ~31.09% for 5F-TiO_2-imp).

Xu, *et al.*, (2008) studied a novel and simple method for preparing F-doped anatase TiO_2 film with high photocatalytic activity using titanium-n-butoxide and NH_4F as TiO_2 and fluorine precursors under mild condition, i.e. low temperature and ambient pressure. The prepared sample was characterized by XRD technique. It was found that the doping F atoms did not cause any shift in peak position of that of TiO_2 phase. This could be understood that the ionic radius of fluoride ion (0.133 nm) is virtually the same as the replaced oxide ion (0.132 nm).

Wang, *et al.*, (2008) studied surface-fluorinated TiO_2 particles prepared via the HF etching method. The X-ray diffraction patterns indicated that the as-prepared TiO_2 consists of a single anatase crystalline phase. No diffraction peaks due to other phases (for example, rutile or brookite TiO_2) were observed. After treating with 5% HF, no new diffraction peaks appeared and positions of the characteristic peaks of anatase TiO_2 also remained unchanged, indicating that the etching of TiO_2 by HF under the present conditions could not change the crystalline phase and that F^- was not incorporated into the bulk of TiO_2 particles. Although TiO_2 can be transformed to $TiOF_2$ by treating with a high concentration of aqueous HF (50%), HF at low concentration (5%) under the present experimental conditions seems to etch only the surface of anatase TiO_2 and, maybe, to dissolve some amorphous TiO_2.

The clues from Xu, *et al* (2008) and Wang, *et al* (2008), and support from the EDX data below led us to conclude that F element was entrapped in surface of 5F-TiO_2-imp and obviously inducing some degrees of an orderly pattern of atoms yielding the improved crystallinity of 5F-TiO_2-imp. The crystalline phase, crystallite size and crystallinity of the synthesized TiO_2 powders are summarized in Table 3.5.

Table 3.5 Phase, crystallite size and crystallinity of the synthesized TiO_2 powders.

TiO_2 samples	Phase	Crystallite size[a] (nm)	Crystallinity[b] (%)	Amorphous[c] (%)
Undoped TiO_2	Amorphous	-	-	Amorphous (100)
Undoped-pH 3.6	Amorphous, Anatase	11.21	Anatase (11.29)	Amorphous (88.71)
5F-TiO_2-imp	Amorphous, Anatase	5.64	Anatase (31.09)	Amorphous (68.91)
7F-TiO_2-imp	Amorphous, Anatase	6.31	Anatase (22.79)	Amorphous (77.21)
10F-TiO_2-imp	Amorphous, Anatase	11.84	Anatase (17.39)	Amorphous (82.61)

[a] The crystallite size was calculated by using Scherrer's equation.

[b] Determined by XRD using standard addition method, Suwanchawalit, *et al.*, 2008.

[c] The amorphous content was calculated by 100 % - Anatase %.

3.2.1.2 Electron microscopy

(1) Scanning electron microscopy (SEM)

Figure 3.10 shows the SEM images of the synthesized TiO_2 powders with different magnifications (1,000×, 5,000×, 10,000×). Amorphous undoped TiO_2 showed high agglomerated particles with various sizes of particles (Figure 3.10a). Fluorine doped TiO_2 showed variation of particles (Figure 3.10c, Figure 3.10d, and Figure 3.10e). The powders are found to be fine and slightly agglomerated. The porous structure of F-TiO_2-imp can be better seen from the SEM images with higher magnification (Figure 3.10c, (10,000×)). It should be emphasized that a small crystallites aggregate to form porous structure. The presence of porous structure might favor the improvement of the photocatalytic activity of TiO_2.

(a) Undoped TiO_2

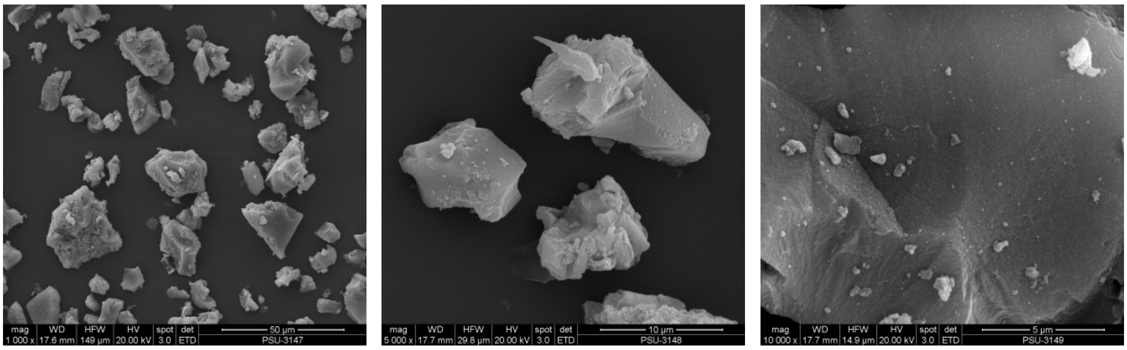

(b) Undoped -pH3.6

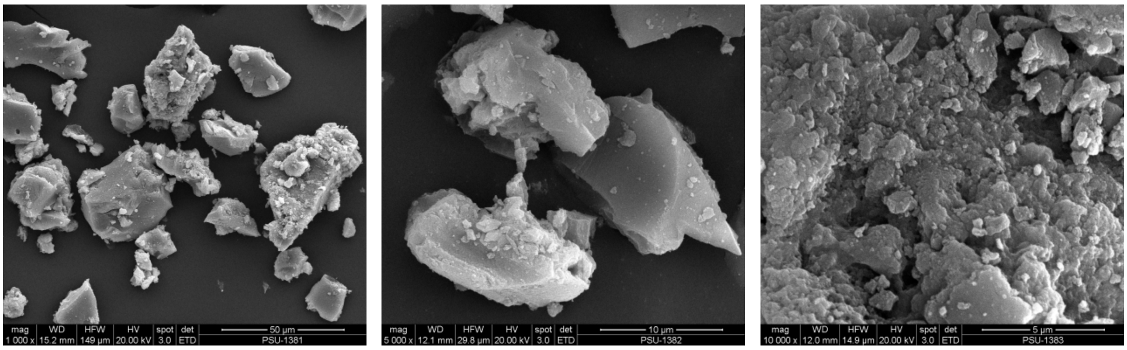

(c) 5F-TiO_2-imp

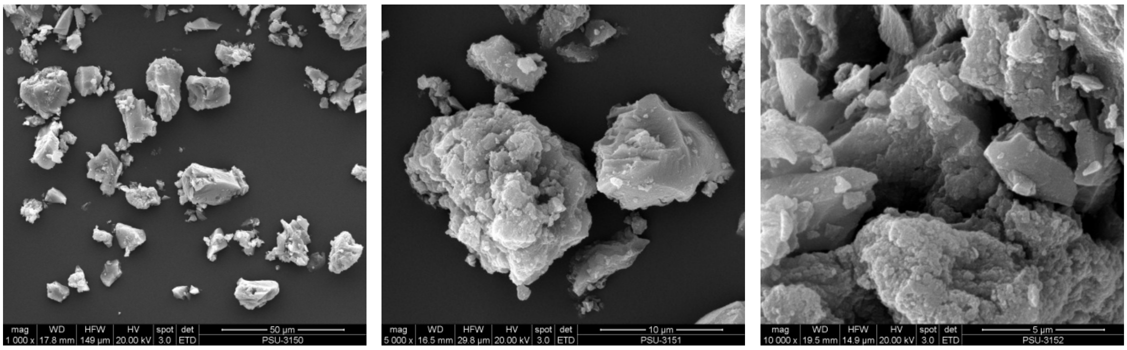

(d) 7F-TiO_2-imp

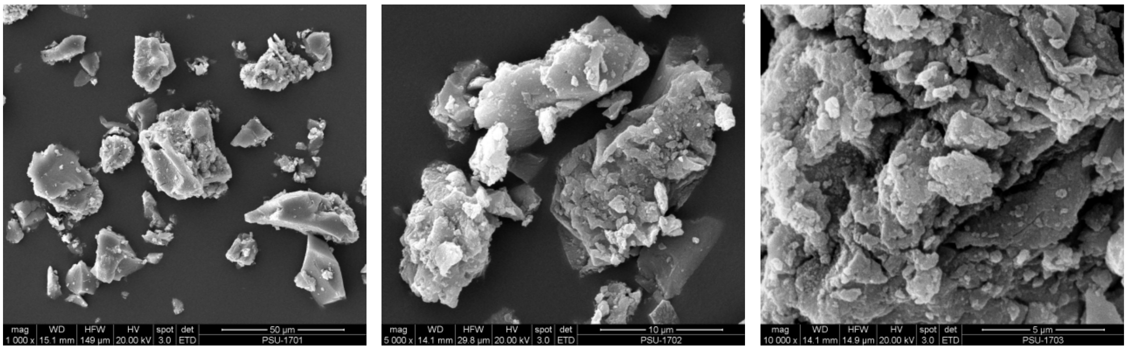

(e) 10F-TiO_2-imp

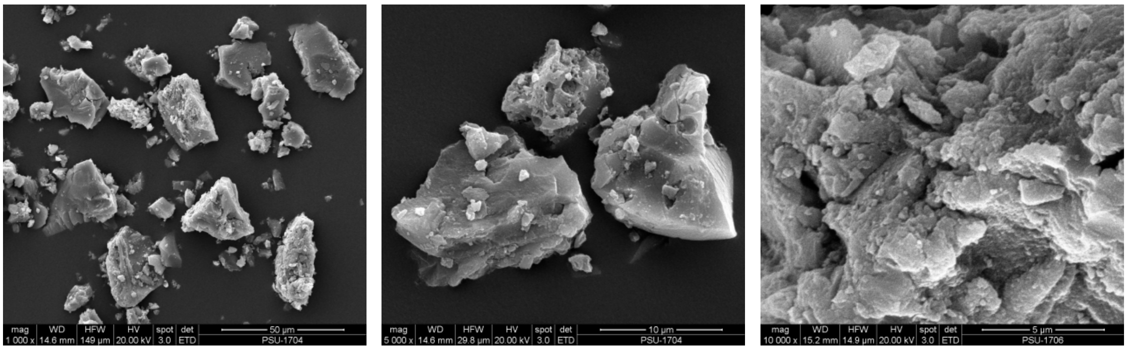

Figure 3.10 SEM images of the synthesized TiO_2 powders; (a) undoped TiO_2, (b) undoped-pH 3.6, (c) 5F-TiO_2-imp, (d) 7F-TiO_2-imp, (e) 10F-TiO_2-imp. Each sample was magnified at low (1,000×) and high (5,000× and 10,000×) magnification.

(2) Energy-dispersive X-ray spectroscopy (EDX)

Chemical composition analysis using energy-dispersive X-ray (EDX) spectroscopy (Figure 3.11a) illustrates that undoped TiO_2 are mainly composed of Ti, O and C elements. Figure 3.11b and Figure 3.11c show peak corresponding to fluorine was detected in F-TiO_2-imp.

(a) Undoped TiO_2

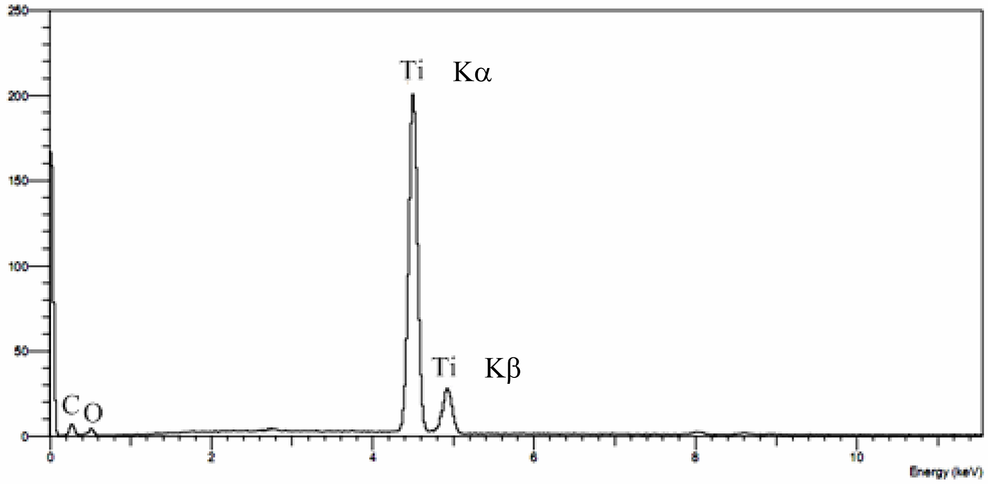

(b) 5F-TiO_2-imp

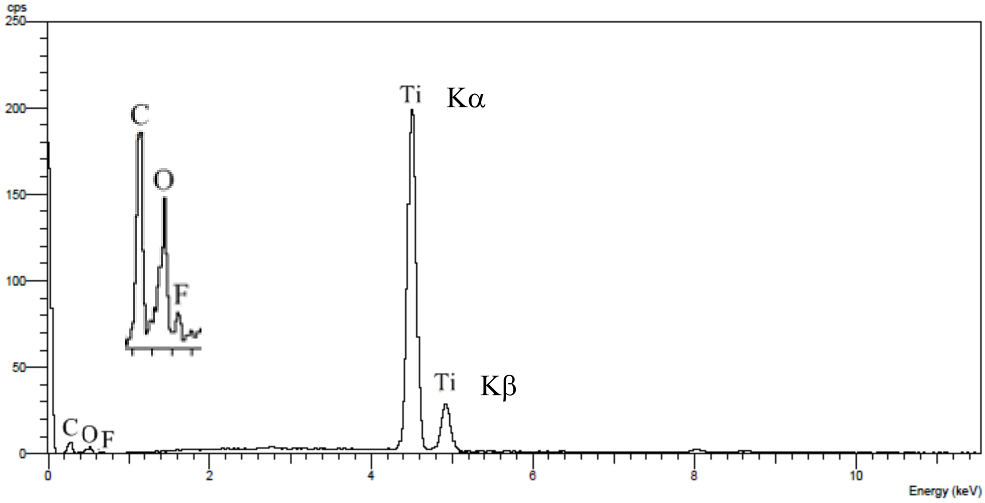

(c) 10F-TiO_2-imp

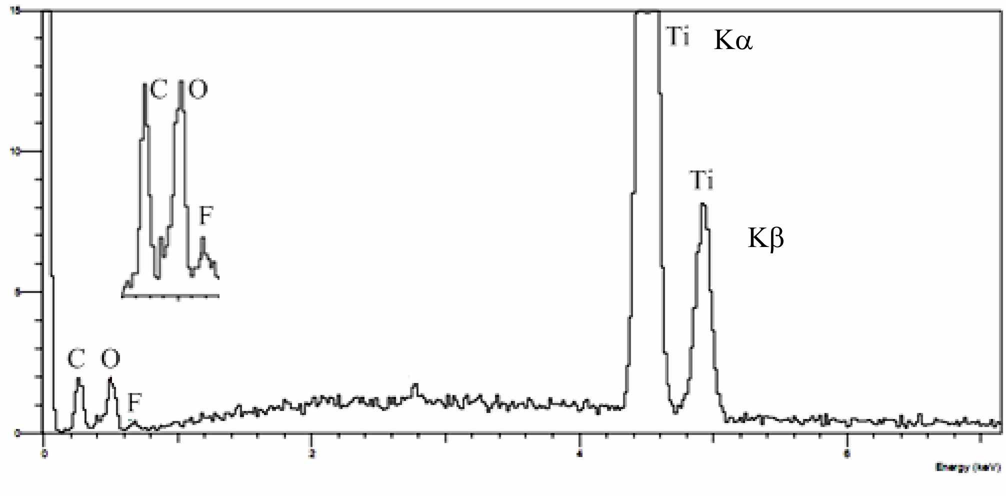

Figure 3.11 EDX spectra of the synthesized TiO_2 powders; (a) undoped TiO_2, (b) 5F-TiO_2-imp, (c) 10F-TiO_2-imp.

(3) Elemental mapping

Elemental mapping using characteristic X-ray intensity measured relative to lateral position on the sample. Variations in X-ray intensity at any characteristic energy value indicate the relative concentration for the applicable element across the surface. One or more maps are recorded simultaneously using image brightness intensity as a function of the local relative concentration of the element present (Jensen, 1982; (http://mee-inc.com/eds.html)).

(a) 5F-TiO_2-imp

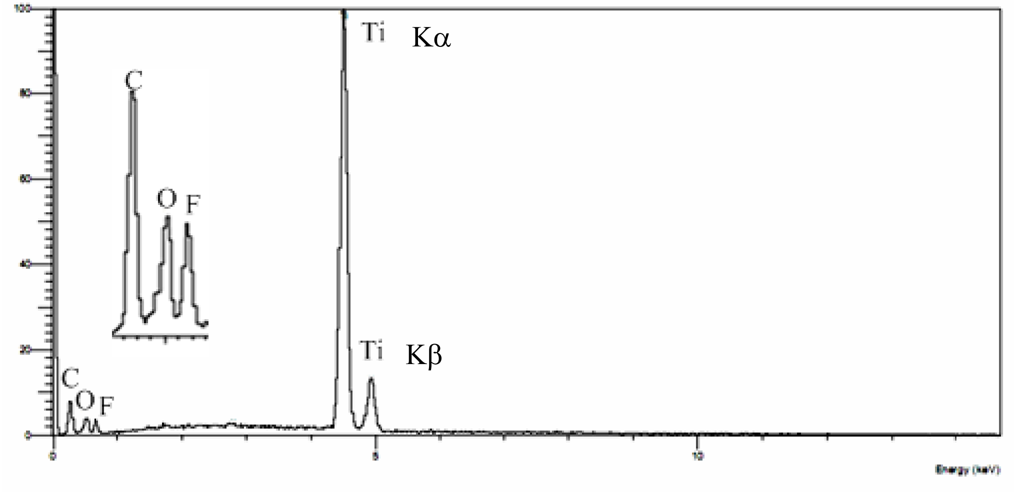

(b) 5F-TiO_2-imp

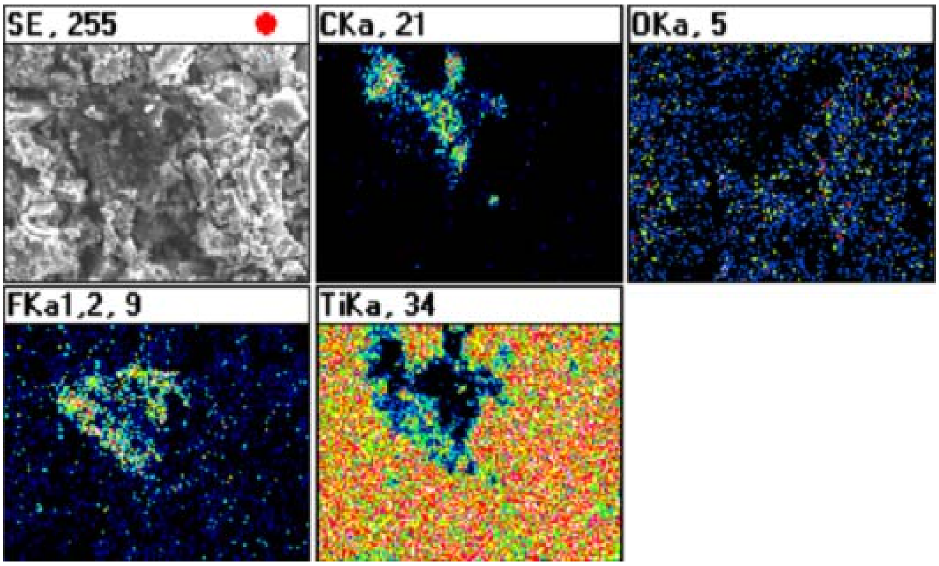

Figure 3.12 EDX mapping image of 5F-TiO_2-imp; (a) EDX spectrum and (b) elemental profile of 5F-TiO_2-imp.

Figure 3.12 shows EDX data of Ti, O, C and F elements and the high resolution EDX mapping analysis corresponding to Ti elements and a top layer that contains of Ti element. Figure 3.12b indicating C, O and F element located on the titanium outer surface. 5F-TiO_2-imp showed high fluorine content on the surface in some positions. F element showed high agglomerated particles and relatively intensity of spectra. In the impregnation method, the ion substitution may take place on the surfaces instead of in the bulk TiO_2 crystals (Qiu, *et al.*, 2006) From these results, it can be assumed that F element was entrapped in surface of 5F-TiO_2-imp.

3.2.1.3 Diffused reflectance UV-Vis spectroscopy (DRS)

The UV-visible DRS spectra of the synthesized TiO_2 powders are shown in Figure 3.13. It was also demonstrated that the absorption edge of F-TiO_2-imp shifted toward a longer wavelength than that of undoped amorphous TiO_2 and undoped-pH 3.6 TiO_2. The band gap energy was calculated by the formula E_g (eV) = 1240/λ. The band gap energy of amorphous undoped TiO_2 and 5F-TiO_2-imp were 3.20 and 3.13 eV, respectively. It can be concluded that the absorption edge shifted toward longer wavelength indicating a decrease in the band gap energy of TiO_2. The data of wavelength at onset of absorbance and band gap energy of the synthesized TiO_2 powders are summarized in Table 3.6.

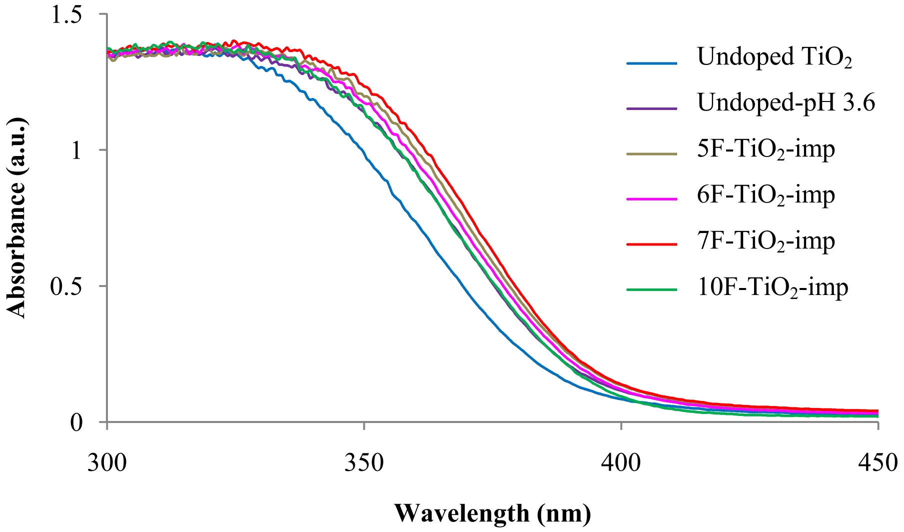

Figure 3.13 Diffused reflectance UV-Vis spectra of the synthesized TiO_2 powders.

Table 3.6 The wavelength at onset of absorption and the band gap energy of the synthesized TiO_2 powders.

TiO_2 samples	DRS	
	λ_{onset} of absorption (nm)	E_g (eV)
Undoped TiO_2	388	3.20
Undoped-pH 3.6	393	3.16
5F-TiO_2-imp	396	3.13
6F-TiO_2-imp	396	3.13
7F-TiO_2-imp	397	3.12
10F-TiO_2-imp	393	3.16

3.2.1.4 Photoluminescence spectroscopy (PL)

PL emission spectra have been widely used to investigate the efficiency of charge carrier trapping, immigration, transfer, and to understand the fate of electron-hole pairs in semiconductor particles (Xu, *et al.*, 2008). Photoluminescence spectra of the synthesized TiO_2 powders are shown in Figure 3.14. The band gap energy of TiO_2 samples were calculated by the Planck's equation. The photoluminescence spectra of amorphous undoped TiO_2 and 5F-TiO_2-imp show the sharp UV emission at 388 nm and 396 nm, respectively. The peak at 650 nm could be ascribed to electron transition mediated by defects level in the band gap (Suwanchawalit and Wongnawa, 2008). It was found that the band gap energy of amorphous undoped TiO_2 and 5F-TiO_2-imp were 3.20 and 3.13 eV, respectively. The data of wavelength at emission of absorption and the band gap energy of the synthesized TiO_2 powders are summarized in Table 3.7.

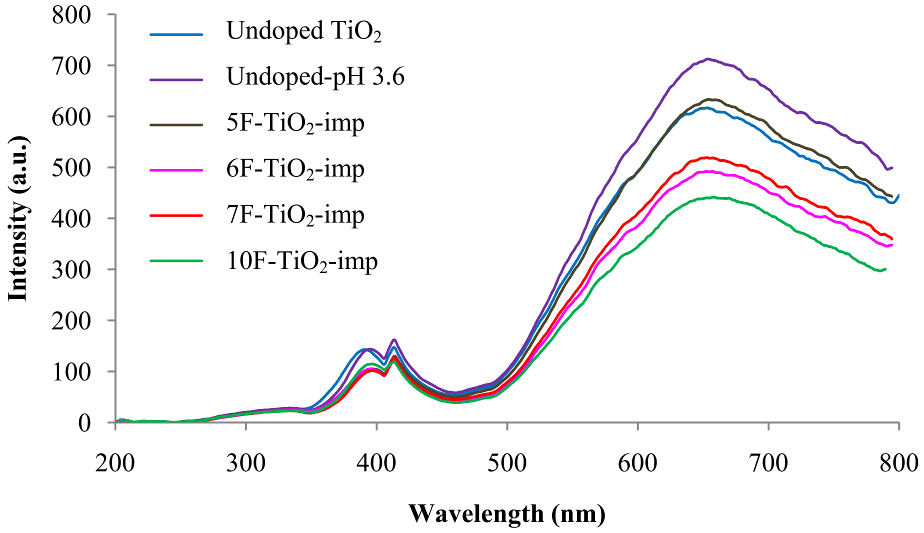

Figure 3.14 Photoluminescence spectra of the synthesized TiO_2 powders.

Table 3.7 The wavelength at emission of absorption and the band gap energy of the synthesized TiO_2 powders.

TiO_2 samples	PL	
	$\lambda_{emission}$ (nm)	E_g (eV)
Undoped TiO_2	388	3.20
Undoped-pH 3.6	394	3.15
5F-TiO_2-imp	396	3.13
6F-TiO_2-imp	396	3.13
7F-TiO_2-imp	397	3.12
10F-TiO_2-imp	395	3.14

3.2.1.5 BET surface area (BET method)

The surface area of the synthesized TiO_2 powders and the pore size distribution were studied by N_2 adsorption-desorption using BET and BJH methods. The BET surface areas and particle size of the synthesized TiO_2 powders are reported in Table 3.8. Amorphous undoped TiO_2 exhibited higher surface area than F-TiO_2-imp and they ranged from 478.41 to 161.98 m^2g^{-1}.

Table 3.8 BET surface area and particle size of the synthesized TiO_2 powders.

TiO_2 samples	Surface area (m^2g^{-1})	Particle size[a] (nm)
Undoped TiO_2	478.41	3.33
Undoped-pH 3.6	265.67	5.79
5F-TiO_2-imp	274.85	5.60
7F-TiO_2-imp	227.18	6.77
10F-TiO_2-imp	161.98	9.49

[a] Determined by BET using D = 6000/(ρ × BET surface area), where ρ is approximated to be 3.90 g/cm^3 of anatase density. (The true value of ρ of amorphous is not known, however, it should be slightly less than that of anatase. In this calculation, we can only use the approximated value.)

The BET surface areas of amorphous undoped TiO_2 and 5F-TiO_2-imp are 478.41 and 274.85 m^2g^{-1}, respectively. Degussa P25 has been used as a standard material which has a surface area of 50 m^2g^{-1} (Saadoun, *et al.*, 2000; Kanna, *et al.*, 2010). The surface area of amorphous TiO_2 is much higher than that of commercially available (Degussa P25, anatase) due to its amorphous morphology. The N_2 adsorption-desorption isotherm of the synthesized TiO_2 powders are shown in Figure 3.15. The isotherm is type I, characteristic of microporous materials. Type I isotherms are given by microporous solids having relatively small external surfaces, the limiting uptake being governed by the accessible micropore volume rather than by the internal surface area (Sing, *et al.*, 1985). It was found that, undoped-pH 3.6 TiO_2, 7F-TiO_2-imp and 7F-TiO_2-imp show the isotherm of type IV. T-plot of N_2 adsorption isotherm of the synthesized TiO_2 powders are shown in Figure 3.16. The t-plot data of the synthesized TiO_2 powders showed straight line passing the origin. The synthesized TiO_2 powders showed microporous structure. The presence of porosity is also documented using t-plots comparing the volume of nitrogen adsorbed on a sample to that adsorbed on a nonporous standard. The t-value is the statistical thickness of the adsorbed gas layer as calculated at a given value of p/p° for a nonporous standard adsorbent. The volume of microporosity can be determined from the intercept of the first straight line segment. If the sample isotherm is identical with that of the standard, the t-plot will be linear and pass through the origin (Brantley and Mollott, 2000). The pore size distribution (BJH) of the synthesized TiO_2 powders is shown in Figure 3.17. The pore size distribution plot calculated using the Barrett-Joyner-Halenda (BJH) equation exhibits a narrow pore size distribution with an average pore diameter at *ca.* 5-10 nm.

(1) N_2 adsorption isotherm of the synthesized TiO_2 powders

(a) Undoped TiO_2

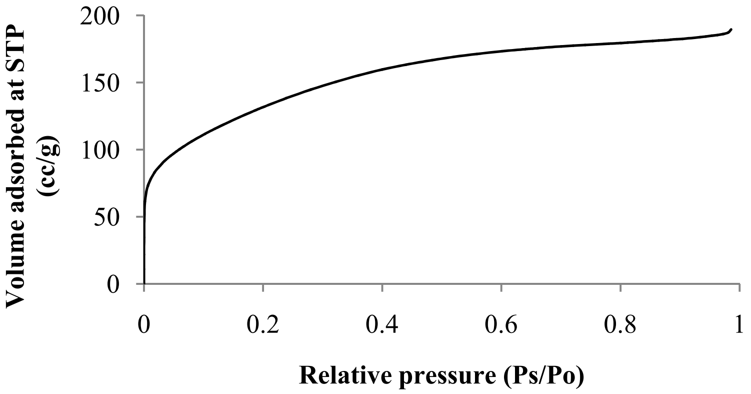

(b) Undoped-pH 3.6

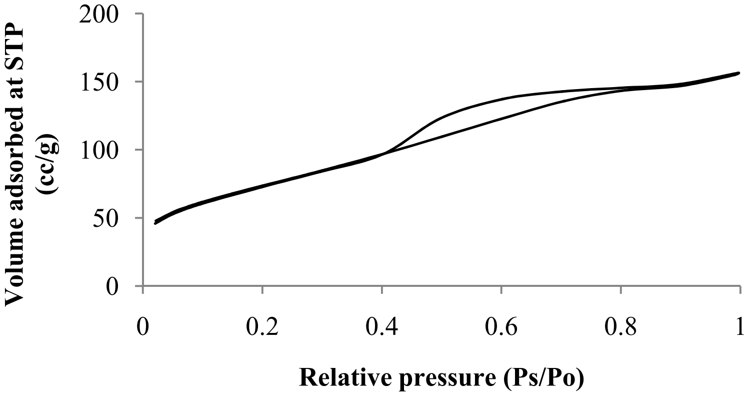

(c) 5F-TiO$_2$-imp

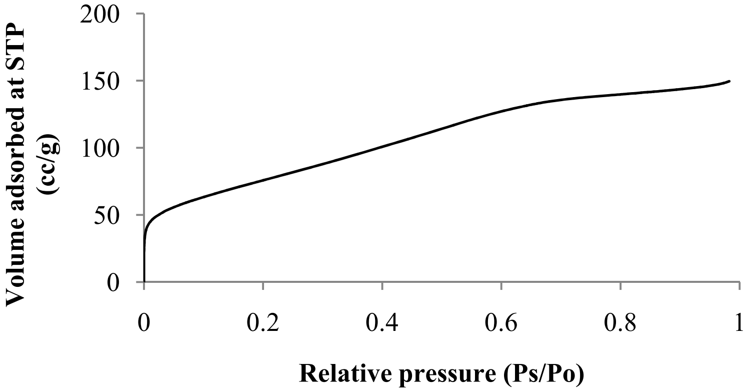

(d) 7F-TiO$_2$-imp

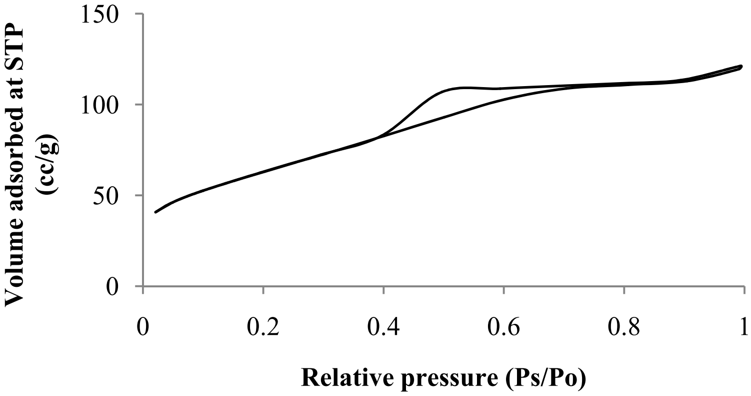

(e) 10F-TiO$_2$-imp

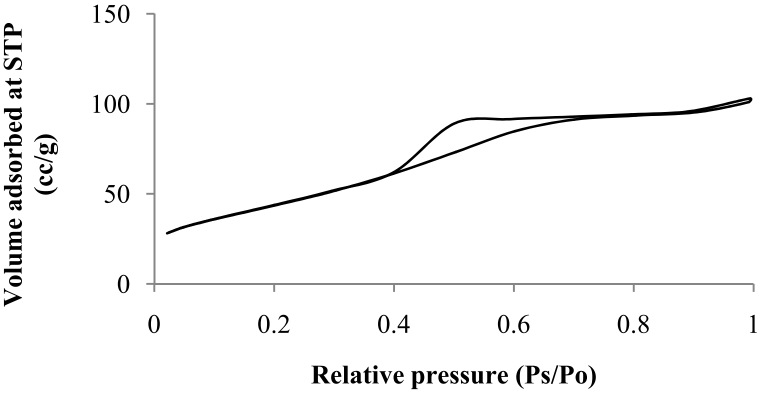

Figure 3.15 N_2 adsorption isotherm of the synthesized TiO$_2$ powders; (a) undoped TiO$_2$, (b) undoped-pH 3.6, (c) 5F-TiO$_2$-imp, (d) 7F-TiO$_2$-imp, (e) 10F-TiO$_2$-imp.

(2) T-plot of N_2 adsorption isotherm of the synthesized TiO_2 powders

(a) Undoped TiO_2

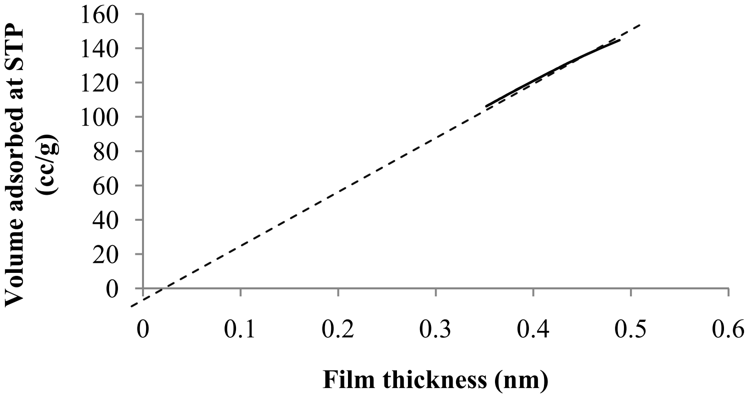

(b) Undoped-pH 3.6

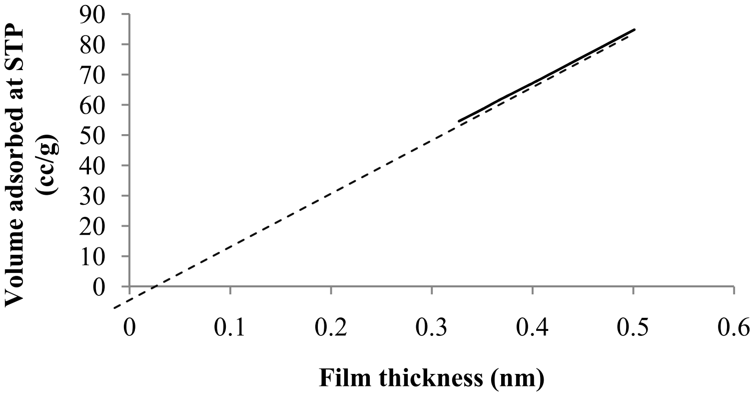

(c) 5F-TiO_2-imp

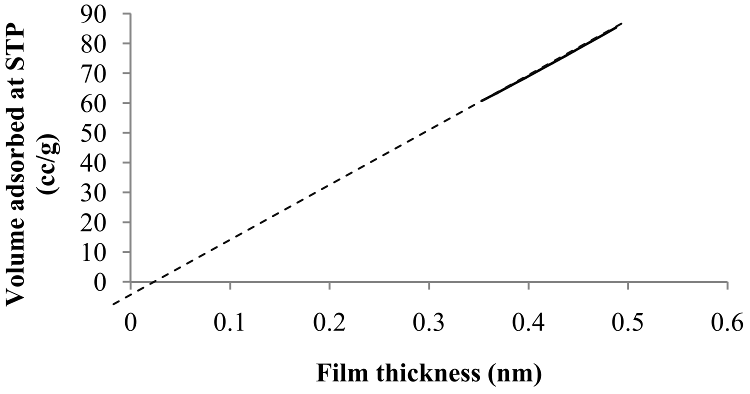

(d) 7F-TiO_2-imp

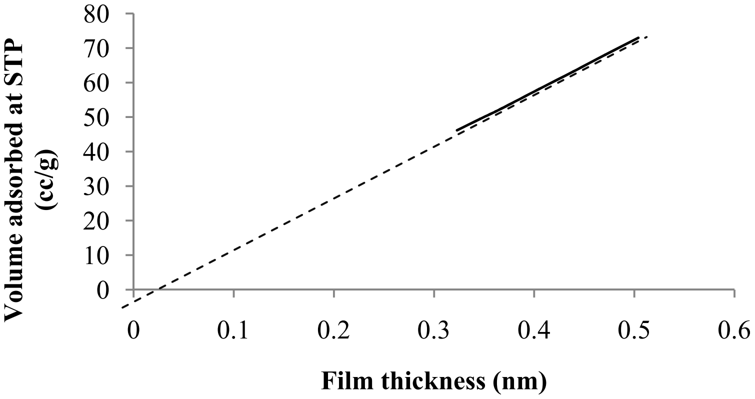

(e) 10F-TiO_2-imp

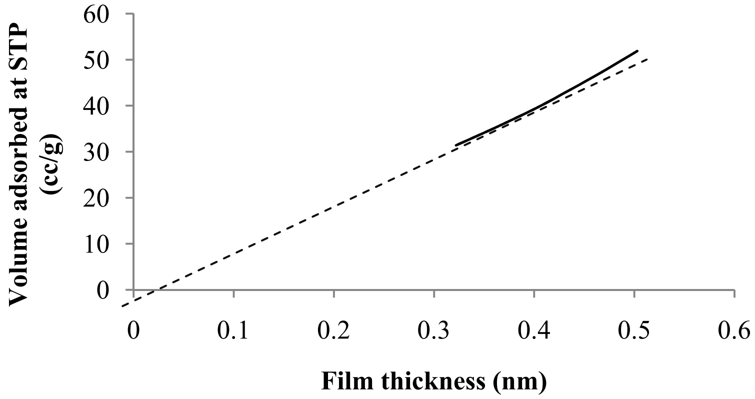

Figure 3.16 T-plot of N_2 adsorption isotherm of the synthesized TiO_2 powders; (a) undoped TiO_2, (b) undoped-pH 3.6, (c) 5F-TiO_2-imp, (d) 7F-TiO_2-imp, (e) 10F-TiO_2-imp.

(3) Pore size distribution curve of the synthesized TiO_2 powders

(a) Undoped TiO_2

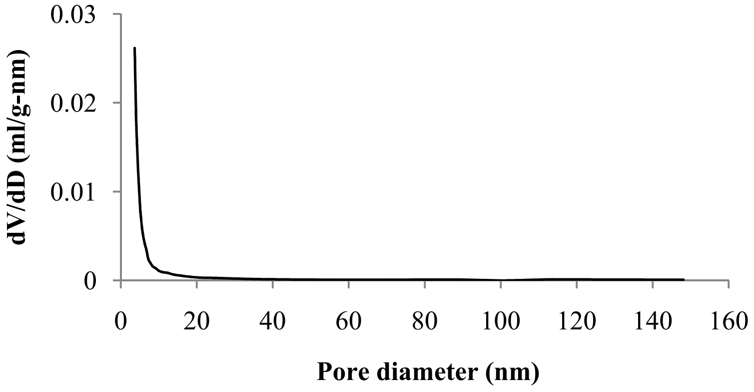

(b) Undoped-pH 3.6

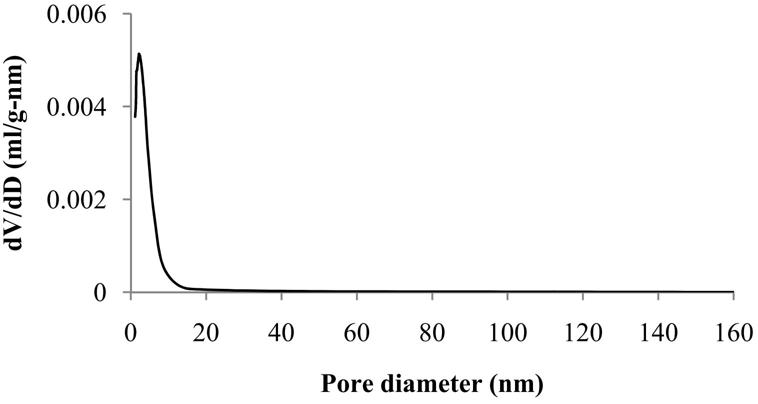

(c) 5F-TiO_2-imp

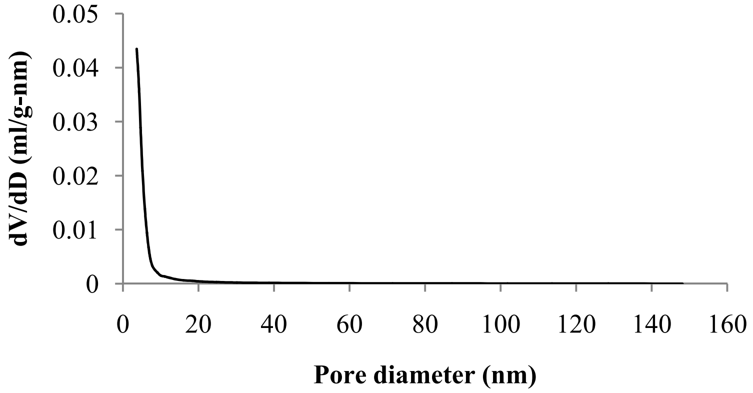

(d) 7F-TiO_2-imp

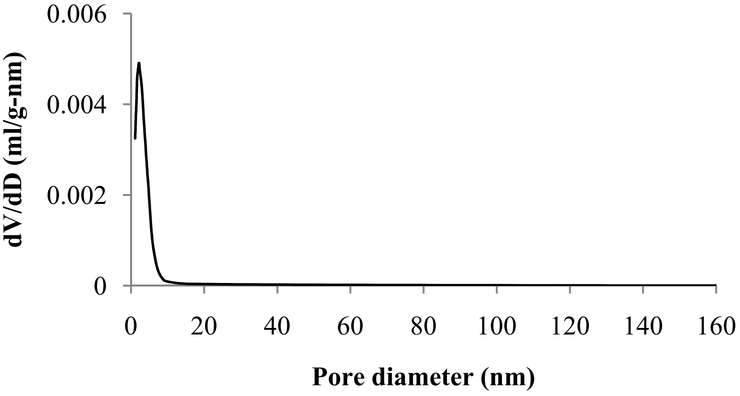

(e) 10F-TiO_2-imp

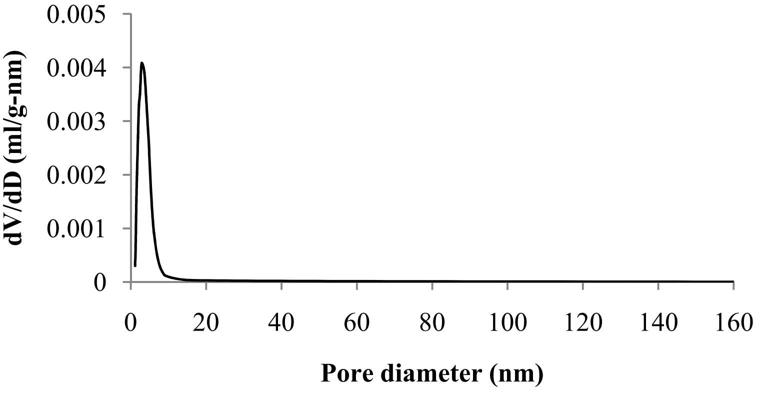

Figure 3.17 Pore size distribution curve of the synthesized TiO_2 powders; (a) undoped TiO_2, (b) undoped-pH 3.6, (c) 5F-TiO_2-imp, (d) 7F-TiO_2-imp, (e) 10F-TiO_2-imp.

3.2.1.6 Fourier-transformed infrared spectroscopy (FT-IR)

The FT-IR spectra of the synthesized TiO_2 powders are shown in Figure 3.18 which can provide the information of functional groups on the surface of materials. In the FT-IR spectrum of the synthesized TiO_2 powders, there are four apparent vibrational bands at 3500-3000, 1640, 1404, and 800-400 cm^{-1}. The bands in the range of 800-400 cm^{-1} are the characteristic of the O-Ti-O lattice (Huo, *et al.*, 2009) and the bands at 1404 cm^{-1} are attributed to NH_4^+ (Youn, *et al.*, 1999). The band at 1640 cm^{-1} is ascribed to the bending vibration absorption of free water (Xu, *et al.*, 2008) and 3500-3000 cm^{-1} is attributed to the stretching vibration absorption of hydroxyl function groups (Zhu, *et al.*, 2007). The FT-IR investigation indicates that F-TiO_2-imp has less surface OH groups and NH_4^+ group as they were replaced by F element which was entrapped at the surface of F-TiO_2-imp. However, no evidence for Ti-F vibration could be found in F-TiO_2-imp. The data of vibrational bands, assignments, functional groups and literatures of TiO_2 samples are summarized in Table 3.9.

(a) Undoped TiO_2

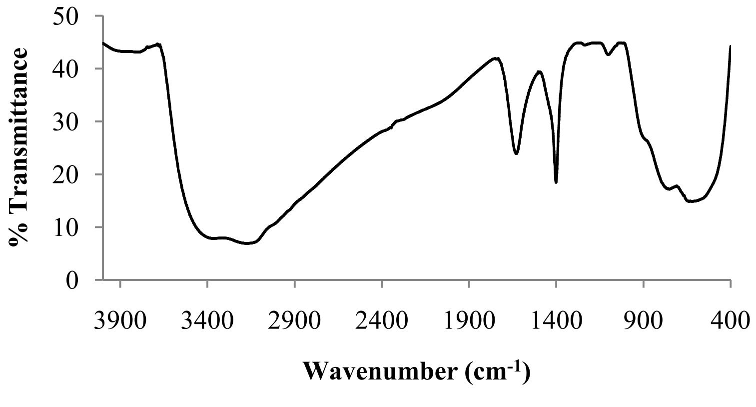

(b) Undoped-pH 3.6

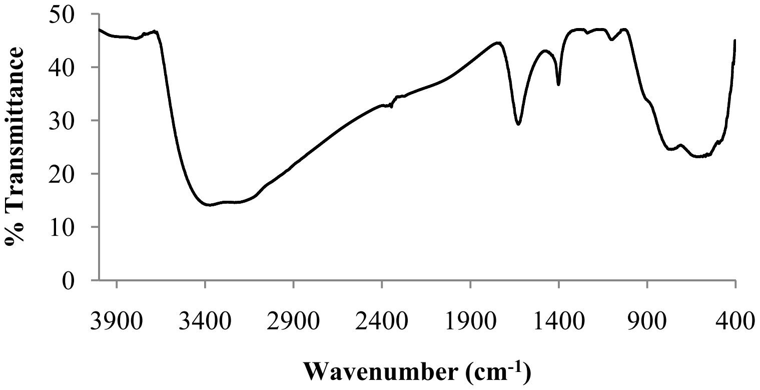

(c) 5F-TiO$_2$-imp

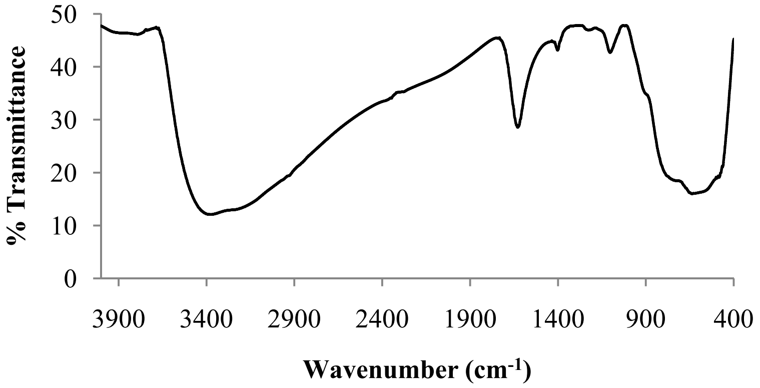

(d) 6F-TiO$_2$-imp

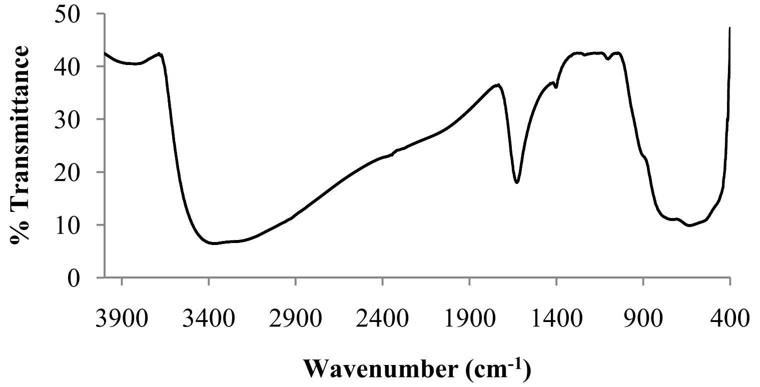

(e) 7F-TiO_2-imp

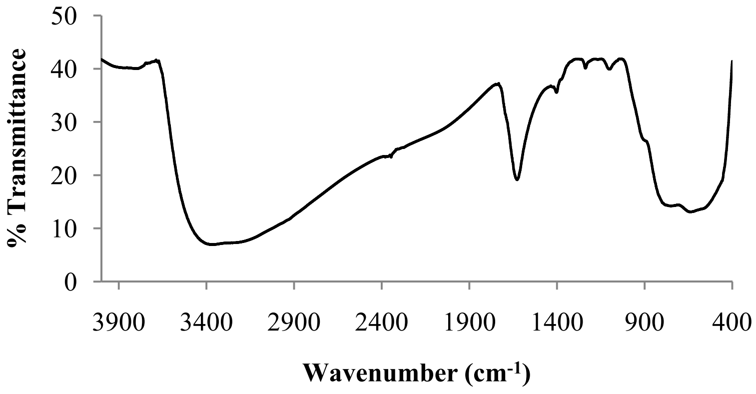

(f) 10F-TiO_2-imp

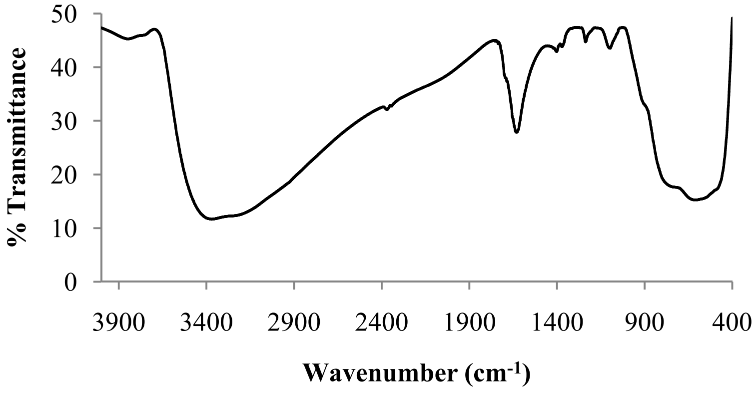

Figure 3.18 FT-IR spectra of the synthesized TiO_2 powders; (a) undoped TiO_2, (b) undoped-pH 3.6, (c) 5F-TiO_2-imp, (d) 6F-TiO_2-imp, (e) 7F-TiO_2-imp, (f) 10F-TiO_2-imp.

Table 3.9 The FT-IR bands of the synthesized TiO_2 powders.

TiO_2	Vibrational bands (cm^{-1})	Assignments	Functional groups	Literatures
Undoped TiO_2	3500-3000	ν_{OH} and ν_{NH}	H_2O and NH_4^+	Zhu, *et al.*, 2007
	2385	ν_{co}	CO_2	Liao, *et al.*, 2003
	1644	δ_{OH}	OH groups	Xu, *et al.*, 2008
	1404	δ_{NH}	NH_4^+ group	Youn, *et al.*, 1999
	below 800	$\nu_{Ti\text{-}O}$	Ti-O bond	Huo, *et al.*, 2009

Table 3.9 The FT-IR bands of the synthesized TiO_2 powders. (Continued)

TiO_2	Vibrational bands (cm^{-1})	Assignments	Functional groups	Literatures
Undoped-pH 3.6	3500-3000	ν_{OH} and ν_{NH}	H_2O and NH_4^+	Zhu, *et al.*, 2007
	2380	ν_{co}	CO_2	Liao, *et al.*, 2003
	1647	δ_{OH}	OH groups	Xu, *et al.*, 2008
	1407	δ_{NH}	NH_4^+ group	Youn, *et al.*, 1999
	below 800	$\nu_{Ti\text{-}O}$	Ti-O bond	Zhu, *et al.*, 2007
5F-TiO_2-imp	3500-3000	ν_{OH} and ν_{NH}	H_2O and NH_4^+	Zhu, *et al.*, 2007
	2389	ν_{co}	CO_2	Liao, *et al.*, 2003
	1647	δ_{OH}	OH groups	Xu, *et al.*, 2008
	1452	δ_{NH}	NH_4^+ group	Youn, *et al.*, 1999
	below 800	$\nu_{Ti\text{-}O}$	Ti-O bond	Huo, *et al.*, 2009
6F-TiO_2-imp	3500-3000	ν_{OH} and ν_{NH}	H_2O and NH_4^+	Zhu, *et al.*, 2007
	2382	ν_{co}	CO_2	Liao, *et al.*, 2003
	1661	δ_{OH}	OH groups	Xu, *et al.*, 2008
	1461	δ_{NH}	NH_4^+ group	Youn, *et al.*, 1999
	below 800	$\nu_{Ti\text{-}O}$	Ti-O bond	Zhu, *et al.*, 2007
7F-TiO_2-imp	3500-3000	ν_{OH} and ν_{NH}	H_2O and NH_4^+	Zhu, *et al.*, 2007
	2385	ν_{co}	CO_2	Liao, *et al.*, 2003
	1646	δ_{OH}	OH groups	Xu, *et al.*, 2008
	1462	δ_{NH}	NH_4^+ group	Youn, *et al.*, 1999
	below 800	$\nu_{Ti\text{-}O}$	Ti-O bond	Huo, *et al.*, 2009
10F-TiO_2-imp	3500-3000	ν_{OH} and ν_{NH}	H_2O and NH_4^+	Zhu, *et al.*, 2007
	2385	ν_{co}	CO_2	Liao, *et al.*, 2003
	1650	δ_{OH}	OH groups	Xu, *et al.*, 2008
	1465	δ_{NH}	NH_4^+ group	Youn, *et al.*, 1999
	below 800	$\nu_{Ti\text{-}O}$	Ti-O bond	Hamadanian, *et al.*, 2010

3.2.1.7 Thermogravimetric analyzer (TGA)

Thermogravimetric analysis (TGA) is important in studying the transformation of the synthesized TiO_2 powders in a thermal process. Figure 3.19 shows the TGA spectra of the synthesized TiO_2 powders in the range of 50-1000 °C. In the TGA spectra of undoped-pH 3.6 (Figure 3.19a), the weight loss is about 22.3% from 34.6 to 264 °C, which represents the evaporation of water and alcohol. In the temperature range of 264-650 °C, the weight loss is about 2.9%, which is due to the removal of strongly bound water or surface hydroxyl groups. The TGA results of 5F-TiO_2-imp in Figure 3.19b show that the weight loss is about 18.75% from 59 to 209 °C which represents the evaporation of water and organic solvent. In the temperature range of 209-479 °C, the weight loss is about 3.6%, which is due to the removal of strongly bound water or surface hydroxyl groups and the weight loss of 1.31% in the range of 479-700 °C corresponds to the oxidation of carbon residue and evaporation of chemisorbed water. These results are in accordance with the values found in the literature of Todorova, *et al.*, 2008 and Yu, *et al.*, 2002.

Todorova, *et al.*, (2008) studied nanocrystalline F-doped TiO_2 powders prepared by the sol-gel route. The thermal behavior of the powders was recorded by DTA/TG technique. For the undoped TiO_2, the first is the main loss of weight (22.3%) that took place between 30 and 180 °C and it was related to the evaporation of water and alcohol included in the xerogel. The second (2.5%) and the third (0.4%) weak losses took place between 180-430 °C and 430-675 °C, respectively, during which the remained water and organics (2.9%) were gradually removed from the powders.

Yu, *et al.*, (2002) synthesized fluorine doped TiO_2 photocatalyst with anatase and brookite phase by hydrolysis of titanium tetraisopropoxide in a mixed NH_4F-H_2O solution. The TG curve can be divided into three stages. The first stage is from room temperature to 200 °C, over which the mass loss is the greatest. A mass loss of up to 8.8% was observed, which was caused by dehydration and evaporation of alcohol from the xerogels. The second stage is from 200 to 400 °C, where the mass loss is 2.5%. This can be assigned to the combustion and carbonization of most organic contents in the xerogels. The third stage is from 400 to 650 °C, where the mass loss is about 0.9%. This is attributed to the oxidation of carbon residue and evaporation of chemisorbed water.

(a) Undoped-pH 3.6

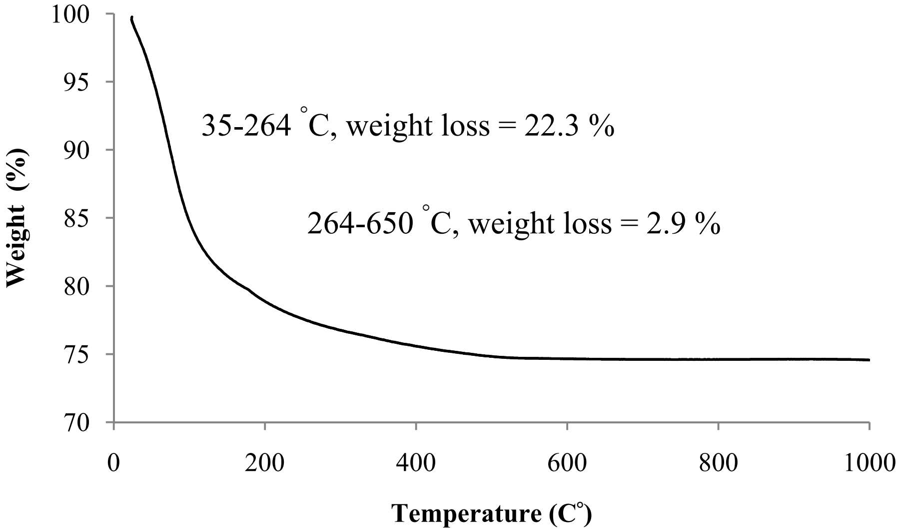

(b) 5F-TiO_2

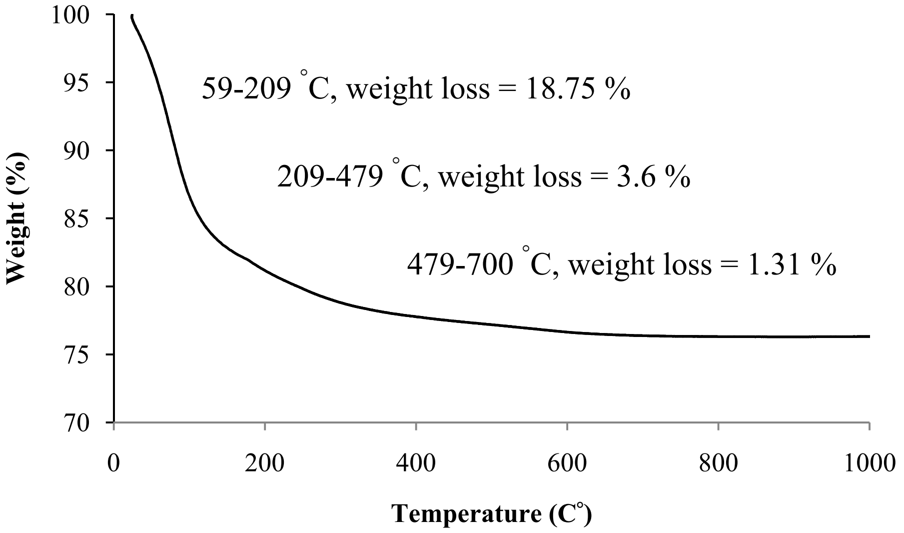

Figure 3.19 TGA spectra of the synthesized TiO_2 powders were measured at a heating rate of 10 °C/min; (a) undoped-pH 3.6, (b) 5F-TiO_2-imp.

3.2.1.8 Differential scanning calorimetry (DSC)

Figure 3.20 shows the DSC spectra of the synthesized TiO_2 powders in the range of 50-500 °C and heating rate of 10 °C /min. In the DSC spectra of undoped-pH 3.6-imp (Figure 3.20a), there are two endothermic peaks at 101 and 427 °C. The endothermic peak at 101 °C corresponds to the desorption of water and alcohol. The endothermic peak at 427 °C corresponds to the decomposition of organic substances. DSC spectra of 5F-TiO_2-imp (Figure 3.20b), the endothermic peak at 97 °C corresponds to the desorption of water and alcohol. The exothermic peak at 284 °C corresponds to the decomposition of organic substances and the exothermic peak at 388 °C can be attributed to formation of anatase phase and it exhibits good crystalline because F accelerates amorphous to be an anatase phase transformation. The results in this work was similar to the results from Yu, *et al.*, (2002) who prepared F^--doped TiO_2 powders and characterized by differential thermal analysis-thermogravimetry (DTA-TG). A broad endothermic peak exists at around 100 °C due to the desorption of water and alcohol. The relatively small exothermic peak at 261 °C comes from the decomposition of organic substances contained in the xerogel. At about 400 °C, a small exothermic peak is observed due to further crystallization or formation of anatase phase.

(a) Undoped-pH 3.6

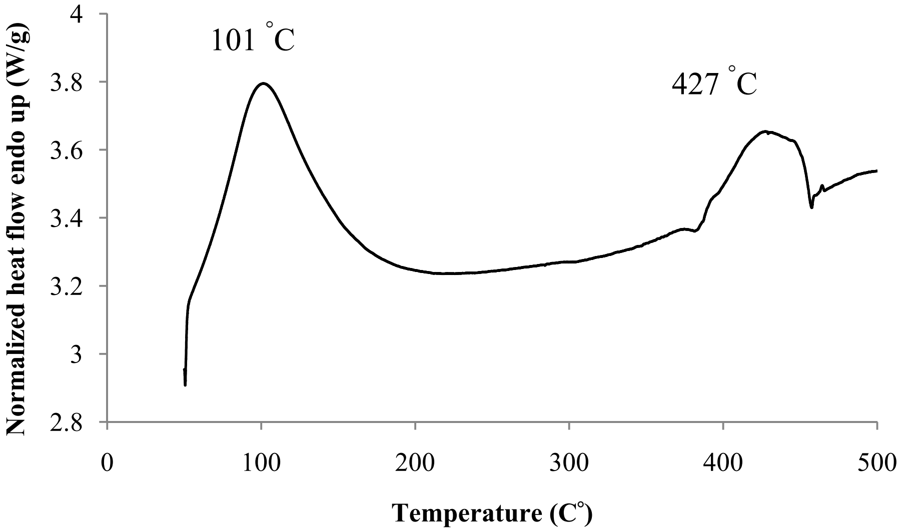

(b) 5F-TiO_2-imp

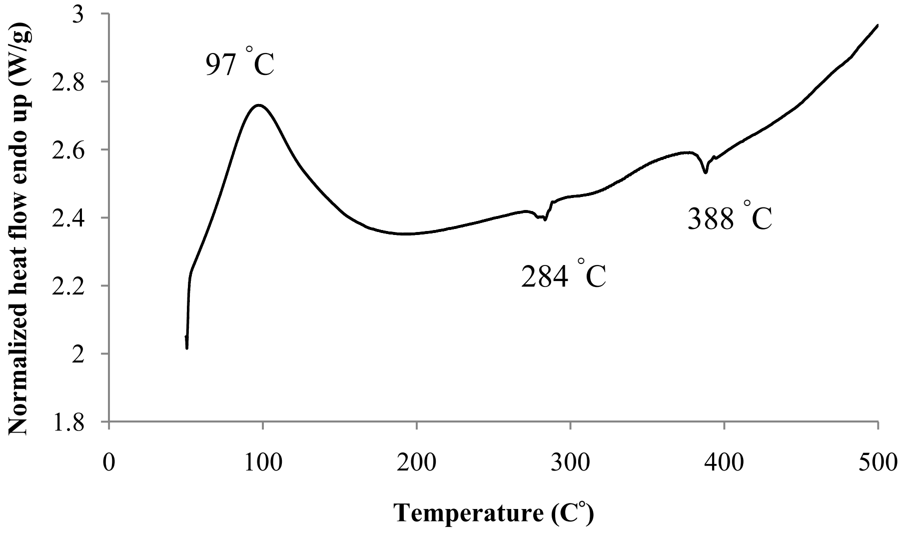

Figure 3.20 DSC spectra of the synthesized TiO_2 powders; (a) undoped-pH 3.6, (b) 5F-TiO_2-imp.

3.2.2 The pH of the point of zero charge (pH_{pzc})

The suspensions were prepared by adding Degussa P25 (0.1 gL^{-1}) and NaCl solution and then stirred for 3 h. The pH of 0.01 M NaCl solution was adjusted using 0.1M HCl or 0.1M NaOH. The point of zero charge (pH_{pzc}) of TiO_2 samples were determined by measuring the final pH and plotted as a function of initial pH. It was found that almost all the change in the pH occurred within 2 h (Figure 3.21) and the system equilibrated for 3 h after the pH reached a new value (pH_{final}). In this work, the pH_{pzc} value was determined by two methods. The first one is the pH drift method and the second is the salt addition method. Similar pH_{pzc} values were obtained from both methods. The pH_{pzc} of Degussa P25 are shown in Figure 3.22 and Figure 3.23. The pH_{pzc} for Degussa P25 is 6.8 which agrees with the literature value of 6.8 ± 0.2 (Dutta, *et al.*, 2004; Zhou, *et al.*, 2006). The pH_{pzc} of TiO_2 samples are shown in Figure 3.24 and Figure 3.25 and the values are summarized in Table 3.10. It can be concluded that the pH_{pzc} values of F-TiO_2-imp are lower than that of Degussa P25. The pH_{pzc} value of the F-TiO_2-imp is significantly different from that of the undoped

TiO_2 and undoped-pH 3.6. Furthermore, with the increase of F dopant concentration for F-TiO_2-imp, the pH_{pzc} value decreased.

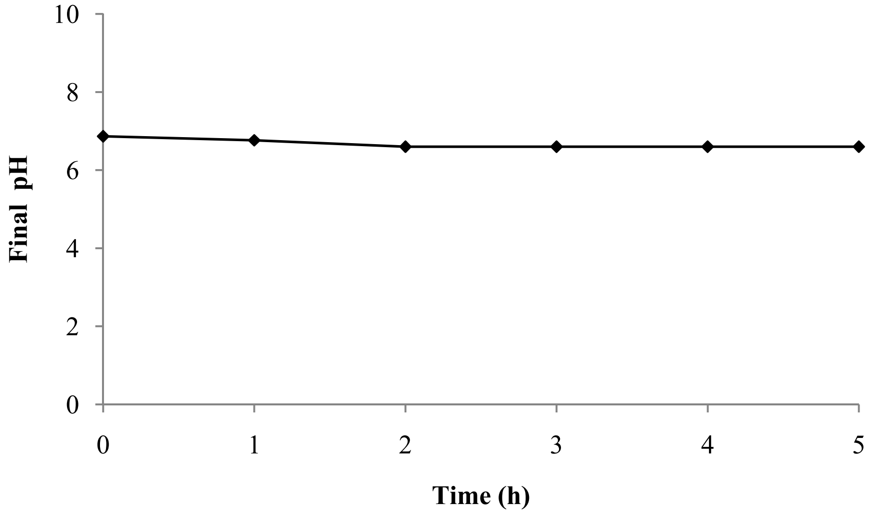

Figure 3.21 Plot of the variation in pH vs. time.

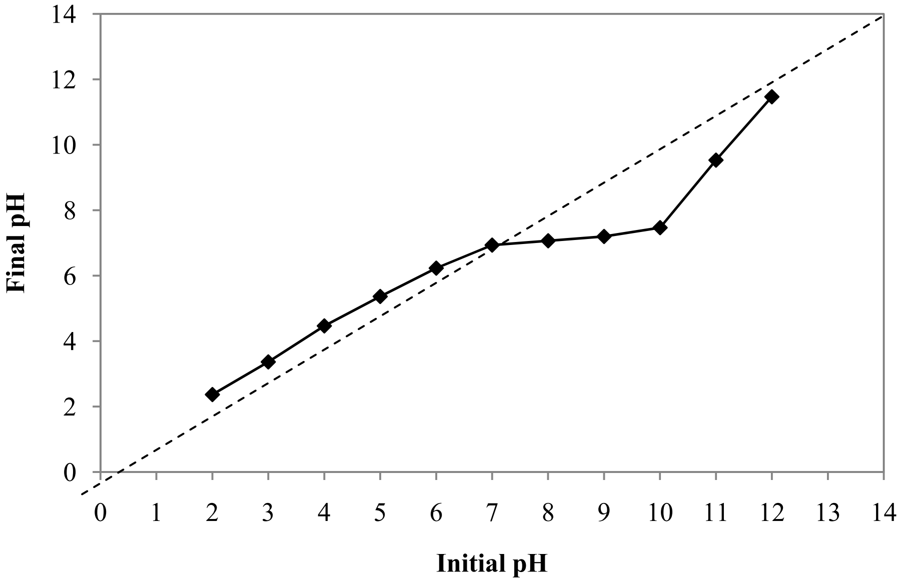

Figure 3.22 pH drift method to obtain pH_{pzc} for Degussa P25.

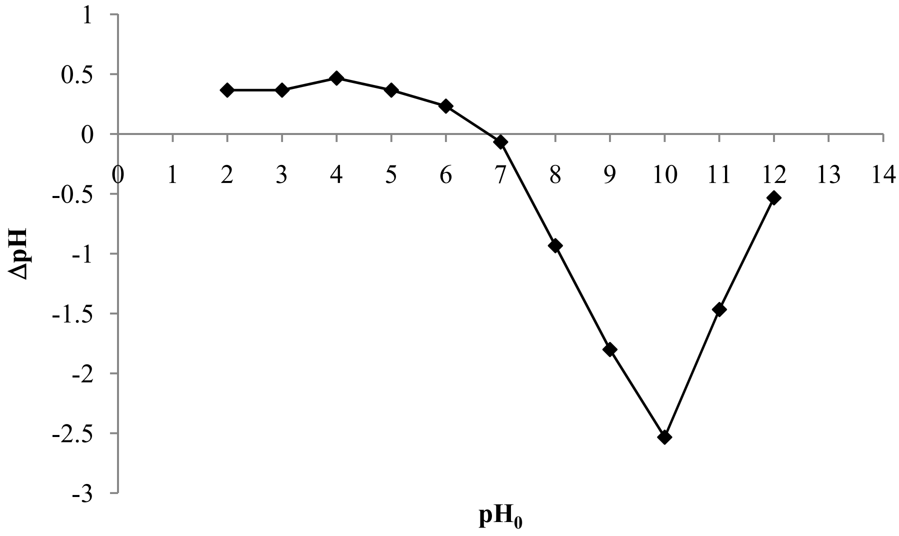

Figure 3.23 Salt addition method ($\Delta pH = pH_{final}-pH_{initial}$) for Degussa P25.

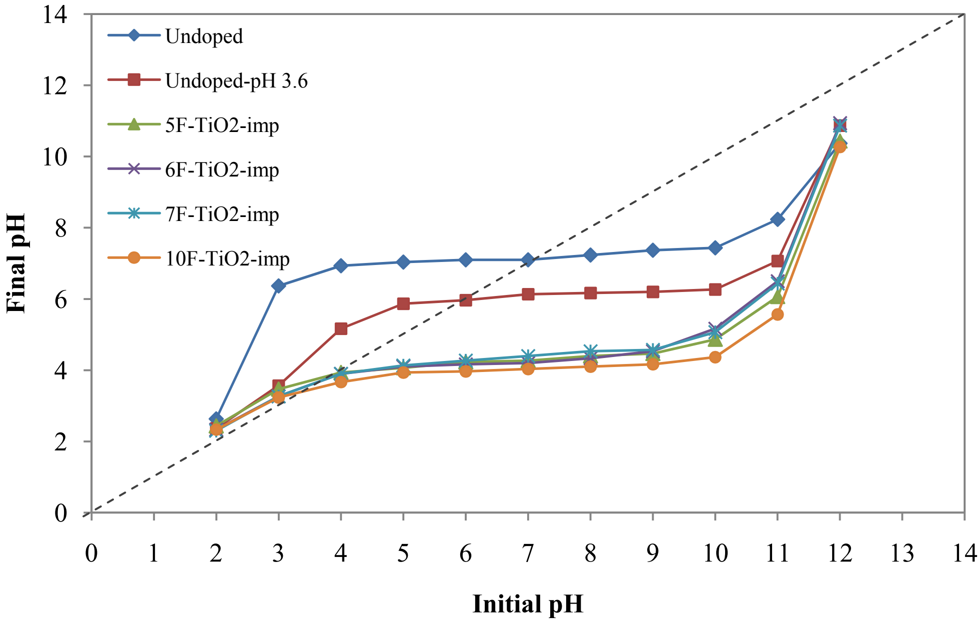

Figure 3.24 pH drift method to obtain pH_{pzc} for TiO_2 samples.

Table 3.10 The pH_{pzc} of TiO_2 samples.

TiO_2 samples	pH_{pzc}	
	pH drift method[a]	Salt addition method[b]
Undoped TiO_2-imp	7.0	7.1
Undoped-pH 3.6-imp	6.0	6.0
5F-TiO_2-imp	3.8	3.8
6F-TiO_2-imp	3.7	3.65
7F-TiO_2-imp	3.6	3.6
10F-TiO_2-imp	3.3	3.4
Degussa P25	6.8	6.8

[a] Bessekhouad, *et al.*, 2004.

[b] Mullet, *et al.*, 1997.

(a) Undoped TiO_2

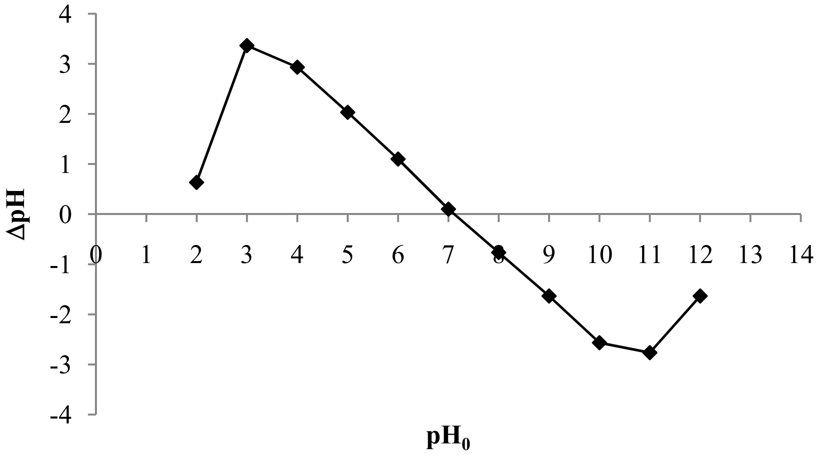

(b) Undoped-pH 3.6

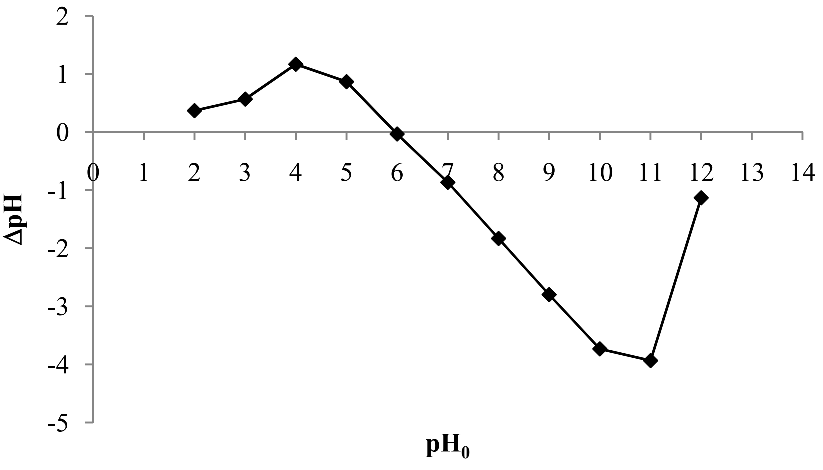

(c) 5F-TiO$_2$-imp

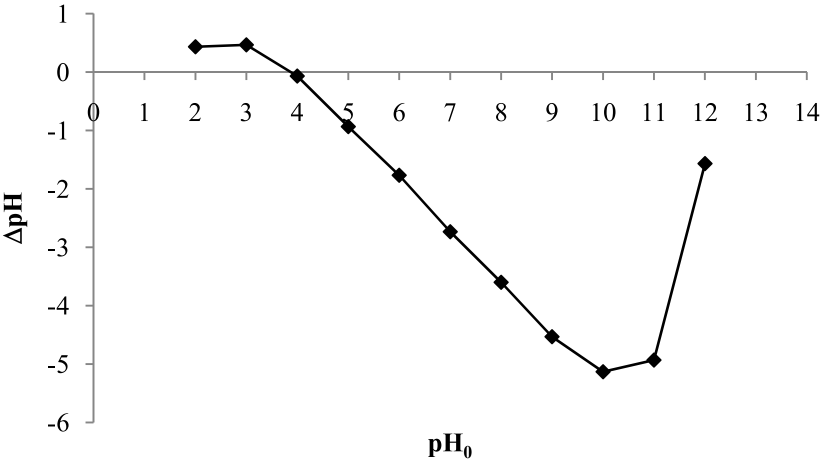

(d) 6F-TiO$_2$-imp

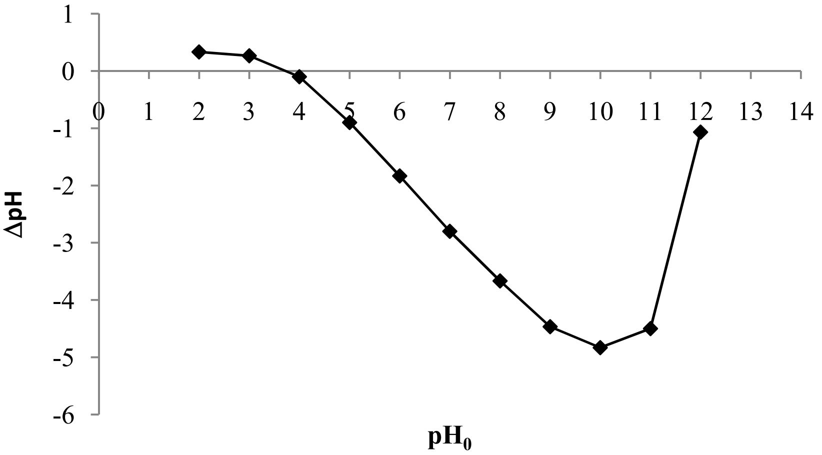

(e) 7F-TiO_2-imp

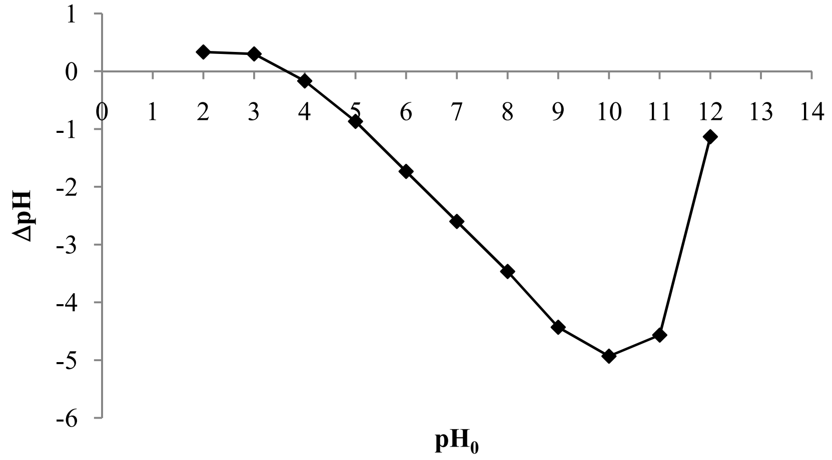

(f) 10F-TiO_2-imp

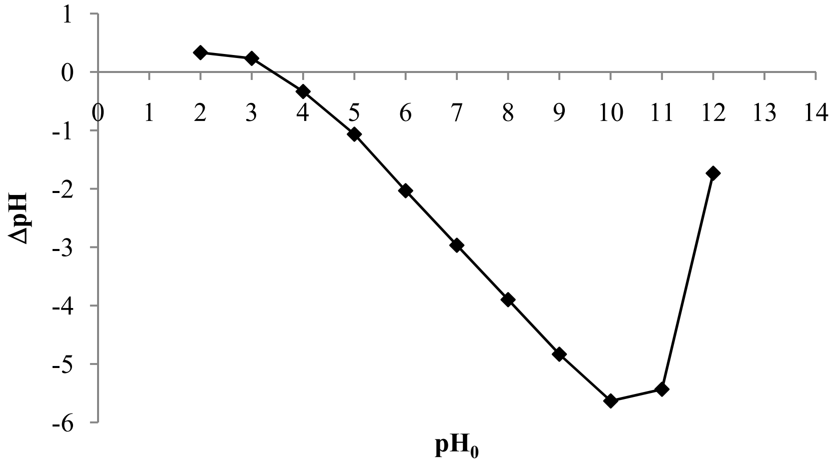

Figure 3.25 Salt addition method ($\Delta pH = pH_{final}$-$pH_{initial}$) for (a) undoped TiO_2, (b) undoped-pH 3.6, (c) 5F-TiO_2-imp, (d) 6F-TiO_2-imp, (e) 7F-TiO_2-imp, (f) 10F-TiO_2-imp.

3.2.3 Titration of the synthesized TiO_2 powders

Surface charge and acidity of oxides are usually measured using acid-base titration of suspended oxide particles in aqueous suspensions. Oxide surface can acquire either a positive or negative charge by association or dissociation of protons. Titration experiments in aqueous solutions were employed to measure the surface charge, acidity, and point of zero charge of TiO_2 (Sabia and Ukrainczyk, 2000). The purpose of this experimental study is to evaluate the effects of surface charge and concentration of H^+ or OH^-. The surface charge was determined by changing the pH value of the synthesized TiO_2 powders. Undoped-pH 3.6 and F-TiO_2-imp have decreased OH content of TiO_2, resulting in a higher surface charge (high concentration, Table 3.11) and enhancement of surface acidity. Undoped TiO_2 have increase OH content of TiO_2, resulting in a low surface charge (low concentration, Table 3.11). The positive surface charge of TiO_2 is markedly increased with the addition of F^- because the dominant surface species of Ti-OH_2^+. Titration data of the synthesized TiO_2 powders are summarized in Table 3.11.

Table 3.11 Titration data of the synthesized TiO_2 powders

TiO_2 samples	Titrated with	Surface OH^- (mol)	Surface H^+ (mol)
Undoped TiO_2	0.01 M HCl	8.23×10^{-3}	-
Undoped-pH 3.6	0.01 M NaOH	-	8.49×10^{-3}
2F-TiO_2-imp	0.01 M NaOH	-	9.47×10^{-3}
5F-TiO_2-imp	0.01 M NaOH	-	5.03×10^{-2}
7F-TiO_2-imp	0.01 M NaOH	-	5.16×10^{-2}
10F-TiO_2-imp	0.01 M NaOH	-	7.57×10^{-2}
30F-TiO_2-imp	0.01 M NaOH	-	1.36×10^{-1}

3.2.4 Photocatalytic activity of TiO_2 samples

In this work, the photocatalytic activities of TiO_2 samples were evaluated using IC as a model organic dye compound under UV and visible light. The primary events occurring at the catalyst surface in the presence of an anion X^- that can undergo surface complexation are summarized in reactions 3.5-3.21. The primary photochemical act, following the near-UV light absorption by TiO_2 ($\lambda < 380$ nm) is the generation of electron/hole pairs in the bulk of the semiconductor (Eq 3.5). The charge carriers can either recombine according to Eq 3.9 or migrate rapidly to the surface where they are ultimately trapped (the electron as a surface Ti(III) and the hole as a surface radical hydroxyl group; Eq 3.7). In the presence of surface complexation by ligands other than OH^- (Eq 3.6), trapping by these species is possible (Eq 3.8). If electron acceptors (Ox_2) or electron donors (Red_1, solvent) are present at the surface (adsorbed), interfacial electron transfers may occur according to reactions 3.12-3.15 and 3.19. Competitive with these are the interfacial recombination (Eqs 3.10 and 3.11), secondary surface trapping (Eq 3.17), and back reactions (Eqs 3.20 and 3.21).

charge separation

$$TiO_2 \longrightarrow e^-_{CB} + h^+_{VB} \qquad (3.5)$$

surface complexationt

$$\equiv TiOH + X^- \overset{K_2}{\rightleftarrows} \equiv TiX + OH^- \qquad (3.6)$$

surface trapping

$$h^+_{VB} + \equiv TiOH \xrightarrow{k_3} TiO^{\bullet +} H^+ \qquad (3.7)$$

$$h^+_{VB} + TiX \xrightarrow{k_4} \equiv TiX^{\bullet +} \qquad (3.8)$$

recombination

$$e^-_{CB} + h^+_{VB} \xrightarrow{k_5} heat \qquad (3.9)$$

$$e^-_{CB} + \equiv TiO^{\bullet +} + H^+ \xrightarrow{k_6} \equiv TiOH \qquad (3.10)$$

$$e^-_{CB} + \equiv TiX^{\bullet +} \xrightarrow{k_7} TiX \qquad (3.11)$$

interfacial charge transfer

$$h^+_{VB} + Red_1 \xrightarrow{k_8} Ox_1 \qquad (3.12)$$

$$\equiv TiO^{\bullet} + Red_1 \xrightarrow{k_9} Ox_1' \qquad (3.13)$$

$$\equiv TiX^{\bullet +} + Red_1 \xrightarrow{k_{10}} Ox_1'' \qquad (3.14)$$

$$h^+_{VB} + H_2O \xrightarrow{k_{11}} H_2O^{\bullet +} \qquad (3.15)$$

$$H_2O^{\bullet +} \xrightarrow{k_{12}} H^+ + OH^{\bullet} \qquad (3.16)$$

$$OH^{\bullet} + \equiv TiOH \xrightarrow{k_{13}} \equiv TiO^{\bullet} + H_2O \qquad (3.17)$$

$$OH^{\bullet} + Red \xrightarrow{k_{14}} Ox_1'' \qquad (3.18)$$

$$e^{-}_{CB} + Ox_2 \xrightarrow{k_{15}} Red_2 \qquad (3.19)$$

backreactions

$$Red_2 + h^{+}_{VB}(\text{or} \equiv TiO^{\bullet} \text{ or} \equiv TiX^{\bullet +}) \xrightarrow{k_{16}} Ox_2 \qquad (3.20)$$

$$Ox_1 \text{ (or } Ox_1' \text{ or } Ox_1'') + e^{-}_{CB} \xrightarrow{k_{17}} Red_1 \qquad (3.21)$$

Reactions 3.12-3.14, 3.18 and 3.19 can generate different (radical) species depending on the type of primary active species and the further chemical reactions (redox, reaction with solvent or oxygen, and dimerization). In aerated systems, oxygen acts as an efficient electron scavenger in reaction 3.19.

$$O_2 \text{ (ads)} + e^{-} \longrightarrow O_2^{-}\text{ads} \qquad (3.22)$$

In the presence of organic compounds, a series of oxidation/reduction processes, both initiated through Eqs 3.12-3.19, and involving other species such as O_2, H_2O_2, and O_2^{-}, may lead to complete degradation of the organic compound to CO_2 and inorganic anions (Minero, *et al.*, 2000). Figure 3.26 shows the primary processes involved in photomineralisation of organic compounds.

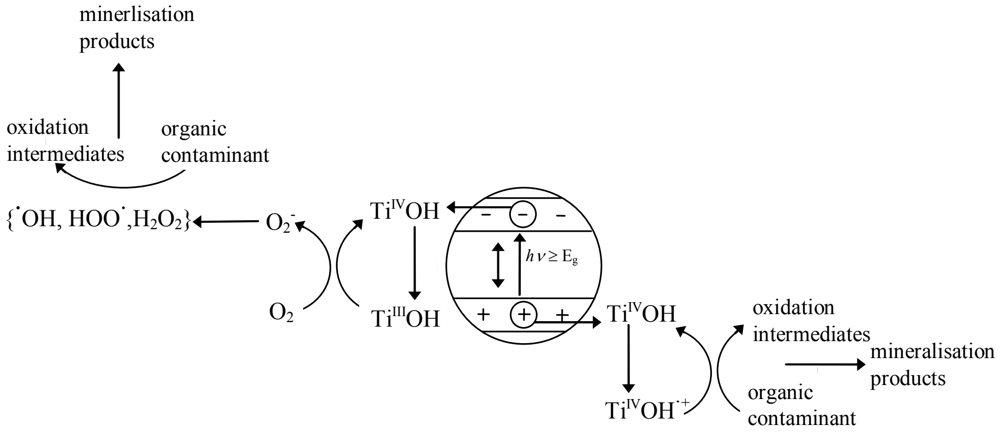

Figure 3.26 The primary processes involved in photomineralisation of organic compounds (Gaya and Abdullah, 2008).

(1) Preparation of calibration graphs

The calibration graph was used to find the concentration of IC. The concentrations of IC solutions were 1.0×10^{-5} M to 1.0×10^{-4} M. The concentration of IC solution was analysed by using a UV-Vis spectrophotometer (Specord S100, Analytik Jena, Germany) and the absorbance measured at 610 nm (λ_{max} of the dye). The resulting plot displayed an excellent linear relationship with R^2= 0.999. The standard calibration graphs of IC solution as shown in Figure 3.27.

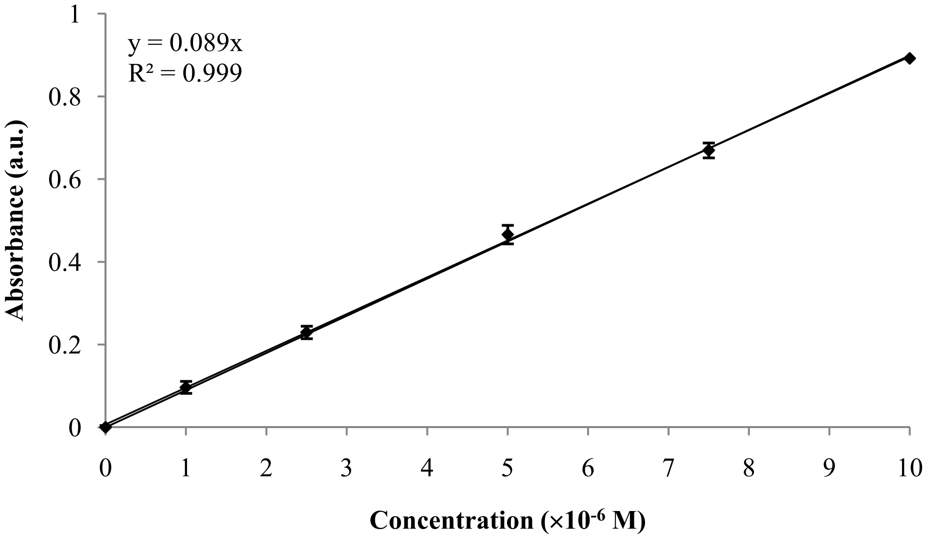

Figure 3.27 The standard calibration graphs of indigo carmine.

(2) The adsorption study of TiO_2 samples

Adsorption tests in dark were carried out in order to evaluate the adsorption of IC dye on the photocatalyst surface. Decolorization of IC dye was carried out in a closed compartment using 100 mL of a 2.5×10^{-5} mol/L dye solution and 1.0 g/L of TiO_2 samples. Decolorization efficiency of TiO_2 samples are shown in Figure 3.28 and Table 3.12. Fluorine doped TiO_2 samples (5F-TiO_2-imp, 6F-TiO_2-imp, 7F-TiO_2-imp) showed enhanced adsorption ability than undoped TiO_2 and undoped-pH 3.6. The decolorization efficiency was greater than 30% after 6 h. Undoped TiO_2 and undoped-pH3.6 showed the decolorization efficiency about 1-3%. F-TiO_2 samples (10F-TiO_2-imp and 30F-TiO_2-imp) showed the decolorization efficiency about 3-4%.

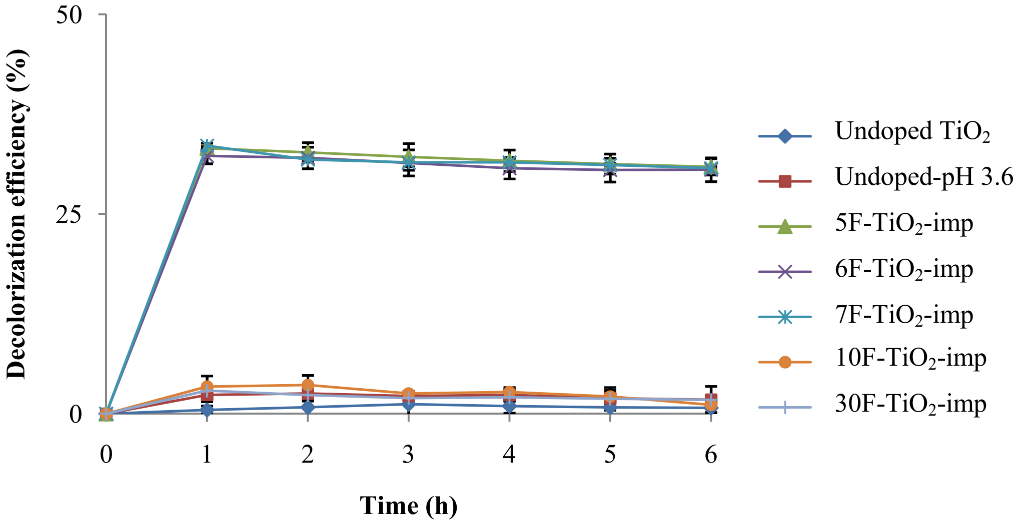

Figure 3.28 Decolorization (adsorption) efficiency of IC by TiO_2 samples.

Table 3.12 The percentage of IC decolorization (adsorption) by TiO_2 samples.

TiO_2 samples	Decolorization (adsorption) efficiency (%) at adsorption time (h)					
	1	2	3	4	5	6
Undoped TiO_2	0.00	1.00	1.00	1.00	1.00	1.00
Undoped-pH 3.6	2.00	3.00	2.00	2.00	2.00	2.00
5F-TiO_2-imp	33.0	33.0	32.0	32.0	31.0	31.0
6F-TiO_2-imp	32.0	32.0	31.0	31.0	31.0	31.0
7F-TiO_2-imp	34.0	32.0	31.0	31.0	31.0	31.0
10F-TiO_2-imp	3.00	4.00	3.00	3.00	2.00	1.00
30F-TiO_2-imp	3.00	2.00	2.00	2.00	2.00	2.00

(3) Test for photocatalytic activity

(a) The photocatalytic activity of TiO_2 samples under UV light

The photocatalytic activity of F-TiO_2-imp was studied by IC dye degradation in aqueous solution under UV light irradiation. The photocatalytic activity of TiO_2 samples under UV light irradiation is shown in Figure 3.29, it can be concluded that the photocatalytic activity of undoped TiO_2 and undoped-pH3.6 are lower than that of F-TiO_2-imp. It is seen that in 30 minute, the removal of IC treated by three samples (5F-TiO_2-imp, 6F-TiO_2-imp, 7F-TiO_2-imp) under UV irradiation is 78%, 74% and 74%, respectively. Three samples degraded 100% of IC in about 1 h.

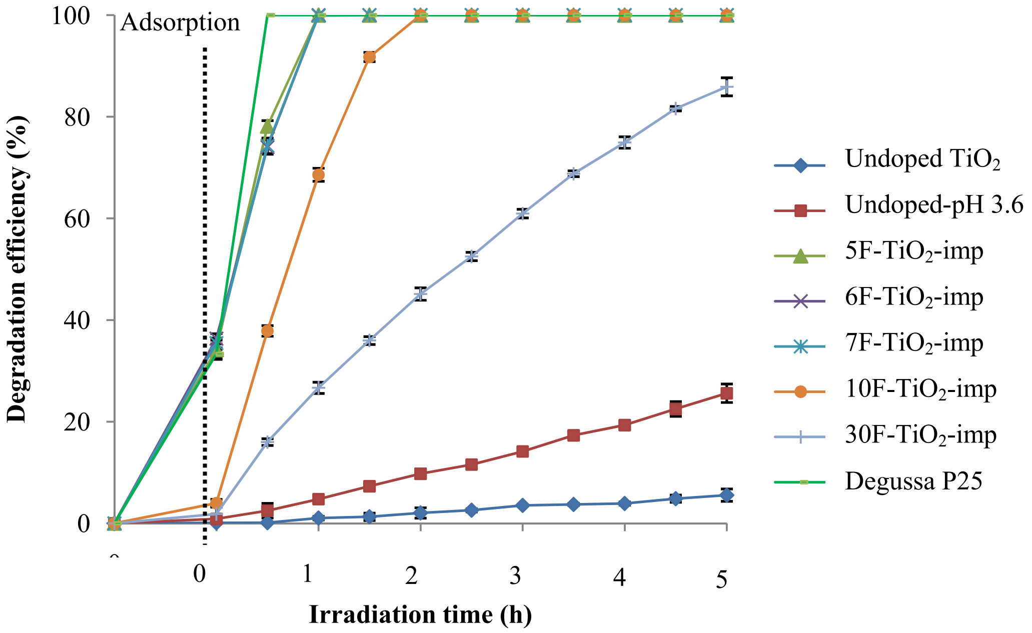

Figure 3.29 Photocatalytic activity of TiO_2 samples under UV light.

(b) The photocatalytic activity of TiO_2 samples under visible light

The photocatalytic activity of F-TiO_2-imp was studied by IC dye degradation in aqueous solution under visible light irradiation and using Degussa P25 for comparison. Figure 3.30 shows the degradation efficiency of IC by undoped TiO_2 and F-TiO_2-imp under visible light. The removal of IC under visible irradiation in about 4 h by three samples (5F-TiO_2-imp, 6F-TiO_2-imp, 7F-TiO_2-imp) is 100%, 92% and 93%, indicating that 5F-doped TiO_2 has the highest photocatalytic activity under visible irradiation (Figure 3.31). Degussa P25 has been accepted by most researchers as standard for testing the photocatalytic activity of TiO_2 samples. The results of adsorption and photocatalytic activity of TiO_2 samples, including Degussa P25 indicates that the photocatalytic activity of undoped TiO_2 and undoped-pH 3.6 are lower than that of F-TiO_2-imp. However, the photocatalytic activity of F-TiO_2-imp is lower than that of Degussa P25. Absorption spectra of indigo carmine solution containing TiO_2 samples under visible light irradiation at different time intervals are shown in Figure 3.32.

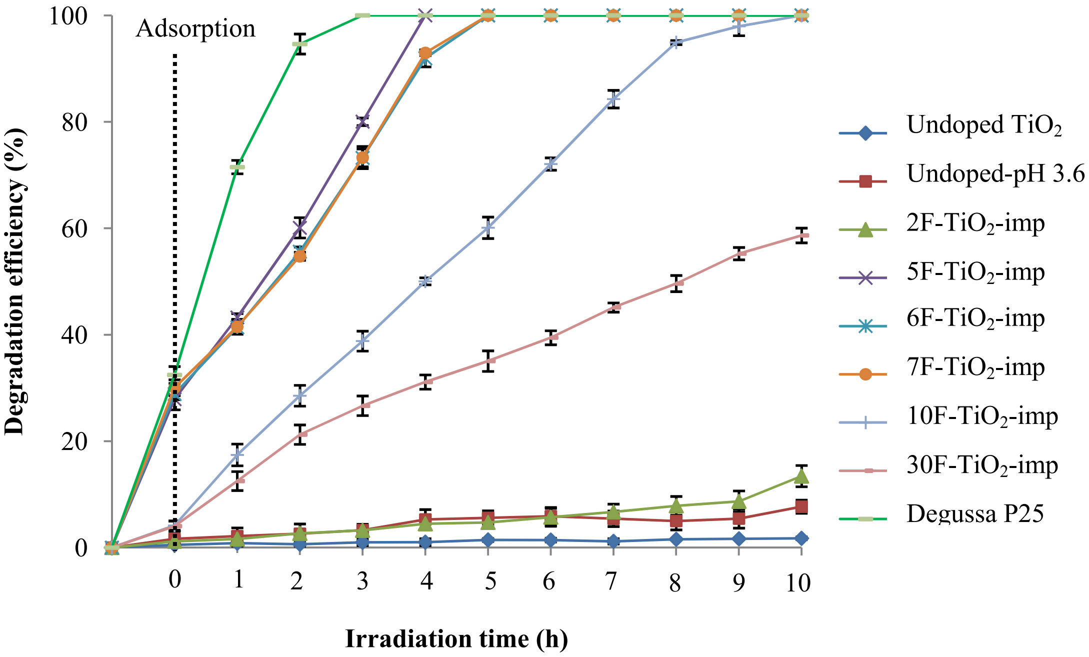

Figure 3.30 Photocatalytic activity of TiO_2 samples under visible light.

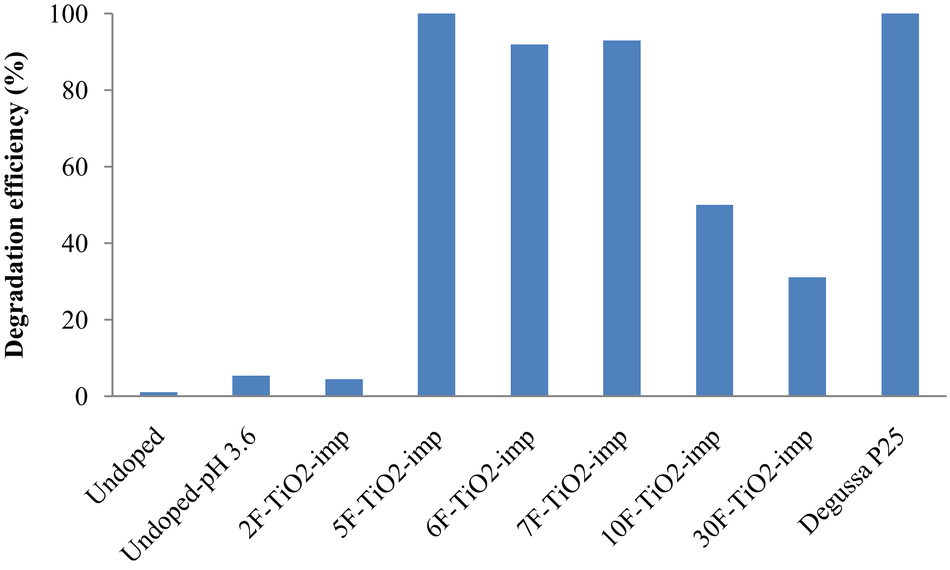

Figure 3.31 Photocatalytic activity of TiO_2 samples under visible light in about 4 h.

(a) Undoped TiO_2

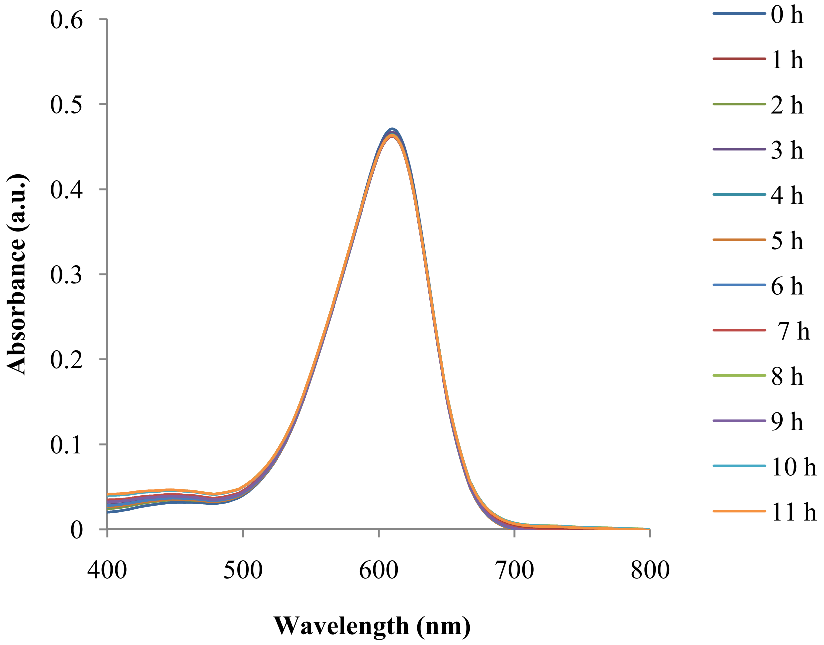

(b) Undoped-pH 3.6

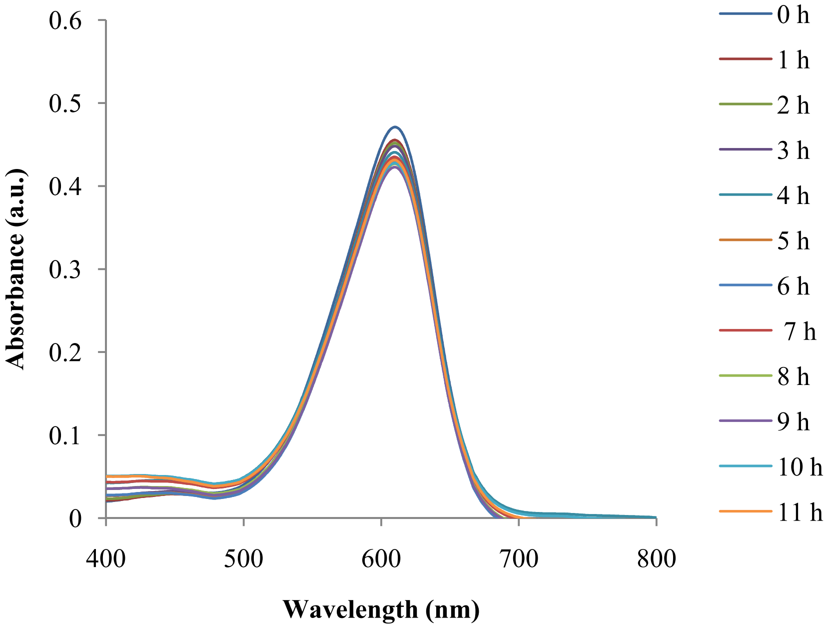

(c) 2F-TiO_2-imp

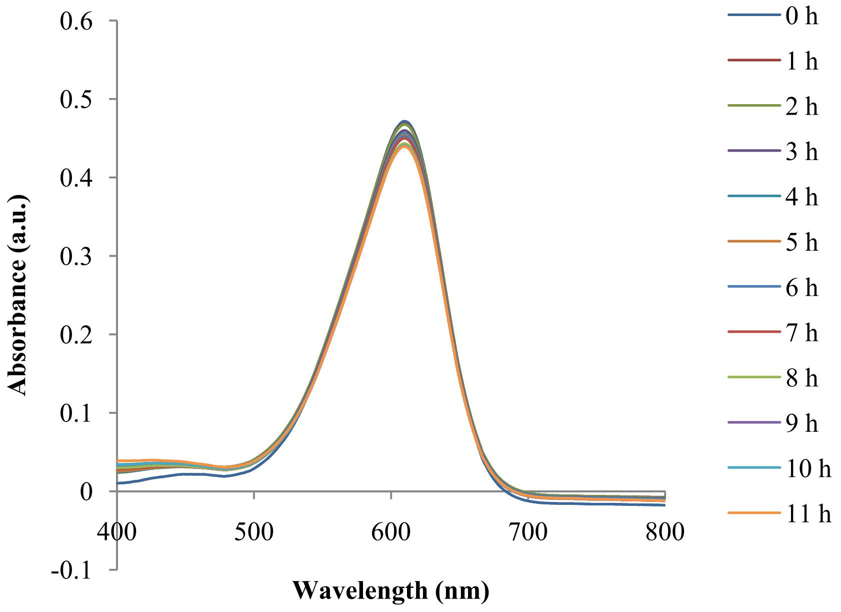

(d) 5F-TiO_2-imp

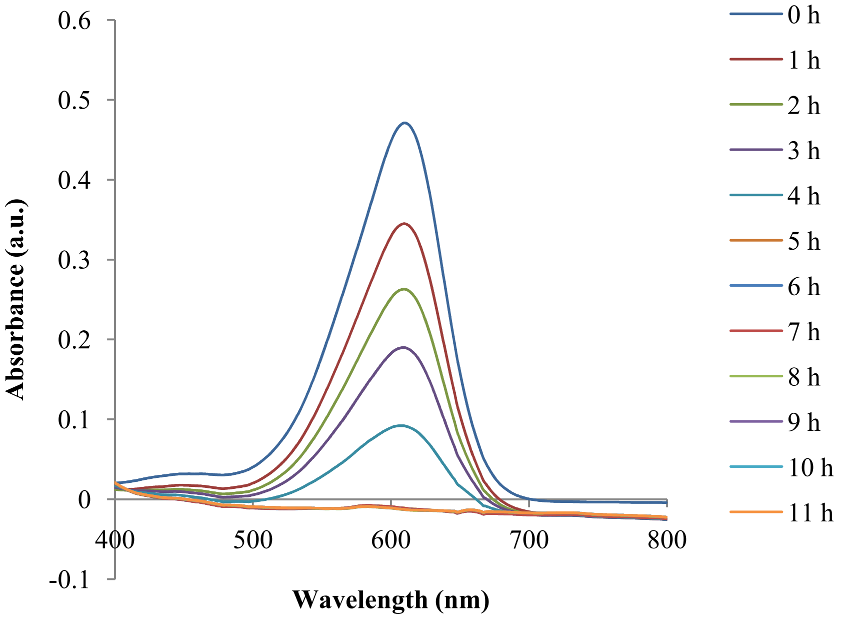

(e) 6F-TiO_2-imp

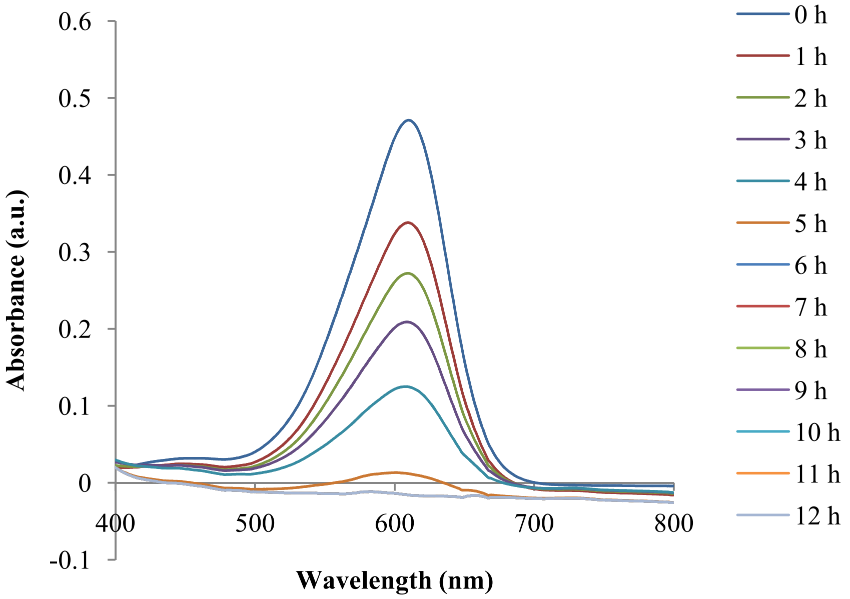

(f) 7F-TiO_2-imp

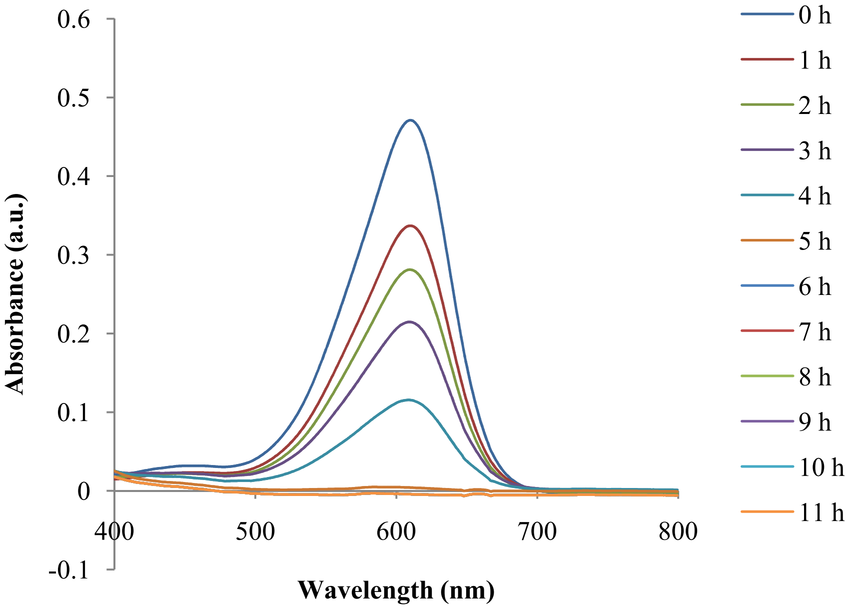

(g) 10F-TiO_2-imp

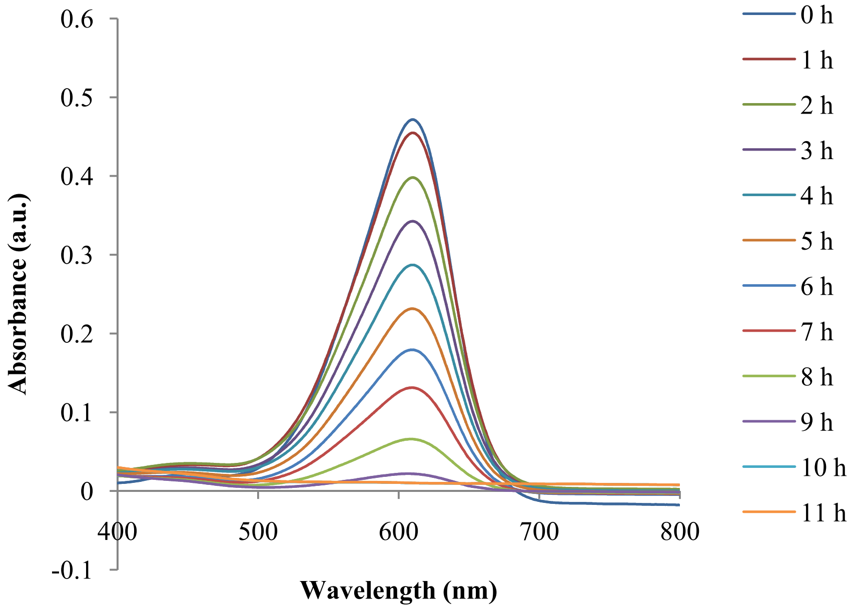

Figure 3.32 Absorption spectra of indigo carmine solution containing TiO_2 samples under visible light irradiation at different time intervals.

(4) Effect of pH

The wastewater from textile industries usually has a wide range of pH values. Generally, the pH of the solution is an important parameter in the photocatalytic processes, since it not only plays an important role in the characteristics of textile wastewater, but also determines the surface charge properties of TiO_2, the size of aggregates formed, the charge of dye molecules, adsorption of dyes onto TiO_2 surface and the concentration of hydroxyl radicals. According to the point of zero charge (pzc), the surface charge property of TiO_2 changes with the change of solution pH. TiO_2 surface is presumably positively charged in acidic solution ($pH < pH_{pzc}$) and negatively charged in alkaline solution ($pH > pH_{pzc}$) as given in Eqs. (3.23) and (3.24) (Sun, *et al.*, 2008).

$$pH < pH_{pzc} : TiOH + H^+ \longleftrightarrow TiOH_2^+ \qquad (3.23)$$

$$pH > pH_{pzc} : TiOH + OH^- \longleftrightarrow TiO^- + H_2O \qquad (3.24)$$

The IC dye in solution is negatively charged as the sulphonated group existing in its structure is hydrolyzed. Due to the electrostatic attraction, the acidic solution favors adsorption of IC dye onto TiO_2 surface, and the degradation efficiency of IC increases accordingly. It was found that the photocatalytic degradation IC dye solution could be enhanced by both H^+ and OH^- ion formation. Under acidic conditions, the perhydroxyl radical is formed by the protonation of superoxide radical. These perhydroxyl radicals combine together to form hydrogen peroxide, which in turn dissociates to give hydroxyl radical (Eqs (3.25-3.30)). Therefore, in the alkaline pH range, the concentration of hydroxyl radicals increases (Eq. 3.31) (Kumar, *et al.*, 2010).

$$O_2 + e^- \xrightarrow{hv} O_2^{-\bullet} \quad (3.25)$$

$$O_2^{-\bullet} + H^+ \longrightarrow HO_2^{\bullet} \quad (3.26)$$

$$HO_2^{\bullet} + HO_2^{\bullet} \longrightarrow H_2O_2 + O_2 \quad (3.27)$$

$$H_2O_2 + e^-_{cb} \xrightarrow{hv} HO^{\bullet} + HO^- \quad (3.28)$$

$$H_2O_2 + O_2^{-\bullet} \longrightarrow HO^{\bullet} + HO^- + O_2 \quad (3.29)$$

$$H_2O_2 \longrightarrow 2HO^{\bullet} \quad (3.30)$$

$$O_2 + HO^- \longrightarrow O^{-\bullet} + HO^{\bullet} \quad (3.31)$$

IC is a dianionic dye in aqueous solution and it can keep its dianionic configuration in the pH range 3-11. At low pH range, electrostatic interactions between the positive catalyst surface and dye anions lead to strong adsorption of the latter on the metal oxide support (Othman, *et al.*, 2007). The photocatalytic activity of F-TiO_2-imp was studied in the effect of pH values on the photodegradation of IC dye in aqueous solution under UV and visible light. The pH of the solution was adjusted with dilute NaOH or HCl solutions and the initial dye concentration was 1×10^{-4} M.

(a) The adsorption study of TiO_2 samples

The results on the decolorization efficiency of IC by 5F-TiO_2-imp are shown in Figure 3.33. The decolorization of IC was higher in acid zone (pH 3) and the decolorization efficiencies decreasing as the pH values increased in the order: (pH) 3 > 5 > 6.5 > 9 > 11.

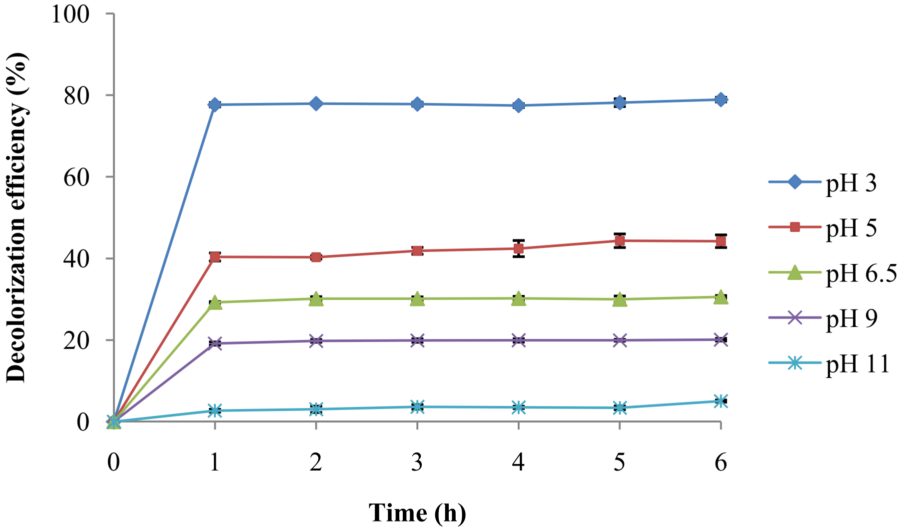

Figure 3.33 Effect of pH on decolorization efficiency of IC by 5F-TiO_2-imp.

(b) The photocatalytic activity of TiO_2 samples under UV light

Figure 3.34 demonstrates the degradation efficiency of IC dye at different pH from 3 to 11 after irradiation of UV light for 6 h. The effect of pH values on the photodegradation was also studied, as shown in Figure 3.35. Under UV light irradiation, the degradation was higher in acid zone (pH 3), with almost all dye being degraded. It is obvious that 5F-TiO_2-imp showed enhanced adsorption ability than undoped TiO_2 and the degradation efficiency was greater than 80% after 1 h. The results showed the higher degradation efficiency region at pH about 3 and 9. At pH > 11, the degradation efficiency of IC was negligible.

(a) pH 3

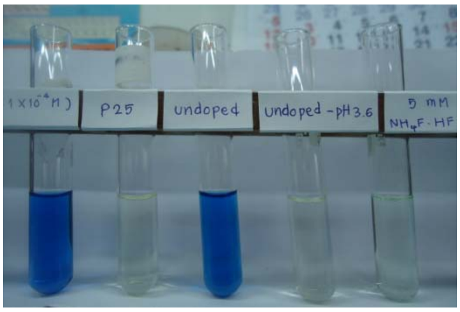

(b) pH 5

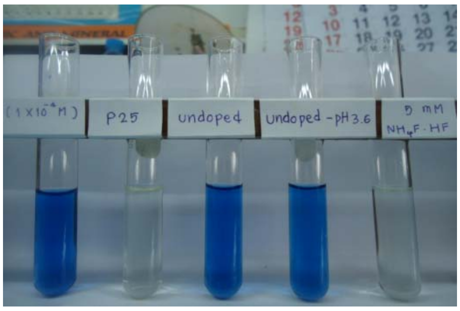

(c) pH 6.5

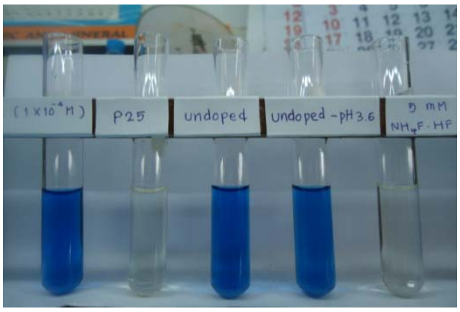

(d) pH 9

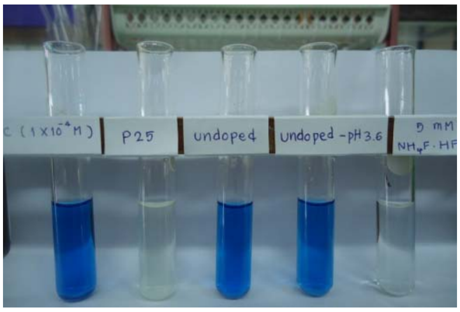

(e) pH 11

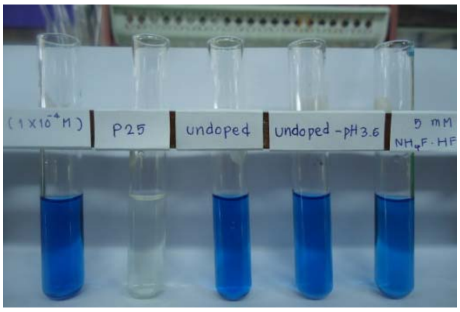

Figure 3.34 Effect of pH on the degradation efficiency of IC by 5F-TiO_2-imp.

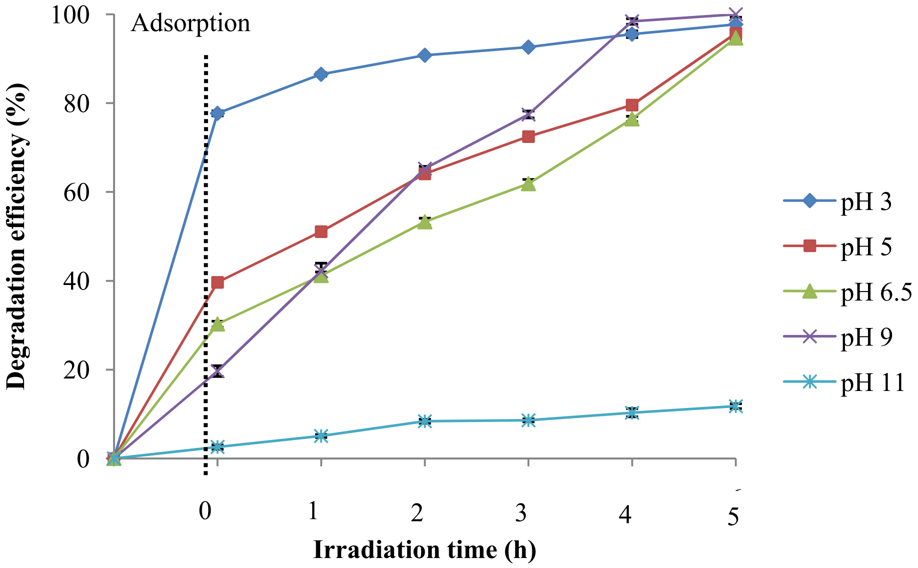

Figure 3.35 Degradation efficiency of IC by 5F-TiO_2-imp under UV light.

(c) The photocatalytic activity of TiO_2 samples under visible light

In the first one hour under dark condition. The concentration of IC dye was decreased because IC dye was physically adsorbed on the surface of 5F-TiO_2-imp. After switching on the light, the concentration of IC dye was gradually decreased in case of 5F-TiO_2-imp (Figure 3.36). The degradation efficiencies decreased as the pH values increased in the order: (pH) 3 > 9 > 5 > 6.5 > 11, whereas, the IC dye was stable in amorphous undoped TiO_2. Amorphous undoped TiO_2 is less efficient in the photocatalytic degradation of IC compared to 5F-TiO_2-imp. The effect of pH on the photodegradation of IC by 5F-TiO_2-imp is shown in Figure 3.37. Under visible light irradiation, 5F-TiO_2-imp degraded almost 95% of IC in about 10 h. The results show the higher degradation efficiency region at pH about 3. Figure 3.38 demonstrates the degradation efficiency of IC at different pH from 3 to 11.

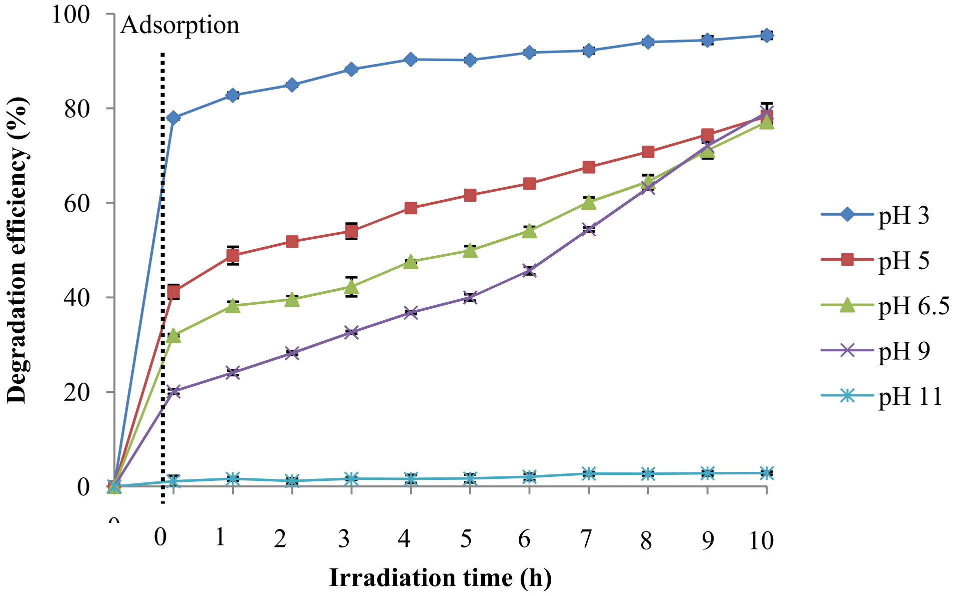

Figure 3.36 Degradation efficiency of IC by 5F-TiO_2-imp under visible light.

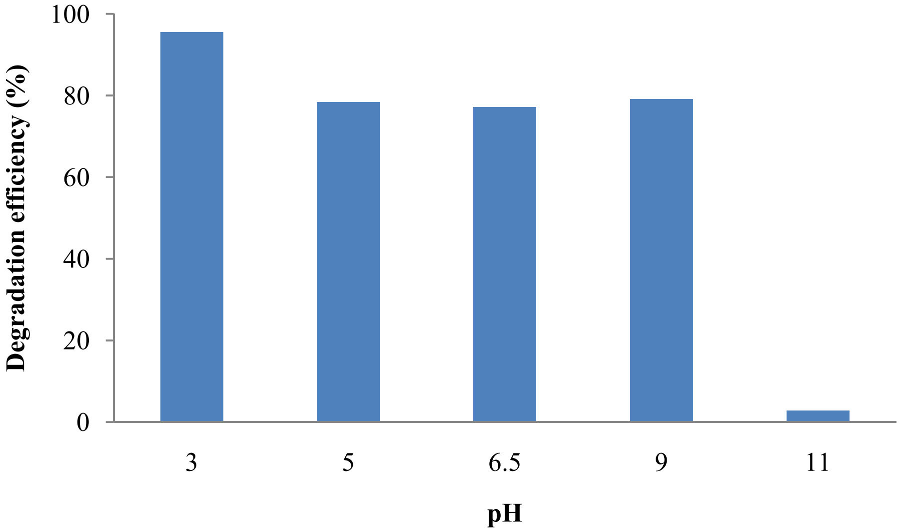

Figure 3.37 Effect of pH versus degradation efficiency of IC by 5F-TiO_2-imp (10 h visible light irradiation).

(a) pH 3

(b) pH 5

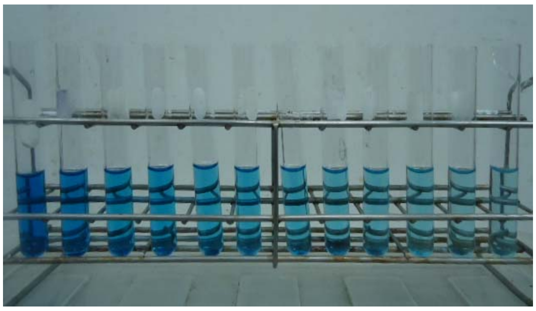

(c) pH 6.5

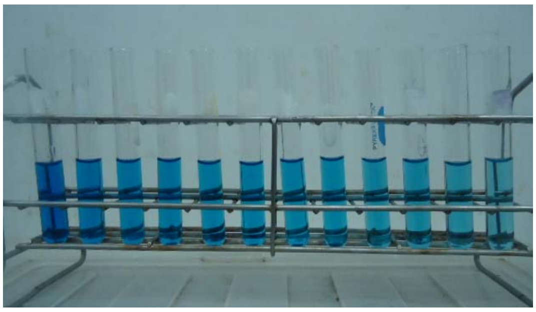

(d) pH 9

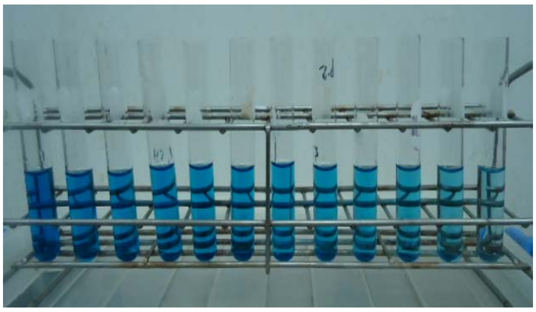

Figure 3.38 Effect of pH on the degradation efficiency of IC by 5F-TiO_2-imp (10 h visible light irradiation)

3.3 Fluorine doped TiO_2 via co-precipitation method and the photocatalytic activity

Fluorine doped TiO_2 (F-TiO_2-PC) was prepared by co-precipitation method using $NH_4F{\cdot}HF$ as a source of dopant. F-TiO_2-PC exists as a white powder solid.

3.3.1 Characterization of fluorine doped TiO_2

3.3.1.1 X-ray diffraction (XRD)

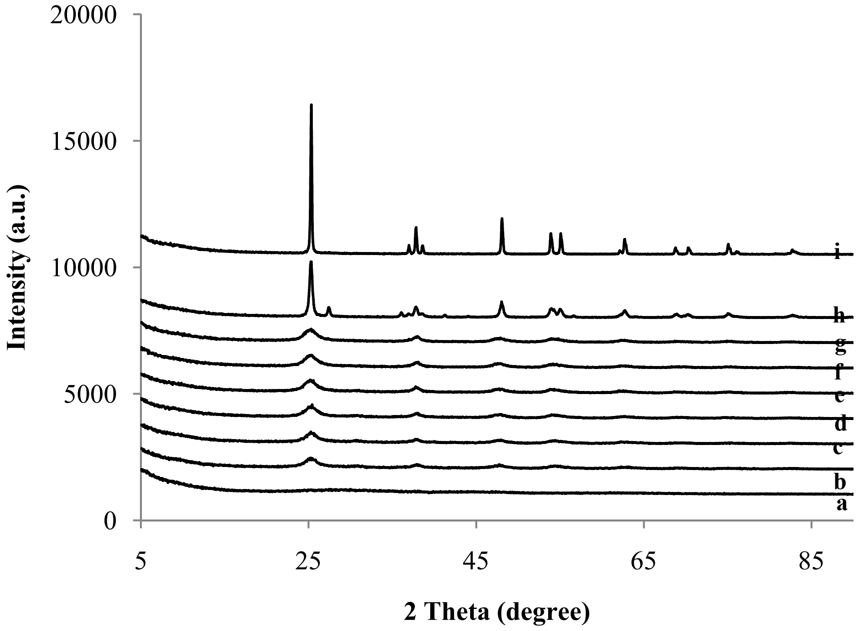

Figure 3.39 X-ray diffraction patterns of the synthesized TiO_2 powders; (a) undoped TiO_2, (b) undoped-pH 3.6, (c) 5F-TiO_2-PC , (d) 10F-TiO_2-PC, (e) 15F-TiO_2-PC, (f) 20F-TiO_2-PC, (g) 30F-TiO_2-PC, (h) Degussa P25, (i) anatase.

Figure 3.39 shows XRD spectra of the synthesized TiO_2 powders and the commercial ones. The undoped powder was amorphous TiO_2 showing a flat base line without any diffraction pattern. F-TiO_2-PC showed broad characteristic diffraction peak of anatase phase. The 30F-TiO_2-PC has diffraction peaks at 2θ = 25.60°, 38.04°, 47.90°, 53.88°. The peaks are broad indicating low crystallinity of anatase phase. The rutile and brookite phases of F-TiO_2-PC were not observed. The undoped-pH 3.6 shows that the peaks at 25.09°, 37.94°, 47.83° and 54.50°. The commercial Degussa P25 (Figure 3.39h) shows pattern of both anatase (2θ = 25.29°)

and rutile (2θ = 27.44°) phase in the ratio of *ca.* 4:1 and the commercial anatase (Figure 3.39i) shows only anatase phase (2θ = 25.33°). It can be concluded that fluorine doping inhibits the grain growth. Compared undoped-pH 3.6 TiO_2 and 30F-TiO_2-PC, the peak position of the (101) plane of 30F-TiO_2-PC shifted slightly to higher 2θ value, which suggested the distortion of the crystal lattice and the smaller particle size of 30F-TiO_2-PC. Crystal lattice distortion is reported to be important for absorption edge shift towards the visible-light region (Xie, *et al.*, 2007). Phase, crystallite size and crystallinity of the synthesized TiO_2 powders are summarized in Table 3.13.

Table 3.13 Phase, crystallite size and crystallinity of the synthesized TiO_2 powders.

TiO_2 samples	Phase	Crystallite size[a] (nm)	Crystallinity[b] (%)	Amorphous[c] (%)
Undoped TiO_2	Amorphous	-	-	100
Undoped-pH 3.6	Amorphous, Anatase	11.81	12.66	87.34
5F-TiO_2-PC	Amorphous, Anatase	16.54	10.49	89.51
10F-TiO_2-PC	Amorphous, Anatase	9.19	21.03	78.97
15F-TiO_2-PC	Amorphous, Anatase	6.54	29.06	70.94
20F-TiO_2-PC	Amorphous, Anatase	8.27	25.73	74.27
30F-TiO_2-PC	Amorphous, Anatase	6.10	29.21	70.79

[a] Calculated from XRD data using Scherrer's formula.

[b] Determined by XRD using standard addition method, Suwanchawalit, *et al.*, 2008.

[c] The amorphous content was calculated by 100 % - Anatase %.

In comparation with XRD patterns of F-TiO_2-PC using five different concentration of dopant. The crystallite size of TiO_2 samples were always found in the range of 6.10-16.54 nm. The crystallite sizes of F-TiO_2-PC are smaller than that of Degussa P25. Undoped-pH 3.6 and F-TiO_2-PC showed a small amount of crystalline anatase phase (~12.66% for undoped-pH 3.6 TiO_2, ~29.21% for 30F-TiO_2-PC). It can be concluded that F element entrapped in surface of 30F-TiO_2-PC or incorporate in the TiO_2 lattice, an orderly repeating pattern of atoms and improved the crystallinity of 30F-TiO_2-PC.

3.3.1.2 Electron microscopy

(1) Scanning electron microscopy (SEM)

Figure 3.40 shows SEM image of the synthesized TiO_2 powders. The SEM images of amorphous undoped TiO_2 showed highly agglomerated particles with various sizes as shown in Figure 3.40a. At high magnification (Figure 3.40a, (5,000×), (10,000×)), the amorphous-like structure with low crystalline phase of TiO_2 can be detected. Figure 3.40b shows SEM images of undoped-pH 3.6 TiO_2 and the powder slightly agglomerated. Figure 3.40c, 3.40d, 3.40e, 3.40f, 3.40g show SEM images of F-TiO_2-PC, the powders are found to be fine and slightly agglomerated.

(a) Undoped TiO_2

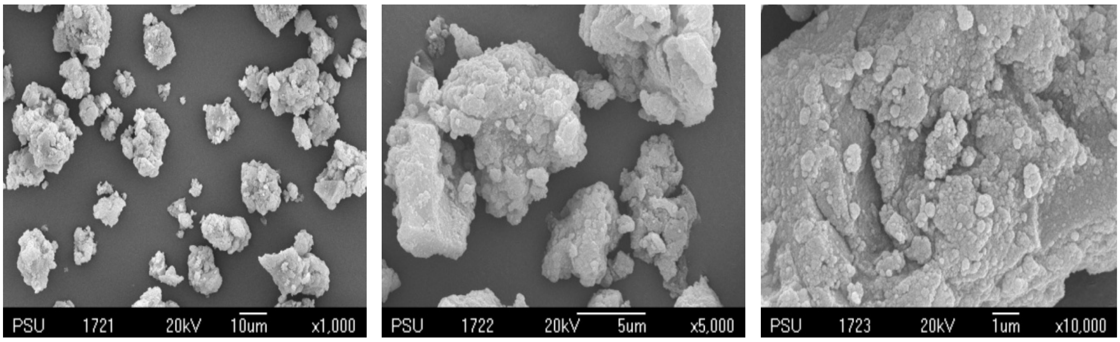

(b) Undoped-pH 3.6

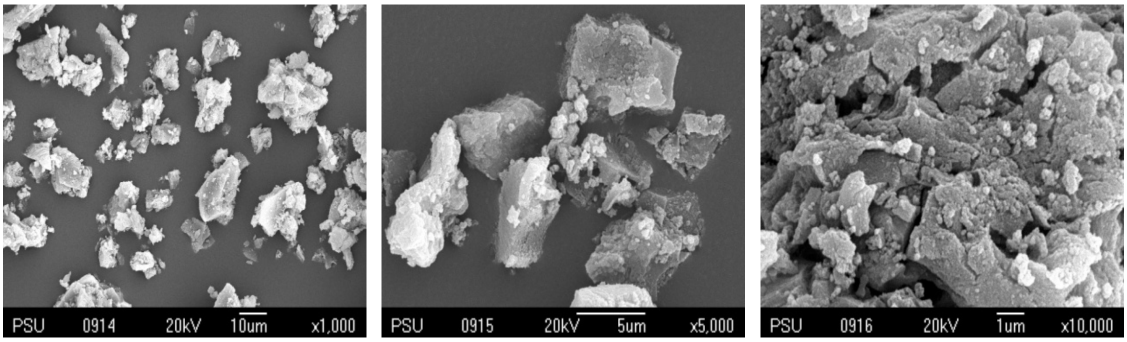

(c) 5F-TiO_2-PC

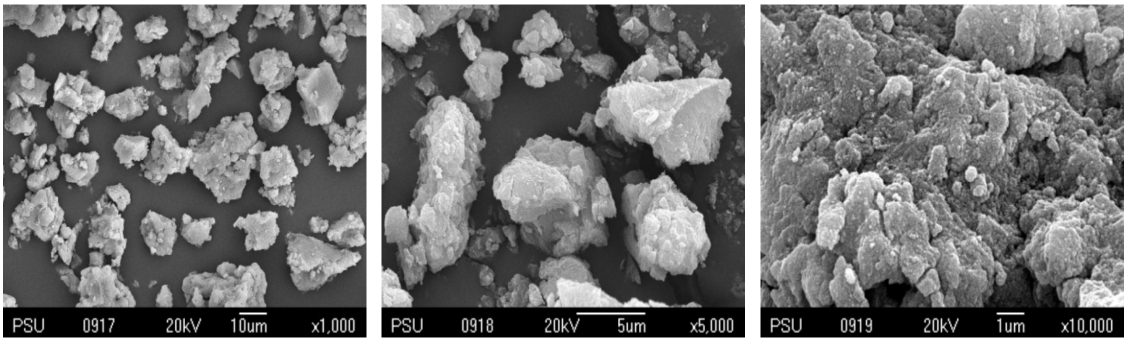

(d) 10F-TiO_2-PC

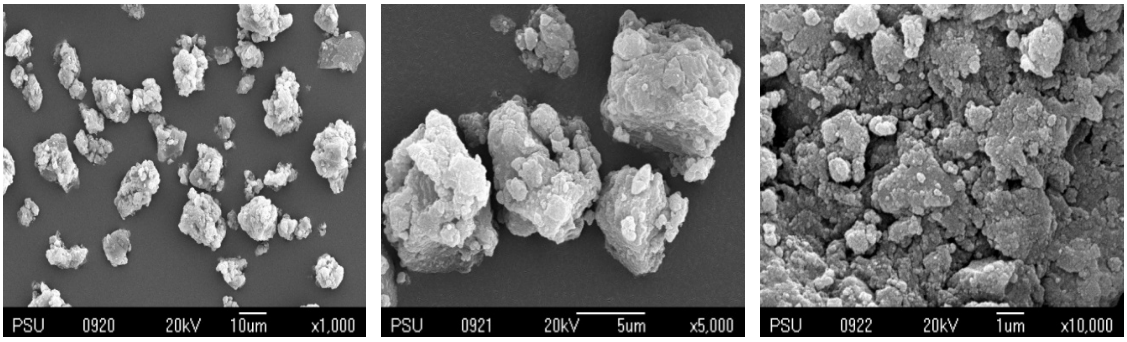

(e) 15F-TiO_2-PC

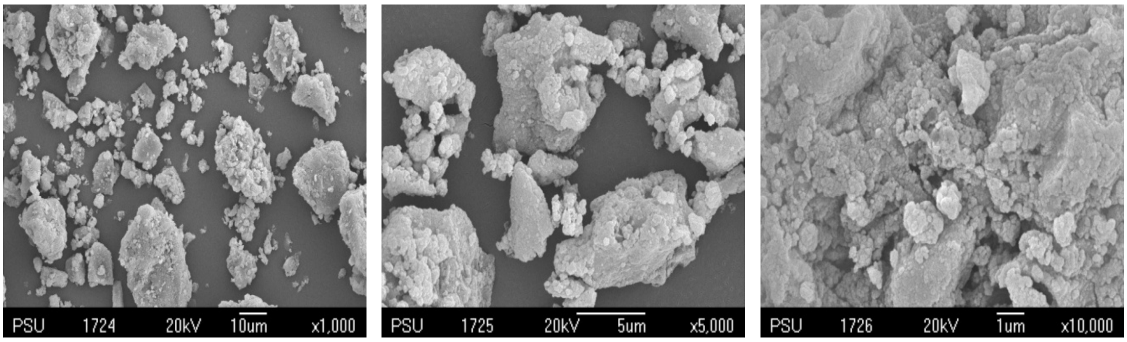

(f) 20F-TiO_2-PC

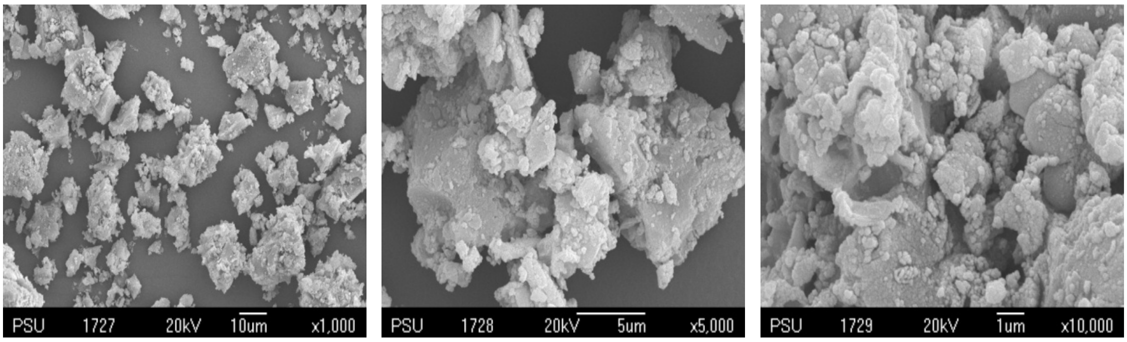

(g) 30F-TiO_2-PC

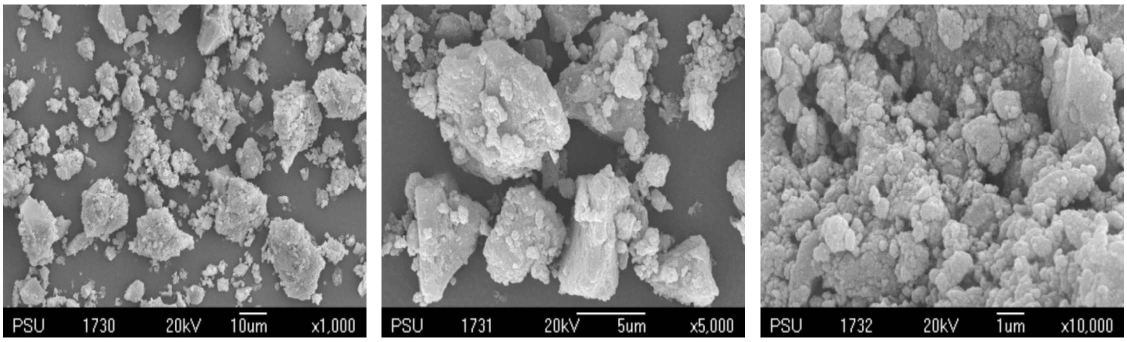

Figure 3.40 SEM images of the synthesized TiO_2 powders; (a) undoped TiO_2, (b) undoped-pH 3.6, (c) 5F-TiO_2-PC, (d) 10F-TiO_2-PC, (e) 15F-TiO_2-PC, (f) 20F-TiO_2-PC, (g) 30F-TiO_2-PC. Each sample was magnified at low (1,000×) and high (5,000× and 10,000×) magnification.

(2) Energy-dispersive X-ray spectroscopy (EDX)

Figure 3.41 shows the EDX microanalyses of the synthesized TiO_2 powders. The EDX spectrum of amorphous undoped TiO_2 (Figure. 3.41a) shows the presence of Ti, O and C elements. Figure 3.41c, 3.41d and Figure 3.41e show peak corresponding to fluorine was detected in F-TiO_2-PC which is not observed in amorphous undoped TiO_2. On the other hand, it was found that 10F-TiO_2-PC (Figure 3.41b) did not show fluorine element because of its very small amount beyond the detection of EDX.

(a) Undoped TiO_2

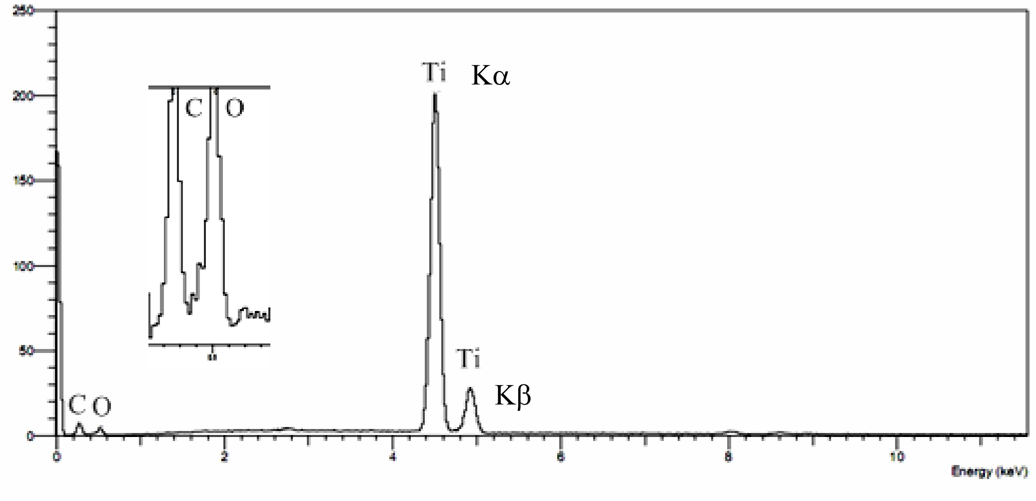

(b) 10F-TiO_2-PC

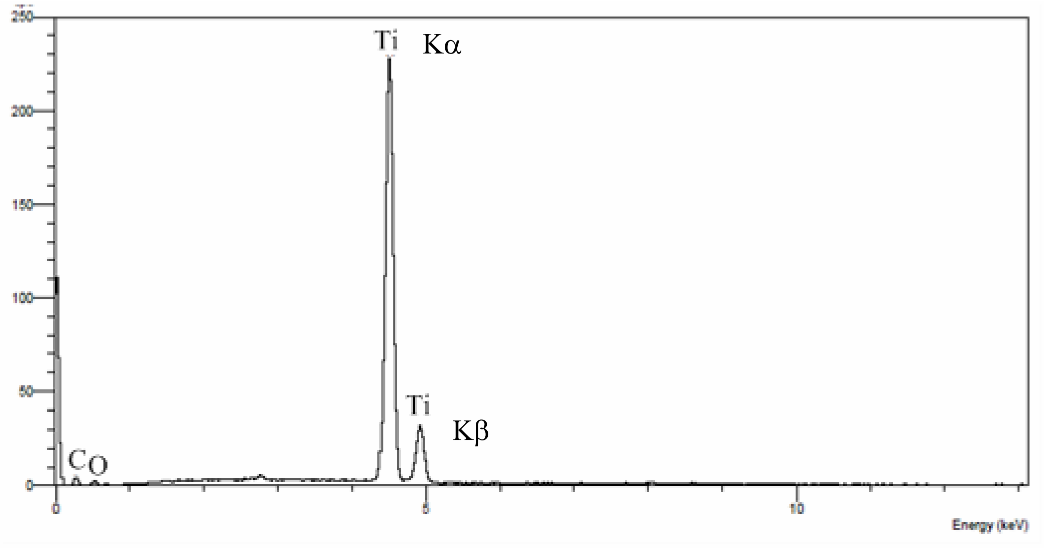

(c) 20F-TiO_2-PC

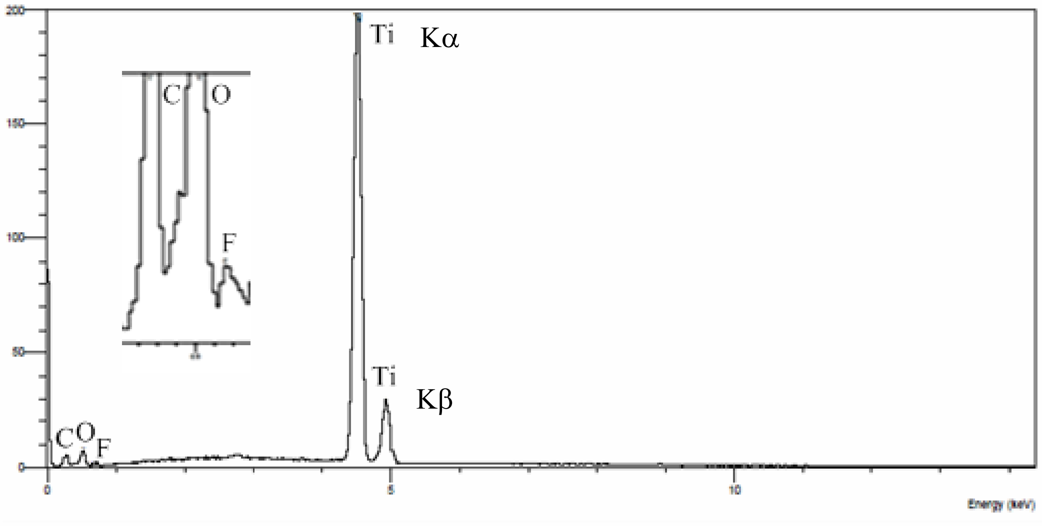

(d) 30F-TiO_2-PC

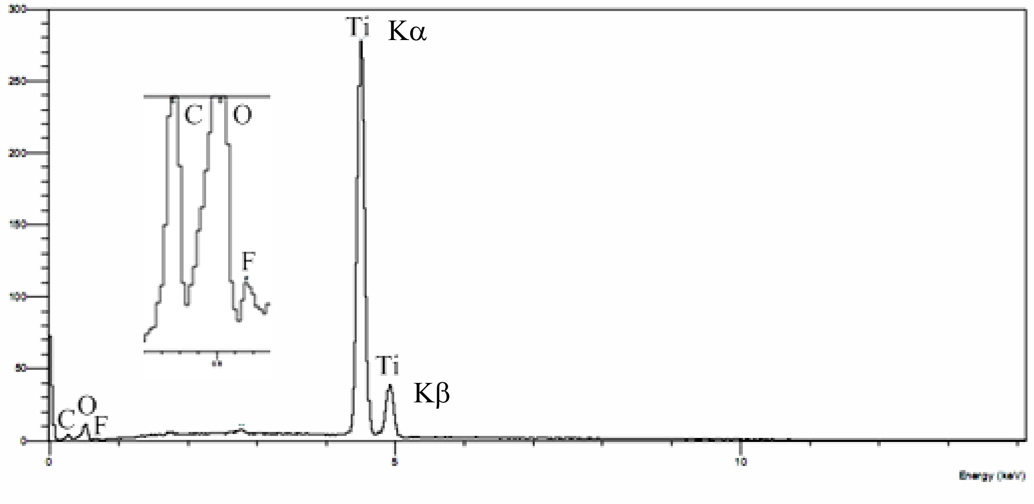

(e) 50F-TiO_2-PC

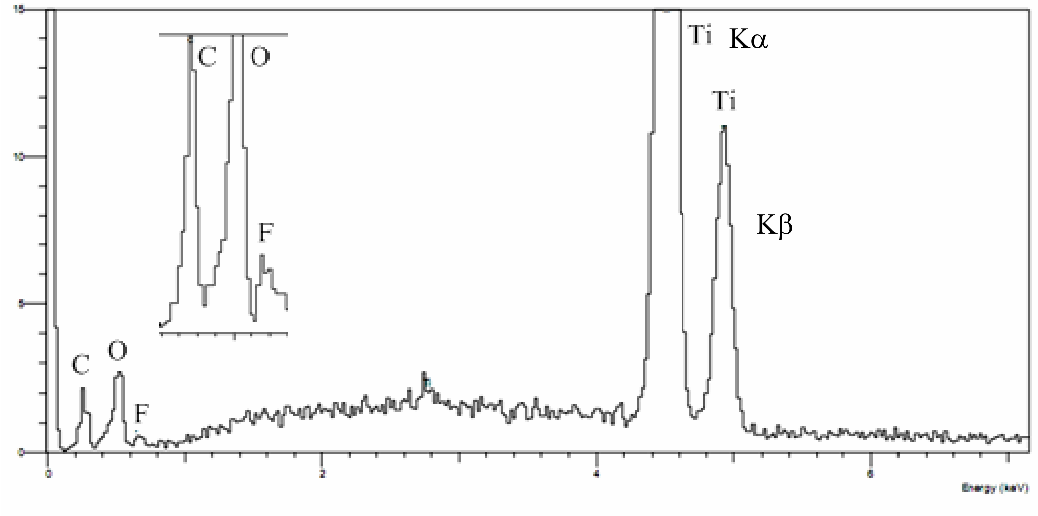

Figure 3.41 EDX spectra of the synthesized TiO_2 powders; (a) undoped TiO_2, (b) 10F-TiO_2-PC, (c) 20F-TiO_2-PC, (d) 30F-TiO_2-PC, (e) 50F-TiO_2-PC.

3.3.1.3 Diffused reflectance UV-Vis spectroscopy (DRS)

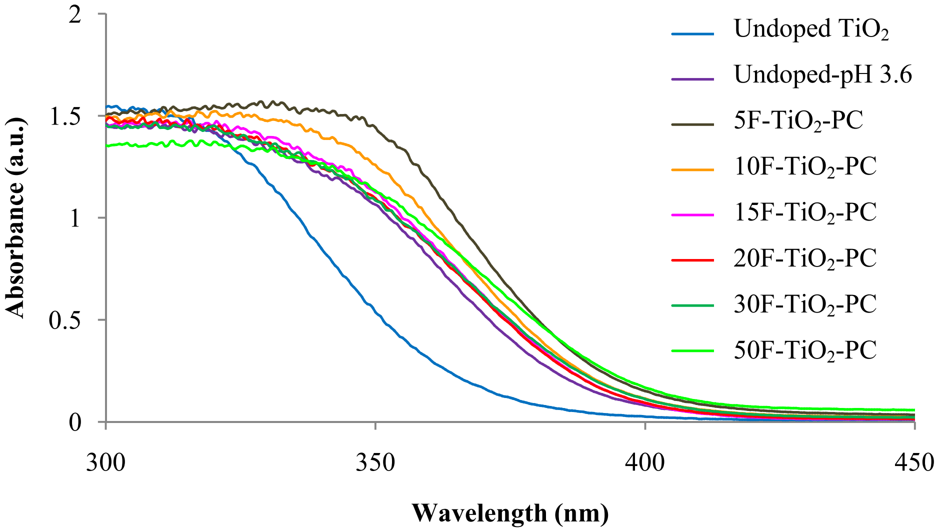

Figure 3.42 Diffused reflectance UV-vis spectra of the synthesized TiO_2 powders.

In Figure 3.42, the UV-vis diffused reflectance of amorphous undoped TiO_2 is compared with F-TiO_2-PC's. The undoped TiO_2 showed absorbance in the shorter wavelength region while F-TiO_2-PC shifted toward a longer wavelength. The band gap energy of amorphous undoped TiO_2 and 30F-TiO_2-PC were 3.35 and 3.13 eV, respectively. It was found that, narrowing of the band gap of TiO_2 upon doping was responsible for the enhanced visible light activity. The data of onset of absorbance and band gap energy of all samples are summarized in Table 3.14.

Table 3.14 Band gap energy from DRS technique of the synthesized TiO_2 powders.

TiO_2 samples	DRS	
	λ_{onset} of absorption (nm)	E_g (eV)
Undoped TiO_2	370	3.35
Undoped-pH 3.6	391	3.17
5F-TiO_2-PC	395	3.15
10F-TiO_2-PC	395	3.14
15F-TiO_2-PC	396	3.13
20F-TiO_2-PC	396	3.13
30F-TiO_2-PC	396	3.13
50F-TiO_2-PC	402	3.08

3.3.1.4 Photoluminescence spectroscopy (PL)

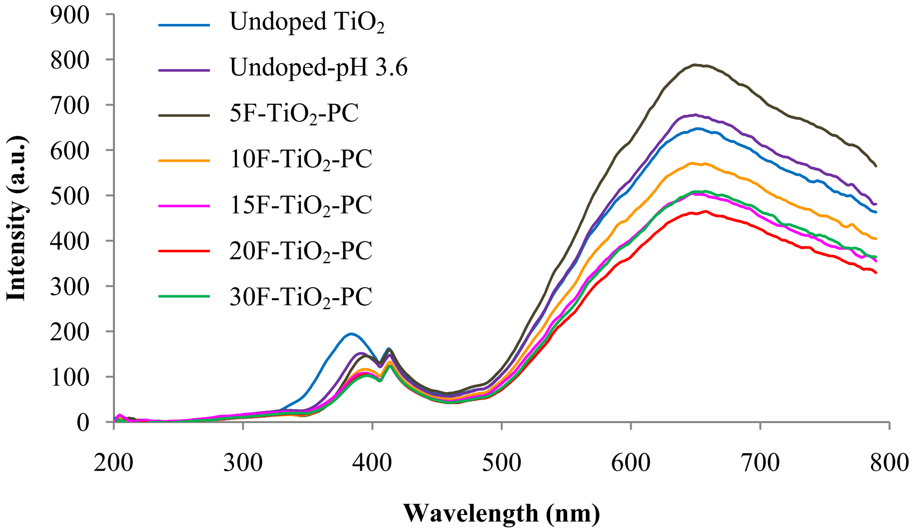

Figure 3.43 Photoluminescence spectra of the synthesized TiO_2 powders.

Figure 3.43 shows the PL spectra of the synthesized TiO_2 powders. The photoluminescence spectra of amorphous undoped TiO_2 and 30F-TiO_2-PC show the sharp UV emission at 383 nm and 396 nm, respectively. The UV band peak at 383 nm and 396 nm has been attributed to the electronic transition from conduction band (CB) to valence band (VB). The peak at 650 nm could be ascribed to electron transition mediated by defects level in the band gap (Suwanchawalit and Wongnawa, 2008). The band gap energy of amorphous undoped TiO_2 and 30F-TiO_2-PC calculated from PL data were 3.24 and 3.13 eV, respectively. The data of emission of absorbance and band gap energy of all samples are summarized in Table 3.15.

Table 3.15 Band gap energy from PL technique of the synthesized TiO_2 powders

TiO_2 samples	PL	
	$\lambda_{emission}$ (nm)	E_g (eV)
Undoped TiO_2	383	3.24
Undoped-pH 3.6	391	3.17
5F-TiO_2-PC	396	3.14
10F-TiO_2-PC	395	3.14
15F-TiO_2-PC	395	3.14
20F-TiO_2-PC	395	3.14
30F-TiO_2-PC	396	3.13

3.3.1.5 BET surface area (BET method)

The BET surface areas, type of isotherm and particle size of the synthesized TiO_2 powders are shown in Table 3.16. The BET surface area of amorphous undoped TiO_2 is 481.84 m^2g^{-1}. Amorphous undoped TiO_2 shows a smaller size and irregular surface lead to high specific surface area, while F-TiO_2-PC's show aggregation of particles having lower specific surface area. The BET surface area of undoped-pH 3.6 is 285.11 m^2g^{-1}. The specific surface area of the synthesized TiO_2 powders relates to the particle size. It was found that F-TiO_2-PC's have large effective surface area which is beneficial to enhance the adsorption of reactants leading to higher reaction activity. In addition, N_2 adsorption isotherms of the synthesized TiO_2 powders are shown in Figure 3.44. It was found that, amorphous undoped TiO_2 and F-TiO_2-PC's show the isotherms of type I (BDDT classification). The type I isotherm is given by microporous solid. The very steep region at low P/P_0 is due to the filling of very narrow pores and limiting uptake is dependent on the accessible micropore volume rather than on the internal surface area (Ryu, *et al.*, 1999). Porosity, T-plot of N_2 adsorption isotherm and pore size distribution curve of the synthesized TiO_2 powders are shown in Table 3.17, Figure 3.45 and Figure 3.46, respectively. The t-plot data of the synthesized TiO_2 powders showed straight line passing the origin indicating they contained micropores structure. The pore size distribution plot calculated using the Barrett-Joyner-Halenda (BJH) equation exhibits a narrow pore size distribution with an average pore diameter at *ca.* 5-15 nm.

Table 3.16 BET surface area, Type of isotherm and particle size of the synthesized TiO_2 powders.

TiO_2 samples	Surface area (m^2g^{-1})	Type of isotherm	particle size[a] (nm)
Undoped TiO_2	481.84	Type I	3.19
Undoped-pH 3.6	285.11	Type I	5.40
5F-TiO_2-PC	269.29	Type I	5.71
10F-TiO_2-PC	272.70	Type I	5.64
15F-TiO_2-PC	285.52	Type I	5.39
20F-TiO_2-PC	281.05	Type I	5.47
30F-TiO_2-PC	303.17	Type I	5.07

[a] Determined by BET using $D = 6000/(\rho \times \text{BET surface area})$, where ρ is approximated to be 3.90 g/cm^3 of anatase density. (The true value of ρ of amorphous is not known, however, it should be slightly less than that of anatase. In this calculation, we can only use the approximated value.)

Table 3.17 Porosity of the synthesized TiO_2 powders.

TiO_2 Sample	Pore volume (%) for pore diameter (nm)								Porosity (mL/g)
	<6	6-8	8-10	10-12	12-16	16-20	20-80	>80	
Undoped TiO_2	41.30	11.05	5.31	5.38	6.54	5.76	17.90	6.76	0.11
Undoped-pH 3.6	32.05	14.95	8.45	9.14	9.39	6.84	15.10	4.09	0.30
5F-TiO_2-PC	33.60	20.17	11.53	11.71	10.38	6.22	5.49	0.89	0.30
10F-TiO_2-PC	37.09	21.04	12.81	10.15	7.14	3.59	6.40	1.77	0.29
15F-TiO_2-PC	48.02	20.26	8.04	5.91	3.13	2.14	8.03	4.47	0.23
20F-TiO_2-PC	40.74	13.06	6.15	5.70	6.63	6.21	17.29	4.22	0.22
30F-TiO_2-PC	52.32	17.12	6.57	5.51	4.29	2.91	8.14	3.14	0.19

(1) N_2 adsorption isotherm of the synthesized TiO_2 powders

(a) Undoped TiO_2

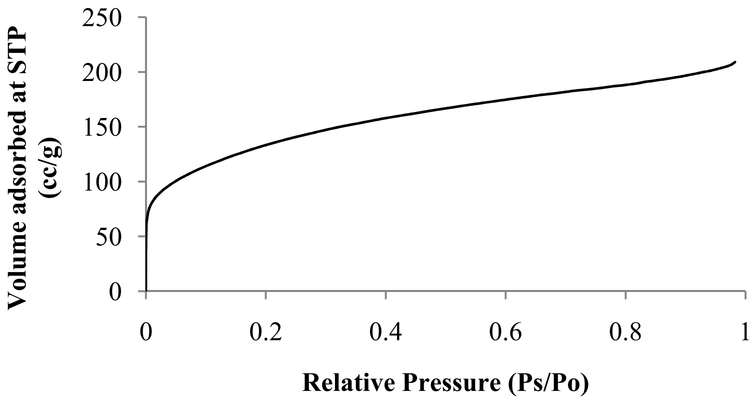

(b) Undoped-pH 3.6

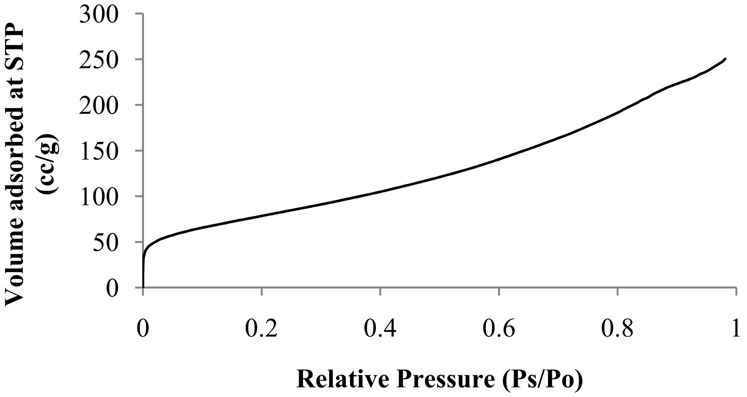

(c) 5F-TiO$_2$-PC

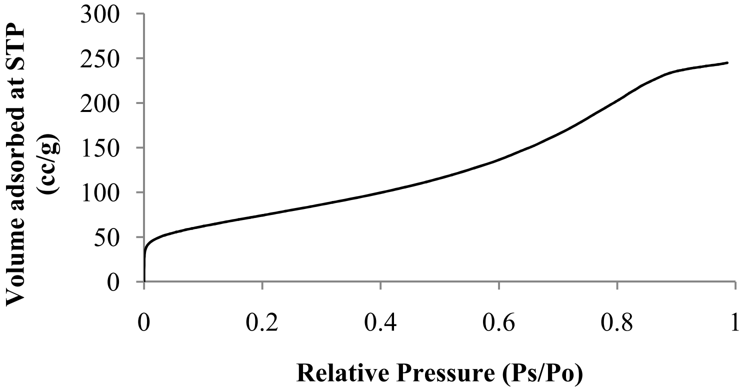

(d) 10F-TiO$_2$-PC

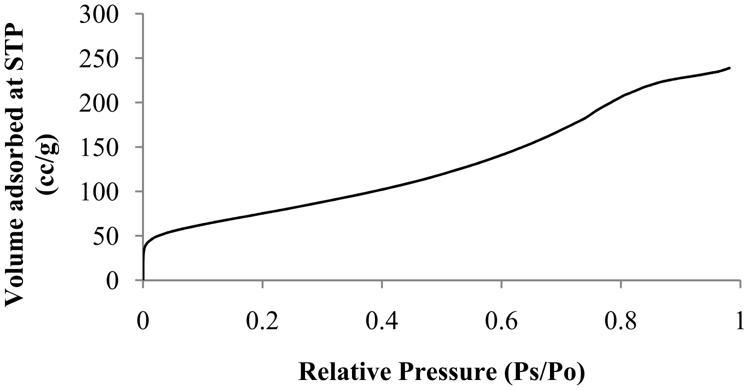

(e) 15F-TiO_2-PC

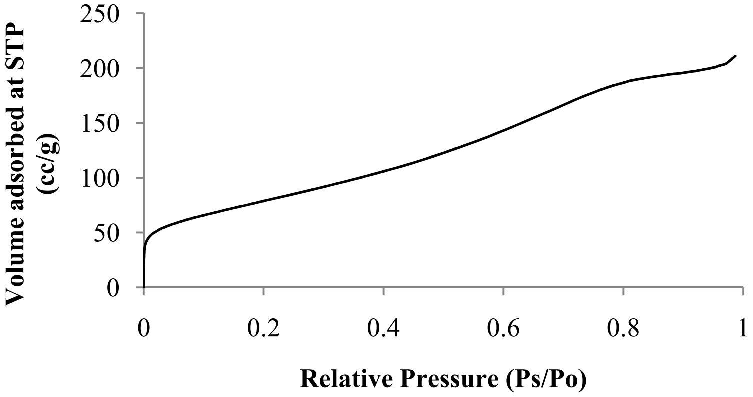

(f) 20F-TiO_2-PC

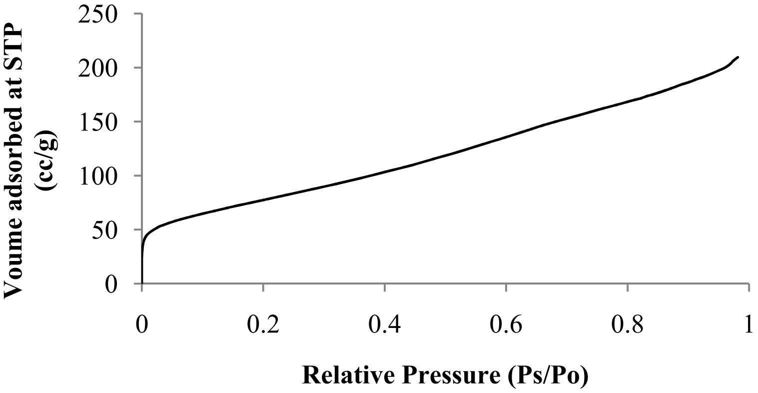

(g) 30F-TiO_2-PC

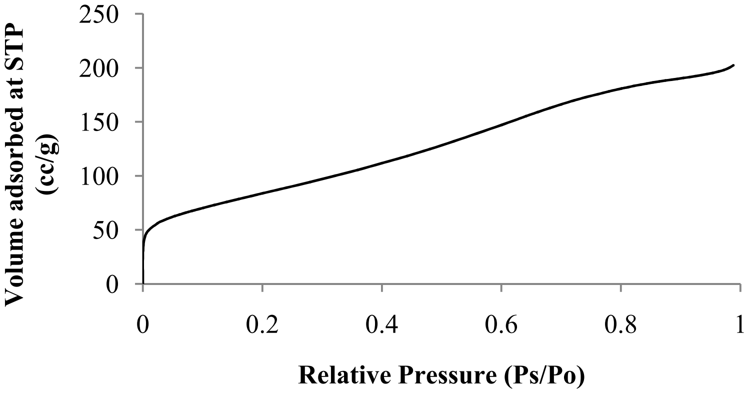

Figure 3.44 N_2 adsorption isotherms of the synthesized TiO_2 powders; (a) undoped TiO_2, (b) undoped-pH 3.6, (c) 5F-TiO_2-PC, (d) 10F-TiO_2-PC, (e) 15F-TiO_2-PC, (f) 20F-TiO_2-PC, (g) 30F-TiO_2-PC.

(2) T-plot of N_2 adsorption isotherm of the synthesized TiO_2 powders

(a) Undoped TiO_2

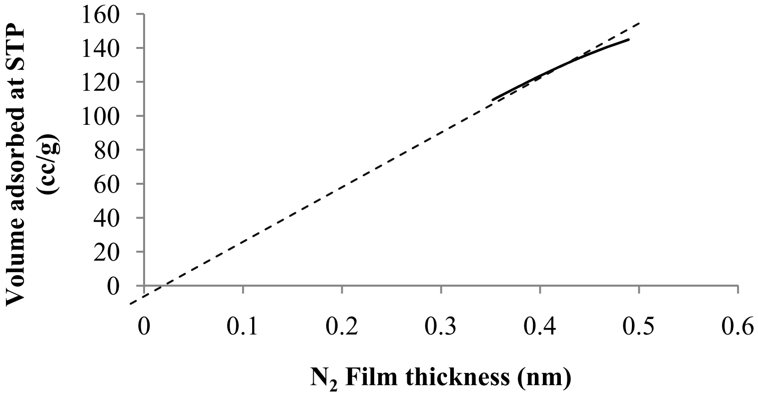

(b) Undoped-pH 3.6

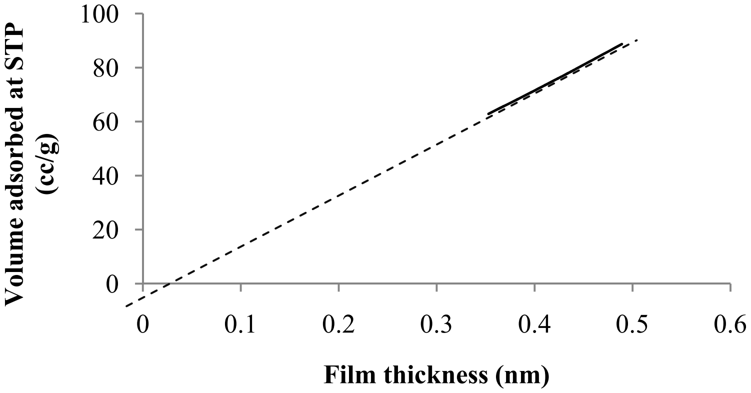

(c) 5F-TiO_2-PC

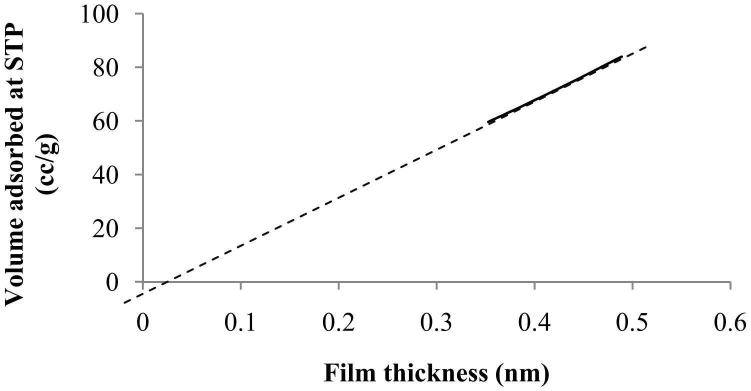

(d) 10F-TiO$_2$-PC

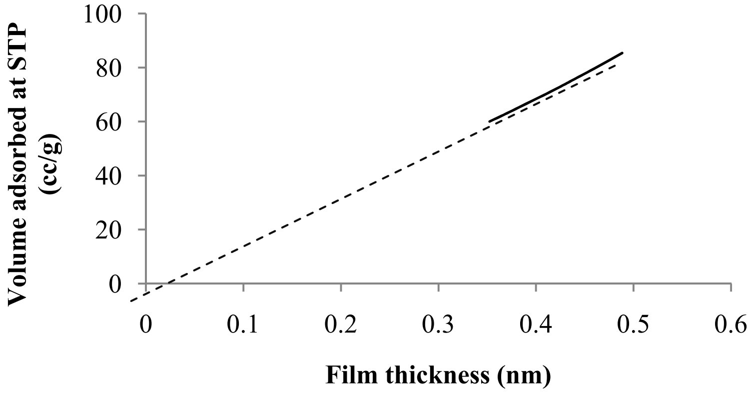

(e) 15F-TiO$_2$-PC

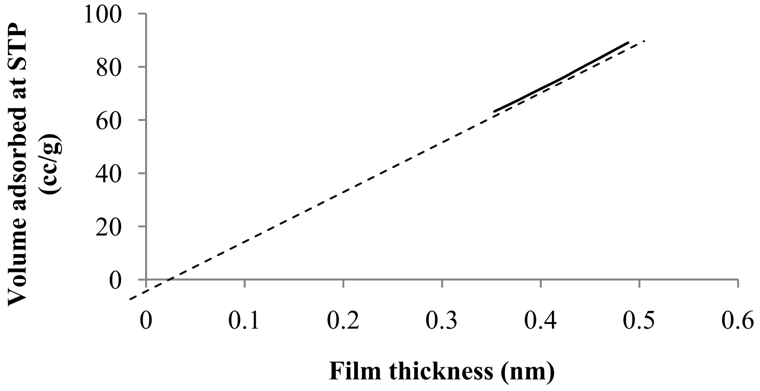

(f) 20F-TiO$_2$-PC

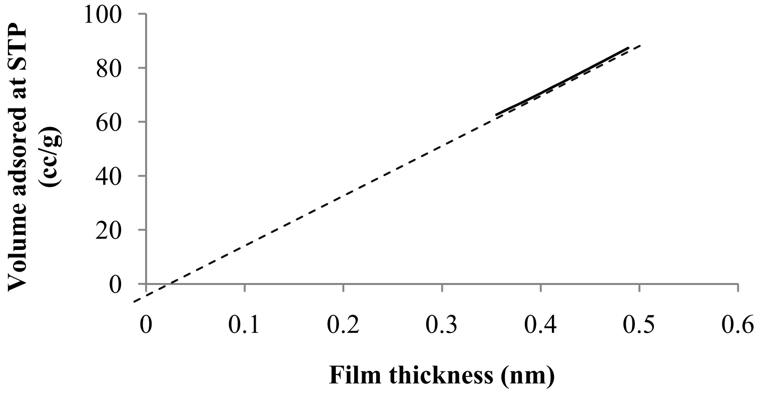

(g) 30F-TiO$_2$-PC

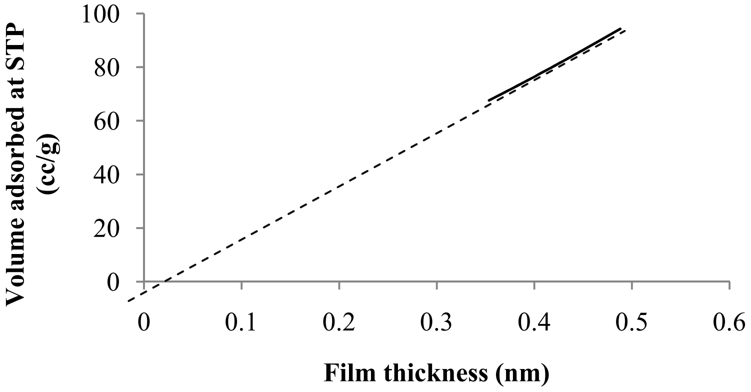

Figure 3.45 T-plot of N_2 adsorption isotherm of the synthesized TiO$_2$ powders; (a) undoped TiO$_2$, (b) undoped-pH 3.6, (c) 5F-TiO$_2$-PC, (d) 10F-TiO$_2$-PC, (e) 15F-TiO$_2$-PC, (f) 20F-TiO$_2$-PC, (g) 30F-TiO$_2$-PC.

(3) Pore size distribution curve of the synthesized TiO_2 powders

(a) Undoped TiO_2

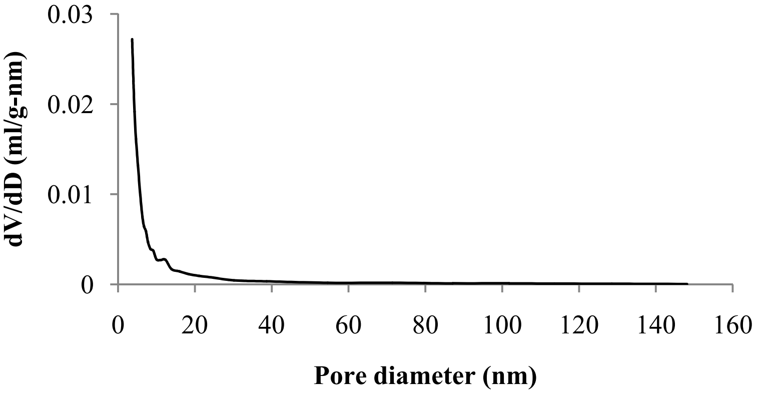

(b) Undoped-pH 3.6

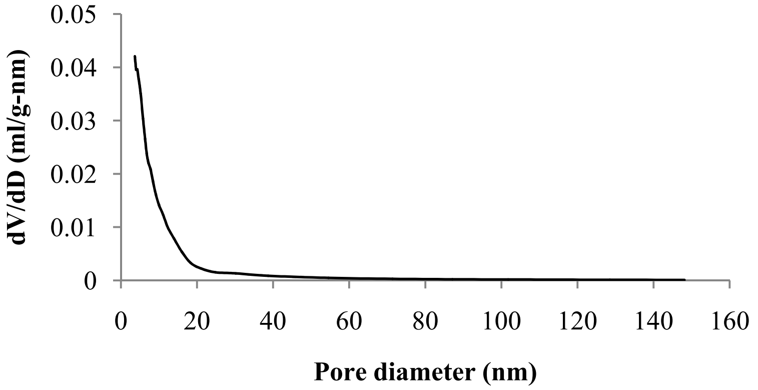

(c) 5F-TiO_2-PC

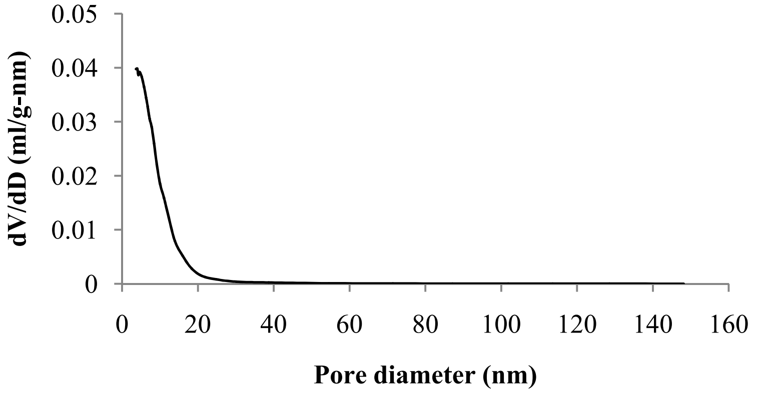

(d) 10F-TiO_2-PC

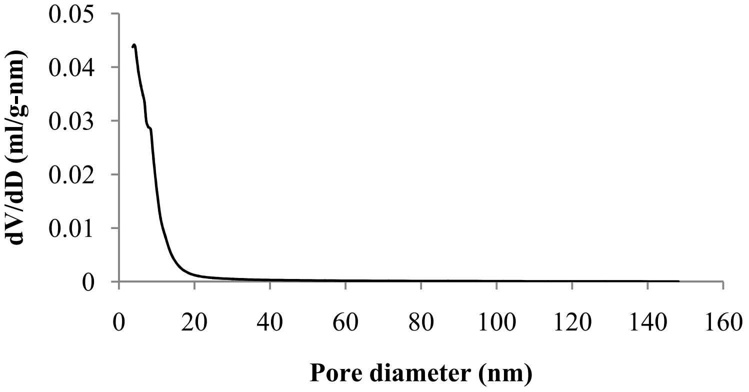

(e) 15F-TiO_2-PC

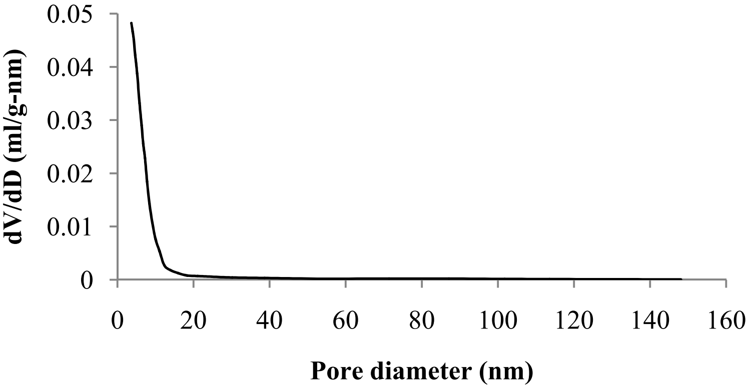

(f) 20F-TiO_2-PC

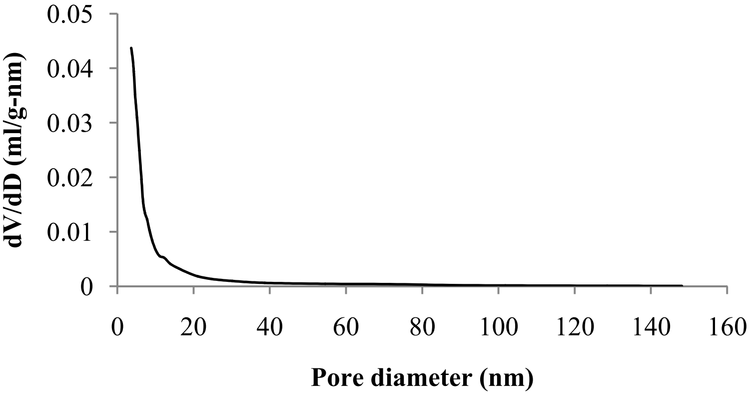

(g) 30F-TiO_2-PC

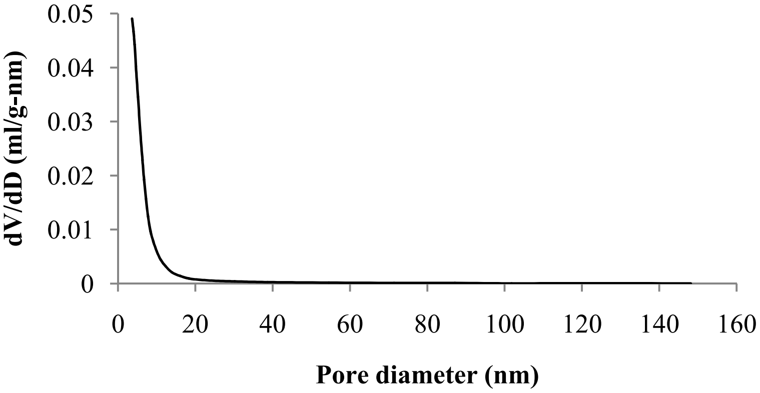

Figure 3.46 Pore size distribution curves of the synthesized TiO_2 powders; (a) undoped TiO_2, (b) undoped-pH 3.6, (c) 5F-TiO_2-PC, (d) 10F-TiO_2-PC, (e) 15F-TiO_2-PC, (f) 20F-TiO_2-PC, (g) 30F-TiO_2-PC.

3.3.1.6 Fourier-transformed infrared spectroscopy (FT-IR)

FT-IR spectra of the synthesized TiO_2 powders are shown in Figure 3.47. The spectra were scanned in wavenumber range of 4000 to 400 cm^{-1}. Four main vibrational bands are displayed for the synthesized TiO_2 powders at 3500-3000, 1639, 1401 and 800-400 cm^{-1}. The bands in the range of 3500-3000 cm^{-1} and 1640-1600 cm^{-1} are assigned to the stretching and bending vibrations of the hydroxyl on the surface of TiO_2 powers, respectively. The band at 1401 cm^{-1} can be attributed to bending regions of NH_4^+. The bands in the range of 800-400 cm^{-1} can be assigned to Ti-O stretching and Ti-O-Ti bridging stretching modes. F-TiO_2-PC's showed the decreasing intensity of the band at 1401 cm^{-1}. The bands in the range of 3500-3000 cm^{-1} (surface OH groups) of F-TiO_2-PC's when compared to amorphous undoped TiO_2. It can be concluded that F element was either entrapped in surface of F-TiO_2-PC or incorporated in the TiO_2 lattice. The Ti-F vibration, if present, showed appear as small band at 889 cm^{-1} (Huang, *et al.*, 2007), however, it was not found in F-TiO_2-PC due to the large and strong band at 800-400 cm^{-1}. The data of vibrational bands, assignments, functional groups and literatures of the synthesized TiO_2 powders are summarized in Table 3.18.

(a) Undoped TiO_2

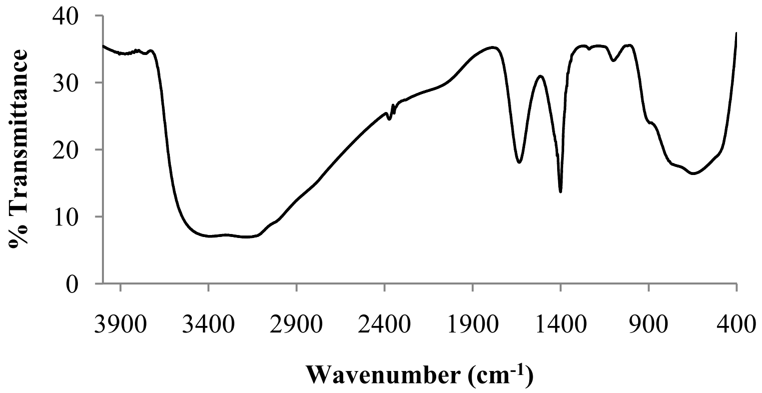

(b) Undoped-pH 3.6

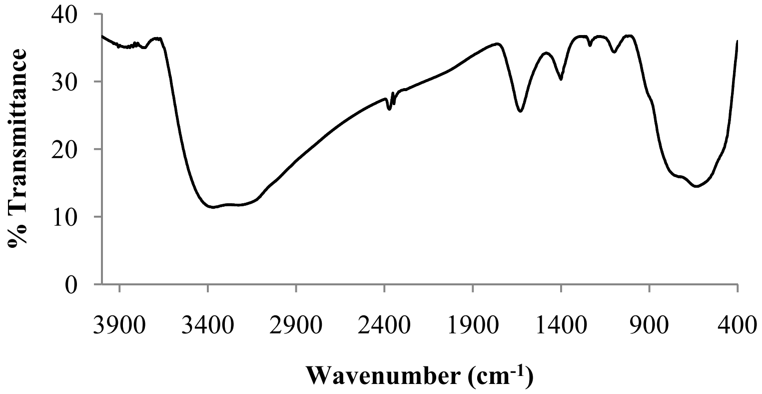

(c) 5F-TiO_2-PC

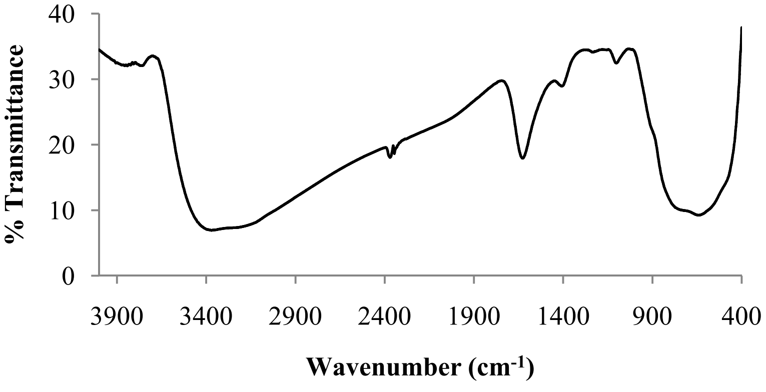

(d) 10F-TiO_2-PC

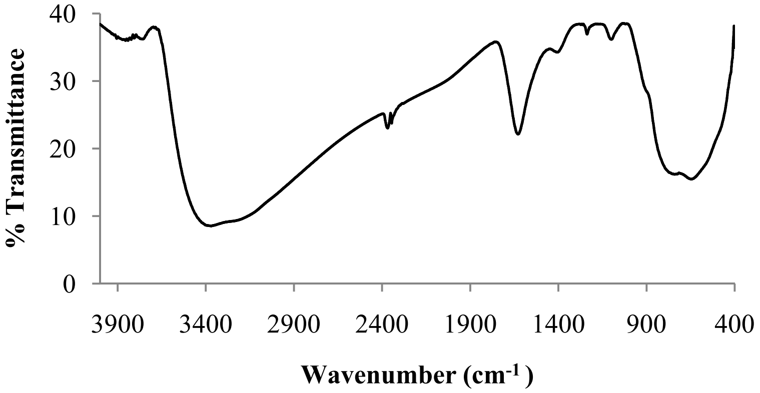

(e) 15F-TiO_2-PC

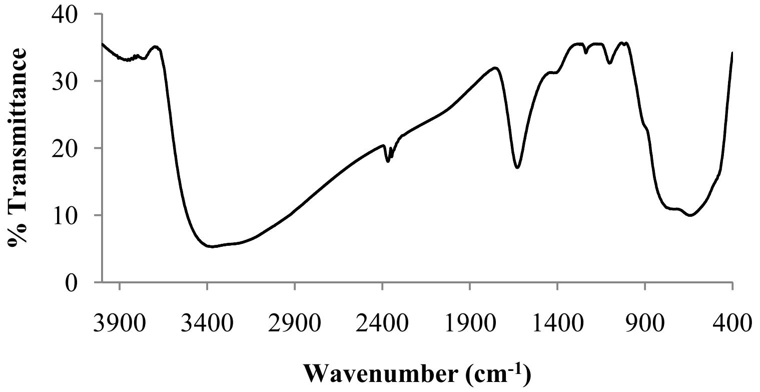

(f) 20F-TiO_2-PC

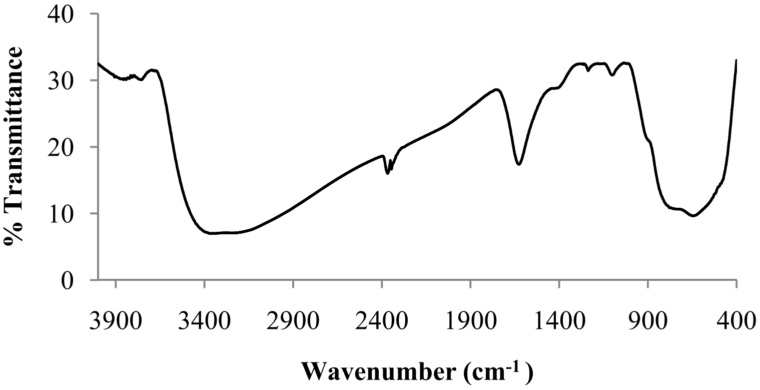

(g) 30F-TiO_2-PC

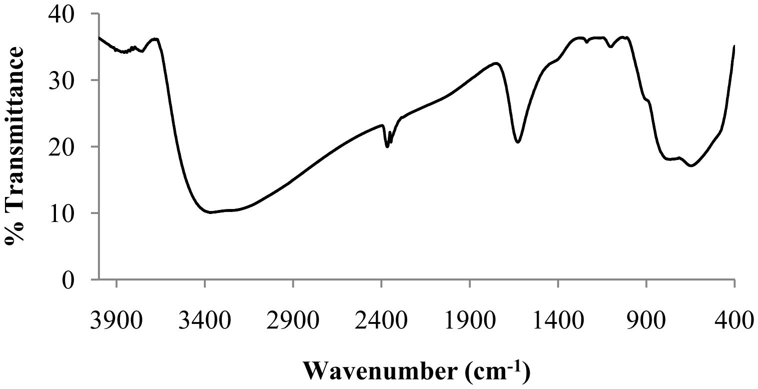

Figure 3.47 FT-IR spectra of the synthesized TiO_2 powders; (a) undoped TiO_2, (b) undoped-pH 3.6, (c) 5F-TiO_2-PC, (d) 10F-TiO_2-PC, (e) 15F-TiO_2-PC, (f) 20F-TiO_2-PC, (g) 30F-TiO_2- PC.

Table 3.18 The FT-IR bands of the synthesized TiO_2 powders.

TiO_2	Vibrational bands (cm^{-1})	Assignments	Functional groups	Literatures
Undoped TiO_2	3500-3000 2380 1639 1402 below 800	ν_{OH} and ν_{NH} ν_{co} δ_{OH} δ_{NH} $\nu_{Ti\text{-}O}$	H_2O and NH_4^+ CO_2 OH groups NH_4^+ group Ti-O bond	Wei, *et al.*, 2008 Yeung, *et al.*, 2003 Yang, *et al.*, 2010 Youn, *et al.*, 1999 Reddy, *et al.*, 2009
Undoped-pH 3.6	3500-3000 2385 1630 1401 below 800	ν_{OH} and ν_{NH} ν_{co} δ_{OH} δ_{NH} $\nu_{Ti\text{-}O}$	H_2O and NH_4^+ CO_2 OH groups NH_4^+ group Ti-O bond	Wei, *et al.*, 2008 Yeung, *et al.*, 2003 Yang, *et al.*, 2010 Youn, *et al.*, 1999 Huo, *et al.*, 2009

Table 3.18 The FT-IR bands of the synthesized TiO_2 powders. (Continued)

TiO_2	Vibrational bands (cm^{-1})	Assignments	Functional groups	Literatures
5F-TiO_2-PC	3500-3000 2385 1630 1402 below 800	ν_{OH} and ν_{NH} ν_{co} δ_{OH} δ_{NH} $\nu_{Ti\text{-}O}$	H_2O and NH_4^+ CO_2 OH groups NH_4^+ group Ti-O bond	Wei, *et al.*, 2008 Yeung, *et al.*, 2003 Yang, *et al.*, 2010 Youn, *et al.*, 1999 Huo, *et al.*, 2009
10F-TiO_2-PC	3500-3000 2385 1631 1402 below 800	ν_{OH} and ν_{NH} ν_{co} δ_{OH} δ_{NH} $\nu_{Ti\text{-}O}$	H_2O and NH_4^+ CO_2 OH groups NH_4^+ group Ti-O bond	Wei, *et al.*, 2008 Yeung, *et al.*, 2003 Yang, *et al.*, 2010 Youn, *et al.*, 1999 Reddy, *et al.*, 2009
15F-TiO_2-PC	3500-3000 2385 1630 1402 below 800	ν_{OH} and ν_{NH} ν_{co} δ_{OH} δ_{NH} $\nu_{Ti\text{-}O}$	H_2O and NH_4^+ CO_2 OH groups NH_4^+ group Ti-O bond	Wei, *et al.*, 2008 Yeung, *et al.*, 2003 Yang, *et al.*, 2010 Youn, *et al.*, 1999 Reddy, *et al.*, 2009
20F-TiO_2-PC	3500-3000 2385 1630 1402 below 800	ν_{OH} and ν_{NH} ν_{co} δ_{OH} δ_{NH} $\nu_{Ti\text{-}O}$	H_2O and NH_4^+ CO_2 OH groups NH_4^+ group Ti-O bond	Wei, *et al.*, 2008 Yeung, *et al.*, 2003 Yang, *et al.*, 2010 Youn, *et al.*, 1999 Huo, *et al.*, 2009
30F-TiO_2-PC	3500-3000 2385 1630 1402 below 800	ν_{OH} and ν_{NH} ν_{co} δ_{OH} δ_{NH} $\nu_{Ti\text{-}O}$	H_2O and NH_4^+ CO_2 OH groups NH_4^+ group Ti-O bond	Wei, *et al.*, 2008 Yeung, *et al.*, 2003 Yang, *et al.*, 2010 Youn, *et al.*, 1999 Huo, *et al.*, 2009

3.3.1.7 Thermogravimetric analysis (TGA)

The TGA results of undoped-pH 3.6- PC in Figure 3.48a shows that the weight loss about 20.54%, from 41 °C to 273 °C, corresponds to the evaporation of water and solvent. In the temperature range of 273-650 °C, the weight loss about 2.45% can be attributed to the oxidation of carbon residue and evaporation of chemisorbed water.

There are three regions of weight loss in the case of 30F-TiO_2-PC. Figure 3.48b shows the TGA spectra of 30F-TiO_2-PC with the weight loss about 17.55% below 178 °C corresponds to the evaporation of water and alcohol. In the temperature range of 178-333 °C, the weight loss about 3.17% is due to the removal of strongly bound water or surface hydroxyl groups and the weight loss of 2.2% in the range of 333-700 °C corresponds to the oxidation of carbon residue and evaporation of chemisorbed water.

(a) Undoped-pH 3.6-PC

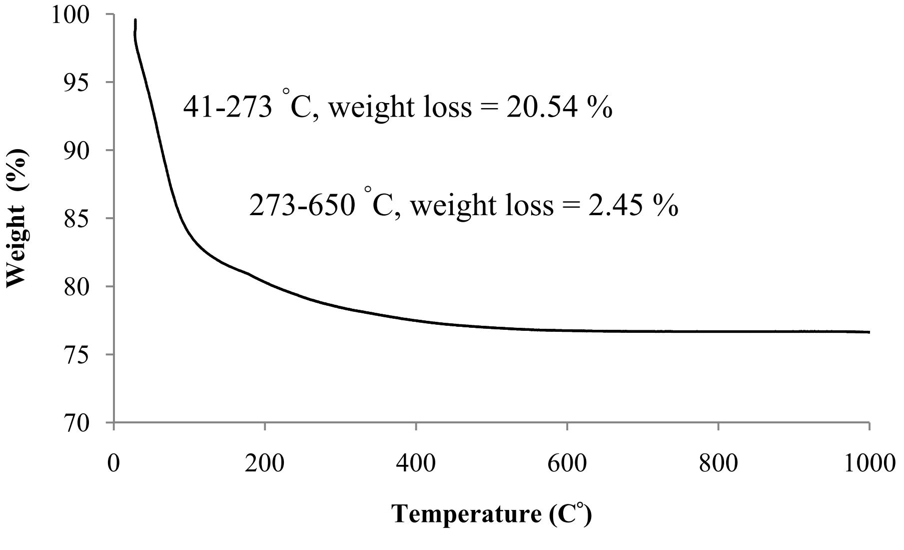

(b) 30F-TiO_2-PC

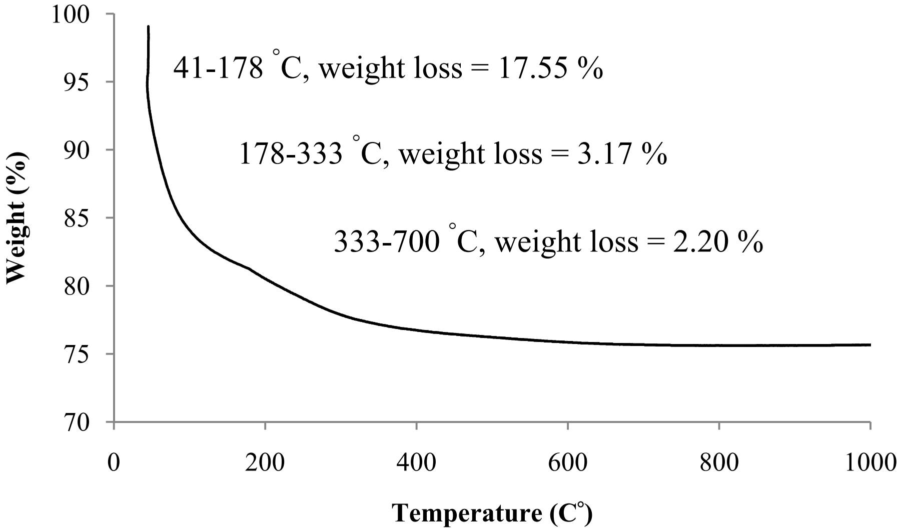

Figure 3.48 TGA spectra of the synthesized TiO_2 powders were measured at a heating rate of 10 °C/min; (a) undoped-pH 3.6-PC, (b) 30F-TiO_2-PC.

3.3.1.8 Differential scanning calorimetry (DSC)

The DSC spectra of undoped-pH 3.6-PC (Figure 3.49a) exhibits the endothermic peak at 91 °C which corresponds to the desorption of the physisorbed water and alcohol. The endothermic peak at 276 °C in DSC curve corresponds to the crystallization of the amorphous phase to anatase. Figure 3.49b shows the DSC spectra of 30F-TiO_2-PC with the endothermic peak at 99 °C which is due to the desorption of water and alcohol. The endothermic peak at 267 °C corresponds to the decomposition of organic substances. The exothermic peak at about 334 °C is possibly the phase transformation from amorphous to anatase. A similar result was reported by Chen, *et al.*, (2009) who studied the thermogravimetry-differential thermal analysis (TG-DTA) of $(NH_4)_2TiF_6$ to further confirm the change of the crystal structures. It was found that there were three apparently endothermic peaks at 283 °C, 343 °C, and 411 °C, respectively. It was deduced that $(NH_4)_2TiF_6$ changed with the increase of temperature as: $(NH_4)_2TiF_6 \longrightarrow NH_4TiOF_3 \longrightarrow TiOF_2 \longrightarrow TiO_2$. NH_4F that was formed during the formation of NH_4TiOF_3 and $TiOF_2$ further decomposed to HF and NH_3 which exhibited strong peaks at 283 °C and 343 °C. When the temperature exceeds 480 °C, the residual weight changed slightly, indicating that TiO_2 became the major component in the product.

Huang, *et al.*, (2006) studied anatase type N-F-codoped TiO_2 powder prepared by a sol-gel solvothermal method using tetrabutyl titanate as precursor. To fully understand the stability of N-F-codoped TiO_2 powders, the thermal behavior of the sol-gel-solvothermal process N-F-TiO_2 sample was investigated. Thermal analysis-thermogravimetry (DTA-TG) curves showed a sharp endothermic peak appeared at 103.73 °C due to the desorption of water and alcohol. The relatively broad exothermic peak at 350.67 °C was assigned to the decomposition of organic substances in the powder.

(a) Undoped-pH 3.6-PC

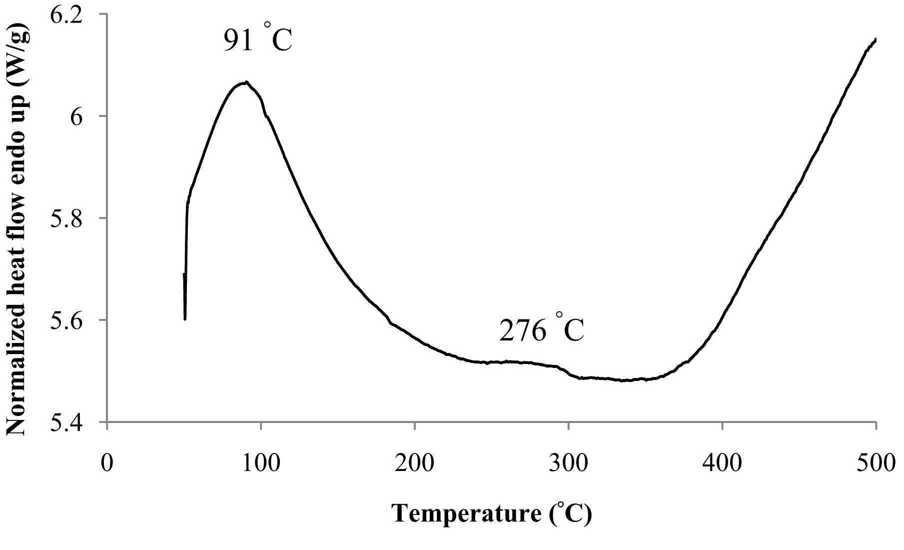

(b) 30F-TiO_2-PC

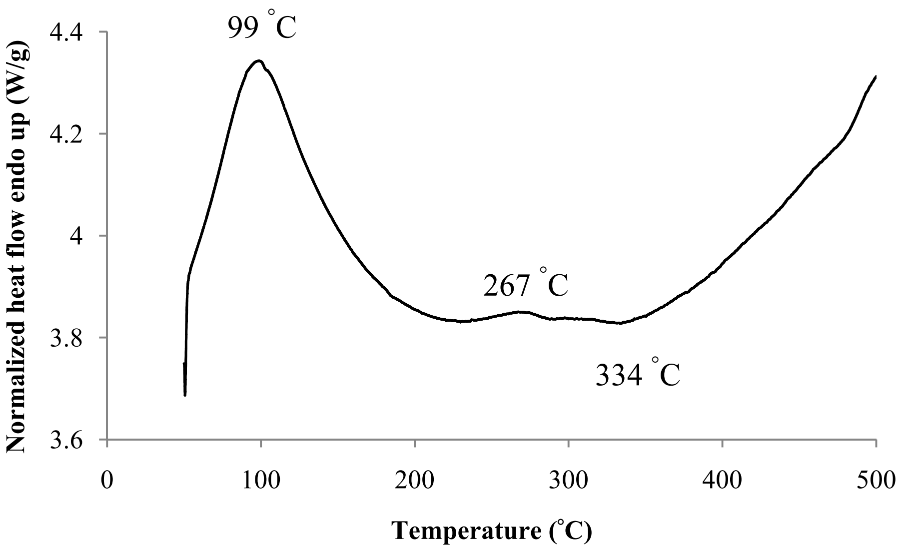

Figure 3.49 DSC spectra of the synthesized TiO_2 powders; (a) undoped-pH 3.6-PC, (b) 30F-TiO_2-PC.

3.3.1.9 X-ray absorption spectroscopy (XAS)

X-ray absorption spectroscopy contains information about the oxidation state of all TiO_2 samples. XAS spectra of the synthesized TiO_2 powders and commercial TiO_2 are shown in Figure 3.50. XAS spectra were recorded the absorption energy between 4950 eV and 5050 eV. The absorption energy for Degussa P25 and anatase occurs at 4979 eV and 4980 eV, respectively. The absorption energy for the synthesized TiO_2 powders occurs at 4978-4976 eV. The XAS spectra of all TiO_2 samples indicate that F-TiO_2-PC's contain titanium in the oxidation state (Ti^{4+}). The position of the edge region is shifted to lower energy with decreasing titanium oxidation state (Geselbracht, *et al.*, 2006).

A similar result was reported by Yang, *et al.*, (2008) who studied the effects of borosilicate glass composition and melting condition on valence state and coordination geometry of polyvalent Ti ions were studied by X-ray absorption experiments. There are three pre-peaks for model compounds rutile and anatase. It is well known that Ti^{4+} ions occupy slightly distorted octahedral sites in rutile and anatase, denoted as Ti^{4+}. The intensities and energies of pre-peaks for these model compounds are also different as shown in Table 3.19.

Geselbracht, *et al.*, (2006) reduced titanates in the ATi_2O_4 (A = Li, Mg) spinel family exhibiting a variety of interesting electronic and magnetic properties, most notably superconductivity in the mixed-valence spinel, $Li_{1+x}Ti_{2-x}O_4$. They showed that sodium and calcium analogs, $NaTi_2O_4$ and $CaTi_2O_4$, each differed in structure, the main features of which were double rutile-type chains composed of edge-sharing TiO_6 octahedra. XANES spectroscopy at the Ti K-edge was used to probe the titanium valence. The absorption edge position and the pre-edge spectral features observed in the XANES data confirmed the assignment of Ti^{3+} in $CaTi_2O_4$ and mixed-valence $Ti^{3+/}Ti^{4+}$ in $NaTi_2O_4$.

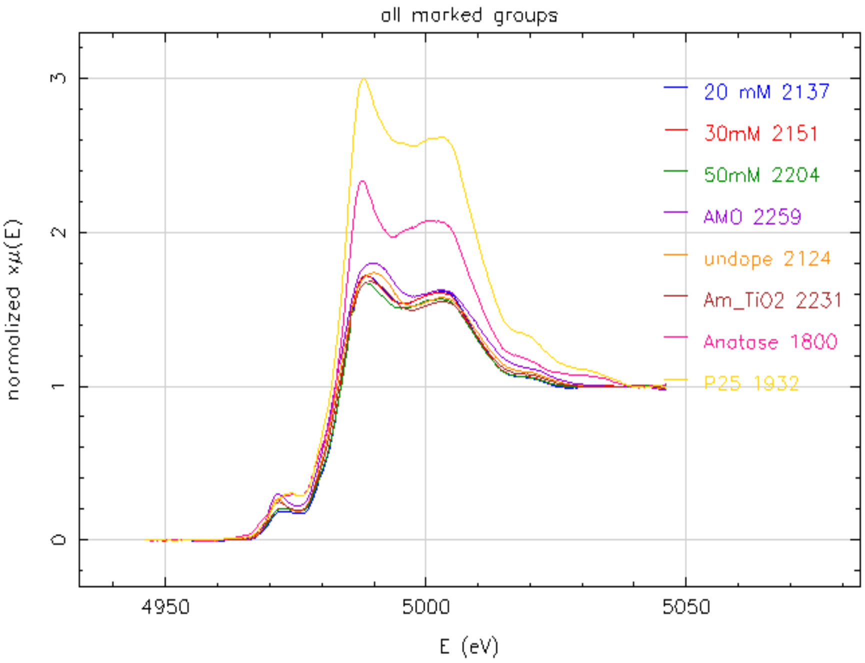

Figure 3.50 XAS spectra of all TiO_2 samples.

Table 3.19 Near Ti K-edge information for selected Ti-containing model compounds and glasses (Yang, *et al.*, 2008).

Samples	Ti-O coordination	Ti K-edge energy (eV)	Edge energy shift (eV)	Pre-edge information	
				Energy (eV)	Relative height
Ti foil	-	4972.8	0	-	-
Ti_2O_3	Ti^{3+}	4975.8	3.0	4970.4	0.2
TiO_2-rutile	Ti^{4+}	4979.5	6.7	4968.7 4971.9 4974.3	0.06 0.22 0.22
TiO_2-anatase	Ti^{4+}	4982.1	9.1	4968.8 4971.9 4974.3	0.09 0.17 0.17
$Sr_2TiSi_2O_8$	Ti^{4+}	4979.7	6.9	4970.4	0.61
$Ba_2TiSi_2O_8$	Ti^{4+}	4979.4	6.6	4970.6	0.52
$CsAlTiO_4$	Ti^{4+}	4979.7	6.9	4969.7	0.68

3.3.2 The pH of the point of zero charge (pH_{pzc})

The pH_{pzc} of the TiO_2 samples were determined from Figure 3.51 and Figure 3.52 and their values are summarized in Table 3.20. The pH_{pzc} for undoped TiO_2, undoped-pH 3.6 and 30F-TiO_2-PC are 7.2, 6.4 and 3.6, respectively. In the presence of F^-, the pH_{pzc} is shifted to lower pH values and the positive charge on TiO_2 surface at acidic pH region is much reduced since the surface $\equiv$Ti-OH_2^+ groups are replaced by $\equiv$Ti-F species (Park and Choi, 2004).

Table 3.20 The pH_{pzc} of the synthesized TiO_2 powders.

TiO_2 samples	pH_{pzc}	
	pH drift method[a]	Salt addition method[b]
Undoped- TiO_2-PC	7.2	7.2
Undoped-pH 3.6-PC	6.4	6.5
10F-TiO_2-PC	5.4	5.4
15F-TiO_2-PC	4.3	4.3
20F-TiO_2-PC	4.1	4.2
30F-TiO_2-PC	3.6	3.6
50F-TiO_2-PC	3.5	3.4

[a] Bessekhouad, *et al*., 2004.

[b] Mullet, *et al*., 1997.

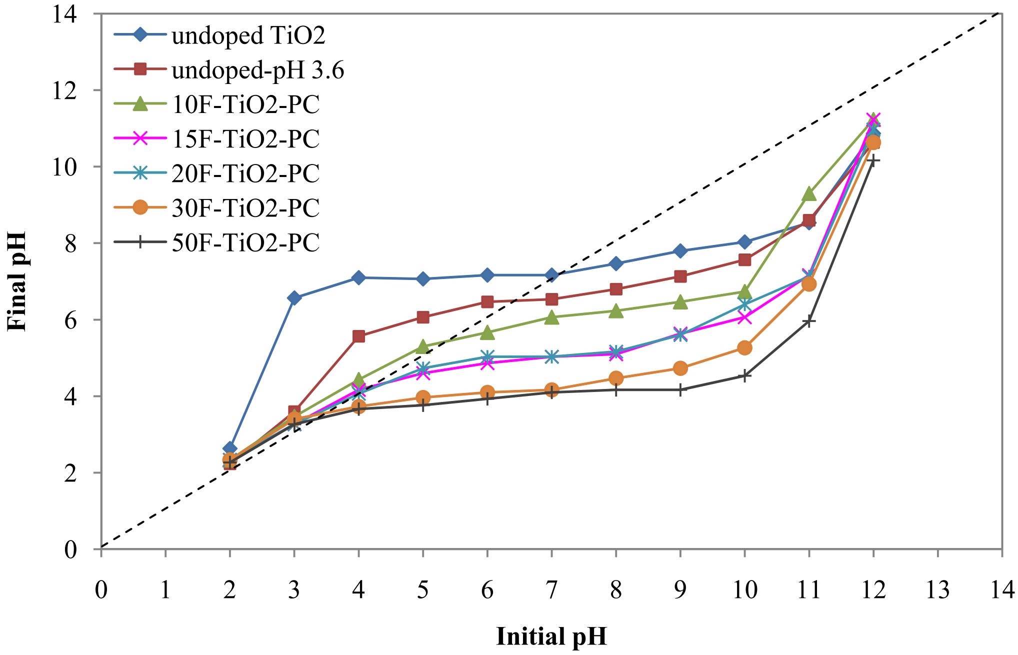

Figure 3.51 pH drift method to obtain pH_{pzc} for TiO_2 samples.

(a) Undoped TiO_2

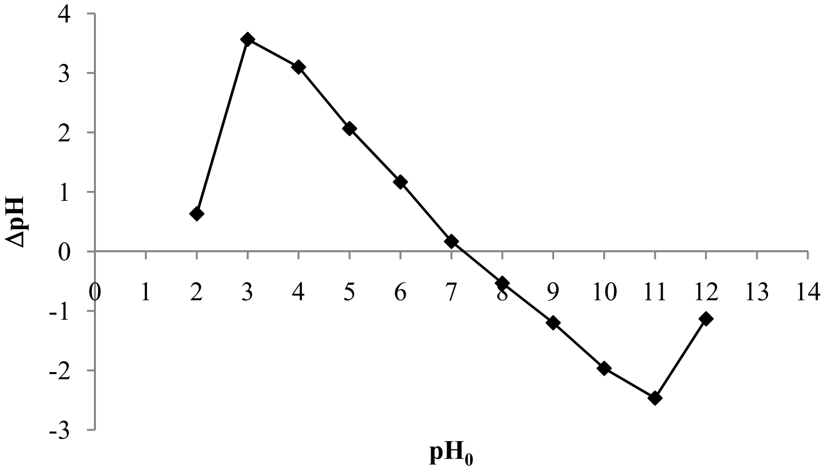

(b) Undoped-pH 3.6-PC

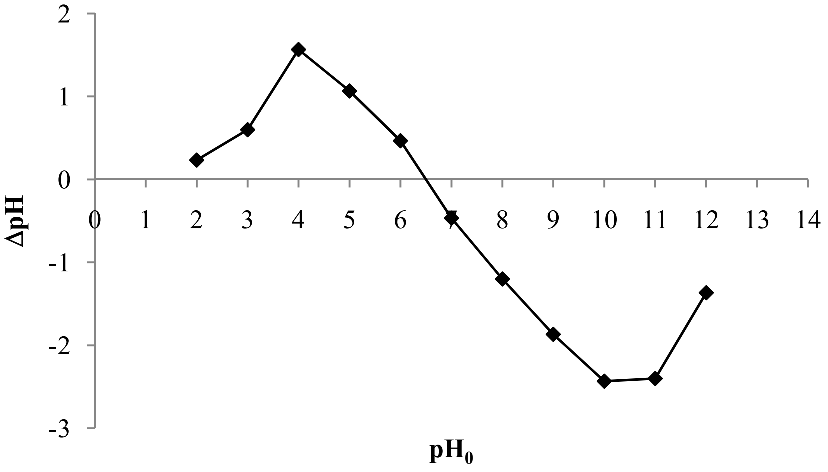

(c) 10F-TiO_2-PC

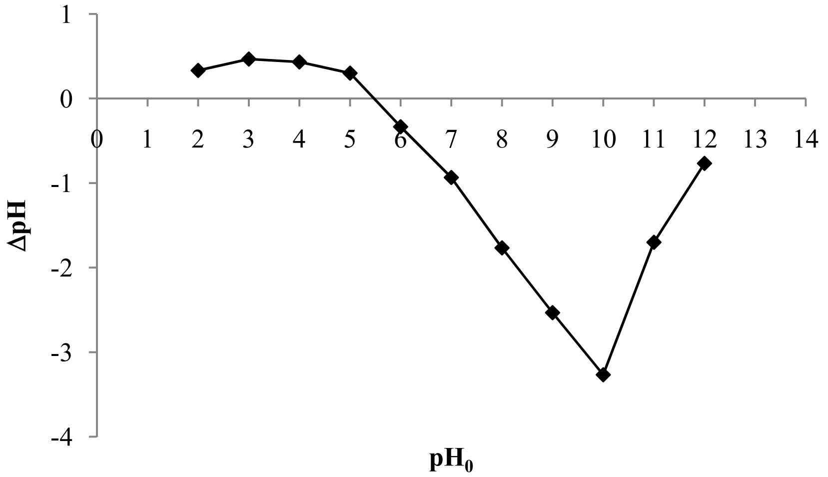

(d) 15F-TiO_2-PC

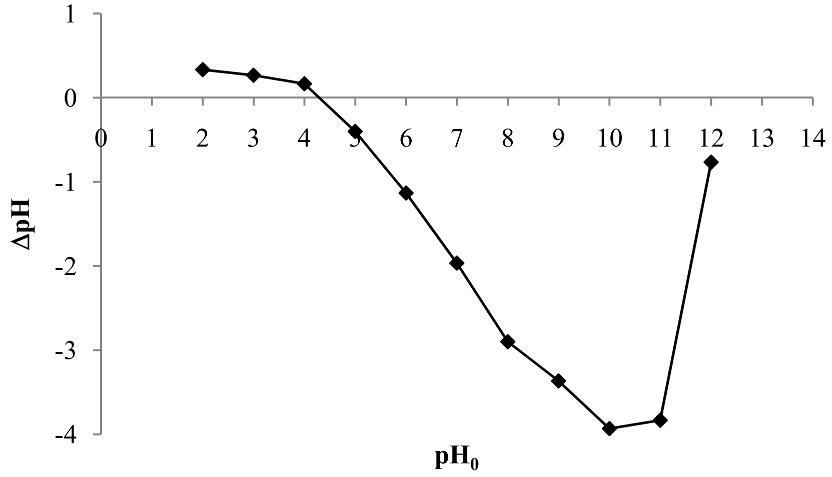

(e) 20F-TiO_2-PC

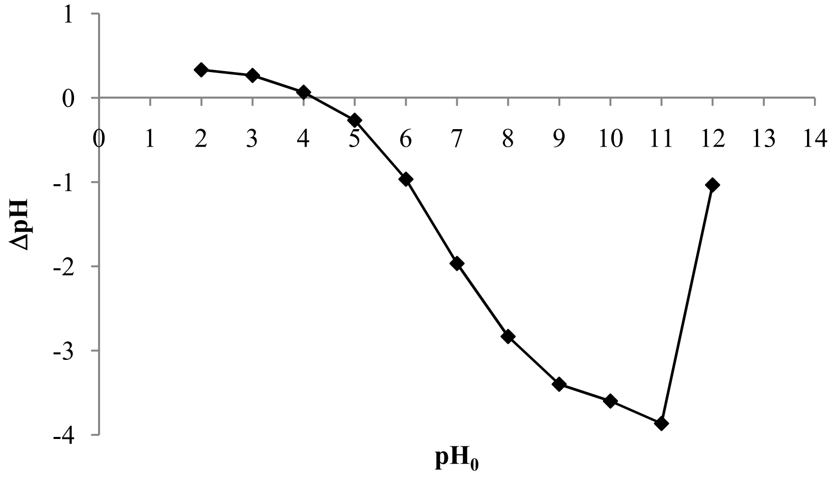

(f) 30F-TiO_2-PC

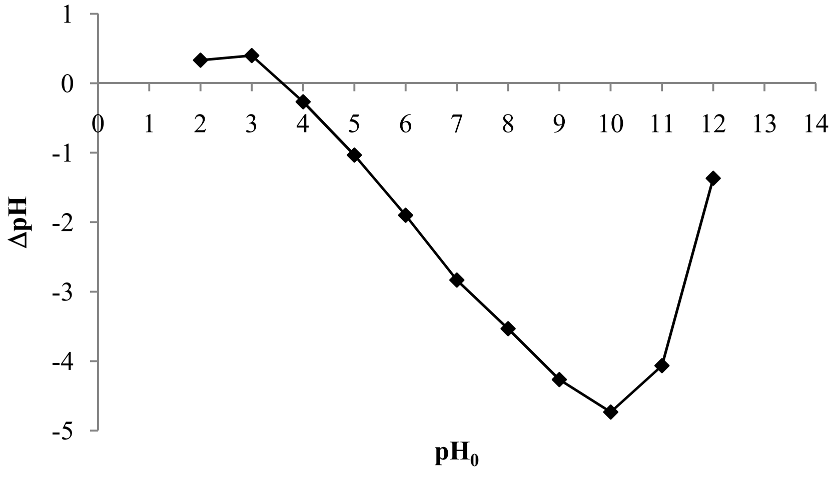

(g) 50F-TiO_2-PC

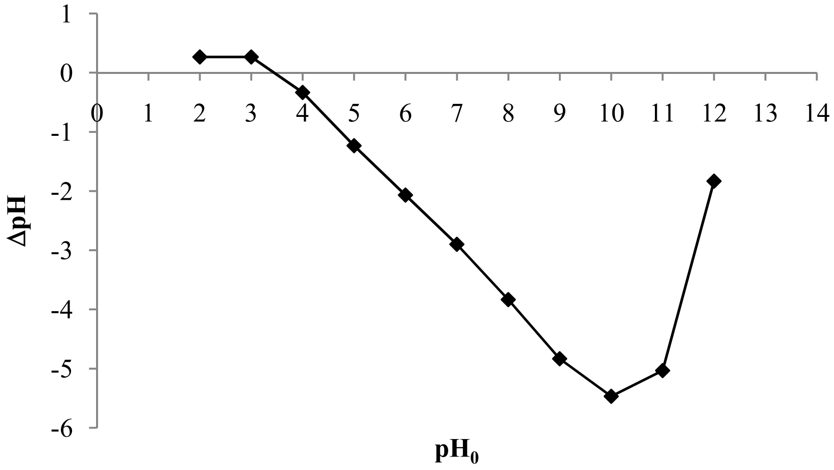

Figure 3.52 Salt addition method ($\Delta pH = pH_{final}-pH_{initial}$) for (a) undoped TiO_2, (b) undoped-pH 3.6-PC, (c) 10F-TiO_2-PC, (d) 15F-TiO_2-PC, (e) 20F-TiO_2-PC, (f) 30F-TiO_2-PC, (g) 50F-TiO_2-PC.

3.3.3 Titration of the synthesized TiO_2 powders

Acid-base titration can be applied for the quantitative characterization of the pH-dependent charge formation on TiO_2 surfaces. Undoped-pH 3.6 and F-TiO_2-PC's have decrease OH content at TiO_2 surface, resulting in a higher surface charge (high concentration, Table 3.21) and enhancement of surface acidity. Undoped TiO_2 have increase OH content of TiO_2, resulting in low surface charge. Titration data of the synthesized TiO_2 powders are shown in Table 3.21.

Table 3.21 Concentration of the synthesized TiO_2 powders

TiO_2 samples	Titrated with	Surface OH^- (mol)	Surface H^+ (mol)
Undoped TiO_2	0.01 M HCl	1.64×10^{-2}	-
Undoped-pH 3.6-PC	0.01 M NaOH	-	4.90×10^{-3}
5F-TiO_2-PC	0.01 M NaOH	-	8.65×10^{-3}
10F-TiO_2-PC	0.01 M NaOH	-	2.48×10^{-2}
15F-TiO_2-PC	0.01 M NaOH	-	2.87×10^{-2}
20F-TiO_2-PC	0.01 M NaOH	-	3.26×10^{-2}
30F-TiO_2-PC	0.01 M NaOH	-	5.25×10^{-2}
50F-TiO_2-PC	0.01 M NaOH	-	8.00×10^{-2}

3.3.4 Photocatalytic activity of TiO_2 samples

(1) The adsorption study of TiO_2 samples

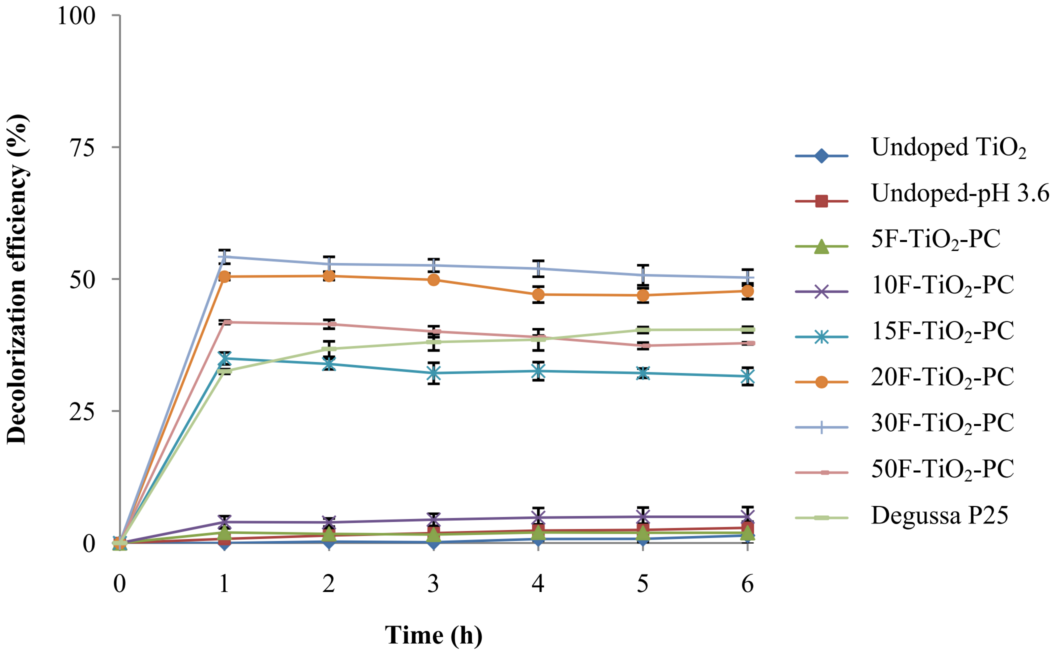

Figure 3.53 Decolorization (adsorption) efficiency of IC by TiO_2 samples.

In this work, the adsorption study of fluorine doped TiO_2 was investigated for the decolorization of IC dye (2.5×10^{-5}M) at 610 nm in the closed wooden compartment. The percentage of IC decolorization by TiO_2 samples are shown in Figure 3.53 and Table 3.22. The decolorization efficiency of IC obeyed the following order: Undoped TiO_2 < Undoped-pH 3.6 < 5F-TiO_2-PC < 10F-TiO_2-PC < 15F-TiO_2-PC < 50F-TiO_2-PC < Degussa P25 < 20F-TiO_2-PC < 30F-TiO_2-PC.

Table 3.22 The percentage of IC decolorization (adsorption) by TiO_2 samples.

TiO_2 samples	Decolorization efficiency (%) at adsorption time (h)					
	1	2	3	4	5	6
Undoped TiO_2	0.00	0.00	0.00	1.00	1.00	1.00
Undoped-pH 3.6	1.00	1.00	2.00	2.00	2.00	2.00
5F-TiO_2-PC	2.00	2.00	2.00	2.00	2.00	2.00
10F-TiO_2-PC	4.00	4.00	4.00	5.00	5.00	5.00
15F-TiO_2-PC	35.0	34.0	32.0	33.0	32.0	31.0
20F-TiO_2-PC	50.0	51.0	49.0	47.0	46.0	47.0
30F-TiO_2-PC	54.0	53.0	53.0	52.0	51.0	50.0
50F-TiO_2-PC	42.0	42.0	40.0	39.0	37.0	38.0
Degussa P25	32.0	37.0	38.0	39.0	40.0	40.0

(2) Test for photocatalytic activity

The photocatalytic activity of TiO_2 samples was studied in the photocatalytic degradation of IC dye in aqueous solution under UV and visible light and results are shown in Figure 3.54 and Figure 3.55. F-TiO_2-PC's exhibited much higher activity than that of undoped TiO_2 and undoped-pH 3.6 TiO_2. The photocatalytic activity of F-TiO_2-PC's are lower than that of Degussa P25. In the first 30 minute under UV light irradiation, the removal of IC treated by three samples (15F-TiO_2-PC, 20F-TiO_2-PC, 30F-TiO_2-PC) were 84%, 85% and 100%, respectively. The degradation efficiency of IC obeyed the following order: Undoped TiO_2 < Undoped-pH 3.6 < 5F-TiO_2-PC < 50F-TiO_2-PC < 10F-TiO_2-PC < 15F-TiO_2-PC < 20F-TiO_2-PC < 30F-TiO_2-PC. Under visible light F-TiO_2 (15F-TiO_2-PC, 20F-TiO_2-PC, 30F-TiO_2-PC) degraded 100% of dye in about 4 h (Figure 3.56). The degradation efficiency of IC obeyed the following order: Undoped TiO_2 < Undoped-pH 3.6 < 5F-TiO_2-PC < 10F-TiO_2-PC < 50F-TiO_2-PC < 15F-TiO_2-PC < 20F-TiO_2-PC < 30F-TiO_2-PC. Figure 3.57 demonstrates degradation efficiency of IC dye by TiO_2 samples under visible light in about 10 h.

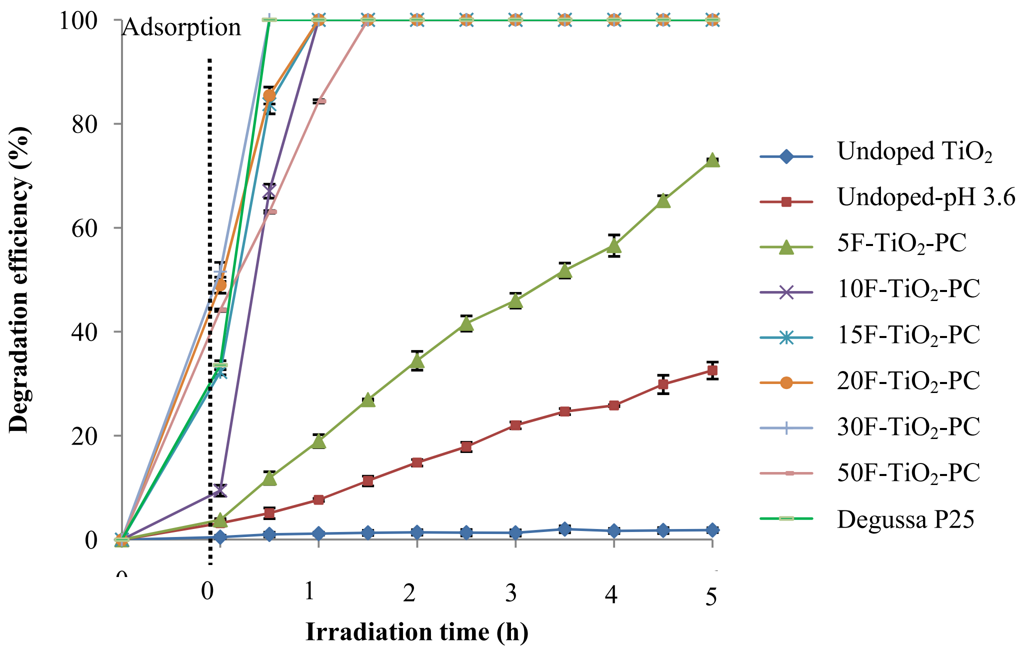
(a) The photocatalytic activity of TiO_2 samples under UV light

Figure 3.54 Photocatalytic activity of TiO_2 samples under UV light.

(b) The photocatalytic activity of TiO_2 samples under visible light

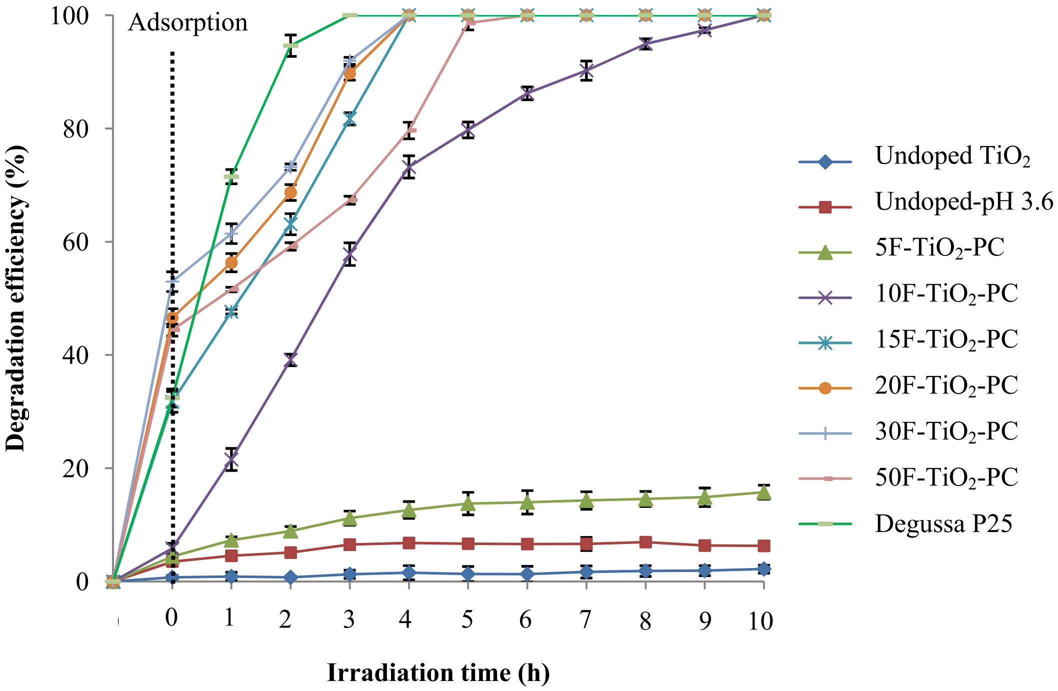

Figure 3.55 Photocatalytic activity of TiO_2 samples under visible light.

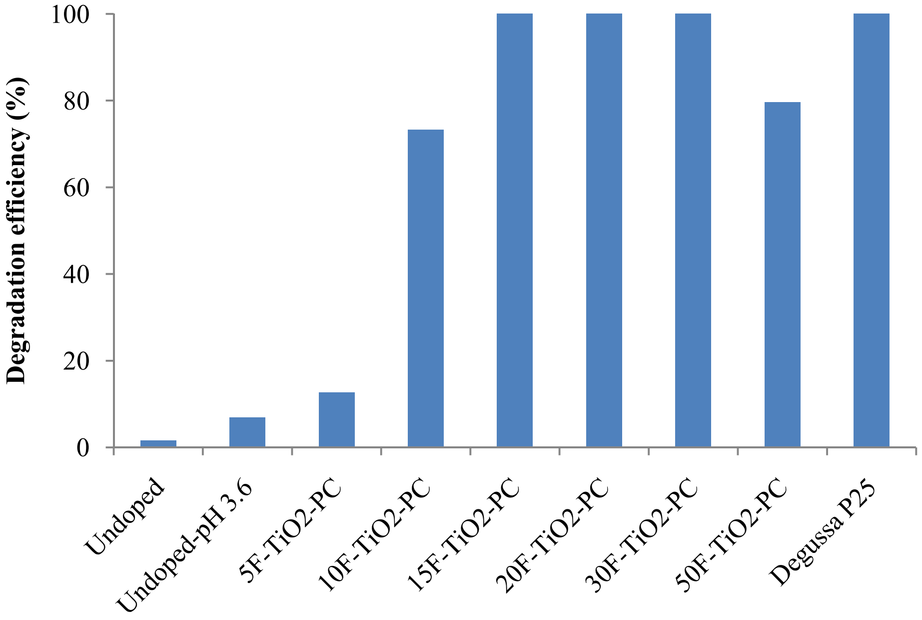

Figure 3.56 Photocatalytic activity of TiO_2 samples under visible light in about 4 h.

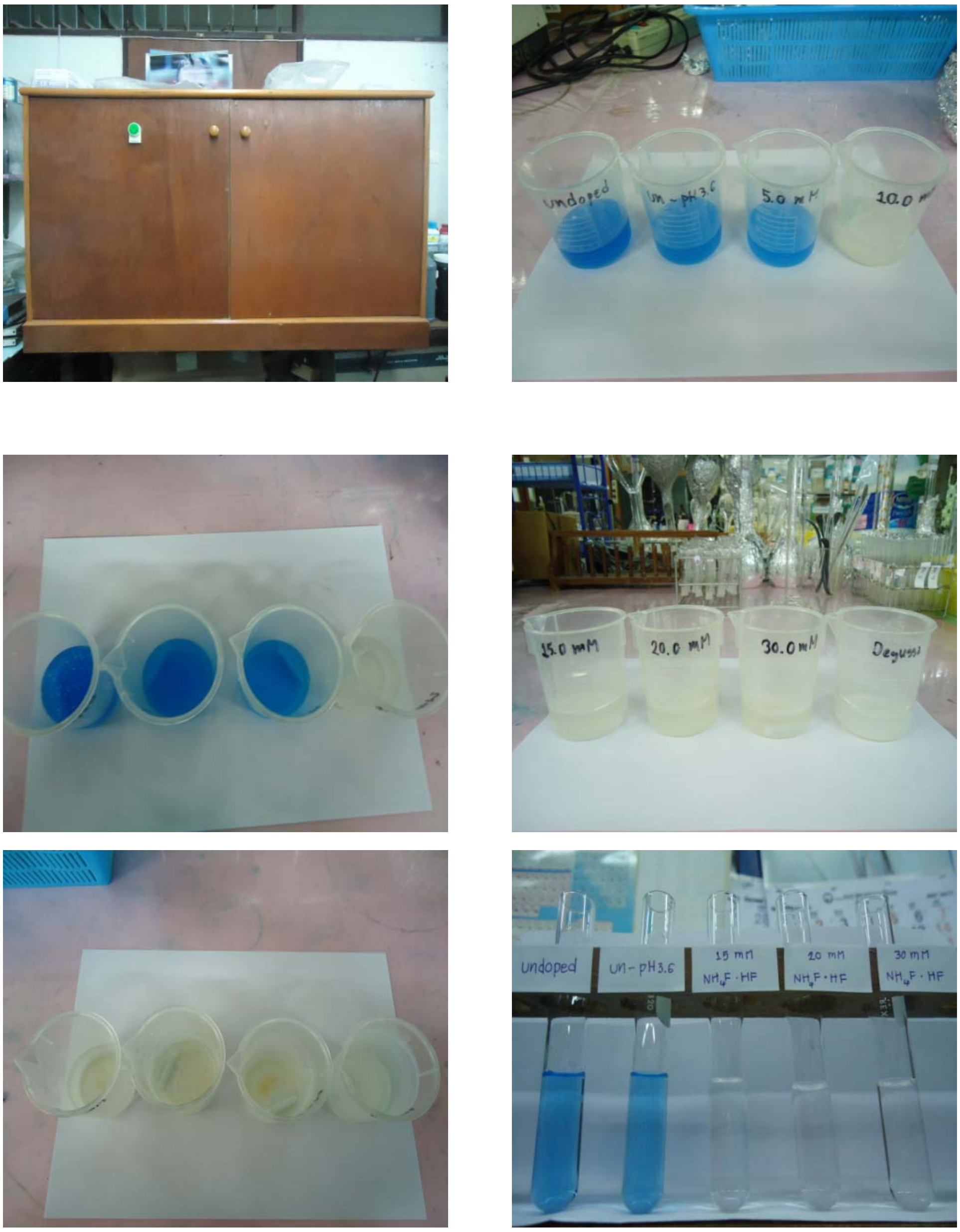

Figure 3.57 Degradation efficiency of IC dye by TiO_2 samples under visible light in about 10 h.

(3) Effect of pH

The efficiency of the photocatalytic activity strongly depends on the pH of the reaction solution. The photocatalytic degradations of IC dye by TiO_2 samples were studied by varying the initial pH of aqueous solution from 3 to 11.

(a) The adsorption study of TiO_2 samples

The decolorization efficiency of IC by 20F-TiO_2-PC at different pH levels are shown in Figure 3.58. It was found that the high adsorption of IC dye on 20F-TiO_2-PC led to a fast decrease of the dye concentration in acid pH zone (pH 3). The decolorization efficiency of IC dye at low pH was higher compared to that at higher pH. The decolorization efficiency of IC dye by 30F-TiO_2-PC is shown in Figure 3.59. The decolorization efficiencies which decreased with the increasing pH values fall in the order: (pH) 3 > 5 > 6.5 > 9 > 11.

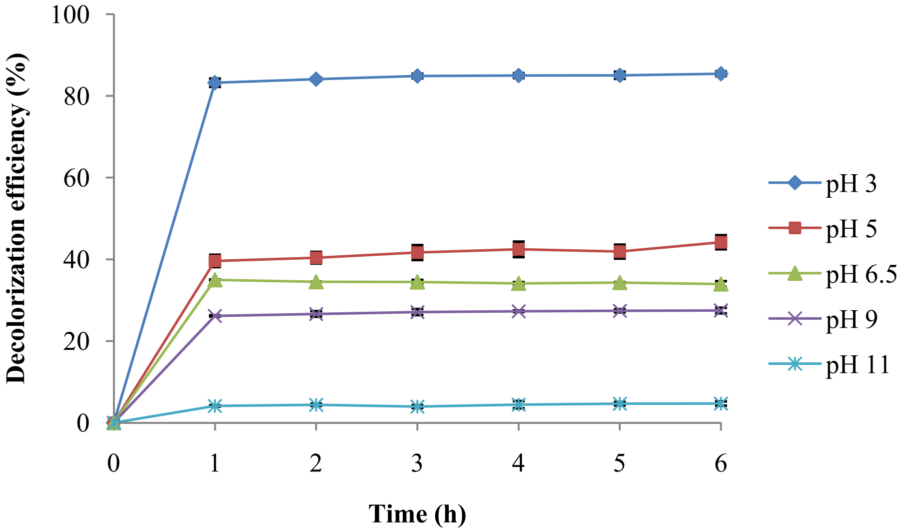

Figure 3.58 Effect of pH on decolorization efficiency of IC by 20F-TiO_2-PC.

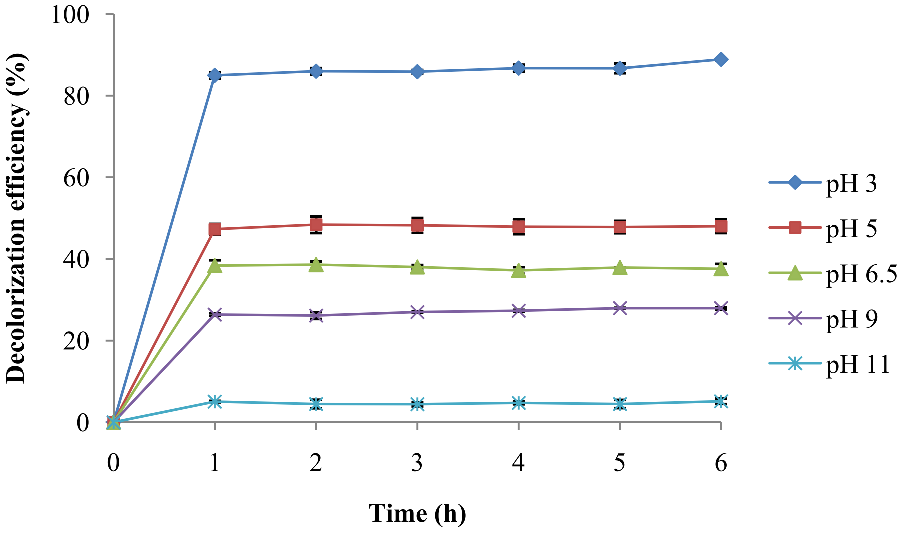

Figure 3.59 Effect of pH on decolorization efficiency of IC by 30F-TiO_2-PC.

(b) The photocatalytic activity of TiO_2 samples

The photodegradation of IC dye by the TiO_2 samples was studied in pH range from 3 to 11. Figure 3.60 demonstrates degradation efficiency of IC by 20F-TiO_2-PC under UV light. It was found that decrease of solution pH from 6.5 to 3 increased the degradation efficiency of IC from 51 to 92 % in 2 h and from 95 to 97 % in 6 h under UV light. The results show the higher degradation efficiency region at pH about 3 and 9. Figure 3.61 shows degradation efficiency of IC by 30F-TiO_2-PC under UV light. 30F-TiO_2-PC trend is noted with higher degradation rates observed at pH 3 and 9 and lower at pH 11.

Figure 3.62 shows the variation of the photocatalytic degradation of 20F-TiO_2-PC with varying the initial pH of aqueous solution from 3 to 11 under visible light. Figure 3.63 shows the degradation efficiency of IC dye by 30F-TiO_2-PC under visible light. In this study, the degradation efficiency was highest at pH 3 whereas lower efficiencies were observed at pH 11. The degradation efficiency decreased as the pH increased in the order: (pH) 3 > 9 > 5 > 6.5 > 11.

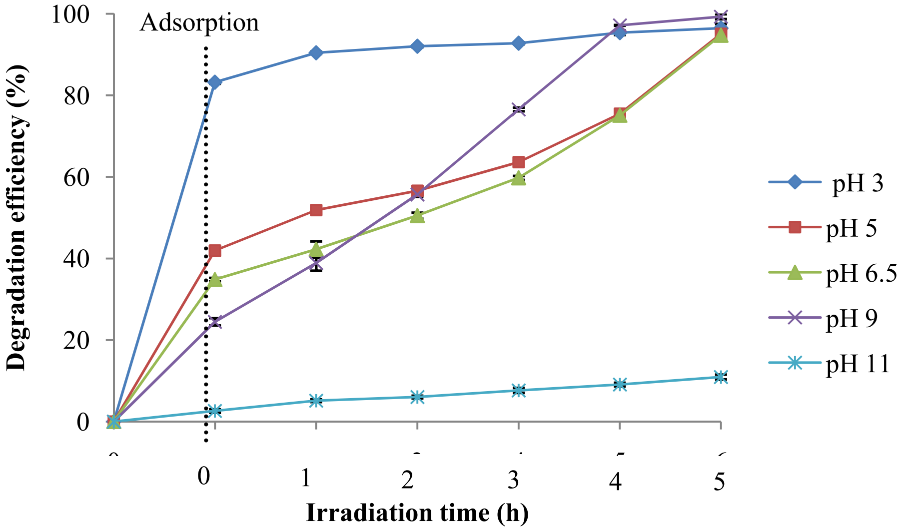

Figure 3.60 Degradation efficiency of IC by 20F-TiO_2-PC under UV light.

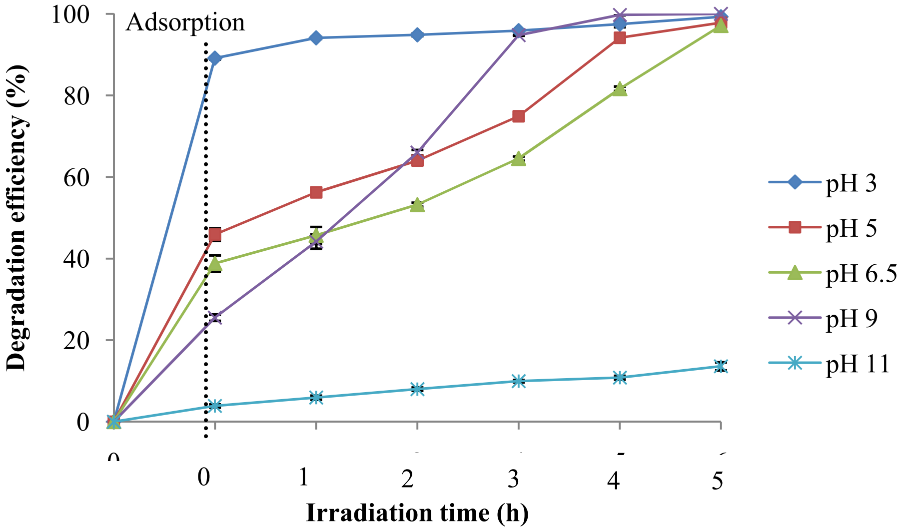

Figure 3.61 Degradation efficiency of IC by 30F-TiO_2-PC under UV light.

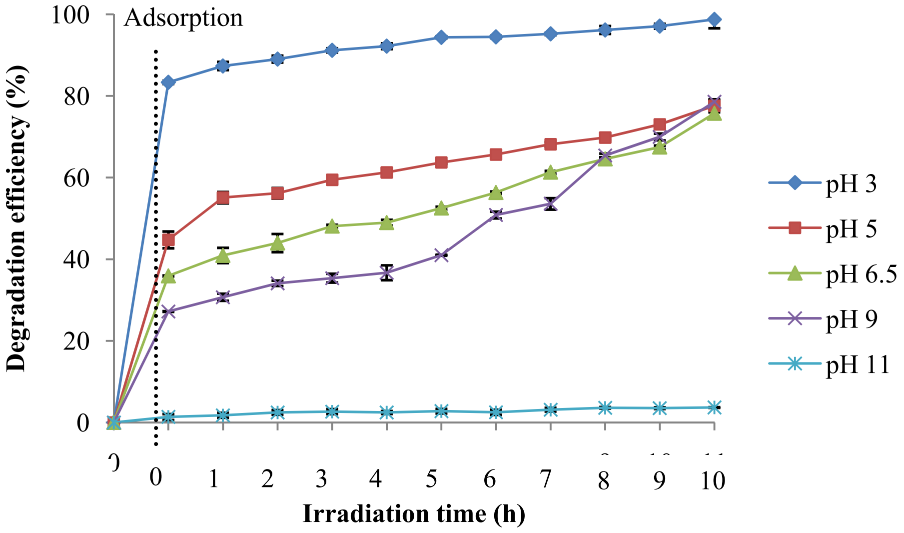

Figure 3.62 Degradation efficiency of IC by 20F-TiO_2-PC under visible light.

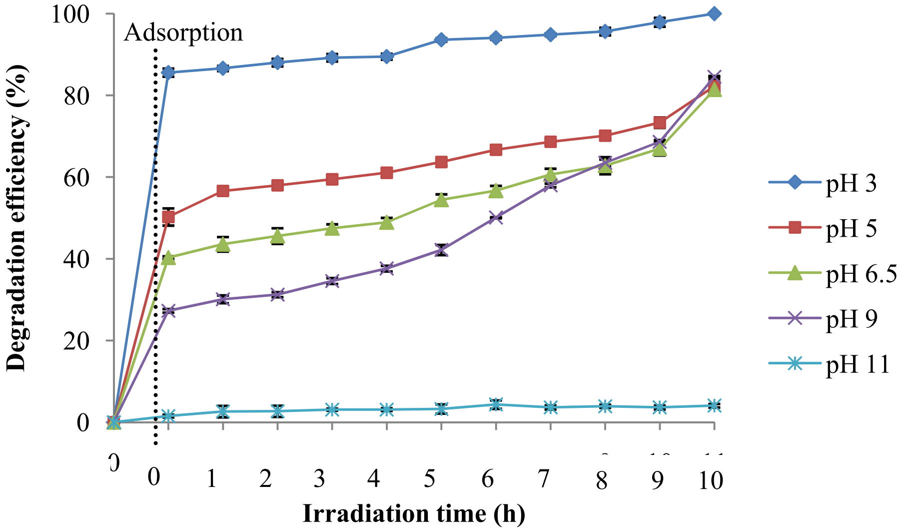

Figure 3.63 Degradation efficiency of IC by 30F-TiO_2-PC under visible light.

3.4 Comparative assessment of the degradation efficiency of fluorine doped TiO_2 prepared by two doping methods

In this section, the efficiencies of fluorine doped TiO_2 prepared by two doping methods are compared with respect to Degussa P25. Fluorine doped TiO_2 samples (20F-TiO_2-PC, 30F-TiO_2-PC) showed enhanced adsorption ability than 5F-TiO_2-imp and Degussa P25. The decolorization efficiency (by adsorption) of IC fell in the following order: 5F-TiO_2-imp < Degussa P25 < 20F-TiO_2-PC < 30F-TiO_2-PC (Figure 3.64). For the photocatalytic degradation under UV light, 30F-TiO_2-PC and Degussa P25 degraded about 100% of IC in about 30 minute (Figure 3.65). Under visible light, the photocatalytic activity of F-TiO_2 samples were lower than that of Degussa P25 (Figure 3.66). The degradation efficiencies of IC treated by TiO_2 samples (Degussa P25, 30F-TiO_2-PC, 20F-TiO_2-PC, 5F-TiO_2-imp) are 100%, 92%, 90% and 80%, respectively.

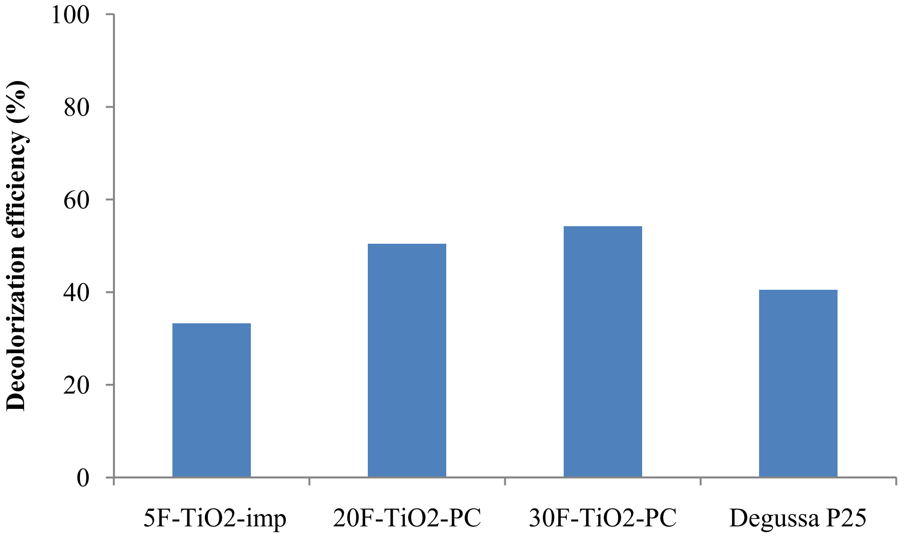

Figure 3.64 Decolorization (by adsorption, 6 h) efficiency of IC by TiO_2 samples.

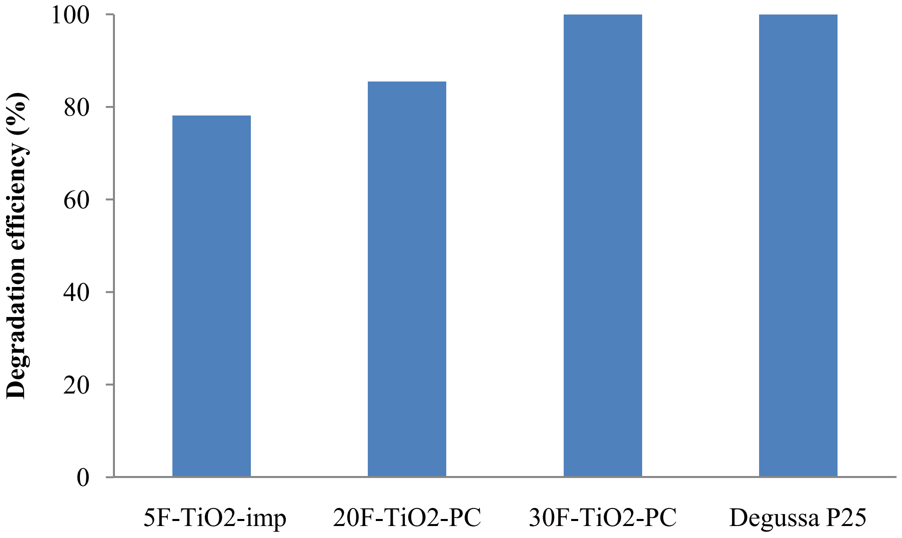

Figure 3.65 Photocatalytic degradation efficiency of IC by TiO_2 samples under UV light (30 minute).

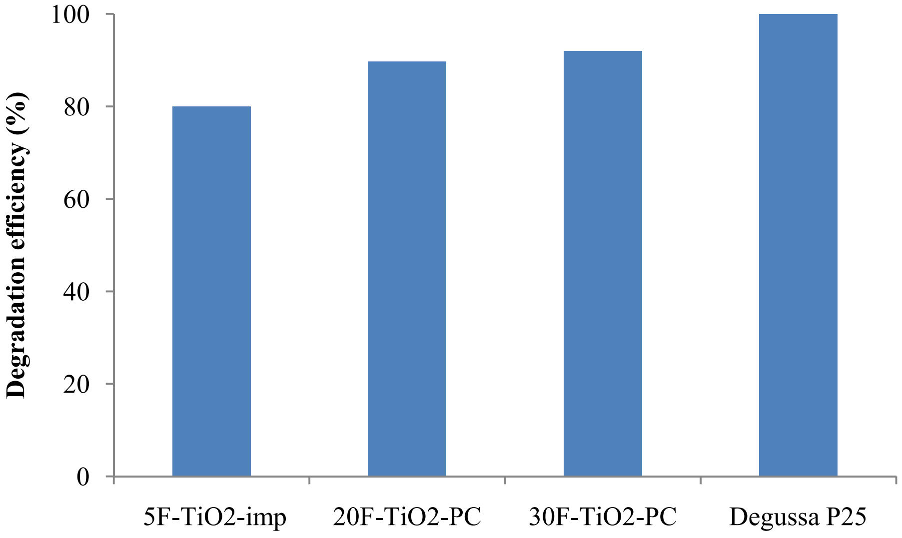

Figure 3.66 Photocatalytic degradation efficiency of IC by TiO_2 samples under visible light (3 h).

In section 3.4.4, the results showed that the prepared samples exhibited high photocatalytic degradation efficiencies at pH 3. In this section, Degussa P25 is shown comparatively with these prepared samples at pH 3 which we can see that the prepared samples outperformed Degussa P25 both under UV light and visible light (Figure 3.67, Figure 3.68).

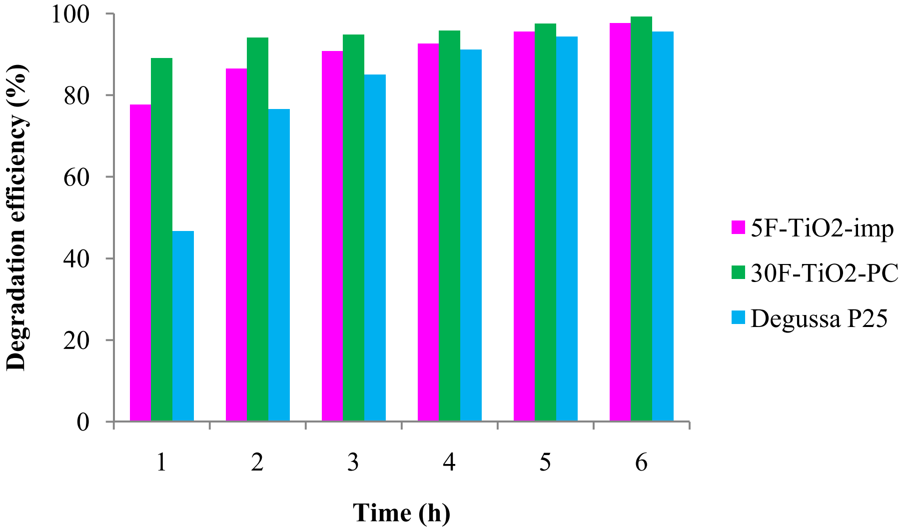

Figure 3.67 Degradation efficiency of IC (pH 3) by TiO_2 samples under UV light.

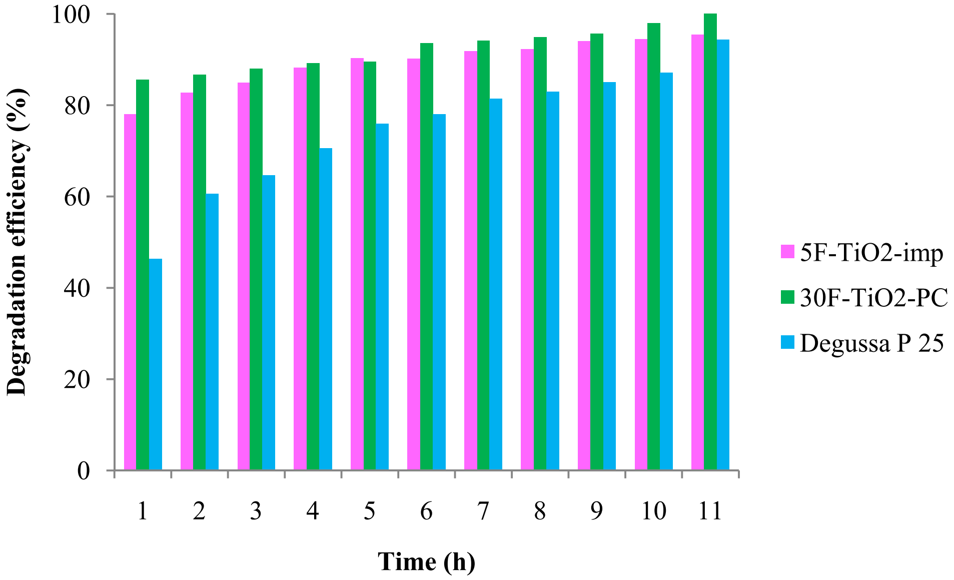

Figure 3.68 Degradation efficiency of IC (pH 3) by TiO_2 samples under visible light.

3.5 The effect of F-doping on the photocatalytic activity

In this work, fluorine doped TiO_2 (F-TiO_2) was successfully synthesized by impregnation and co-precipitation methods. F-TiO_2 showed higher photocatalytic activity than undoped TiO_2 and undoped pH 3.6 under UV light and visible light. It has been reported that the improved photocatalytic activity could be ascribed to the increase in the anatase crystallinity induced by F^- ion. The introduction of F^- ion is also promising to reduce the hydrophilic nature of TiO_2 particle surface, which could enhance the affinity of TiO_2 surface toward organic compounds by the replacement of OH^- group by F^- (Mori, *et al.*, 2008). The formation of surface fluorides on TiO_2 affects both photocatalytic reactions and photoelectrochemical behaviors. The fluoride adsorption is favored at acidic pH and greatly reduces the positive surface charge on TiO_2 by replacing $\equiv Ti\text{-}OH_2^+$ with $\equiv$Ti-F species. The surface fluorination of TiO_2 is a simple ligand exchange between fluoride anions (F^-) and surface hydroxide groups on TiO_2 in water (Eq 3.32).

$$\equiv Ti\text{-}OH + F^- \longrightarrow \equiv Ti\text{-}F + OH^- \qquad (3.32)$$

The extent of fluorination on TiO_2 highly depends on pH, showing a maximum (~99%) around pH 3-4 (Park and Choi, 2004). Fluorine is the most active element among all halogens and it is easy to obtain an electron to form an ion with chemical state of -1 (Sun, *et al.*, 2010). Fluoride ion replaces the basic hydroxide according to the above reaction. The reaction rate was strongly dependent on the surface coverage by $\equiv$Ti-F species (concentration of fluoride ions and pH). It was argued that, for a surface covered by fluorine, the redox process of degradation would follow different routes from those in the presence of $\equiv$Ti-OH species. When the surface is hydroxylated the reaction would proceed with surface-trapped holes and direct electron transfer. When the surface is covered by fluorine, it was concluded that the kinetic pathways for reaction with subsurface holes and with free $^{\bullet}OH$ in solution are predominant (Minero, *et al.*, 2000). The higher photocatalytic oxidation rate in the F-TiO_2 suspension has been ascribed to the enhanced generation of mobile free OH radicals (Eq 3.33) whereas most OH radicals generated on naked TiO_2 surface prefer to remain adsorbed (Eq 3.34).

$$\equiv\text{Ti-F} + H_2O \text{ (or } OH^-) + h_{vb}^+ \longrightarrow \equiv\text{Ti-F} + {}^\bullet OH_{free} + H^+ \quad (3.33)$$

$$\equiv\text{Ti-OH} + h_{vb}^+ \longrightarrow \equiv\text{Ti-OH}^{\bullet+} \quad (3.34)$$

This implies that the photocatalytic reactions in the F-TiO_2 suspension could be initiated in the solution bulk remote from the TiO_2 surface (Park and Choi, 2004).

In fact fluorine, one of halogen elements, was firstly used to improve the UV activity of TiO_2. It was found that fluorine would influence the photocatalytic reactions by changing the interfacial e^-/h^+ transfer, surface charge distribution and substrate-surface interaction, which were attributed to the enhancement of surface acidity, formation of surface hydroxyl radicals, and creation of oxygen vacancies or Ti^{3+}, etc. It is known that the ions with a similar radius to either Ti^{4+} or O^{2-} in TiO_2 crystal can occupy a substituted site. Table 3.23 shows the ionic radii of halogen elements and it reveals that many halogen ions are able to be doped into TiO_2 crystal to improve the optical property of TiO_2. Therefore, F-doping produced two types of species, oxygen vacancy and Ti^{3+}. These species have low energy barrier in response to visible light and can activate organic molecules or oxygen to induce redox reaction. Previous investigations indicated that the oxygen vacancies and Ti^{3+} in TiO_2 would result in significant changes of UV-vis absorption (Sun, *et al.*, 2010).

Table 3.23 Ionic radius of halogens, Ti^{4+} and O^{2-} in TiO_2 matrix (Sun, *et al.*, 2010).

Elements	Anion radius (nm)	Cation radius (nm)
Ti		Ti^{4+} (TiO_2) : 0.068
O	O^{2-} (TiO_2) : 0.124	
F	F^- (HF) : 0.133	F^{7+} (FO_4^-) : 0.008
Cl	Cl^- (HCl) : 0.181	Cl^+(ClO^-): 0.130; Cl^{3+} (ClO_2^-): 0.105; Cl^{5+}(ClO_3^-): 0.012; Cl^{7+}(ClO_4^-): 0.020
Br	Br^- (HBr) : 0.196	Br^+(BrO^-): 0.106; Br^{3+}(BrO_2^-): 0.082; Br^{5+}(BrO_3^-): 0.059; Br^{7+} (BrO_4^-): 0.039
I	I^- (HI) : 0.220	I^+(IO^-): 0.170; I^{3+}(IO_2^-): 0.139; I^{5+}(IO_3) :0.062; I^{7+}($IO4^-$): 0.050

Yu, *et al.*, (2002) who studied the crystallinity of anatase was improved upon F^- doping. Moreover, fluoride ions not only suppressed the formation of brookite phase but also prevented phase transition of anatase to rutile. The F^--doped TiO_2 samples exhibited stronger absorption in the UV-visible range with a red shift in the band gap transition. One possible explanation for this photocatalytic activity enhancement is that F doping converts some Ti^{4+} to Ti^{3+} by charge compensation. Since TiO_2 is an *n*-type semiconductor, the Ti^{3+} surface states in TiO_2 form a donor level between the band gaps of TiO_2. The Ti^{3+} surface states may trap the photogenerated electrons and then transfer them to O_2 adsorbed on the surface of TiO_2. Therefore, the existence of a certain amount of Ti^{3+} surface states in TiO_2 results in the reduction of the electron and hole recombination rate and enhances photocatalytic activity. Figure 3.69 shows the energy level diagram for Ti^{3+} and charge-carrier dynamics in F^--doped TiO_2. Upon UV excitation, photogenerated electrons accumulate at the lower lying surface state of Ti^{3+}, whereas holes accumulate at the valence band of TiO_2. Accumulated electrons at the surface state of Ti^{3+} can be transferred to oxygen adsorbed on the surface. This slows down the recombination of the electron-hole pairs.

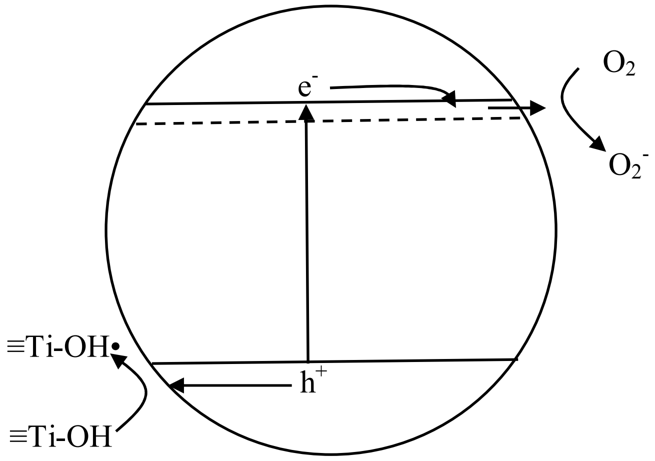

Figure 3.69 Energy level diagram for Ti^{3+} and charge-carrier dynamics in F^--doped TiO_2 (Yu, *et al.*, 2002).

The possible approaches to increasing the reactivity of TiO_2 involve (1) extending the optical absorption from UV to the visible light region; (2) decreasing the recombination of photogenerated charge carriers; and (3) improving the adsorption and subsequent reaction of the reactants on the surface of TiO_2. The factors relevant to surface properties of TiO_2 include surface acidity, defects, hydroxyl groups, crystalline phase, and so on. Among them, the surface acidity, defects, and OH groups can give rise to a great influence on the chemical properties of TiO_2. It has been reported that the surface acidization of TiO_2 can improve the adsorption and reaction of polar molecules. Fluorination is a very effective way to increase the surface acidity of a material because of the strongest electronegativity of fluorine (Tang, *et al*., 2007).

CHAPTER 4

Conclusions

In this work, fluorine doped TiO_2 (F-TiO_2) was successfully synthesized by impregnation and co-precipitation methods at low temperature. The physico-chemical properties of the synthesized TiO_2 powders were characterized by XRD, SEM, EDX, UV-Vis DRS, PL, FT-IR, XAS, DSC, TGA, UV-Vis spectroscopy and surface area measurement by BET techniques.

The X-ray diffraction patterns of the synthesized TiO_2 powders indicated that the undoped powder was amorphous TiO_2 showing a flat base line without any diffraction pattern. F-TiO_2 showed broad characteristic diffraction peak of anatase phase and a small effect on the crystal structure of the original TiO_2. The surface feature and morphology of the synthesized TiO_2 powders were investigated by using SEM. Amorphous undoped TiO_2 showed high agglomerated particles of various sizes. F-TiO_2 powders were fine and slightly agglomerated. EDX technique was used to confirm that F-TiO_2 are mainly composed of Ti, O, C and F elements. DRS and PL techniques were used to determine and confirm the band gap energy of the synthesized TiO_2 powders. The adsorption edge of F-TiO_2 shifted toward a longer wavelength than that of amorphous undoped TiO_2 and undoped-pH 3.6 TiO_2. Generally, the synthesized TiO_2 powders have high surface area with amorphous undoped TiO_2 exhibits higher surface area than F-TiO_2. The effect of dopant content on the photocatalytic activity was noted that F-doped TiO_2 exhibited a small crystallite size when increasing the dopant and the photocatalytic efficiency was higher. The highest enhancement in photocatalytic activity was obtained in 30F-TiO_2-PC. The photocatalytic activity of fluorine doped TiO_2 was investigated for the degradation of IC dye at 610 nm under UV and visible light. F-TiO_2 prepared in this work showed higher photocatalytic activity for IC dye than that of amorphous undoped TiO_2 and undoped-pH3.6 TiO_2 both under UV and visible light irradiation. This can be assumed that some fluorine species entrapped in surface of TiO_2 and improved the photocatalytic degradation of IC dye. However, the photocatalytic activity of F-TiO_2 was lower than that of Degussa P25. The photodegradation of IC on the TiO_2 samples was studied in the range pH 3-11. The degradation efficiency was highest at pH 3 with 30F-TiO_2-PC and 5F-TiO_2-imp show higher photocatalytic efficiency than Degussa P25 both under UV and visible light irradiation. The pH_{pzc} of 30F-TiO_2-PC is 3.6. When solution pH is below the pH_{pzc}, the adsorbent surface is positively charged, and anion adsorption occurred. When solution pH is above the pH_{pzc}, the adsorbent surface is negative charged, and cation adsorption occurred.

From all of these results, it can be concluded that the present study demonstrates preparation of fluorine doped TiO_2 and photocatalytic degradation of IC dye. The higher activity of F-TiO_2 may be due to low crystallinity of anatase phase, an absorption edge shift toward longer wavelength, high surface area, there by increasing the photocatalytic activity.

References

Ahmad, A.; Awan, G.H. and Aziz, S. 2006. Synthesis and applications of TiO_2 nanoparticles. Proceeding, 70th Annual Session. Engineering Congress, Pakistan, 405-412.

Akpan, U.G. and Hameed, B.H. 2010. The advancements in sol-gel method of doped-TiO_2 photocatalysts. Appl Catal A- Gen. 375, 1-11.

Alexiou, M.S. and Sermon, P.A. 1993. Aspects of the preparation of heterogeneous catalysts by impregnation. React Kinet Catal L. 51, 1-7.

Ammar, S.; Abdelhedi, R.; Flox, C.; Arias, C. and Brillas, E. 2006. Electrochemical degradation of the dye indigo carmine at boron-doped diamond anode for wastewaters remediation. Environ Chem Lett. 4, 229-233.

Barka, N.; Assabbane, A.; Nounahb, A. and Ichou, Y.A. 2008. Photocatalytic degradation of indigo carmine in aqueous solution by TiO_2-coated non-woven fibres. J Hazard Mater. 152, 1054-1059.

Bessekhouad, Y; Robert, D.; Weber, J.V. and Chaoui, N. 2004. Effect of alkaline-doped TiO_2 on photocatalytic efficiency. J Photoch Photobio A. 167, 49-57.

Brantley, S.L. and Mollott, N.P. 2000. Surface area and porosity of primary silicate minerals. Am Mineral, 85, 1767-1783.

Brophy, J.J. 1964. Semiconductor devices. McGraw-Hill, Inc. U.S.A. 25.

Buchner, W.; Schliebs, S.; Winter, G. and Buchel. K.H. 1989. Industrial Inorganic Chemistry. New York : VCH, 553-558.

Carp, O.; Huisman, C.L. and Reller, A. 2004. Photoinduced reactivity of titanium dioxide. Prog Solid State Ch. 32, 33-177.

Cassignol, E.J. 1966. Semiconductors. N.V. Philips'Gloeilampenfabrieken, Eindhoven, Natherlands, 1.

Chen, D.; Jiang, Z.; Geng, J.; Zhu, J. and Yang, D. 2009. A facile method to synthesize nitrogen and fluorine co-doped TiO_2 nanoparticles by pyrolysis of $(NH_4)_2TiF_6$. J Nanopart Res. 11, 303-313.

Chen, X. and Mao, S.S. 2007. Titanium Dioxide Nanomaterials: Synthesis, Properties, Modifications, and Applications. Chem. Rev. 107, 2891-2959.

Czoska, A.M.; Livraghi, S.; Chiesa, M.; Giamello, E.; Agnoli, S.; Granozzi, G.; Finazzi, E.; Valentin, C.D. and Pacchioni, G. 2008. The Nature of Defects in Fluorine-Doped TiO_2. J. Phys. Chem. C. 112, 8951-8956.

Devi, L.G. and Kumar, S.G. 2011. Influence of physicochemical-electronic properties of transition metal ion doped polycrystalline titania on the photocatalytic degradation of Indigo Carmine and 4-nitrophenol under UV/solar light. Appl Surf Sci. 257, 2779-2790.

Dong, X.; Tao, J.; Li, Y. and Zhu, H. 2009. Enhanced photoelectrochemical properties of F-containing TiO_2 sphere thin film induced by its novel hierarchical structure. Appl Surf Sci. 255, 7183-7187.

Doping (semiconductor) from Wikipedia, the free encyclopedia : http://en.wikipedia.org/wiki/Doping_(semiconductor) (accessed 29/07/11).

Duplyakin, V.K.; Belyi, A.S.; Rodionov, A.V. and Alfeev, V.S. 1991, New impregnation process for producing coated catalysts. Chem Tech Fuels Oil. 27, 39-42.

Dutta, P.K.; Raya, A.K.; Sharma, V.K. and Millero, F.J. 2004. Adsorption of arsenate and arsenite on titanium dioxide suspensions. J Colloid Interf Sci. 278, 270-275.

Dye from Wikipedia, the free encyclopedia : http://en.wikipedia.org/wiki/Dye (accessed 15/07/11).

Eufinger, K. 2007. Effect of deposition conditions and doping on the structure, optical properties and photocatalytic activity of d.c. magnetron sputtered TiO_2 thin films. Gent. 9.

Fagerlund, G. Determination of specific surface by the BET method. Mater Struct. 6, 239-245.

Fujishima, A.; Rao, T.N. and Tryk, D.A. 2000. Titanium dioxide photocatalysis. J Photoch Photobio C. 1, 1-21.

Gaya, U.I. and Abdullah, A.H. 2008. Heterogeneous photocatalytic degradation of organic contaminants over titanium dioxide: A review of fundamentals, progress and problems. J Photoch Photobio C. 9, 1-12.

Gemeay, A.H.; Mansour, I.A.; El-Sharkawy, R.G. and Zaki, A.B. 2003. Kinetics and mechanism of the heterogeneous catalyzed oxidative degradation of indigo carmine. J Mol Catal A-Chem. 193, 109-120.

Geselbracht, J.M.; Erickson, A.S.; Rogge, M.P.; Greedan, J.E.; Richard I. Walton, R.I.; Stoltzfus, M.W.; Eng, H.W. and Woodward, P.M. 2006. Structure property relationships in the ATi_2O_4 (A = Na, Ca) family of reduced titanates. J Solid State Chem. 179, 3489−3499.

Gil, K.R.R.; Garcia, E.A.R. and Raftery, D. 2006. Photoelectrochemical Analysis of Anion-Doped TiO_2 Colloidal and Powder Thin-Film Electrodes. J Electrochem Soc. 153, 1296-1301.

Golubovic, A.; Scepanovic, M.; Kremenovic, A.; Askrabic, S.; Berec, V.; Mitrovic, Z.D. and Popovic, Z.V. 2009. Raman study of the variation in anatase structure of TiO_2 nanopowders due to the changes of sol-gel synthesis conditions. J Sol-Gel Sci Technol. 49, 311-319.

Habibi, M.H. and Esfahani, M.N. 2007. Preparation, characterization and photocatalytic activity of a novel nanostructure composite film derived from nanopowder TiO_2 and solegel process using organic dispersant. Dyes Pigments. 75, 714-722.

Hamadanian, M.; Vanani, A.R. and Majedi, A. 2010. Sol-Gel Preparation and Characterization of Co/TiO_2 Nanoparticles: Application to the Degradation of Methyl Orange. J. Iran. Chem. Soc., Vol. 7, Suppl., July 2010, S52-S58.

Han, F.; Kambala, V.S.R.; Srinivasan, M.; Rajarathnam, D. and Naidu, R. 2009. Tailored titanium dioxide photocatalysts for the degradation of organic dyes in wastewater treatment: A review. Appl Catal A-Gen. 359, 25-40.

Hashimoto, K.; Irie, H. and Fujishima, A. 2005. TiO_2 Photocatalysis: A Historical Overview and Future Prospects. Jpn J Appl Phys. 44, 8269-8285.

Herrmann, J.M. 1999. Heterogeneous photocatalysis: fundamentals and applications to the removal of various types of aqueous pollutants. Catal Today. 53, 115-129.

Hoffmann, M.R.; Martin, S.T.; Choi, W. and Bahnemann, D.W. 1995. Environmental Applications of Semiconductor Photocatalysis. Chem. Rev. 95, 69-96.

Huang, B.S.; Tseng H.H. and Wey, M.Y. 2009. Comparison of visible light driven routes of anion-doped TiO_2 and composite photocatalyst. J Ceram Soc Jpn. 117, 753-758.

Huang, D.G.; Liao, S.J.; Liu, J.M.; Dang, Z. and Petrik, L. 2006. Preparation of visible-light responsive N-F-codoped TiO_2 photocatalyst by a sol-gel-solvothermal method. J Photoch Photobio A. 184, 282-288.

Huang, D.; Liao, S.; Quan, S.; Liu, L.; He, Z.; Wan, J. and Zhou, W. 2007. Preparation and characterization of anatase N-F-codoped TiO_2 sol and its photocatalytic degradation for formaldehyde. J. Mater. Res., Vol. 22, No. 9, 2389-2397.

Huo, Y.; Jin, Y.; Zhu, J. and Li, H. 2009. Highly active $TiO_{2-x-y}N_xF_y$ visible photocatalyst prepared under supercritical conditions in NH_4F/EtOH fluid. Appl Catal B-Environ. 89, 543-550.

Ibrahim, S.A. and Sreekantan, S. 2010. Effect of pH on TiO_2 nanoparticles via sol gel method. Proceedings, ICXRI, Malaysia, 84-87.

Incipient wetness impregnation from Wikipedia, the free encyclopedia : http://en.wikipedia.org/wiki/Incipient_wetness_impregnation (accessed 30/03/09).

Jensen, H.; Soloviev, A.; Li, Z. and Sqgaard, E.G. 2005. XPS and FTIR investigation of the surface properties of different prepared titania nano-powders. Appl Surf Sci. 246, 239-249.

Kanna, M.; Wongnawa, S.; Buddee, S.; Dilokkhunakul, K. and Pinpithak, P. 2010. Amorphous titanium dioxide: a recyclable dye remover for water treatment. J Sol-Gel Sci Technol. 53, 162-170.

Kanna, M. and Wongnawa, S. 2008. Mixed amorphous and nanocrystalline TiO_2 powders prepared by sol-gel method: Characterization and photocatalytic study. Mater Chem Phys. 110, 166-175.

Khalfaoui, M.; Knani, S; Hachicha, M.A. and Lamine, A.B. 2003. New theoretical expressions for the five adsorption type isotherms classified by BET based on statistical physics treatment. J Colloid Interf Sci. 263, 350-356.

Khalil, K.M.S. and Zaki, M.I. 1997. Synthesis of high surface area titania powders via basic hydrolysis of titanium (IV) isopropoxide. Powder Technol. 92, 233-239.

Konstantinou, I.K. and Albanis, T.A. 2004. TiO_2-assisted photocatalytic degradation of azo dyes in aqueous solution: kinetic and mechanistic investigations A review. Appl Catal B- Environ. 49, 1-14.

Kumar, B.V.S.; Sajan, C.P.; Rai, K.M.L. and Byrappa, K. 2010. Photocatalytic activity of TiO_2:$AlPO_4$-5 zeolites for the degradation of indigo carmine dye. Indian J chem Techn. 17, 191-197.

Lakshminarasimhan, N.; Bae, E. and Choi, W. 2007. Enhanced Photocatalytic Production of H_2 on Mesoporous TiO_2 Prepared by Template-Free Method: Role of Interparticle Charge Transfer. J. Phys. Chem. C. 111, 15244-15250.

Liao, L.F.; Lien, C.F.; Chen, M.T.; Lin, Y.F. and Lin, J.L. 2003. CH_2I_2 adsorption and reactions on TiO_2. Phys Chem Chem Phys. 5, 1912-1916.

Li, D.; Haneda, H.; Hishita, S.; Ohashi, N. and Labhsetwar, N.K. 2005. Fluorine-doped TiO_2 powders prepared by spray pyrolysis and their improved photocatalytic activity for decomposition of gas-phase acetaldehyde. J Fluorine Chem. 126, 69-77.

Li, D.; Haneda, H; Labhsetwar, N.K.; Hishita, S. and Ohashi, N. 2005. Visible-light-driven photocatalysis on fluorine-doped TiO_2 powders by the creation of surface oxygen vacancies. Chem Phys Lett. 401, 579-584.

Li, D.; Ohashi, N.; Hishita, S.; Kolodiazhnyi, T. and Haneda, H. 2005. Origin of visible-light-driven photocatalysis: A comparative study on N/F-doped and N-F-codoped TiO_2 powders by means of experimental characterizations and theoretical calculations. J Solid State Chem. 178, 3293-3302.

Linsebigler, A.L.; Lu, G. and Yates, J.T. 1995. Photocatalysis on TiO_2 Surfaces: Principles, Mechanisms, and Selected Results. Chem. Rev. 95, 735-758.

Li, X. and Liu, S. 2008. Characterization of Visible Light Response N-F Codoped TiO_2 Photocatalyst Prepared by Acid Catalyzed Hydrolysis. Acta Phys.-Chim. Sin. 24, 2019-2024.

Lokshin, E.P.; Sedneva, T.A.; Belyaevskii, A.T. and Kalinnikov, V.T. 2008. Photocatalytic Activity of Fluorine-Doped Titanium Dioxide. Theor Found Chem Eng. 42, 590-594.

Liu, Y.H.; Lin, C.W.; Chang, M.C.; Shao, H. and Yang, A.C.M. 2008. The hydrothermal analogy role of ionic liquid in transforming amorphous TiO_2 to anatase TiO_2: elucidating effects of ionic liquids and heating method. J Mater Sci. 43, 5005-5013.

Maikala, R.V. 2010. Modified Beer’s Law-historical perspectives and relevance in near-infrared monitoring of optical properties of human tissue. Int J Ind Ergonom. 40, 125-134.

Materials Evaluation and Engineering, Inc. 2009. Energy dispersive x-ray spectroscopy. http://mee-inc.com/eds.html (accessed 15/07/11).

Mays, T.J. 2007. A new classification of pore sizes. Stud Surf Sci Catal. 160, 57-62.

Meng, Y.; Chen, J.; Wang, Y.; Dingy, H. and Shan, Y. 2009. (N, F)-codoped TiO_2 Nanocrystals as Visible Light-activated Photocatalyst. J. Mater. Sci. Technol. 25, 73-76.

Mills, A. and Hunte, S.L. 1997. An overview of semiconductor photocatalysis. J Photoch Photobio A. 108, 1-35.

Minero, C.; Mariella, G.; Maurino, V. and Pelizzetti, E. 2000. Photocatalytic Transformation of Organic Compounds in the Presence of Inorganic Anions. 1. Hydroxyl-Mediated and Direct Electron-Transfer Reactions of Phenol on a Titanium Dioxide-Fluoride System. Langmuir. 16, 2632-2641.

Minero, C.; Mariella, G.; Maurino, V.; Vione, D. and Pelizzetti, E. 2000. Photocatalytic Transformation of Organic Compounds in the Presence of Inorganic Ions. 2. Competitive Reactions of Phenol and Alcohols on a Titanium Dioxide-Fluoride System. Langmuir. 16, 8964-8972.

Mohamed, M.M.; Othman, I. and Mohamed, R.M. 2007. Synthesis and characterization of MnO_x/TiO_2 nanoparticles for photocatalytic oxidation of indigo carmine dye. J Photoch Photobio A. 191, 153-161.

Mohamed, R.M. 2009. Characterization and catalytic properties of nano-sized Pt metal catalyst on TiO_2-SiO_2 synthesized by photo-assisted deposition and impregnation methods. J Mater Process Tech. 209, 577-583.

Mori, K; Maki, K.; Kawasaki, S.; Yuan, S. and Yamashita, H. 2008. Hydrothermal synthesis of TiO_2 photocatalysts in the presence of NH_4F and their application for degradation of organic compounds. Chem Eng Sci. 63, 5066-5070.

Mullet, M; Fievet, P.; Reggiani, J.C. and Pagetti, J. 1997. Surface electrochemical properties of mixed oxide ceramic membranes: Zeta-potential and surface charge density. J Membrane Sci. 123, 255-265.

Nagaveni, K.; Sivalingam, G.; Hegde, M.S. and Madras, G. 2004. Solar photocatalytic degradation of dyes: high activity of combustion synthesized nano TiO_2. Appl Catal B-Environ. 48, 83-93.

Nagaveni, K.; Hegde, M. S.; Ravishankar, N.; Subbanna, G. N., and Madras, G. 2004. Synthesis and Structure of Nanocrystalline TiO_2 with Lower Band Gap Showing High Photocatalytic Activity. LANGMUIR. 20, 2900-2907.

Ngamsopasiriskun, C.; Charnsethikul, S.; Thachepan, S. and Songsasen, A. 2010. Removal of Phenol in Aqueous Solution by Nanocrystalline TiO_2/Activated Carbon Composite Catalyst. Kasetsart J. 44, 1176-1182.

Othman, I.; Mohamed, R.M. and Ibrahem, F.M. 2007. Study of photocatalytic oxidation of indigo carmine dye on Mn-supported TiO_2. J Photoch Photobio A. 189, 80-85.

Park, H. and Choi, W. 2004. Effects of TiO_2 Surface Fluorination on Photocatalytic Reactions and Photoelectrochemical Behaviors. J. Phys. Chem. B. 108, 4086-4093.

Pelaez, M.; Cruz, A.D.; Stathatos, E.; Falaras, P. and Dionysiou, D.D. 2009. Visible light-activated N-F-codoped TiO_2 nanoparticles for the photocatalytic degradation of microcystin-LR in water. Catal Today. 144, 19-25.

Pore, V. 2010. Atomic Layer Deposition and Photocatalytic Properties of Titanium Dioxide Thin Films. Finland, 14.

Prado, A.G.S.; Bolzon, L.B.; Pedroso, C.P.; Moura, A.O. and Costa, L.L. 2008. Nb_2O_5 as efficient and recyclable photocatalyst for indigo carmine degradation. Appl Catal B-Environ. 82, 219-224.

Qiu, S. and Starr, T.L. 2007. Zirconium Doping in Titanium Oxide Photocatalytic Films Prepared by Atomic Layer Deposition. J Electrochem Soc. 154, 472-475.

Rajeshwar, K. 1995. Photoelectrochemistry and the environment. J electrochem. 25, 1067-1082.

Raj, K.J.A. and Viswanathan, B. 2009. Effect of surface area, pore volume and particle size of P25 titania on the phase transformation of anatase to rutile. Indian J chem. 48, 1378-1382.

Rauf, M.A. and Ashraf, S.S. 2009. Fundamental principles and application of heterogeneous photocatalytic degradation of dyes in solution. Chem Eng J. 151, 10-18.

Reddy, B.M.; Rao, K.N.; Reddy, G.K. and Bharali, P. 2006. Characterization and catalytic activity of V_2O_5/Al_2O_3-TiO_2 for selective oxidation of 4-methylanisole. J Mol Catal A-Chem. 253, 44-51.

Ryu, Z.; Zheng, J.; Wang, M. and Zhang, B. 1999. Characterization of pore size distributions on carbonaceous adsorbents by DFT. Carbon. 37, 1257-1264.

Saadoun, L.; Ayllon, J.A.; Becerril, J.J.; Peral, J.; Domenech, X. and Clemente, R.R. 2000. Synthesis and photocatalytic activity of mesoporous anatase prepared from tetrabutylammonium-titania composites. Materials Research Bulletin. 35, 193-202.

Sing, K.S.W.; Everett, D.H.; Haul, R.A.W.; Moscou, L; Pierotti, R.A.; Rouquerol, J. and Siemieniewska, T. 1985. Reporting physisorption data for gas/solid systems with Special Reference to the Determination of Surface Area and Porosity. Pure & Appl. Chem. 57, 603-619.

Sriwong, C.; Wongnawa, S. and Patarapaiboolchai, O. 2010. Degradation of indigo carmine by rubber sheet impregnated with TiO_2 particles. Science Asia. 36, 52-58.

Stengl, V.; Bakardjieva, S. and Murafa, N. 2009. Preparation and photocatalytic activity of rare earth doped TiO_2 nanoparticles. Mater Chem Phys. 114, 217-226.

Sabia, R. and Ukrainczyk, L. 2003. Surface chemistry of SiO_2 and TiO_2-SiO_2 glasses as determined by titration of soot particles. J Non-Cryst Solids. 277, 1-9.

Sayilkan, F.; Asilturk, M.: Sayilkan, H.; Sayilkan, H.; Onal, Y.; Akarsu, M. and Arpac. E. 2005. Characterization of TiO_2 Synthesized in Alcohol by a Sol-Gel Process: The Effects of AnnealingTemperature and Acid Catalyst. Turk J Chem. 29, 697-706.

Shi, D.; Li, Z.; Zhang, Y.; Kou, X.; Wang, L.; Wang, J. and Li, J. 2009. Synthesis and Characterizations of Amorphous Titania Nanoparticles. Nanosci Nanotec Lett. 1, 165-170.

Subramani, A.K.; Byrappa, K.; Ananda, S.; Rai, K.M.L.; Ranganathaiah, C. and Yoshimura. M. 2006. Photocatalytic degradation of indigo carmine dye using TiO_2 impregnated activated carbon. Bull. Mater. Sci. 30, 37-41.

Su, C.; Hong, B.Y. and Tseng, C.M. 2004. Sol-gel preparation and photocatalysis of titanium dioxide. Catal Today. 96, 119-126.

Sun, H.; Wang, S.; Ang, H.M.; Tade, M.O. and Li, Q. 2010. Halogen element modified titanium dioxide for visible light photocatalysis. Chem Eng J. 162, 437-447.

Sun, J. and Gao, L. 2002. pH Effect on Titania-Phase Transformation of Precipitates from Titanium Tetrachloride Solutions. J. Am. Ceram. Soc. 85, 2382-2384.

Sun, J.; Qiao, L.; Sun, S. and Wang,G. 2008. Photocatalytic degradation of Orange G on nitrogen-doped TiO_2 catalysts under visible light and sunlight irradiation. J Hazard Mater. 155, 312-319.

Suwanchawalit, C. 2009. Syntheses of TiO_2 Powders via Sol-Gel Process with Different Precursors and Their Photocatalytic Properties. Prince of Songkla University. 137-142.

Suwanchawalit, C and Wongnawa, S. 2008. Influence of calcination on the microstructures and photocatalytic activity of potassium oxalate-doped TiO_2 powders. Appl Catal A-Gen. 338, 87-99.

Tang, J.; Quan, H. and Ye, J. 2007. Photocatalytic Properties and Photoinduced Hydrophilicity of Surface-Fluorinated TiO_2. Chem. Mater. 19, 116-122.

The TiO_2 group is composed of rutile, anatase, and brookite. University of Colorado: http://ruby.colorado.edu/~smyth/min/tio2.html (accessed 1/07/11).

Todorova, N.; Giannakopoulou, T.; Romanos, G.; Vaimakis, T.; Yu, J. and Trapalis, C. 2008. Preparation of Fluorine-Doped TiO_2 Photocatalysts with Controlled Crystalline Structure. Int J Photoenergy. V. ID 534038, 1-9.

Todorova, N.; Giannakopoulou, T; Vaimakis, T. and Trapalis, C. 2008. Structure tailoring of fluorine-doped TiO_2 nanostructured powders. Mater Sci Eng. 152, 50-54.

Tong, T.; Zhang, J.; Tian, B.; Chen, F.; He, D. 2008. Preparation and characterization of anatase TiO_2 microspheres with porous frameworks via controlled hydrolysis of titanium alkoxide followed by hydrothermal treatment. Mater Lett. 62, 2970-2972.

Tseng, T.K.; Lin, S.Y.; Chen, Y.J. and Chu, H. 2010. A Review of Photocatalysts Prepared by Sol-Gel Method for VOCs Removal. Int. J. Mol. Sci. 11, 2336-2361.

Utrilla, J.R.; Toledo, I.B.; Garcia, M.A.F. and Castilla, C.M. 2001. Activated carbon surface modifications by adsorption of bacteria and their effect on aqueous lead adsorption. J ChemTechnol Biot. 16, 1209-1215.

Vautier, M.; Guillard, C. and Herrmann, J.M. 2001. Photocatalytic Degradation of Dyes in Water: Case Study of Indigo and of Indigo Carmine. J Catal. 201, 46-59.

Wang, Q.; Chen, C.; Zhao, D.; Ma, W. and Zhao, J. 2008. Change of Adsorption Modes of Dyes on Fluorinated TiO_2 and Its Effect on Photocatalytic Degradation of Dyes under Visible Irradiation. Langmuir. 24, 7338-7345.

Watson, S.; Beydoun, D.; Scott, J. and Amal, R. 2004. Preparation of nanosized crystalline TiO_2 particles at low temperature for photocatalysis. J Nanopart Res. 6, 193-207.

Wei, F.; Ni, L. and Cui, P. 2008. Preparation and characterization of N-S-codoped TiO_2 photocatalyst and its photocatalytic activity. J Hazard Mater. 156, 135-140.

Xie, Y; Li, Y. and Zhao, X. 2007. Low-temperature preparation and visible-light-induced catalytic activity of anatase F-N-codoped TiO_2. J Mol Catal A-Chem. 277, 119-126.

Xu, J.; Ao, Y.; Fu, D. and Yuan, C. 2008. Low temperature preparation of F-doped TiO_2 film and its photocatalytic activity under solar light. Appl Surf Sci. 254, 3033-3038.

Xu, J.; Ao, Y.; Fu, D. and Yuan, C. 2008. Synthesis of fluorine-doped titania-coated activated carbon under low temperature with high photocatalytic activity under visible light. J Phys Chem Solids. 69, 2366-2370.

Yamashita, H.; Nose, H.; Kuwahara, Y.; Nishida, Y.; Yuan, S. and Mori, K. 2008. TiO_2 photocatalyst loaded on hydrophobic Si_3N_4 support for efficient degradation of organics diluted in water. Appl Catal A-Gen. 350, 164-168.

Yamaki, T.; Umebayashi, T.; Sumita, T.; Yamamoto, S.; Maekawa, M.; Kawasuso, A. and Itoh, H. 2003. Fluorine-doping in titanium dioxide by ion implantation technique. Nucl Instrum Methods. 206, 254-258.

Yang, G.; Jiang, Z.; Shi, H.; Jones, M.O.; Xiao, T.; Edwards, P.P. and Yan, Z. 2010. Study on the photocatalysis of F-S co-doped TiO_2 prepared using solvothermal method. Appl Catal B-Environ. 96, 458-465.

Yang, K; Dai, Y.; Huang, B. and Whangbo, M.B. 2008. Density Functional Characterization of the Band Edges, the Band Gap States, and the Preferred Doping Sites of Halogen-Doped TiO_2. Chem. Mater. 20, 6528-6534.

Yang, S.; Sun, C.; Li, X.; Gong, Z. and Quan, X. 2010. Enhanced photocatalytic activity for titanium dioxide by co-modifying with silica and fluorine. J Hazard Mater. 175, 258-266.

Yang, X. 2008. Sol-gel synthesized nanomaterials for environment applications. China. 1-6.

Yano, T.; Shimomura, N.; Uchiyama, I.; Fukawa, F. and Teranishi, K. 2009. Decolorization of Indigo Carmine Solution Using Nanosecond Pulsed Power. IEEE Transactions on Dielectrics and Electrical Insulation. 16, 1070-9878.

Yeung, K.L.; Yau, S.T.; Maira, A.J.; Coronado, J.M.; Soria, J. and Yue, P.L. 2003. The influence of surface properties on the photocatalytic activity of nanostructured TiO_2. J Catal. 219, 107-116.

Youn, H.J.; Ha, P.S.; Jung, H.S.; Hong, K.S.; Park, Y.H. and Ko, K.H. 1999. Alcohol Rinsing and Crystallization Behavior of Precipitated Titanium Oxide. J Colloid Interf Sci. 211, 321-325.

Yu, J.C.; Yu, J.; Ho, W.; Jiang, Z. and Zhang, L. 2002. Effects of F- Doping on the Photocatalytic Activity and Microstructures of Nanocrystalline TiO_2 Powders. Chem. Mater. 14, 3808-3816.

Zhang, Q.; Gao, L. and Guo, J. 2000. Effect of hydrolysis conditions on morphology and crystallization of nanosized TiO_2 powder. J Eur Ceram Soc. 20, 2153-2158.

Zhou, J.; Zhang, Y.; Zhao, X.S. and Ray, A.K. 2006. Photodegradation of Benzoic Acid over Metal-Doped TiO_2. Ind. Eng. Chem. Res. 45, 3503-3511.

Zhu, J.; Yang, J.; Bian, Z.F.; Ren, J.; Liu, Y.M.; Cao, Y.; Li, H.X.; He, H.Y.; Fan, K.N. 2007. Nanocrystalline anatase TiO_2 photocatalysts prepared via a facile low temperature nonhydrolytic sol-gel reaction of $TiCl_4$ and benzyl alcohol. Appl Catal B-Environ. 76, 82-91.

Appendices

Photocatalytic activity test

Fluorine doped TiO_2 via impregnation method and the photocatalytic activity

Table 1 The percentage of IC decolorization by TiO_2 samples.

TiO_2 samples	Decolorization efficiency (%) at adsorption time (h)		
	1	2	3
Undoped TiO_2	0.00 0.51	1.00 1.15	1.00 1.42
Undoped-pH 3.6	2.00 0.85	3.00 0.94	2.00 0.47
5F-TiO_2-imp	33.0 0.23	33.0 1.21	32.0 1.67
6F-TiO_2-imp	32.0 0.97	32.0 1.35	31.0 1.62
7F-TiO_2-imp	34.0 0.32	32.0 0.26	31.0 0.56
10F-TiO_2-imp	3.00 1.33	4.00 1.20	3.00 0.22
30F-TiO_2-imp	3.00 0.51	2.00 0.46	2.00 0.31

Table 1 The percentage of IC decolorization by TiO_2 samples. (Continued)

TiO_2 samples	Decolorization efficiency (%) at adsorption time (h)		
	4	5	6
Undoped TiO_2	1.00 0.88	1.00 1.06	1.00 0.59
Undoped-pH 3.6	2.00 0.78	2.00 0.73	2.00 0.49
5F-TiO_2-imp	32.0 1.34	31.0 1.25	31.0 1.03
6F-TiO_2-imp	31.0 1.34	31.0 1.48	31.0 1.49
7F-TiO_2-imp	31.0 0.49	31.0 0.19	31.0 0.20
10F-TiO_2-imp	3.00 0.56	2.00 0.77	1.00 0.96
30F-TiO_2-imp	2.00 0.46	2.00 1.42	2.00 1.69

Table 2 Photocatalytic activity of TiO_2 samples under UV light.

TiO_2 samples	Degradation efficiency (%) at time (h)		
	1	1.5	2
Undoped TiO_2	0.00 0.06	0.00 0.04	1.00 0.36
Undoped-pH 3.6	1.00 0.70	2.00 1.44	5.00 0.83
5F-TiO_2-imp	34.0 1.87	78.0 1.09	100 0.00
6F-TiO_2-imp	36.0 1.00	74.0 1.40	100 0.00
7F-TiO_2-imp	35.0 0.96	74.0 1.53	100 0.08
10F-TiO_2-imp	4.00 0.76	38.0 1.05	69.0 1.28
30F-TiO_2-imp	2.00 1.45	16.0 0.66	27.0 1.10
Degussa P25	34.0 0.87	100 0.00	100 0.00

Table 2 Photocatalytic activity of TiO_2 samples under UV light. (Continued)

TiO_2 samples	Degradation efficiency (%) at time (h)		
	2.5	3	3.5
Undoped TiO_2	1.00 0.72	2.00 1.02	3.00 0.31
Undoped-pH 3.6	7.00 0.66	10.0 0.96	12.0 0.19
5F-TiO_2-imp	100 0.00	100 0.00	100 0.00
6F-TiO_2-imp	100 0.00	100 0.00	100 0.00
7F-TiO_2-imp	100 0.00	100 0.00	100 0.00
10F-TiO_2-imp	92.0 0.90	100 0.00	100 0.00
30F-TiO_2-imp	36.0 0.77	45.0 1.21	53.0 0.81
Degussa P25	100 0.00	100 0.00	100 0.00

Table 2 Photocatalytic activity of TiO_2 samples under UV light. (Continued)

TiO_2 samples	Degradation efficiency (%) at time (h)		
	4	4.5	5
Undoped TiO_2	4.00 0.11	4.00 0.21	4.00 0.32
Undoped-pH 3.6	14.0 0.77	17.0 0.52	19.0 0.75
5F-TiO_2-imp	100 0.00	100 0.00	100 0.00
6F-TiO_2-imp	100 0.00	100 0.00	100 0.00
7F-TiO_2-imp	100 0.00	100 0.00	100 0.00
10F-TiO_2-imp	100 0.00	100 0.00	100 0.00
30F-TiO_2-imp	61.0 0.85	69.0 0.57	75.0 1.12
Degussa P25	100 0.00	100 0.00	100 0.00

Table 3 Photocatalytic activity of TiO_2 samples under visible light.

TiO_2 samples	Degradation efficiency (%) at time (h)			
	1	2	3	4
Undoped TiO_2	1.00 0.70	1.00 0.51	1.00 0.37	1.00 0.58
Undoped-pH 3.6	2.00 1.44	2.00 1.54	3.00 1.82	3.00 1.11
2F-TiO_2-imp	1.00 0.93	2.00 1.31	3.00 0.50	3.00 0.27
5F-TiO_2-imp	28.0 2.00	43.0 0.70	60.0 1.91	80.0 0.71
6F-TiO_2-imp	29.0 1.07	41.0 1.32	56.0 0.87	73.0 1.67
7F-TiO_2-imp	30.0 1.49	42.0 1.37	55.0 0.75	73.0 2.00
10F-TiO_2-imp	4.00 0.86	17.0 2.00	29.0 1.96	39.0 1.87
30F-TiO_2-imp	4.00 0.99	13.0 1.78	21.0 1.82	27.0 1.84
Degussa P25	32.0 1.58	71.0 1.26	94.0 1.88	100 0.00

Table 3 Photocatalytic activity of TiO_2 samples under visible light. (Continued)

TiO_2 samples	Degradation efficiency (%) at time (h)		
	5	6	7
Undoped TiO_2	1.00 0.65	1.00 0.26	1.00 0.35
Undoped-pH 3.6	5.00 1.84	6.00 1.30	6.00 1.68
2F-TiO_2-imp	4.00 1.05	5.00 1.14	6.00 1.69
5F-TiO_2-imp	100 0.00	100 0.00	100 0.00
6F-TiO_2-imp	92.0 1.60	100 0.00	100 0.00
7F-TiO_2-imp	93.0 0.47	100 0.00	100 0.00
10F-TiO_2-imp	50.0 0.66	60.0 2.00	72.0 1.16
30F-TiO_2-imp	31.0 1.34	35.0 1.93	39.0 1.31
Degussa P25	100 0.00	100 0.00	100 0.00

Table 3 Photocatalytic activity of TiO_2 samples under visible light. (Continued)

TiO_2 samples	Degradation efficiency (%) at time (h)		
	8	9	10
Undoped TiO_2	1.00 0.50	2.00 0.10	2.00 0.12
Undoped-pH 3.6	5.00 1.46	5.00 1.67	5.00 1.78
2F-TiO_2-imp	7.00 1.45	8.00 1.77	9.00 1.97
5F-TiO_2-imp	100 0.00	100 0.00	100 0.00
6F-TiO_2-imp	100 0.00	100 0.00	100 0.00
7F-TiO_2-imp	100 0.00	100 0.00	100 0.00
10F-TiO_2-imp	84.0 1.65	95.0 0.38	98.0 1.77
30F-TiO_2-imp	45.0 0.86	50.0 1.52	55.0 1.15
Degussa P25	100 0.00	100 0.00	100 0.00

Table 4 Effect of pH on decolorization efficiency of IC by 5F-TiO_2-imp.

Time (h)	Decolorization efficiency (%) at adsorption time (h)				
	pH 3	pH 5	pH 6.5	pH 9	pH 11
1	78.0 0.55	40.0 0.98	29.0 0.21	19.0 0.39	3.00 0.35
2	78.0 0.27	40.0 0.42	30.0 0.51	20.0 0.32	3.00 0.78
3	78.0 0.48	41.0 0.84	30.0 0.46	20.0 0.44	4.00 0.55
4	77.0 0.47	42.0 1.99	30.0 0.51	20.0 0.41	4.00 0.28
5	78.0 0.97	44.0 1.66	30.0 0.79	20.0 0.21	3.00 0.45
6	79.0 0.57	44.0 1.56	31.0 0.32	20.0 0.31	5.00 0.27

Table 5 Effect of pH on degradation efficiency of 5F-TiO_2-imp under UV light

Time (h)	Degradation efficiency (%) at time (h)				
	pH 3	pH 5	pH 6.5	pH 9	pH 11
1	78.0 ± 0.57	40.0 ± 0.66	30.0 ± 0.66	20.0 ± 1.20	3.00 ± 0.48
2	86.0 ± 0.38	51.0 ± 0.13	41.0 ± 0.81	42.0 ±1.80	5.00 ± 0.33
3	91.0 ± 0.06	64.0 ± 1.30	53.0 ± 0.80	65.0 ± 0.49	8.00 ± 0.44
4	93.0 ± 0.06	72.0 ± 0.93	62.0 ± 0.99	77.0 ± 0.77	9.00 ± 0.33
5	96.0 ± 0.76	80.0 ± 0.70	76.0 ± 0.58	98.0 ± 0.64	10.0 ± 0.91
6	98.0 ± 1.64	96.0 ± 0.41	95.0 ± 0.32	100 ± 0.00	12.0 ± 0.54

Table 6 The photocatalytic activity of 5F-TiO_2-imp under visible light

Time (h)	Degradation efficiency (%) at time (h)				
	pH 3	pH 5	pH 6.5	pH 9	pH 11
1	78.0 ± 0.38	41.0 ± 1.43	32.0 ± 0.31	20.0 ± 0.48	1.00 ±1.14
2	83.0 ± 0.56	49.0 ± 1.83	38.0 ± 0.84	24.0 ± 0.48	2.00 ± 0.38
3	85.0 ± 0.34	52.0 ± 0.95	39.0 ± 0.72	28.0 ± 0.33	1.00 ± 0.57
4	88.0 ± 0.34	54.0 ± 1.61	42.0 ± 2.00	33.0 ± 0.31	2.00 ± 0.23
5	90.0 ± 0.27	59.0 ± 0.68	48.0 ± 0.28	37.0 ± 0.29	2.00 ± 0.85
6	90.0 ± 0.38	62.0 ± 1.07	59.0 ± 0.92	40.0 ± 0.68	2.00 ± 0.84
7	92.0 ± 0.42	64.0 ± 0.86	53.0 ± 0.83	46.0 ± 0.76	2.00 ± 0.68
8	93.0 ± 0.57	68.0 ± 0.61	59.0 ± 0.97	54.0 ± 0.41	3.00 ± 0.35
9	94.0 ± 0.47	71.0 ± 0.79	63.0 ± 1.39	63.0 ± 0.27	3.00 ± 0.36
10	94.0 ± 0.79	74.0 ± 0.55	69.0 ± 1.66	72.0 ± 0.41	3.00 ± 0.48
11	95.0 ± 0.72	78.0 ± 1.06	77.0 ± 0.38	79.0 ± 1.94	3.00 ± 0.34

Fluorine doped TiO_2 via co-precipitation method and the photocatalytic activity

Table 7 The percentage of IC decolorization by TiO_2 samples

TiO_2 samples	Decolorization efficiency (%) at adsorption time (h)		
	1	2	3
Undoped TiO_2	0.00 ± 0.40	0.00 ± 0.52	0.00 ± 0.58
Undoped-pH 3.6	1.00 ± 0.77	1.00 ± 0.79	2.00 ± 0.86
5F-TiO_2-PC	2.00 ± 0.97	2.00 ± 1.00	2.00 ± 1.36
10F-TiO_2-PC	4.00 ± 1.16	4.00 ± 0.77	4.00 ± 1.15
15F-TiO_2-PC	35.0 ± 1.13	34.0 ± 1.01	32.0 ± 1.99
20F-TiO_2-PC	50.0 ± 0.63	51.0 ± 0.78	49.0 ± 0.06
30F-TiO_2-PC	54.0 ± 1.29	53.0 ± 1.40	53.0 ± 1.18
50F-TiO_2-PC	42.0 ± 0.35	42.0 ± 0.83	40.0 ± 1.03
Degussa P25	32.0 ± 0.45	37.0 ± 1.47	38.0 ± 1.56

Table 7 The percentage of IC decolorization by TiO_2 samples. (Continued)

TiO_2 samples	Decolorization efficiency (%) at adsorption time (h)		
	4	5	6
Undoped TiO_2	1.00 ± 0.14	1.00 ± 0.17	1.00 ± 0.28
Undoped-pH 3.6	2.00 ± 1.11	2.00 ± 1.10	3.00 ± 1.20
5F-TiO_2-PC	2.00 ± 1.56	2.00 ± 1.72	2.00 ± 2.03
10F-TiO_2-PC	5.00 ± 1.83	5.00 ± 1.79	5.00 ± 1.87
15F-TiO_2-PC	33.0 ± 1.71	32.0 ± 0.89	31.0 ± 1.63
20F-TiO_2-PC	47.0 ± 1.50	46.0 ± 1.34	47.0 ± 1.49
30F-TiO_2-PC	52.0 ± 1.51	51.0 ± 1.90	50.0 ± 1.52
50F-TiO_2-PC	39.0 ± 0.32	37.0 ± 0.62	38.0 ± 0.20
Degussa P25	39.0 ± 2.00	40.0 ± 0.57	40.0 ± 0.54

Table 8 Photocatalytic activity of TiO_2 samples under UV light.

TiO_2 samples	Degradation efficiency (%) at time (h)		
	1	1.5	2
Undoped TiO_2	0.00 ± 0.41	1.00 ± 0.44	1.00 ± 0.28
Undoped-pH 3.6	3.00 ± 0.56	5.00 ± 1.03	8.00 ± 0.29
5F-TiO_2-PC	4.00 ± 0.24	12.0 ± 1.22	19.0 ± 1.25
10F-TiO_2-PC	9.00 ± 1.04	67.0 ± 1.34	100 ± 0.00
15F-TiO_2-PC	32.0 ± 0.51	84.0 ± 1.85	100 ± 0.00
20F-TiO_2-PC	49.0 ± 1.54	85.0 ± 1.62	100 ± 0.00
30F-TiO_2-PC	52.0 ± 1.82	100 ± 0.00	100 ± 0.00
50F-TiO_2-PC	44.0 ± 0.24	63.0 ± 0.26	84.0 ± 0.32
Degussa P25	34.0 ± 0.87	100 ± 0.00	100 ± 0.00

Table 8 Photocatalytic activity of TiO_2 samples under UV light. (Continued)

TiO_2 samples	Degradation efficiency (%) at time (h)		
	2.5	3	3.5
Undoped TiO_2	1.00 ± 0.50	1.00 ± 0.51	1.00 ± 0.63
Undoped-pH 3.6	11.0 ± 0.94	15.0 ± 0.62	18.0 ± 0.89
5F-TiO_2-PC	27.0 ± 0.16	34.0 ± 1.80	42.0 ± 1.46
10F-TiO_2-PC	100 ± 0.00	100 ± 0.00	100 ± 0.00
15F-TiO_2-PC	100 ± 0.00	100 ± 0.00	100 ± 0.00
20F-TiO_2-PC	100 ± 0.00	100 ± 0.00	100 ± 0.00
30F-TiO_2-PC	100 ± 0.00	100 ± 0.00	100 ± 0.00
50F-TiO_2-PC	100 ± 0.00	100 ± 0.00	100 ± 0.00
Degussa P25	100 ± 0.00	100 ± 0.00	100 ± 0.00

Table 8 Photocatalytic activity of TiO_2 samples under UV light. (Continued)

TiO_2 samples	Degradation efficiency (%) at time (h)		
	4	4.5	5
Undoped TiO_2	1.00 ± 0.60	2.00 ± 0.67	2.00 ± 0.51
Undoped-pH 3.6	22.0 ± 0.66	25.0 ± 0.58	26.0 ± 0.19
5F-TiO_2-PC	46.0 ± 1.42	52.0 ± 1.44	56.0 ± 2.06
10F-TiO_2-PC	100 ± 0.00	100 ± 0.00	100 ± 0.00
15F-TiO_2-PC	100 ± 0.00	100 ± 0.00	100 ± 0.00
20F-TiO_2-PC	100 ± 0.00	100 ± 0.00	100 ± 0.00
30F-TiO_2-PC	100 ± 0.00	100 ± 0.00	100 ± 0.00
50F-TiO_2-PC	100 ± 0.00	100 ± 0.00	100 ± 0.00
Degussa P25	100 ± 0.00	100 ± 0.00	100 ± 0.00

Table 9 Photocatalytic activity of TiO_2 samples under visible light.

TiO_2 samples	Degradation efficiency (%) at time (h)			
	1	2	3	4
Undoped TiO_2	1.00 ± 0.34	1.00 ± 0.76	1.00 ± 0.23	1.00 ± 0.72
Undoped-pH 3.6	4.00 ± 0.06	5.00 ± 0.03	5.00 ± 0.34	7.00 ± 0.87
5F-TiO_2-PC	4.00 ± 0.55	7.00 ± 0.60	9.00 ± 0.81	11.0 ± 1.25
10F-TiO_2-PC	6.00 ± 0.90	22.0 ± 1.95	39.0 ± 1.01	58.0 ± 2.00
15F-TiO_2-PC	32.0 ± 1.84	48.0 ± 0.40	63.0 ± 1.86	82.0 ± 1.08
20F-TiO_2-PC	47.0 ± 1.61	56.0 ± 1.62	68.0 ± 1.40	90.0 ± 1.19
30F-TiO_2-PC	53.0 ± 1.74	61.0 ± 1.74	73.0 ± 0.56	92.0 ± 0.61
50F-TiO_2-PC	44.0 ± 1.06	52.0 ± 0.39	59.0 ± 0.67	67.0 ± 0.71
Degussa P25	32.0 ± 1.58	71.0 ± 1.26	94.0 ± 1.88	100 ± 0.00

Table 9 Photocatalytic activity of TiO_2 samples under visible light. (Continued)

TiO_2 samples	Degradation efficiency (%) at time (h)		
	5	6	7
Undoped TiO_2	2.00 ± 1.24	1.00 ± 1.32	1.00 ± 1.38
Undoped-pH 3.6	7.00 ± 0.66	7.00 ± 0.67	7.00 ± 0.81
5F-TiO_2-PC	13.0 ± 1.47	14.0 ± 1.99	14.0 ± 2.07
10F-TiO_2-PC	73.0 ± 1.97	80.0 ± 1.40	86.0 ± 1.13
15F-TiO_2-PC	100 ± 0.00	100 ± 0.00	100 ± 0.00
20F-TiO_2-PC	100 ± 0.00	100 ± 0.00	100 ± 0.00
30F-TiO_2-PC	100 ± 0.00	100 ± 0.00	100 ± 0.00
50F-TiO_2-PC	80.0 ± 1.46	99.0 ± 1.20	100 ± 0.00
Degussa P25	100 ± 0.00	100 ± 0.00	100 ± 0.00

Table 9 Photocatalytic activity of TiO_2 samples under visible light. (Continued)

TiO_2 samples	Degradation efficiency (%) at time (h)		
	8	9	10
Undoped TiO_2	2.00 ± 1.07	2.00 ± 0.95	2.00 ± 0.88
Undoped-pH 3.6	7.00 ± 1.16	6.00 ± 0.52	6.00 ± 0.30
5F-TiO_2-PC	14.0 ± 1.54	15.0 ± 1.33	15.0 ± 1.65
10F-TiO_2-PC	90.0 ± 1.69	95.0 ± 0.90	97.0 ± 0.43
15F-TiO_2-PC	100 ± 0.00	100 ± 0.00	100 ± 0.00
20F-TiO_2-PC	100 ± 0.00	100 ± 0.00	100 ± 0.00
30F-TiO_2-PC	100 ± 0.00	100 ± 0.00	100 ± 0.00
50F-TiO_2-PC	100 ± 0.00	100 ± 0.00	100 ± 0.00
Degussa P25	100 ± 0.00	100 ± 0.00	100 ± 0.00

Table 10 Effect of pH on decolorization efficiency of IC by 20F-TiO_2-PC.

Time (h)	Decolorization efficiency (%) at adsorption time (h)				
	pH 3	pH 5	pH 6.5	pH 9	pH 11
1	83.0 ± 1.00	39.0 ± 1.48	35.0 ± 0.06	26.0 ± 0.16	4.00 ± 0.14
2	84.0 ± 0.36	40.0 ± 1.42	34.0 ± 0.01	27.0 ± 0.69	4.00 ± 0.27
3	85.0 ± 0.58	41.0 ± 1.80	34.0 ± 0.50	27.0 ± 0.73	4.00 ± 0.33
4	85.0 ± 0.59	42.0 ± 1.88	34.0 ± 0.30	27.0 ± 0.19	4.00 ± 0.88
5	85.0 ± 0.88	42.0 ± 1.69	34.0 ± 0.09	27.0 ± 0.37	5.00 ± 0.43
6	85.0 ± 0.58	44.0 ± 1.71	34.0 ± 0.71	27.0 ± 0.69	5.00 ± 0.52

Table 11 Effect of pH on decolorization efficiency of IC by 30F-TiO_2-PC.

Time (h)	Decolorization efficiency (%) at adsorption time (h)				
	pH 3	pH 5	pH 6.5	pH 9	pH 11
1	85.0 ± 0.77	47.0 ±1.30	38.0 ± 1.30	26.0 ± 0.34	5.00 ± 0.18
2	86.0 ± 0.79	48.0 ± 2.05	39.0 ± 0.79	26.0 ± 0.83	4. 00 ± 1.04
3	86.0 ± 0.46	48.0 ± 1.85	38.0 ± 0.52	27.0 ± 0.16	4. 00 ± 0.50
4	87.0 ± 0.85	48.0 ± 1.82	37.0 ± 0.82	27.0 ± 0.21	5. 00 ± 0.34
5	87.0 ± 1.20	48.0 ± 1.52	38.0 ± 0.11	28.0 ± 0.14	4. 00 ± 1.00
6	89.0 ± 0.32	48.0 ± 1.68	38.0 ± 1.19	28.0 ± 0.29	5. 00 ± 0.66

Table 12 Effect of pH on degradation efficiency of IC by 20F-TiO_2-PC under UV light.

Time (h)	Degradation efficiency (%) at time (h)				
	pH 3	pH 5	pH 6.5	pH 9	pH 11
1	83.0 ±0.34	42.0 ± 1.12	35.0 ± 0.42	24.0 ± 0.90	3.00 ± 0.42
2	90.0 ± 0.31	52.0 ± 0.37	42.0 ± 1.98	39.0 ± 1.88	5.00 ± 0.33
3	92.0 ± 0.22	57.0 ± 0.27	51.0 ± 0.74	56.0 ± 0.58	6.00 ± 0.32
4	93.0 ± 0.24	64.0 ± 0.34	60.0 ± 0.48	77.0 ± 0.45	8.00 ± 0.60
5	95.0 ± 0.54	76.0 ± 0.22	75.0 ± 0.38	97.0 ± 0.09	9.00 ± 0.44
6	97.0 ± 1.03	95.0 ± 0.65	95.0 ± 0.84	99.0 ± 0.60	11.0 ± 0.59

Table 13 Effect of pH on degradation efficiency of IC by 30F-TiO_2-PC under UV light.

Time (h)	Degradation efficiency (%) at time (h)				
	pH 3	pH 5	pH 6.5	pH 9	pH 11
1	89.0 ± 0.30	46.0 ± 1.54	39.0 ± 2.00	26.0 ± 0.78	4.00 ± 0.40
2	94.0 ± 0.28	56.0 ± 0.62	46.0 ± 2.08	44.0 ± 1.78	6.00 ± 0.49
3	95.0 ± 0.31	64.0 ± 0.53	53.0 ± 0.49	66.0 ± 0.66	8.00 ± 0.40
4	96.0 ± 0.11	75.0 ± 0.41	65.0 ± 0.52	95.0 ± 0.09	10.0 ± 0.30
5	98.0 ± 0.74	94.0 ± 0.39	82.0 ± 0.54	100 ± 0.09	11.0 ± 0.45
6	99.0 ± 1.22	98.0 ± 0.60	97.0 ± 0.63	100 ± 0.00	14.0 ± 1.00

Table 14 Effect of pH on degradation efficiency of IC by 20F-TiO_2-PC under visible light.

Time (h)	Degradation efficiency (%) at time (h)				
	pH 3	pH 5	pH 6.5	pH 9	pH 11
1	83.0 ± 0.41	45.0 ± 2.05	36.0 ± 0.11	27.0 ± 0.08	1.00 ± 0.73
2	87.0 ± 1.00	55.0 ± 1.40	41.0 ± 1.86	31.0 ± 0.88	2.00 ± 0.60
3	89.0 ± 0.85	56.0 ± 1.30	44.0 ± 2.23	34.0 ± 0.65	2.00 ± 0.58
4	91.0 ± 0.52	59.0 ± 1.09	48.0 ± 0.36	35.0 ± 1.07	3.00 ± 0.61
5	92.0 ± 0.71	61.0 ± 0.91	49.0 ± 0.71	37.0 ± 1.87	2.00 ± 0.36
6	94.0 ± 0.27	64.0 ± 0.34	53.0 ± 0.37	41.0 ± 0.12	3.00 ± 0.56
7	94.0 ± 0.32	66.0 ± 0.83	56.0 ± 0.29	51.0 ± 0.83	3.00 ± 0.64
8	95.0 ± 0.31	68.0 ± 0.54	61.0 ± 0.35	54.0 ± 1.39	3.00 ± 0.46
9	96.0 ± 0.98	70.0 ± 0.66	65.0 ± 0.35	65.0 ± 0.45	4.00 ± 0.19
10	97.0 ± 0.59	73.0 ± 1.00	67.0 ± 0.40	70.0 ± 0.84	4.00 ± 0.20
11	99.0 ± 2.15	78.0 ± 1.58	76.0 ± 1.19	79.0 ± 0.41	4.00 ± 0.09

Table 15 Effect of pH on degradation efficiency of IC by 30F-TiO_2-PC under visible light.

Time (h)	Degradation efficiency (%) at time (h)				
	pH 3	pH 5	pH 6.5	pH 9	pH 11
1	86.0 ± 0.99	50.0 ± 2.10	40.0 ± 0.35	27.0 ± 0.44	2.00 ± 0.31
2	87.0 ± 0.63	57.0 ± 0.56	44.0 ± 1.78	30.0 ± 0.95	3.00 ± 1.40
3	88.0 ± 0.93	58.0 ± 0.86	46.0 ± 1.90	31.0 ± 0.61	3.00 ± 1.38
4	89.0 ± 0.90	59.0 ± 0.86	47.0 ± 0.97	35.0 ± 0.71	3.00 ± 0.23
5	90.0 ± 0.74	61.0 ± 1.12	49.0 ± 1.11	38.0 ± 0.70	3.00 ± 0.31
6	94.0 ± 0.43	64.0 ± 0.96	54.0 ± 1.33	42.0 ± 1.24	3.00 ± 1.11
7	94.0 ±0.39	66.0 ± 0.95	57.0 ± 1.19	50.0 ± 0.13	4.00 ± 1.02
8	95.0 ± 0.35	69.0 ± 0.75	61.0 ± 1.42	58.0 ± 0.45	4.00 ± 0.48
9	96.0 ± 0.92	70.0 ± 0.99	63.0 ± 2.07	64.0 ± 0.82	4.00 ± 0.36
10	98.0 ± 1.07	73.0 ± 1.27	67.0 ± 1.66	69.0 ± 0.43	4.00 ± 0.48
11	100 ± 0.00	82.0 ± 1.50	81.0 ± 0.50	85.0 ± 0.15	4.00 ± 0.45

Table 16 Effect of pH on degradation efficiency of IC by Degussa P25 under visible light.

Time (h)	Degradation efficiency (%) at time (h)				
	pH 3	pH 5	pH 6.5	pH 9	pH 11
1	46.0 ± 2.00	33.0 ± 0.34	11.0 ± 0.56	2.00 ± 0.79	2.00 ± 0.52
2	61.0 ± 0.35	53.0 ± 0.28	27.0 ± 0.37	20.0 ± 0.90	8.0 ± 0.60
3	65.0 ± 0.28	56.0 ± 0.14	38.0 ± 0.21	39.0 ± 0.31	11.0 ± 0.29
4	71.0 ± 0.64	65.0 ± 0.07	46.0 ± 0.91	58.0 ± 0.28	14.0 ± 0.36
5	76.0 ± 0.29	67.0 ± 0.24	53.0 ± 0.43	74.0 ± 0.09	17.0 ± 0.17
6	78.0 ± 0.55	72.0 ± 0.18	59.0 ± 0.60	85.0 ± 0.44	19.0 ± 1.03
7	81.0 ± 0.32	77.0 ± 0.06	64.0 ± 0.53	94.0 ± 0.17	31.0 ± 0.28
8	83.0 ± 0.52	80.0 ± 0.26	69.0 ± 0.63	96.0 ± 0.73	39.0 ± 0.66
9	85.0 ± 0.13	84.0 ± 0.26	75.0 ± 0.37	100 ± 0.00	44.0 ± 1.82
10	87.0 ± 0.11	87.0 ± 0.09	80.0 ± 1.35	100 ± 0.00	50.0 ± 0.49
11	94.0 ± 0.54	88.0 ± 0.36	86.0 ± 0.80	100 ± 0.00	55.0 ± 0.54

Table 17 Titration data of F-TiO_2-imp

TiO_2 samples	Titration	1	2	3	Average (mL)
Undoped TiO_2	0.01 M HCl	0.8	0.8	0.9	0.83 ± 0.06
Undoped-pH 3.6	0.01 M NaOH	0.9	0.8	0.9	0.87 ± 0.06
2F-TiO_2-imp	0.01 M NaOH	0.9	1.0	1.0	0.97 ± 0.06
5F-TiO_2-imp	0.01 M NaOH	5.2	5.1	5.1	5.13 ± 0.06
7F-TiO_2-imp	0.01 M NaOH	5.3	5.2	5.3	5.27 ± 0.06
10F-TiO_2-imp	0.01 M NaOH	7.8	7.7	7.7	7.73 ± 0.06
30F-TiO_2-imp	0.01 M NaOH	13.9	13.9	13.8	13.87 ± 0.06

Table 18 Titration data of F-TiO_2-PC

TiO_2 samples	Titration	1	2	3	Average (mL)
Undoped TiO_2	0.01 M HCl	1.6	1.7	1.7	1.67 ± 0.06
Undoped-pH 3.6	0.01 M NaOH	0.5	0.5	0.5	0.50 ± 0.00
5F-TiO_2- PC	0.01 M NaOH	0.9	0.85	0.9	0.88 ± 0.03
10F-TiO_2- PC	0.01 M NaOH	2.5	2.5	2.6	2.53 ± 0.06
15F-TiO_2- PC	0.01 M NaOH	2.9	2.9	3.0	2.93 ± 0.06
20F-TiO_2- PC	0.01 M NaOH	3.3	3.3	3.4	3.33 ± 0.06
30F-TiO_2- PC	0.01 M NaOH	5.4	5.3	5.4	5.37 ± 0.06
50F-TiO_2- PC	0.01 M NaOH	8.2	8.1	8.2	8.17 ± 0.06

VITAE

Name Miss Sutatip Jainsiri

Student ID 5210220142

Education Attainment

Degree	Name of Institution	Year of Graduation
B. Sc. (Chemistry)	Prince of Songkla University	2007

Scholarship Awards during Enrolment

1. The Center for Innovation in Chemistry: Post Graduate Education and Research Program in Chemistry (PERCH-CIC), Commission on Higher Education, Ministry of Education.
2. Graduate School, Prince of Songkla University.

List of Publications and Proceedings

Jainsiri, S. and Wongnawa, S. “Photocatalytic degradation of dye by TiO_2 doped with some anions” International Congress for Innovation in Chemistry (PERCH-CIC Congress VII). Jomtien Palm Beach Hotel & Resort, Pattaya, Thailand. 4-7 May 2011.

Jainsiri, S. and Wongnawa, S. “Enhancing photocatalytic activity of amorphous TiO_2 by doping with anion” 14th Asian Chemical Congress 2011 (14 ACC). Queen Sirikit National Convention Center, Bangkok, Thailand. 5-8 September 2011.